Charles University in Prague
Faculty of Mathematics and Physics

DOCTORAL THESIS

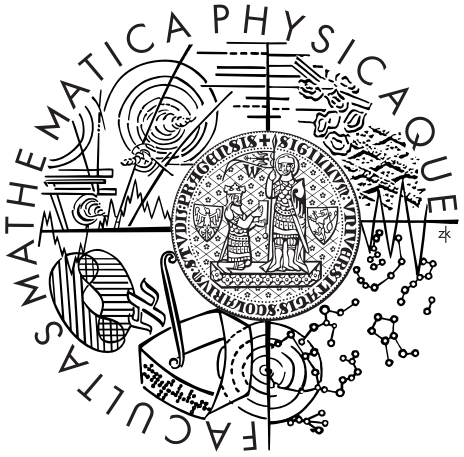

Karel Tůma

Identification of rate type fluids suitable for modeling geomaterials

Mathematical Institute, Charles University

Supervisor of the doctoral thesis:	prof. RNDr. Josef Málek, CSc., DSc.
Study programme:	Physics
Specialization:	Mathematical and Computational Modeling

Prague 2013

To my parents.

I am indebted to my supervisor Professor Josef Málek for numerous pieces of advice and invaluable help during writing this thesis. I am also grateful to Jaroslav Hron who provided me his numerical code and helped me with its modification.

I am very thankful to Professor K.R. Rajagopal for the fruitful collaboration and the possibility to stay six months at Texas A&M University. I also thank to Atul Narayan and Murali Krishnan for providing me their experimental data.

Finally, I would like to thank to Ondřej Souček and to my wife Petra Suková for numerous discussions.

During my Ph.D. studies I have been supported by several projects. I acknowledge explicitly the support of those that financed my research during last month: project MORE, ERC-CZ LL1202 supported by the Czech Ministry of Education, Youth and Sports, project GAČR 201/09/0917 financed by the Grant agency of the Czech Republic. I have been also a member of University Center of Excellence MathMAC financed by the Charles University in Prague.

I declare that I carried out this doctoral thesis independently, and only with the cited sources, literature and other professional sources.

I understand that my work relates to the rights and obligations under the Act No. 121/2000 Coll., the Copyright Act, as amended, in particular the fact that the Charles University in Prague has the right to conclude a license agreement on the use of this work as a school work pursuant to Section 60 paragraph 1 of the Copyright Act.

In Prague December 17, 2013

Název práce: Identifikace tekutin rychlostního typu vhodných k modelování geomateriálů

Autor: Karel Tůma

Ústav: Matematický ústav Univerzity Karlovy

Vedoucí disertační práce: prof. RNDr. Josef Málek, CSc., DSc., Matematický ústav Univerzity Karlovy

Abstrakt: V této práci studujeme a porovnáváme různé viskoelastické modely rychlostního typu, které jsou vhodné pro popis odezvy geomateriálů jako asfalt. Pomocí termodynamického přístupu navrženého Rajagopalem a Srinivasou (2000) odvodíme nové viskoelastické modely, které jsou zobecněním standardních modelů Oldroyd-B a Burgers. Rovněž ukážeme, že nové modely dosahují lepších výsledků při fitování experimentálních dat s asfaltem než dříve uvažované modely (Oldroyd-B, Burgers, Rajagopal a Srinivasa (2000)) a identifikujeme ty modely, které jsou schopné zachytit pozoruhodné chování asfaltu pozorované v nedávných experimentech (překmit momentu síly a dva relaxační mechanismy s rozdílnou časovou škálou). Dále provádíme počítačové simulace úloh zachycující proudění viskoelastických tekutin popsaných oběma standardními modely a nově odvozenými modely metodou konečných prvků jak na pevné, tak časově se měnící výpočetní oblasti. Procesy probíhající v deformující oblasti převedeme na pevnou výpočetní oblast použitím smíšeného Lagrangeova-Eulerova popisu (ALE metoda). Využitím odvozeného postupu simulujeme proces válcování asfaltu nebo vytváření vyjetých kolejí na silnici se skutečnými materiálovými parametry získanými předchozím nafitováním experimentů.

Klíčová slova: viskoelastické tekutiny, tekutiny rychlostního typu, asfalt, fitování experimentů, metoda konečných prvků, numerické simulace.

Title: Identification of rate type fluids suitable for modeling geomaterials

Author: Karel Tůma

Institute: Mathematical Institute, Charles University

Supervisor: prof. RNDr. Josef Málek, CSc., DSc., Mathematical Institute, Charles University

Abstract: In the present thesis we study and compare different viscoelastic rate-type fluid models capable of describing response of geomaterials such as asphalt. Using new thermodynamic approach proposed by Rajagopal and Srinivasa (2000) we derive several classes of non-linear viscoelastic models that generalize standard Oldroyd-B and Burgers models. We show that the new models achieve better results in fitting experimental data with asphalt than the previously considered models (Oldroyd-B, Burgers, Rajagopal and Srinivasa (2000)). In particular they are able to capture the behavior of asphalt observed recently in experiments (torque overshoot and two relaxation mechanisms), which is not possible to describe by the other models. Using both the standard and the newly derived models we compute full simulations of viscoelastic flow with the finite element method in fixed domains and incorporating the Arbitrary Lagrangian-Eulerian description also in deforming domains. For example, we study rolling of asphalt or creation of ruts in the road with the real material parameters obtained by fitting the experiments.

Keywords: viscoelastic, rate-type fluid, asphalt binder, experiment fitting, finite element method, numerical simulation.

Contents

Introduction

In the present thesis we study viscoelastic rate type fluid models capable of describing response of geomaterials like asphalt. Asphalt binder is a complex mixture of hydrocarbons and as such it is difficult to predict its non-linear viscoelastic response. However, mainly for its special properties it is used in many applications. One of the most known application is its use as a glue in asphalt concrete for constructions of roadways and runways.

Being viscous and elastic at the same time makes this material perfect for absorption of the impact of the wheels of the landing plane on the runway. The viscous behavior is exhibited in one of the longest experiment ever done, where dropping of pitch is observed on the time scale of tens of years, see [13]. Asphalt was also used in the early 19th century for making the the oldest surviving photograph of nature, which stemmed from the fact, that the exposure of light hardened the material. Mastic asphalt, which has higher content of asphalt binder than usual asphalt concrete, is also used for waterproofing of roofs, etc. For more information on asphalt see a thorough review paper by Krishnan and Rajagopal [28].

Since asphalt binder is almost incompressible material we are mainly interested in incompressible fluids with constant density ρ that are described by two balance equations (for more details see Chapter 1)

$$\operatorname{div} \mathbf{v} = 0, \tag{1}$$

$$\rho \left(\frac{\partial \mathbf{v}}{\partial t} + \mathbf{v} \cdot \nabla \mathbf{v} \right) = \operatorname{div} \mathbf{T}, \quad \mathbf{T} = \mathbf{T}^{\mathrm{T}}, \tag{2}$$

where $\mathbf{v}$ is fluid velocity and $\mathbf{T}$ is Cauchy stress tensor in the form

$$\mathbf{T} = -p\mathbf{I} + \mathbf{S}. \tag{3}$$

In case of incompressible Navier-Stokes equations $\mathbf{S} = 2\mu\mathbf{D} = \mu \left(\nabla \mathbf{v} + (\nabla \mathbf{v})^{\mathrm{T}} \right)$, where μ is the fluid viscosity. Such model can not capture non-linear response of the stress relaxation test or creep test and other non-Newtonian phenomena (described in Chapter 1). Some rate type fluid models, i.e. the model where $\mathbf{S}$ satisfies some evolutionary equation, are capable of capturing these features. Maxwell model ([40]), the simplest example of rate type fluid model, is given through

$$\mathbf{S} + \tau \overset{\triangledown}{\mathbf{S}} = 2\mu_1 \mathbf{D}, \tag{4}$$

where τ is a relaxation time saying how fast the stress decreases in the stress relaxation test, μ_1 is the viscosity and $\triangledown$ is an objective material time derivative called upper

convected Oldroyd derivative. If we add a viscous Newtonian term $2\mu_2\mathbf{D}$ to the Maxwell model, we obtain Oldroyd-B model ([46]) in the form

$$\mathbf{S} = 2\mu_2\mathbf{D} + \mathbf{A}, \tag{5}$$

$$\mathbf{A} + \tau \overset{\triangledown}{\mathbf{A}} = 2\mu_1\mathbf{D}. \tag{6}$$

This model behaves more viscously than the Maxwell model and it is a popular standard viscoelastic fluid model. Using a new tensor $\mathbf{B} = \mathbf{I}+\mathbf{A}/G$, where $G = \mu_1/\tau$ is the elastic modulus (5)–(6) can be rewritten into the form

$$\mathbf{S} = 2\mu_2\mathbf{D} + G(\mathbf{B} - \mathbf{I}), \tag{7}$$

$$\overset{\triangledown}{\mathbf{B}} = -\frac{G}{\mu_1}(\mathbf{B} - \mathbf{I}). \tag{8}$$

In this thesis we present three ways how to obtain this standard model. In Chapter 1 we show how to get one-dimensional version of this model using mechanical analogs, in Chapter 2 we generalize this one-dimensional model to three-dimensional setting. The problem with such derivation is that it is not unique and we can not fully control how the elastic and viscous part of the deformation looks like. In Chapter 2 there is also given the other possibility of the derivation from microscopical principles (as originally given in [30] by Kuhn). Both derivations do not guarantee that the second law of thermodynamics is satisfied. The other standard viscoelastic model, the Burgers model, is also presented in Chapter 2. Both these models are linear models in the sense that the evolutionary equation for the extra stress tensor $\mathbf{S}$, $\mathbf{A}$, or $\mathbf{B}$ is linear with respect to these tensors.

The properties of asphalt binder, which is the glue that holds the stones in the asphalt concrete together and chemically it is a mixture of many hydrocarbons, were measured in several experiments. One of the experiments shows an interesting non-linear non-monotone response of asphalt binder, the other shows that asphalt binder exhibits at least two different relaxation mechanisms. In Chapter 4 we show that these experiments can not be explained with standard viscoelastic models mentioned above.

On that account we derive new non-linear models that would be able to describe those experiments using a new approach proposed by Rajagopal and Srinivasa ([57]). This approach provides a way how to derive a thermodynamically compatible model where we can control the elastic and dissipative response of the body using the natural configuration. In order to do this, two scalar functions have to be constituted. The first one, which corresponds to the elastic response, is the thermodynamical potential. The other one, which includes the energy dissipation of the body, is the rate of entropy production $\tilde{\xi}$. If it is non-negative, the second law of thermodynamics is satisfied. Finally, the assumption of maximum rate of entropy production is used. This approach is described in Chapter 3.

In [57] Rajagopal and Srinivasa derived a non-linear version of incompressible Maxwell model under the assumption that the Helmholtz free energy ψ is in the form corresponding to incompressible neo-Hookean solid

$$\psi = \frac{G}{2\rho}\left(\operatorname{tr}\mathbf{B}_{\kappa_{p(t)}} - 3\right), \tag{9}$$

where G is the elastic modulus and $\mathbf{B}_{\kappa_{p(t)}}$ is the left Cauchy-Green tensor corresponding to the natural configuration. For the rate of entropy production $\tilde{\xi}$ they chose a non-negative scalar

$$0 \leq \tilde{\xi} = \mu_1 \mathbf{D}_{\kappa_{p(t)}} \mathbf{B}_{\kappa_{p(t)}} \cdot \mathbf{D}_{\kappa_{p(t)}}, \tag{10}$$

where $\mathbf{D}_{\kappa_{p(t)}}$ is the rate of deformation of the natural configuration. They obtained the following model

$$\mathbf{S} = G\mathbf{B}^d_{\kappa_{p(t)}}, \tag{11}$$

$$\overset{\triangledown}{\mathbf{B}}_{\kappa_{p(t)}} = -\frac{G}{\mu_1}\left(\mathbf{B}_{\kappa_{p(t)}} - \frac{3}{\mathrm{tr}\left(\mathbf{B}^{-1}_{\kappa_{p(t)}}\right)}\mathbf{I}\right), \tag{12}$$

which is very similar to Maxwell model. The upper convected Oldroyd derivative comes naturally from the derivation and it does not have to be artificially included as in case of generalization of the one-dimensional model.

Later, in 2007 Málek and Rajagopal derived a different model using the same neo-Hookean free energy with a different rate of entropy production

$$0 \leq \tilde{\xi} = \mu_2 \mathbf{D} \cdot \mathbf{D} + \mu_1 \mathbf{D}_{\kappa_{p(t)}} \mathbf{C}_{\kappa_{p(t)}} \cdot \mathbf{D}_{\kappa_{p(t)}} \tag{13}$$

and obtained a model that is a non-linear version of Oldroyd-B model. They also split the tensor $\mathbf{B}_{\kappa_{p(t)}}$ into its deviatoric and spherical part and obtained a model that is – at least at first sight – far different from the model by Rajagopal and Srinivasa with additional Newtonian dissipation. In this work we show that both models are equivalent and that they reduce to standard Oldroyd-B model if the elastic response is linearized. We use this model to fit the first set of experiments and we obtain better results than that obtained with the linear models. However, the agreement with the experiment is still not satisfactory. We therefore derive several new models in order to fit the experiment as accurate as is possible. First model that we derive is a modification of the derivation by Rajagopal and Srinivasa with the same free energy, but power-law like type of rate of entropy production. We obtain a model with six material parameters (twice more than the Oldroyd-like models have) that is described by the set of algebraic-differential equations. This model captures the first set of experiments quite well.

Furthermore, we use again the same assumption for the elastic part, i.e. the neo-Hookean one, but for the rate of entropy production we use a simple quadratic form

$$0 \leq \tilde{\xi} = \mu_2 \mathbf{D} \cdot \mathbf{D} + \mu_1 \mathbf{D}_{\kappa_{p(t)}} \cdot \mathbf{D}_{\kappa_{p(t)}}, \tag{14}$$

and we obtain an incompressible model with three material parameters denoted as Quad1

$$\mathbf{S} = 2\mu_2 \mathbf{D} + G\mathbf{B}^d_{\kappa_{p(t)}}, \tag{15}$$

$$\overset{\triangledown}{\mathbf{B}}_{\kappa_{p(t)}} = -\frac{G}{\mu_1}\mathbf{B}_{\kappa_{p(t)}}\mathbf{B}^d_{\kappa_{p(t)}}. \tag{16}$$

Again we show that this model reduces to standard Oldroyd-B model when the elastic response is linearized. This model captures the first set of experiments very well, better than the power-law like model.

The other set of experiments shows that asphalt binder exhibits at least two different relaxation mechanisms which can not be captured with any so far presented non-linear models. That is why we derive another model using two natural configurations where every natural configuration corresponds to one individual relaxation mechanism. Using the incompressible neo-Hookean elastic response and the rate of entropy production in the form

$$0 \leq \tilde{\xi} = \mu_3 \mathbf{D} \cdot \mathbf{D} + \mu_1 \mathbf{D}_{\kappa_{p_1(t)}} \cdot \mathbf{D}_{\kappa_{p_1(t)}} + \mu_2 \mathbf{D}_{\kappa_{p_2(t)}} \cdot \mathbf{D}_{\kappa_{p_2(t)}} \tag{17}$$

we derive an incompressible model with two rate-type equations and five material parameters denoted as Quad2

$$\mathbf{S} = 2\mu_3 \mathbf{D} + G_1 \mathbf{B}^d_{\kappa_{p_1(t)}} + G_2 \mathbf{B}^d_{\kappa_{p_2(t)}}, \tag{18}$$

$$\overset{\triangledown}{\mathbf{B}}_{\kappa_{p_1(t)}} = -\frac{G_1}{\mu_1} \mathbf{B}_{\kappa_{p_1(t)}} \mathbf{B}^d_{\kappa_{p_1(t)}}, \tag{19}$$

$$\overset{\triangledown}{\mathbf{B}}_{\kappa_{p_2(t)}} = -\frac{G_2}{\mu_2} \mathbf{B}_{\kappa_{p_2(t)}} \mathbf{B}^d_{\kappa_{p_2(t)}}. \tag{20}$$

We show that this model reduces to Burgers model again when both elastic responses are linearized. This model captures both sets of experiments very well and it is a generalization of model Quad1.

All non-linear models presented above are fully incompressible which means that not only the whole deformation is incompressible (i.e. the motion is isochoric) but both elastic and dissipative parts of the deformation are incompressible. In order to obtain an incompressible model with the compressible neo-Hookean elastic response we use the following thermodynamical potential

$$\psi = \frac{G}{2\rho} \left(\operatorname{tr} \mathbf{B}_{\kappa_{p(t)}} - 3 - \ln \det \mathbf{B}_{\kappa_{p(t)}} \right) \tag{21}$$

and derive few incompressible-compressible models. Furthermore, we also derive one fully compressible viscoelastic model. Doing so, we find out that if the compressible elastic response given by (21) and the rate of entropy production given by (13) are used, the Oldroyd-B model is obtained. Thus, we show that this model is not an approximative model, as the standard ways of derivation suggest, but it is an exact model with compressible neo-Hookean response, which satisfies the second law of thermodynamics. Furthermore, we derive also Burgers model in similar way using two natural configurations. The derivation of all models from the thermodynamical point of view is described in Chapter 3.

In Chapter 5 we derive formal apriori estimates for Burgers and model Quad2 and we define a weak formulation which underlies finite element method. Since we are interested in the simulation of asphalt that flows very slowly, it is sufficient for us to compute problems with a low Weissenberg number (for problems concerning high Weissenberg number problem see for example [67]). First we test our FEM code by computing two benchmark tests with Oldroyd-B model and model Quad1. Further, we do the full simulation of the experiment using our real fitted experiment parameters with the model Quad2 and verify that our full simulation agrees with simplified computation used for the fitting.

We also compute the problems in time-varying deforming domains and simulate real life problems. For this purpose we transform the equations from the physical deforming

domain to the fixed domain using Arbitrary Lagrangian-Eulerian (ALE) method. We study the properties of the numerical solution on two problems.

First, we compare abilities of two different time schemes on the problem of rotating viscoelastic square. It turns out that the higher order time scheme is needed. Next, we study the dependence of the solution on mesh size and time step on the problem of loaded rectangle that corresponds to the real problem of an impact of the plane on the runway. Moreover, we find that the model behaves more elastically with a longer relaxation time.

Finally, full simulations of two real problems with the fitted material parameters are computed. One of the problems corresponds to the important technological problem of "rutting" of roadways, wherein a depression is observed in a portion of the roadways due to the repeated motion of vehicles. The other problem describes the rolling of the asphalt which is caused by the constant load moving forward and back.

Some of the results presented in this thesis are published or submitted for publication in the peer-reviewed journals:

Hron J., Kratochvíl J., Málek J., Rajagopal K. R., Tůma, K.: ***A Thermodynamically Compatible Rate Type Fluid to Describe the Response of Asphalt.*** Elsevier, Mathematics and Computers in Simulation, Volume 82, Issue 10, 1853–1873, 2012.

In this paper we derived a viscoelastic power-law like model and we showed that it captures the torque overshoot experimental data by Krishnan and Narayan (2007) better than the model by Rajagopal and Srinivasa with additional Newtonian dissipation and standard Oldroyd-B model.

Málek J., Rajagopal K. R., Tůma, K.: ***A thermodynamically compatible model for describing the response of asphalt binders.*** Second revised version submitted for publication to Elsevier, Mechanics of Materials, 2013.

In this paper we derived models Quad1 and Quad2, we showed that if the elastic response is linearized they reduce to standard Oldroyd-B and Burgers model and we showed that they capture the experimental data by Krishnan and Narayan (2007) better than power-law like model and that they capture the experiment by Narayan et al. (2012).

Hron J., Rajagopal K. R., Tůma, K.: ***Flow of a Burgers fluid due to time varying loads on deforming boundaries.*** To be submitted for publication to Journal of Non-Newtonian Fluid Mechanics.

In this paper we computed the simulations of standard Maxwell, Oldroyd-B and Burgers model in time varying domain. In particular, we computed the pressing of the viscoelastic rectangle, problem of rutting and rolling of viscoelastic material described by Burgers model.

Some subtle results are also published in the following proceedings:

Tůma, K.: ***Numerical simulation of viscoelastic fluid described by Oldroyd-B model using finite element method and finite volume method.*** Proceedings of Seminar on Numerical Analysis, Technical University of Liberec, ISBN 978-80-7372-821-2, 2012.

Bodnár T., Pirkl L., Tůma K.: ***Viscoelastic Fluid Flows at Moderate Weissenberg Numbers Using Oldroyd Type Model.*** AIP Conf. Proc. 1389, 102–105, 2011.

Tůma K.: ***On Capability of a Class of Incompressible Rate-type Fluid Models to Fit Experimental Data for Asphalt.*** Proceedings of the 18th Annual Conference of Doctoral Students – WDS 2009, MatfyzPress, 2009.

Chapter 1

Non-Newtonian fluids

1.1 Continuum mechanics

In this thesis we study viscoelastic fluids using continuum mechanics which means that we suppose that the material entirely fills whole space and we ignore the fact that the fluid is made of atoms and molecules. Thus continuum mechanics can be used only on scales that are much greater than the distances between molecules.

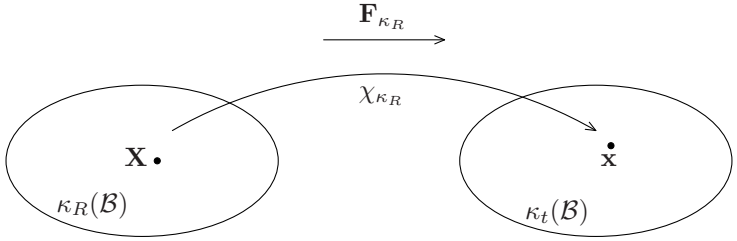

Figure 1.1: Reference and current configuration.

We briefly introduce the basic kinematical quantities and balance equations. For more details see for example [24]. Let $\kappa_R(\mathcal{B})$ and $\kappa_t(\mathcal{B})$ denote the reference and current configuration at time t (see Figure 1.1) of the body $\mathcal{B}$. Let $X \in \kappa_R$ and $x \in \kappa_t$ denote the material point $P \in \mathcal{B}$ at the reference and current configuration, respectively. Then we define the motion χ_{κ_R} of the body as one-to-one mapping

$$x = \chi_{\kappa_R}(X, t). \tag{1.1}$$

The velocity $\mathbf{v}$ is defined through

$$\mathbf{v}(X, t) = \frac{\partial \chi_{\kappa_R}}{\partial t}(X, t), \tag{1.2}$$

the acceleration in Lagrangian formulation (for fixed X) is given by

$$\mathbf{a}(X, t) = \frac{\partial \mathbf{v}(X, t)}{\partial t}. \tag{1.3}$$

However, it is more convenient to compute velocity and acceleration in spatial (Eulerian) description (for fixed x)

$$\mathbf{a}(x, t) = \dot{\mathbf{v}} = \frac{\mathrm{d}\mathbf{v}(x, t)}{\mathrm{d}t} = \frac{\partial \mathbf{v}}{\partial t} + \frac{\partial \mathbf{v}(\chi_{\kappa_R}(X, t), t)}{\partial x} \frac{\partial \chi_{\kappa_R}}{\partial t} = \frac{\partial \mathbf{v}}{\partial t} + [\nabla \mathbf{v}]\mathbf{v}, \tag{1.4}$$

where the last term is usually written in the form $[\nabla \mathbf{v}]\mathbf{v} = (\mathbf{v} \cdot \nabla)\mathbf{v}$ and

$$\dot{s} = \frac{\mathrm{d}s}{\mathrm{d}t} = \frac{\partial s}{\partial t} + \mathbf{v} \cdot \nabla s \tag{1.5}$$

denotes the material time derivative of scalar s. Furthermore, we define the deformation gradient

$$\mathbf{F}_{\kappa_R} = \frac{\partial \chi_{\kappa_R}}{\partial X}, \tag{1.6}$$

and left and right Cauchy-Green tensor

$$\mathbf{B}_{\kappa_R} = \mathbf{F}_{\kappa_R}\mathbf{F}_{\kappa_R}^{\mathrm{T}}, \quad \mathbf{C}_{\kappa_R} = \mathbf{F}_{\kappa_R}^{\mathrm{T}}\mathbf{F}_{\kappa_R}. \tag{1.7}$$

It can be shown that the velocity gradient is equal to

$$\mathbf{L} := \nabla \mathbf{v} = \dot{\mathbf{F}}_{\kappa_R}\mathbf{F}_{\kappa_R}^{-1}, \tag{1.8}$$

the symmetric part of velocity gradient is denoted by

$$\mathbf{D} = \frac{1}{2}(\mathbf{L} + \mathbf{L}^{\mathrm{T}}) \tag{1.9}$$

and the antisymmetric part of velocity gradient by

$$\mathbf{W} = \frac{1}{2}(\mathbf{L} - \mathbf{L}^{\mathrm{T}}). \tag{1.10}$$

1.1.1 Balance equations

In this section we introduce balance equations used in the study of fluids. Using the Reynolds' transport theorem the following balance equations can be derived:

Balance of mass

$$\dot{\rho} + \rho \operatorname{div} \mathbf{v} = 0, \tag{1.11}$$

where ρ is fluid density. If the fluid is incompressible, it can only undergo isochoric motion (i.e. $\det \mathbf{F}_{\kappa_R} = 1$) and hence

$$\operatorname{tr} \mathbf{D} = \operatorname{div} \mathbf{v} = 0\,. \tag{1.12}$$

If the fluid is also homogeneous, then it follows from (1.11) and (1.12) that density is constant everywhere.

Balance of linear momentum

$$\rho \dot{\mathbf{v}} = \rho \mathbf{b} + \operatorname{div} \mathbf{T}\,, \tag{1.13}$$

where $\mathbf{b}$ is the volume force (for example gravity) and $\mathbf{T}$ is the Cauchy stress tensor.

Balance of angular momentum

The balance of angular momentum in the absence of internal body couples leads to

$$\mathbf{T} = \mathbf{T}^{\mathrm{T}}\,. \tag{1.14}$$

Balance of energy

$$\rho\dot{E} = \operatorname{div}(\mathbf{T}\mathbf{v}) - \operatorname{div}\mathbf{q} + \rho r + \rho\mathbf{b}\cdot\mathbf{v}\,, \tag{1.15}$$

where E is the specific total energy, $\mathbf{q}$ is heat flux and r is density of energy sources.

Multiplying (1.13) scalarly by $\mathbf{v}$ and subtracting the result from (1.15), we obtain balance for internal energy e

$$\rho\dot{e} = \mathbf{T}\cdot\mathbf{D} - \operatorname{div}\mathbf{q} + \rho r\,. \tag{1.16}$$

Balance of entropy

$$\rho\dot{\eta} + \operatorname{div}\left(\frac{\mathbf{q}}{\theta}\right) = \frac{\rho r}{\theta} + \frac{\xi}{\theta} \tag{1.17}$$

where η is the entropy, θ is thermodynamical temperature and ξ is the rate of entropy production. The second law of thermodynamics says that $\xi \geq 0$.

In general, the entropy flux does not need to take the form of the heat flux $\mathbf{q}$ divided by temperature θ, the setting given here is however sufficient as we are mostly dealing with isothermal processes.

Note: If we define Helmholtz free energy $\psi := e - \theta\eta$ and we assume only isothermal processes, we obtain a reduced thermodynamical inequality

$$0 \leq \xi = \mathbf{T}\cdot\mathbf{D} - \rho\dot{\psi}. \tag{1.18}$$

1.2 Properties of non-Newtonian fluid

The description of non-Newtonian phenomena given in this section stems from the lecture notes written by the author and the supervisor. These lecture notes have been written as a study text for the series of lectures given by his supervisor at the University of Warsaw (see [34]). For even more information about non-Newtonian fluids see [60], [68], [53] and [35].

Definition 1.2.1. *The fluid is non-Newtonian if it does not behave as a Newtonian fluid described by the model of Navier-Stokes fluid where the Cauchy stress tensor is in the form*

$$\begin{aligned} &\textit{compressible} && \mathbf{T} = -p(\rho,\theta)\mathbf{I} + 2\mu(\rho,\theta)\mathbf{D} + \lambda(\rho,\theta)(\operatorname{div}\mathbf{v})\mathbf{I}, \\ &\textit{incompressible} && \mathbf{T} = -p\mathbf{I} + 2\mu(\rho,\theta)\mathbf{D}. \end{aligned}$$

Most of fluids are not Newtonian and they exhibit different non-Newtonian phenomena that characterize non-Newtonian fluids (fluid does not have to exhibit all phenomena to be non-Newtonian). Consider a fluid flowing in the channel with the velocity in the form

$$\mathbf{v} = (u(y), 0, 0) \tag{1.19}$$

and the Cauchy stress tensor in the form

$$\mathbf{T} = -p\mathbf{I} + \mathbf{S}.$$

For description of non-Newtonian phenomena we need to define few quantities. Shear rate is a shear component of the symmetric part of velocity gradient $\mathbf{D}$, in case of of the velocity (1.19) it is $2D_{12} = u'(y)$, which is sometimes denoted by $\dot{\gamma}$. Corresponding shear stress is equal to S_{12}, sometimes denoted by σ.

Furthermore, we define a generalized viscosity μ_g as

$$\mu_g(D_{12}) := \frac{S_{12}(D_{12})}{D_{12}}.$$

1.2.1 Shear thinning, shear thickening

Response of Newtonian fluid For the Newtonian fluid it holds that S_{12} is a linear function of D_{12} with the proportionality coefficient viscosity μ (see Figure 1.2), i.e. $S_{12} = \mu D_{12}$. The generalized viscosity is constant, i.e. $\mu_g = \mu = const.$, the graph μ_g vs. $\dot{\gamma}$ is depicted in Figure 1.3.

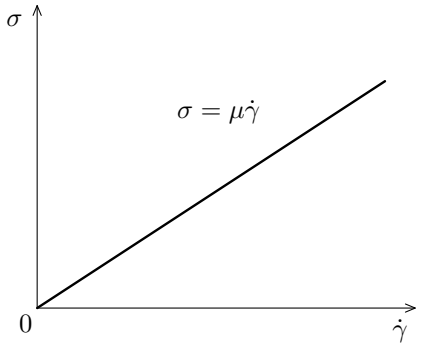

Figure 1.2: Newtonian fluid (shear stress / shear rate)

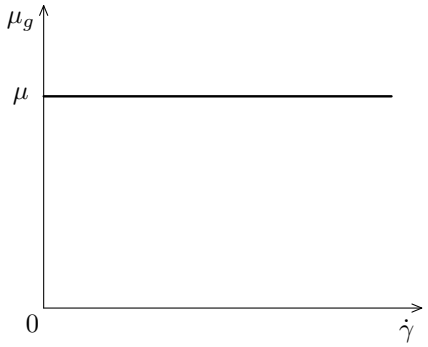

Figure 1.3: Newtonian fluid (generalized viscosity / shear rate)

Response of non-Newtonian fluid A fluid is shear thickening if σ grows faster than linearly with $\dot{\gamma}$ (Figure 1.4). The generalized viscosity μ_g is an increasing function, Figure 1.5 gives the example where the generalized viscosity is degenerate at the beginning, usually the generalized viscosity is positive in zero.

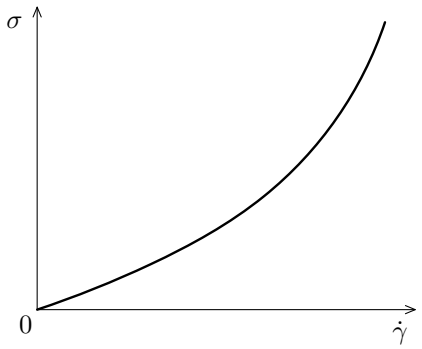

Figure 1.4: Shear thickening (shear stress / shear rate)

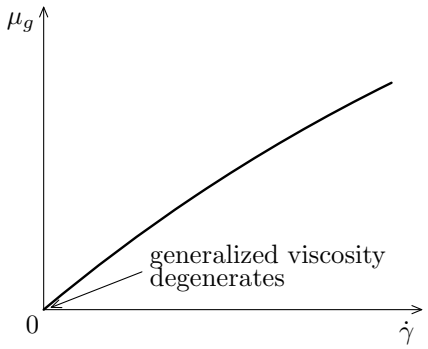

Figure 1.5: Shear thickening (generalized viscosity / shear rate)

Non-Newtonian fluid is shear thinning if σ is a sublinear function of $\dot{\gamma}$ (Figure 1.6). The generalized viscosity μ_g is a decreasing function, in Figure 1.7 is the example where the generalized viscosity is singular at the beginning, usually the generalized viscosity is finite in zero.

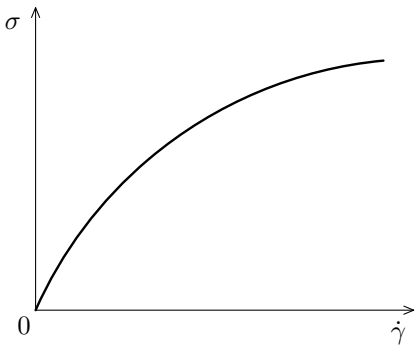

Figure 1.6: Shear thinning, (shear stress / shear rate)

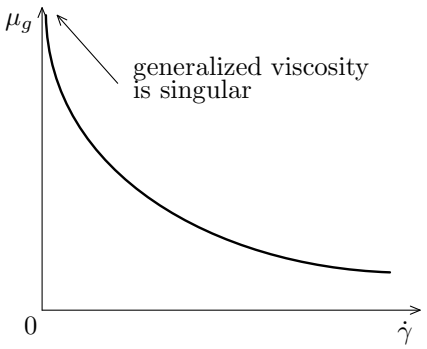

Figure 1.7: Shear thinning, (generalized viscosity / shear rate)

Typical power law model has the generalized viscosity in the form

$$\mu_g = \mu(1 + |\mathbf{D}|^2)^{\frac{r-2}{2}}. \tag{1.20}$$

For $r = 2$ it reduces to Newtonian fluid, for $r > 2$ to shear thickening fluid and for $r < 2$ to shear thinning fluid, see Figures 1.8 and 1.9.

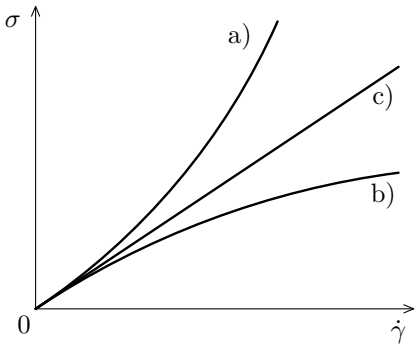

Figure 1.8: Shear stress / shear rate a) $r > 2$, b) $r < 2$, c) $r = 2$

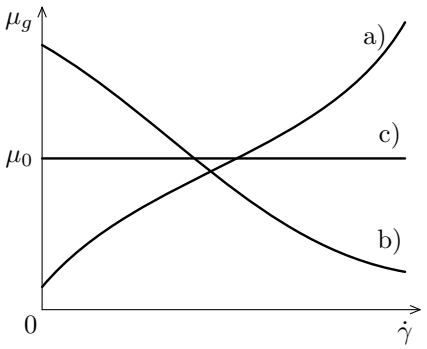

Figure 1.9: Generalized viscosity / shear rate a) $r > 2$, b) $r < 2$, c) $r = 2$

1.2.2 Pressure thickening

Experimental data show that the generalized viscosity μ_g of most fluids is not constant as in case of Newtonian fluid, but it is an increasing function of the pressure (see Figure 1.11).

One of the largest experimental studies concerning the pressure dependence was done in 1926 by Bridgman [9] and recently by Bair [2]. He studied 43 fluids, most of them organic, but including water. He verified that mostly all fluids are pressure

thickening. He also studied water whose behavior is very interesting, for cold water (below about 15 °C) its viscosity is decreasing with the pressure to around 1000 atm, then it is increasing.

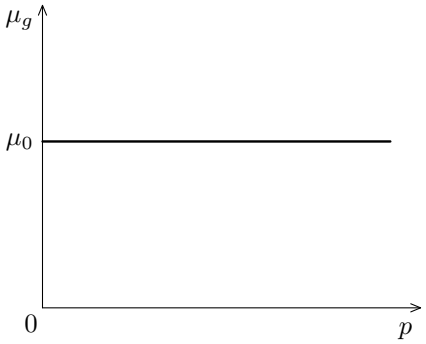

Figure 1.10: Newtonian fluid

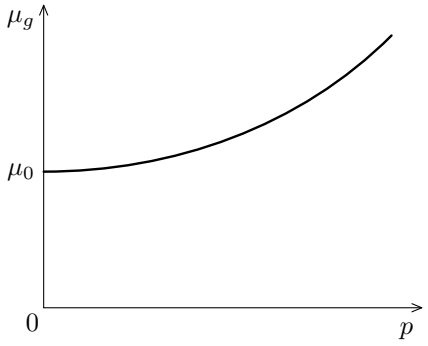

Figure 1.11: Viscosity dependent on pressure

In [3] Barus proposed a pressure thickening model

$$\mu_g(p) = \mu \exp(\alpha p),\ \alpha > 0.$$

1.2.3 Presence of activation/deactivation criteria

Some fluids start to flow after they reach the critical value of the stress (threshold) τ, called the yield stress. In case that the following dependence of the stress on the shear rate is linear, or nonlinear, we call the fluid Bingham fluid named after Bingham [5], or the Herschel-Bulkley fluid, respectively.

The standard formulation is the following:

$$\mathbf{D} = 0 \Leftrightarrow |\mathbf{S}| \leq \tau,$$
$$\mathbf{T} = -p\mathbf{I} + 2\tau\frac{\mathbf{D}}{|\mathbf{D}|} + \tilde{\mu}_g(|\mathbf{D}|^2)\mathbf{D} \Leftrightarrow |\mathbf{S}| > \tau.$$

If $\tilde{\mu}_g$ is constant, it is the Bingham fluid, if not, it is Herschel-Bulkley fluid (see Figure 1.12). Further example is the fluid where the response is connected with the chemical processes. At some value D_{12} the fluid locks and does not flow, see Figure 1.13.

Three non-Newtonian phenomena introduced in Subsections 1.2.1 – 1.2.3 can be described by a non-linear explicit relation between the shear stress S_{12} and shear rate D_{12}. But we can consider a general implicit relation between the Cauchy stress $\mathbf{T}$ and symmetric part of velocity gradient $\mathbf{D}$

$$\mathbf{G}(\mathbf{T}, \mathbf{D}) = \mathbf{0}. \tag{1.21}$$

1.2.4 Presence of non-zero normal stress differences in a simple shear flow

In three dimensional space we define three viscometric functions:

μ	viscosity
$N_1 := T_{11} - T_{22}$	first normal stress difference
$N_2 := T_{22} - T_{33}$	second normal stress difference

In the simple shear flow we suppose a fluid velocity in the form $\mathbf{v} = (u(y), 0, 0)$.

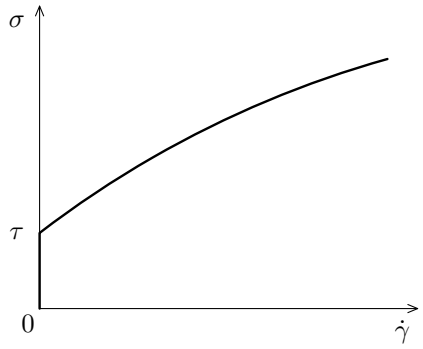

Figure 1.12: Herschel-Bulkley.

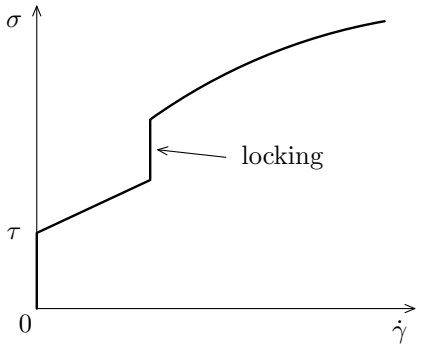

Figure 1.13: Locking.

Response of a Newtonian fluid Let us compute the Cauchy stress $\mathbf{T}$

$$\mathbf{D} = \frac{1}{2}\begin{pmatrix} 0 & u'(y) & 0 \\ u'(y) & 0 & 0 \\ 0 & 0 & 0 \end{pmatrix}, \quad \mathbf{T} = -p\mathbf{I} + 2\mu\mathbf{D} = \begin{pmatrix} -p & \mu u'(y) & 0 \\ \mu u'(y) & -p & 0 \\ 0 & 0 & -p \end{pmatrix}.$$

We can see that $N_1 = N_2 = 0$, and so there are no normal stress differences in the Newtonian case.

Non-Newtonian fluid Non-Newtonian fluids like for example the amyl dissolved in the water, exhibit the presence of non-zero stress differences in the simple shear flow. If we press the fluid in one direction, it reacts in other direction, usually perpendicular. This phenomenon is usually associated with the following effects: rod climbing (Weissenberg effect), die swell, delayed die swell, flow through the sloping channel.

1.2.5 Stress relaxation and non-linear creep

Stress relaxation test Stress relaxation test gives as an output the relation of σ w.r.t. time (see Figure 1.14): At time $t = 0$ we deform the material to the relative prolongation ε_0, keep it constant as time evolves and we study the evolution of shear stress σ.

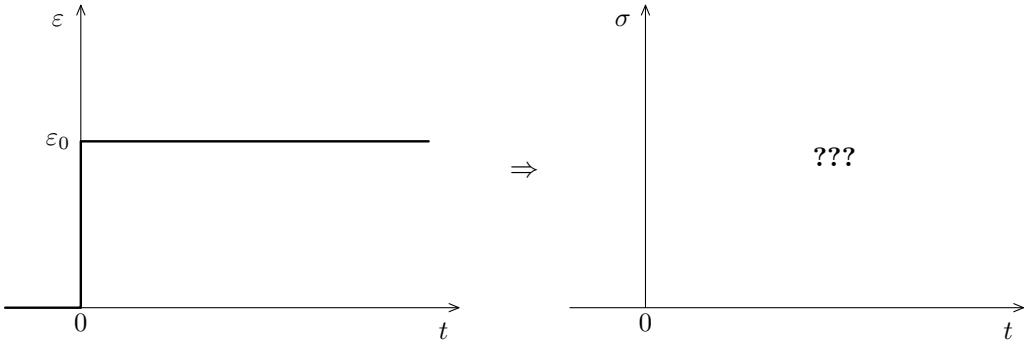

Figure 1.14: Stress relaxation test.

Consider two basic materials – linear elastic material and Newtonian fluid. Linear

elastic material is described by Hookean law $\sigma = G\varepsilon$, where G is the elastic modulus, Newtonian fluid is described by the relation $\sigma = \mu\dot{\varepsilon}$, where μ is the viscosity.

The result of the stress relaxation test is in case of elastic material depicted in Figure 1.15, in case of Newtonian fluid in Figure 1.16. In case of Newtonian fluid the stress is singular in zero (derivative of the Heaviside function).

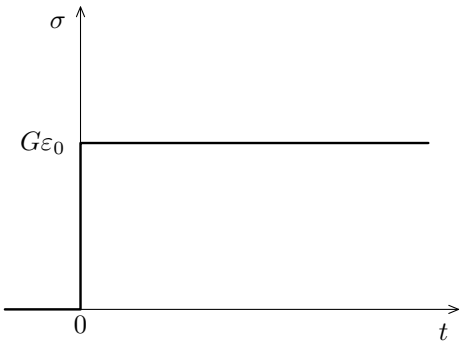

Figure 1.15: Stress relaxation test, linear spring.

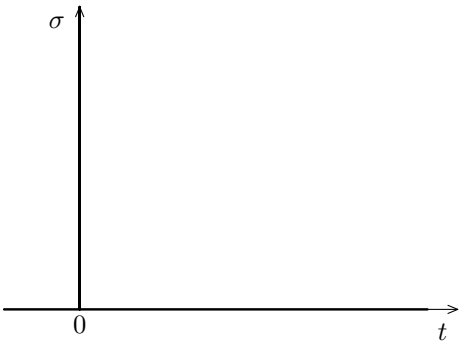

Figure 1.16: Stress relaxation test, linear dashpot.

Creep test Creep test is the following (see Figure 1.17): At time $t = 0$ we put the material into the state corresponding to σ_0 and we keep this value upto time $t = t^*$, then we turn off the stress and study the relative prolongation ε.

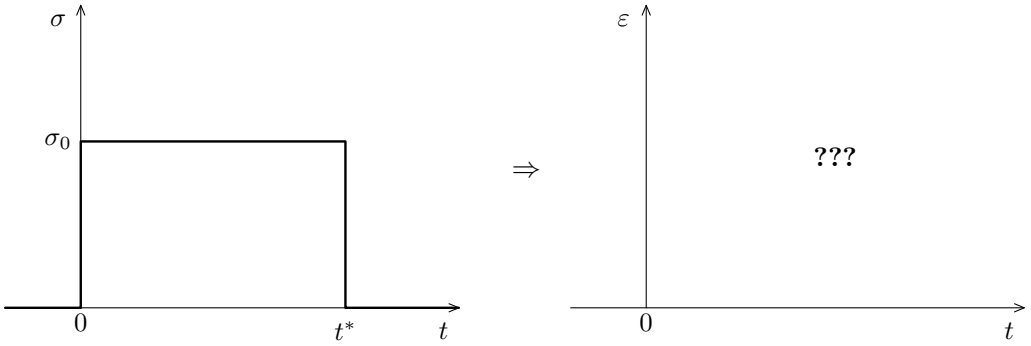

Figure 1.17: Creep test.

The result of the creep test is in case of elastic material depicted in Figure 1.18, in case of Newtonian fluid in Figure 1.19.

The results of the stress relaxation test and creep test are usually described in terms of the stress relaxation function

$$\mathcal{G}(t) = \frac{\sigma(t)}{\varepsilon_0}$$

and the creep function

$$\mathcal{J}(t) = \frac{\varepsilon(t)}{\sigma_0},$$

in order to eliminate the dependence of the responses on the initial deformation or stress.

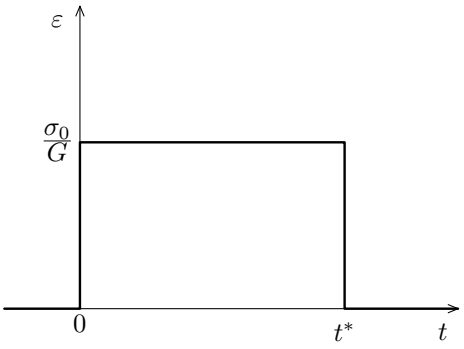

Figure 1.18: Creep test, linear spring.

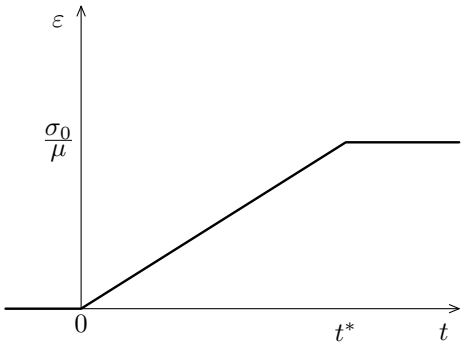

Figure 1.19: Creep test, linear dashpot.

Most of materials exhibit both viscous and elastic characteristic, their response is viscoelastic. The typical response of material in stress relaxation test for viscoelastic solid like and viscoelastic fluid like material is depicted in Figure 1.20, response of material in creep test is given in Figure 1.21, τ is a relaxation time defined later in the text. For more details on the response of real viscoelastic materials see for example [68].

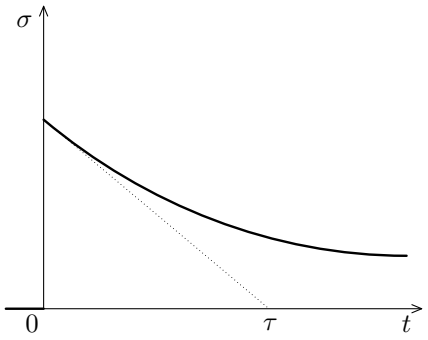

Figure 1.20: Viscoelastic solid

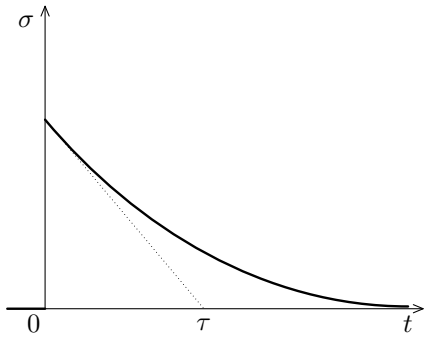

Viscoelastic fluid

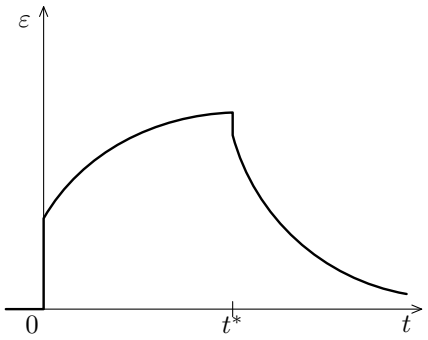

Figure 1.21: Viscoelastic solid

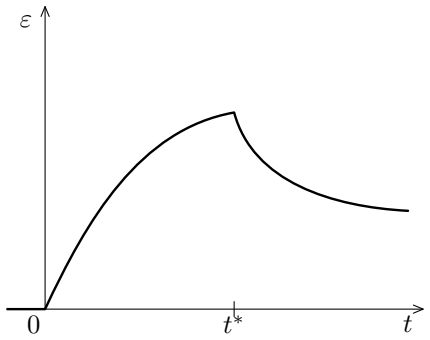

Viscoelastic fluid

In the next Section we introduce models that are capable of capturing viscoelastic stress relaxation and creep. In this work we are interested in so called rate-type models which are models where the Cauchy stress or the symmetric part of velocity gradient (or their parts) satisfy an evolutionary differential equation. Such models are a special

version of a general implicit relation (1.21).

1.3 One-dimensional viscoelasticity

In this section we introduce five one-dimensional viscoelastic models: Maxwell, Oldroyd, Kelvin-Voigt, Burgers and Burgers with an additional Newtonian dissipation. We derive one-dimensional stress-strain relation for all models and compute the stress relaxation function $\mathcal{G}$ and the creep function $\mathcal{J}$ for the first four models. The result of the creep test is not provided for these models in most of literature, usually the result is given for the test in which the stress is not released after some time. We computed the full creep test as described in the previous Section.

1.3.1 Mechanical analogs

We consider two basic materials: a linear elastic material and a Newtonian fluid. The mechanical analog representing the linear elastic material is a Hookean spring (see Figure 1.22(a)), where the relation between the stress and strain is described by $\sigma = G\varepsilon$ where G is the elastic modulus.

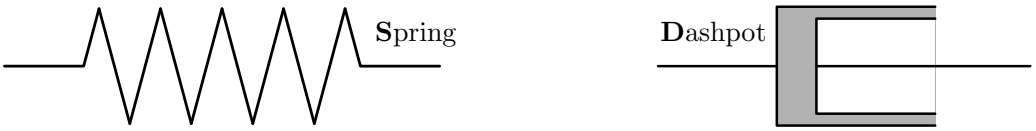

(a) Spring (b) Dashpot

Figure 1.22: Linear spring and linear dashpot.

Newtonian fluid is represented by a linear dashpot. Linear dashpot consists of two concentric cylinders, the gap between them is filled with a Newtonian fluid (see Figure 1.22(b)). The relation between the stress and strain is $\sigma = \mu\dot{\varepsilon}$, where μ is the fluid viscosity.

We use these two basic mechanical analogs for composing one-dimensional structure of viscoelastic fluids, for more details on this topic see [65] and [68].

1.3.2 Maxwell model

Maxwell element is one of the basic mechanical analogs. It consists of two elements, linear spring and linear dashpot connected in series, see Figure 1.23 for the device at rest. We denote by F resp. F_S resp. F_D the force in the whole element resp. in the spring resp. in the dashpot, and Δ resp. Δ_S resp. Δ_D the prolongation of the whole element resp. of the spring resp. of the dashpot. Then for the linear spring it holds

$$F_{\mathrm{S}} = G\Delta_{\mathrm{S}}, \quad \sigma_{\mathrm{S}} = G\varepsilon_{\mathrm{S}},$$

where $\varepsilon_{\mathrm{S}} = \Delta_{\mathrm{S}}/l_0$ and $\sigma_{\mathrm{S}} = F_{\mathrm{S}}/l_0$. For the linear dashpot we have

$$F_{\mathrm{D}} = \mu\dot{\Delta}_{\mathrm{D}}, \quad \sigma_{\mathrm{D}} = \mu\dot{\varepsilon}_{\mathrm{D}},$$

where $\varepsilon_{\mathrm{D}} = \Delta_{\mathrm{D}}/l_0$ and $\sigma_{\mathrm{D}} = F_{\mathrm{D}}/l_0$. First, we derive the constitutive relation between the stress $\sigma = F/l_0$ and strain $\varepsilon = \Delta/l_0$ where l_0 is the length of the whole element at

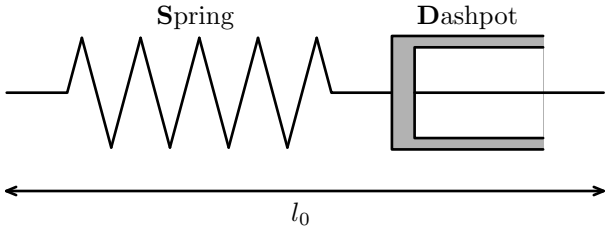

Figure 1.23: Maxwell element.

rest. In the series connection is the stress in the spring and in the dashpot the same, i.e. $\sigma = \sigma_{\mathrm{D}} = \sigma_{\mathrm{S}}$, the whole prolongation is the sum of the prolongation of the spring and the dashpot, i.e. $\Delta = \Delta_{\mathrm{S}} + \Delta_{\mathrm{D}}$. We substitute from the constitutive relation for the linear spring and the linear dashpot

$$\dot{\Delta} = \dot{\Delta}_{\mathrm{S}} + \dot{\Delta}_{\mathrm{D}} = \frac{\dot{F}_{\mathrm{S}}}{G} + \frac{F_{\mathrm{D}}}{\mu},$$

and get the constitutive equation for the Maxwell element

$$G\dot{\varepsilon} = \dot{\sigma} + \frac{G}{\mu}\sigma. \tag{1.22}$$

The initial condition $\sigma(0_+)$ and $\varepsilon(0_+)$ for (1.22) is needed. We briefly show how it is obtained (for details see [68]). For example in the creep test with a jump discontinuity of σ at $t = 0$, ε can be obtained upto constant from (1.22) by direct integration. Instead of considering the jump of stress σ at $t = 0$ we replace it by a sequence of stresses that smoothly (and very fast) grow from zero to a given value. Let $\sigma_n(t), \varepsilon_n(t) \in C^1(\mathbb{R})$ be sequences converging to $\sigma(t)$ and $\varepsilon(t)$ such that $\sigma_n(t) = \sigma(t), \varepsilon_n(t) = \varepsilon(t)$ for $t \geq \delta_n$ and

$$\delta_n \overset{n\to\infty}{\longrightarrow} 0, \quad \sigma_n(t) \overset{n\to\infty}{\longrightarrow} \sigma(t), \quad \varepsilon_n(t) \overset{n\to\infty}{\longrightarrow} \varepsilon(t) \quad \forall t > 0$$

satisfying

$$\dot{\sigma}_n + \frac{G}{\mu}\sigma_n = G\dot{\varepsilon}_n \text{ for } t \geq \delta_n \tag{1.23}$$

and $\sigma_n(0) = \varepsilon_n(0) = 0$.

From the initial condition we obtain. Integrating (1.23) over $(0, \delta_n)$ we obtain

$$\sigma_n(\delta_n) + \frac{G}{\mu}\int_0^{\delta_n} \sigma_n = G\varepsilon_n(\delta_n), \tag{1.24}$$

taking the limit $n \to \infty$ gives the initial condition

$$\sigma(0+) = G\varepsilon(0+). \tag{1.25}$$

Stress relaxation test

Now we compute how the Maxwell element behaves in the stress relaxation test, see Figure 1.14. Let $\varepsilon(t) = \varepsilon_0 H(t)$, where $H(t)$ is the Heaviside function, then the equation (1.22) for $t > 0$ reduces to

$$\dot{\sigma} + \frac{G}{\mu}\sigma = 0$$

with $\sigma(0+) = G\varepsilon_0$. The solution of this initial value problem is

$$\sigma(t) = G\varepsilon_0 e^{-\frac{G}{\mu}t}$$

and the stress relaxation function is equal to

$$\mathcal{G}(t) = \frac{\sigma(t)}{\varepsilon_0} = Ge^{-\frac{G}{\mu}t}.$$

Thus, Maxwell model exhibits stress relaxation of viscoelastic fluid as can be seen in Figure 1.20. The ratio μ/G denotes relaxation time, in Figure 1.20 denoted by τ, and it is a time when the stress decreases by a factor of e.

Creep test

In the creep test the stress is prescribed as

$$\sigma(t) = \begin{cases} \sigma_0 & 0 < t \leq t_0 \\ 0 & t > t_0. \end{cases}$$

We divide the computation of the strain ε into two parts – for t between zero and t_0 and for $t > t_0$. First, we integrate (1.22) from zero to $t \leq t_0$ and obtain

$$\varepsilon(t) = \varepsilon(0+) + \frac{1}{\mu}\sigma_0 t, \quad 0 \leq t \leq t_0, \tag{1.26}$$

where $\varepsilon(0+) = \frac{1}{G}\sigma_0$ according to (1.25). For $t > t_0$ we integrate (1.22) from t_0 to arbitrary $t > t_0$ and obtain

$$\varepsilon(t) = \varepsilon(t_0) - \frac{1}{G}\sigma_0 = \varepsilon(0+) + \sigma_0\left(\frac{t_0}{\mu} - \frac{1}{G}\right), \quad t > t_0, \tag{1.27}$$

where $\varepsilon(t_0)$ is computed from (1.26). The result of creep test is described by (1.26) and (1.27), see Figure 1.24.

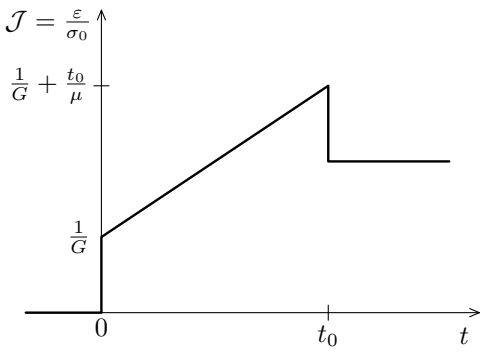

Figure 1.24: Creep function of Maxwell element.

The creep function is equal to

$$\mathcal{J}(t) = \begin{cases} \frac{1}{G} + \frac{t}{\mu} & 0 < t \leq t_0 \\ \frac{t_0}{\mu} & t > t_0. \end{cases}$$

1.3.3 Kelvin-Voigt model

The other basic mechanical analog is Kelvin-Voigt element, it is a model for solid like viscoelastic material. It consists of one linear spring and one linear dashpots connected in parallel, see Figure 1.25. Due to geometry the total strain ε is equal to the strain of

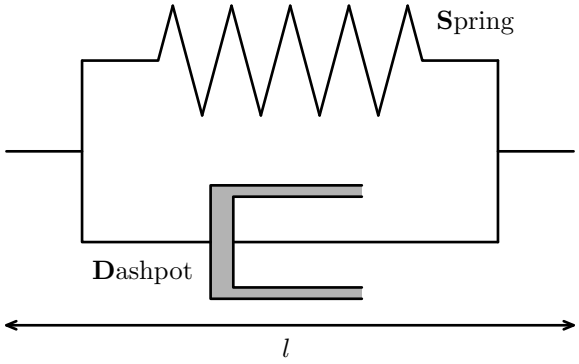

Figure 1.25: Kelvin-Voigt element.

the dashpot ε_D and it is the same as the strain of the spring ε_S, i.e.

$$\varepsilon_D = \varepsilon_S = \varepsilon. \tag{1.28}$$

Stress in the whole element σ is equal to the sum of the stresses in the spring σ_S and the dashpot σ_D, i.e.

$$\sigma = \sigma_D + \sigma_S. \tag{1.29}$$

Combining (1.28), (1.29) and stress-strain relations for the spring and the dashpot we get

$$\sigma = \mu\dot{\varepsilon} + G\varepsilon. \tag{1.30}$$

Similarly to the case of Maxwell element we obtain the initial conditions for Kelvin-Voigt element from the limit

$$\lim_{n\to\infty} \int_0^{\delta_n} \sigma_n = \mu\varepsilon_0(0+), \tag{1.31}$$

which is for the stress relaxation test equal to

$$\sigma(t) = \mu\varepsilon(0+)\delta_0(t) \text{ near } t = 0. \tag{1.32}$$

and for the creep test

$$\varepsilon(0+) = 0. \tag{1.33}$$

Stress relaxation test

Now we compute the response of stress relaxation test for the Kelvin-Voigt element. Let $\varepsilon(t) = \varepsilon_0 H(t)$, where $H(t)$ is the Heaviside function, then the solution of (1.30) with (1.32) is

$$\sigma(t) = \mu\delta_0\varepsilon_0 + G\varepsilon_0,$$

where $\delta_0 = \dot{H}(t)$ is a Dirac distribution. The stress relaxation function, that is equal to

$$\mathcal{G}(t) = \mu\delta_0 + G,$$

is a pure combination of the linear spring and the linear dashpot (see Figure 1.26) and it is not satisfactory in the sense that it does not reflect well the behavior of real materials.

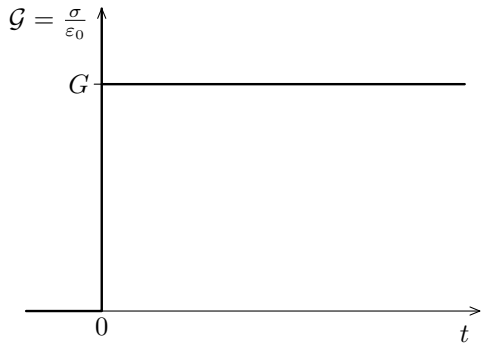

Figure 1.26: Stress relaxation function of Kelvin-Voigt element.

Creep test

Kelvin-Voigt element is deformed with the stress

$$\sigma(t) = \begin{cases} \sigma_0 & 0 < t \leq t_0 \\ 0 & t > t_0. \end{cases}$$

Again we divide the computation into two parts – for $0 < t \leq t_0$ and for $t > t_0$. First, we solve (1.30) on the interval $(0, t_0)$ with the initial condition (1.33) and obtain

$$\varepsilon(t) = \frac{\sigma_0}{G}\left(1 - \exp\left(-\frac{G}{\mu}t\right)\right), \quad 0 \leq t \leq t_0. \tag{1.34}$$

For $t > t_0$ we solve (1.30) with the initial condition $\varepsilon(t_0)$ given by (1.34) and obtain

$$\varepsilon(t) = \varepsilon(t_0)\exp\left(-\frac{G}{\mu}(t - t_0)\right). \tag{1.35}$$

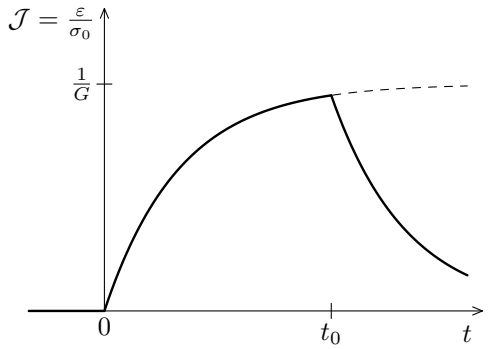

Figure 1.27: Creep function of Kelvin-Voigt element.

The response of material in creep test for Kelvin-Voigt element is given by (1.34) and (1.35) which is a nice example result of creep test for solid like viscoelastic material (strain goes to zero for $t \to \infty$), see Figure 1.27.

1.3.4 Oldroyd model

Oldroyd element consists of two linear dashpots (thus it is more fluid like than the Maxwell model) and one linear spring, it is a parallel connection of the Maxwell element and one dashpot (D_2), see Figure 1.28. For the Maxwell element it holds

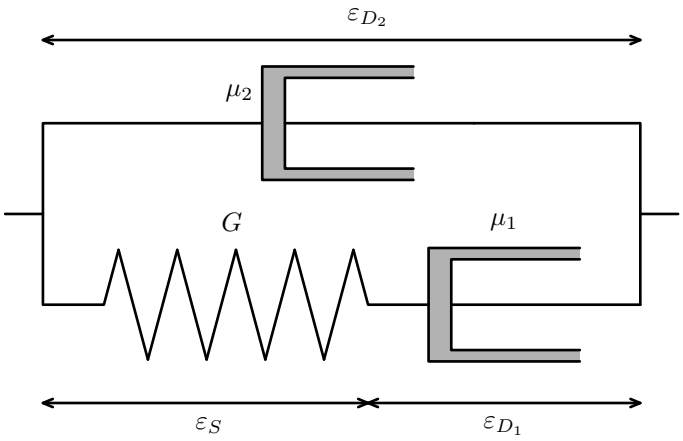

Figure 1.28: Oldroyd element.

$$\dot{\varepsilon}_M = \frac{1}{G}\dot{\sigma}_M + \frac{1}{\mu_1}\sigma_M \tag{1.36}$$

and due to geometry the total strain ε is equal to the strain of the dashpot D_2 ε_{D_2} and it is the same as the strain of the Maxwell element ε_M, i.e.

$$\varepsilon_{D_2} = \varepsilon_M = \varepsilon. \tag{1.37}$$

The stress in the whole element σ is equal to the sum of the stresses in the Maxwell element and the dashpot D_2, i.e.

$$\sigma = \sigma_{D_2} + \sigma_M. \tag{1.38}$$

Combining (1.36)–(1.38) we get

$$\begin{aligned}\frac{1}{G}\dot{\sigma} + \frac{1}{\mu_1}\sigma &= \frac{1}{G}\dot{\sigma}_{D_2} + \frac{1}{\mu_1}\sigma_{D_2} + \dot{\varepsilon}_M = \\ &= \frac{\mu_2}{G}\ddot{\varepsilon}_{D_2} + \frac{\mu_2}{\mu_1}\dot{\varepsilon}_{D_2} + \dot{\varepsilon}_M = \frac{\mu_2}{G}\ddot{\varepsilon} + \left(1 + \frac{\mu_2}{\mu_1}\right)\dot{\varepsilon}.\end{aligned} \tag{1.39}$$

Multiplying (1.39) by μ_1 we obtain stress-strain relation for Oldroyd element in more usual form

$$\sigma + \frac{\mu_1}{G}\dot{\sigma} = \frac{\mu_1\mu_2}{G}\ddot{\varepsilon} + (\mu_1 + \mu_2)\,\dot{\varepsilon}. \tag{1.40}$$

Similarly to the case of Maxwell element we obtain the initial conditions for Oldroyd element. We replace ε and σ by sufficiently smooth sequences ε_n and σ_n with $\sigma_n(0+) = \varepsilon_n(0+) = \dot{\varepsilon}_n(0+) = 0$ and integrate two times over $(0, \delta_n)$. We obtain

$$\varepsilon(0+) = 0, \quad \sigma(0+) = \mu_2\dot{\varepsilon}(0+). \tag{1.41}$$

Note: Using (1.36) – (1.38) Oldroyd model can be also written alternatively in the form

$$\sigma = \mu_2\dot{\varepsilon} + \sigma_M, \tag{1.42a}$$

$$\frac{1}{G}\dot{\sigma}_M + \frac{1}{\mu_1}\sigma_M = \dot{\varepsilon}. \tag{1.42b}$$

Stress relaxation test

Now we compute the response of stress relaxation test for the Oldroyd element. Let $\varepsilon(t) = \varepsilon_0 H(t)$, where $H(t)$ is the Heaviside function, then the equation (1.22) for $t > 0$ reduces to

$$\dot{\sigma} + \frac{G}{\mu_1}\sigma = 0$$

with $\sigma(0+) = \mu_2\dot{\varepsilon}(0+)$. The solution is similar to the case of Maxwell model

$$\sigma(t) = \mu_2\delta_0(t)\varepsilon_0 + G\varepsilon_0 e^{-\frac{G}{\mu_1}t}$$

and the stress relaxation function is equal to

$$\mathcal{G}(t) = \frac{\sigma(t)}{\varepsilon_0} = \mu_2\delta_0 + Ge^{-\frac{G}{\mu_1}t},$$

which is a combination of the result for the dashpot and the Maxwell element. The stress relaxation test exhibits non-linear viscoelastic fluid-like behavior, see Figure 1.29.

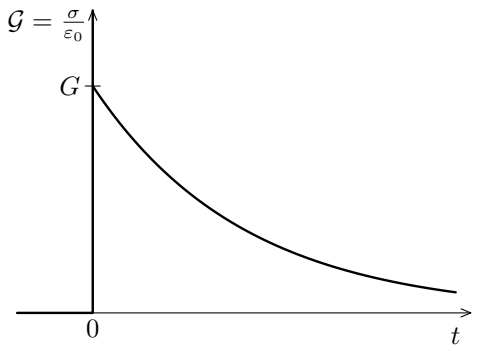

Figure 1.29: Stress relaxation function of Oldroyd element.

Creep test

Oldroyd element is deformed with the stress

$$\sigma(t) = \begin{cases} \sigma_0 & 0 < t \leq t_0 \\ 0 & t > t_0. \end{cases}$$

Again we divide the computation into two parts – for $0 < t \leq t_0$ and for $t > t_0$. First, we integrate (1.40) over $(0, t_0)$, use initial conditions (1.41) and after this we look for

the solution of ODE

$$\mu_2 \left(\dot{\varepsilon} - \frac{1}{\mu_2}\sigma_0 \right) + G \left(1 + \frac{\mu_2}{\mu_1} \right) \varepsilon = \frac{G}{\mu_1}\sigma_0 t, \quad 0 \leq t \leq t_0. \tag{1.43}$$

The solution of (1.43) together with initial conditions (1.41) is

$$\varepsilon(t) = \frac{\mu_1^2 + G(\mu_1+\mu_2)t}{(\mu_1+\mu_2)^2 G}\sigma_0 - \frac{\mu_1^2}{(\mu_1+\mu_2)^2 G}\sigma_0 \exp\left(-\frac{G(\mu_1+\mu_2)t}{\mu_1\mu_2} \right), \quad 0 \leq t \leq t_0. \tag{1.44}$$

For $t > t_0$ we integrate (1.40) from t_0 to arbitrary $t > t_0$ and obtain

$$\mu_2(\dot{\varepsilon} - \dot{\varepsilon}(t_0)) + G \left(1 + \frac{\mu_2}{\mu_1} \right) (\varepsilon - \varepsilon(t_0)) = -\sigma_0, \quad t > t_0 \tag{1.45}$$

where $\varepsilon(t_0)$ and $\dot{\varepsilon}(t_0)$ are obtained from (1.44). The solution of (1.45) with the initial conditions (1.41) is

$$\varepsilon(t) = \frac{-\sigma_0\mu_1 + \mu_1\mu_2\dot{\varepsilon}(t_0) + G(\mu_1+\mu_2)\varepsilon(t_0)}{G(\mu_1+\mu_2)} \left(1 - \exp\left(-\frac{G(\mu_1+\mu_2)(t-t_0)}{\mu_1\mu_2} \right) \right) + \varepsilon(t_0) \exp\left(-\frac{G(\mu_1+\mu_2)(t-t_0)}{\mu_1\mu_2} \right), \quad t > t_0. \tag{1.46}$$

The response of creep test for Oldroyd element is given by (1.43) and (1.46), concretely the result for $\mu_1 = 10$ Pa s, $\mu_2 = 1$ Pa s, $G = 1$ Pa, $\sigma_0 = 1$ Pa, $t_0 = 5$ s is depicted in Figure 1.30 and it is a satisfactory result of non-linear creep test for viscoelastic fluid like model.

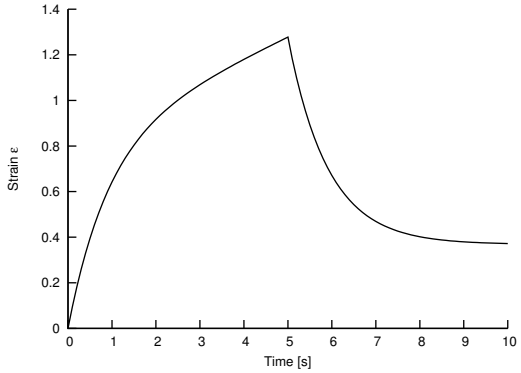

Figure 1.30: Creep function of Oldroyd element for $\mu_1 = 10$ Pa s, $\mu_2 = 1$ Pa s, $G = 1$ Pa, $\sigma_0 = 1$ Pa, $t_0 = 5$ s.

Thus, Oldroyd element gives nice results for both stress relaxation and creep test.

1.3.5 Burgers element

Burgers element consists of two linear dashpots and two linear springs, in this subsection we introduce two types of Burgers models.

Original Burgers element

The first element is a classical Burgers element by Burgers [10] and it is a connection of the Maxwell element and the Kelvin-Voigt element in series, see Figure 1.31. For the Maxwell element it holds

$$\dot{\varepsilon}_M = \frac{1}{G_2}\dot{\sigma}_M + \frac{1}{\mu_2}\sigma_M. \tag{1.47}$$

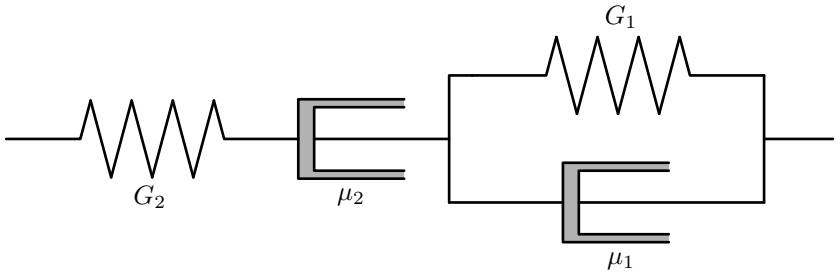

Figure 1.31: Burgers element from [10].

The Kelvin-Voigt element is described by

$$\dot{\sigma}_K = \mu_1\dot{\varepsilon}_K + G_1\varepsilon_K \tag{1.48}$$

and due to geometry the total strain $\varepsilon = \varepsilon_M + \varepsilon_K$ and the stresses in both elements as well as in the whole connection are the same, i.e. $\sigma = \sigma_M = \sigma_K$. Using (1.47) and (1.48) we obtain

$$G_1(\dot{\varepsilon}_K + \dot{\varepsilon}_M) + \mu_1(\ddot{\varepsilon}_K + \ddot{\varepsilon}_M) = \dot{\sigma}_K + \frac{G_1}{\mu_2}\sigma_M + \left(\frac{G_1}{G_2} + \frac{\mu_1}{\mu_2}\right)\dot{\sigma}_M + \frac{\mu_1}{G_2}\ddot{\sigma}_M \tag{1.49}$$

which reduces to

$$\sigma + \left(\frac{\mu_2}{G_1} + \frac{\mu_1}{G_1} + \frac{\mu_2}{G_2}\right)\dot{\sigma} + \frac{\mu_1\mu_2}{G_1G_2}\ddot{\sigma} = \mu_2\dot{\varepsilon} + \frac{\mu_1\mu_2}{G_1}\ddot{\varepsilon}. \tag{1.50}$$

Similarly to the case of Oldroyd element we obtain the initial conditions by integrating (1.50) two times over $(0, \delta_n)$. We obtain

$$\varepsilon(0+) = \frac{1}{G_2}\sigma(0+), \quad \left(\frac{\mu_2}{G_1} + \frac{\mu_1}{G_1} + \frac{\mu_2}{G_2}\right)\sigma(0+) + \frac{\mu_1\mu_2}{G_1G_2}\dot{\sigma}(0+) = \mu_2\varepsilon(0+) + \frac{\mu_1\mu_2}{G_1}\dot{\varepsilon}(0+). \tag{1.51}$$

Burgers element – parallel connection of two Maxwell elements

The other other type of Burgers element is the element consisting of two Maxwell elements connected in parallel, see Figure 1.32. For both Maxwell elements it hold

$$\dot{\varepsilon}_1 = \frac{1}{G_1}\dot{\sigma}_1 + \frac{1}{\mu_1}\sigma_1, \tag{1.52}$$

and

$$\dot{\varepsilon}_2 = \frac{1}{G_2}\dot{\sigma}_2 + \frac{1}{\mu_2}\sigma_2. \tag{1.53}$$

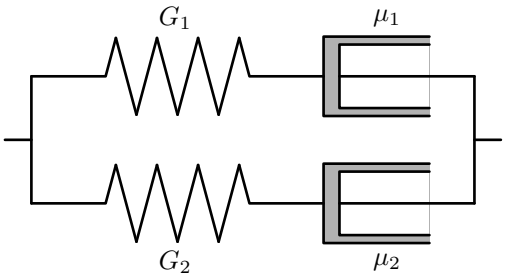

Figure 1.32: Burgers element – two Maxwell elements.

The total strain is equal to the strain of both Maxwell elements, i.e. $\varepsilon = \varepsilon_1 = \varepsilon_2$ and the total stress is equal to the sum of both stresses, i.e. $\sigma = \sigma_1 + \sigma_2$. In order to obtain the final stress-strain relation we take the sum

$$\dot{(1.52)} + \frac{G_2}{\mu_2}(1.52) + \dot{(1.53)} + \frac{G_1}{\mu_1}(1.53)$$

and obtain

$$\sigma + \left(\frac{\mu_1}{G_1} + \frac{\mu_2}{G_2}\right)\dot{\sigma} + \frac{\mu_1\mu_2}{G_1G_2}\ddot{\sigma} = (\mu_1 + \mu_2)\dot{\varepsilon} + \left(\frac{\mu_1\mu_2}{G_1} + \frac{\mu_1\mu_2}{G_2}\right)\ddot{\varepsilon} \tag{1.54}$$

with the initial conditions

$$\varepsilon(0+) = \frac{1}{G_1 + G_2}\sigma(0+), \tag{1.55}$$

$$\left(\frac{\mu_1}{G_1} + \frac{\mu_2}{G_2}\right)\sigma(0+) + \frac{\mu_1\mu_2}{G_1G_2}\dot{\sigma}(0+) = (\mu_1 + \mu_2)\varepsilon(0+) + \left(\frac{\mu_1\mu_2}{G_1} + \frac{\mu_1\mu_2}{G_2}\right)\dot{\varepsilon}(0+). \tag{1.56}$$

Both Burgers models can be written in the same form

$$\sigma + p_1\dot{\sigma} + p_2\ddot{\sigma} = q_1\dot{\varepsilon} + q_2\ddot{\varepsilon} \tag{1.57}$$

with the initial conditions

$$p_2\sigma(0+) = q_2\varepsilon(0+), \quad p_1\sigma(0+) + p_2\dot{\sigma}(0+) = q_1\varepsilon(0+) + q_2\dot{\varepsilon}(0+). \tag{1.58}$$

The initial conditions for Burgers model are a complicated problem, for much more details see [51]. In this text we for simplicity suppose that $\dot{\varepsilon}_0(0) = 0$ in the stress relaxation test and $\dot{\sigma}(0+) = 0$ in the creep test.

Stress relaxation test

Now we compute the response of stress relaxation test for the Burgers element described by (1.57) and (1.58). Let $\varepsilon(t) = \varepsilon_0 H(t)$, then the equation (1.50) for $t > 0$ reduces to

$$\sigma + p_1\dot{\sigma} + p_2\ddot{\sigma} = 0$$

and the solution is

$$\sigma(t) = \varepsilon_0 \left[C_1 \exp(\lambda_1 t) + C_2 \exp(\lambda_2 t)\right],$$

where

$$\lambda_1 = \frac{-p_1 + \sqrt{p_1^2 - 4p_2}}{2}, \quad \lambda_2 = \frac{-p_1 - \sqrt{p_1^2 - 4p_2}}{2},$$

$$C_2 = \frac{q_1 p_2 - p_1 q_2 - \lambda_1 q_2 p_2}{p_2^2(\lambda_2 - \lambda_1)}, \quad C_1 = \frac{q_2}{p_2} - C_2$$

and from the concrete form of p_1, p_2, q_1, q_2 given by (1.50) and (1.54) we have

$$p_1^2 \geq 4p_2, \quad q_1 p_2 \leq p_1 q_2, \quad \lambda_2 \leq \lambda_1 < 0.$$

The stress relaxation function is equal to

$$\mathcal{G}(t) = \frac{\sigma(t)}{\varepsilon_0} = C_1 \exp(\lambda_1 t) + C_2 \exp(\lambda_2 t).$$

The model has two relaxation times $-1/\lambda_1$ and $-1/\lambda_2$. For $p_1 = 4, p_2 = 3, q_1 = q_2 = 1$ we obtain

$$\mathcal{G}(t) = \frac{1}{9}\left[4\exp(-t) - \exp(-3t)\right],$$

and Burgers model exhibits non-linear viscoelastic behavior in the stress relaxation test (see Figure 1.33).

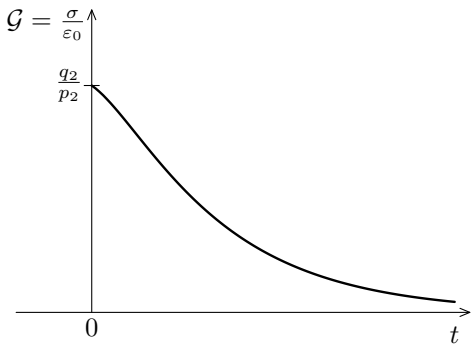

Figure 1.33: Stress relaxation function of Burgers element.

Creep test

The result of the creep test for the Burgers model is similar to the result for Oldroyd model. The difference between these two models is that the term $\ddot{\sigma}$ is missing in the stress-strain relation for Oldroyd and that $\varepsilon(0+) \neq 0$ for Burgers. This causes that in case of Burgers there are jumps of the strain at the beginning $t = 0$ when the stress is applied and at $t = t_0$ when the stress is released.

Burgers element is deformed with the stress

$$\sigma(t) = \begin{cases} \sigma_0 & 0 < t \leq t_0 \\ 0 & t > t_0. \end{cases}$$

As in case of Oldroyd we divide the computation into two parts – for $0 < t \leq t_0$ and for $t > t_0$. First, we integrate (1.57) over $(0, t < t_0)$, use initial conditions (1.58) and after this we look for the solution of ODE

$$q_1 \left(\varepsilon - \varepsilon(0+)\right) + q_2 \left(\dot{\varepsilon} - \dot{\varepsilon}(0+)\right) = \sigma_0 t, \quad 0 \leq t \leq t_0. \tag{1.59}$$

The solution of (1.59) together with initial conditions (1.58) is

$$\varepsilon(t) = \frac{q_1 p_1 - q_2}{q_1^2}\sigma_0 \left(1 - \exp\left(-\frac{q_1}{q_2}t\right)\right) + \frac{p_2}{q_2}\sigma_0 \exp\left(-\frac{q_1}{q_2}t\right) + \frac{\sigma_0}{q_1}t, \quad 0 \leq t \leq t_0. \tag{1.60}$$

For $t > t_0$ we integrate (1.57) from t_0 to arbitrary $t > t_0$ and obtain

$$q_1 \left(\varepsilon - \varepsilon(t_0)\right) + q_2 \left(\dot{\varepsilon} - \dot{\varepsilon}(t_0)\right) = -p_1\sigma_0, \quad t > t_0, \tag{1.61}$$

where $\varepsilon(t_0)$ and $\dot{\varepsilon}(t_0)$ are obtained from (1.60)[1]. The solution of equation (1.61) is

$$\varepsilon(t) = \left(\varepsilon(t_0) + \frac{q_2}{q_1}\dot{\varepsilon}(t_0) - \frac{p_1}{q_1}\sigma_0\right)\left(1 - \exp\left(-\frac{q_1}{q_2}(t - t_0)\right)\right) + \left(\varepsilon(t_0) - \frac{p_2}{q_2}\sigma_0\right)\exp\left(-\frac{q_1}{q_2}(t - t_0)\right), \quad t > t_0. \tag{1.62}$$

The response of creep test for Burgers element is given by (1.59) and (1.62), concretely the result for $p_1 = 20, p_2 = 2, q_1 = q_2 = 1$ is depicted in Figure 1.34 and it is a satisfactory result of non-linear creep test for viscoelastic fluid like model (for $t \to \infty$ the strain is positive).

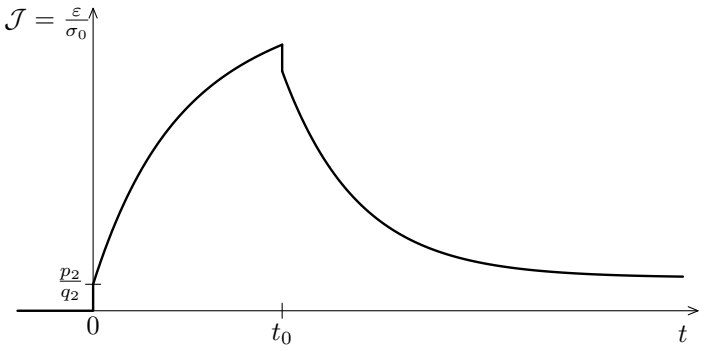

Figure 1.34: Creep function of Burgers element for $p_1 = 20, p_2 = 2, q_1 = q_2 = 1$.

[1] In order to solve ODE (1.61) we need to know the initial condition at $t = t_0$, let us denote it by $\varepsilon^*(t_0)$ (different from $\varepsilon(t_0)$ which is obtained from (1.60)). First, in (1.57) we replace ε and σ by sufficiently smooth sequences ε_n and σ_n with $\sigma_n(t_0) = \sigma_0$ and $\varepsilon_n(t_0)$ and $\dot{\varepsilon}_n(t_0)$ given by (1.60). Then integrate two times over $(t_0, t_0 + \delta_n)$ and take the limit $n \to \infty$. We obtain

$$\varepsilon^*(t_0) = \varepsilon(t_0) - \frac{p_2}{q_2}\sigma_0, \quad \dot{\varepsilon}^*(t_0) = \dot{\varepsilon}(t_0) + \frac{q_1 p_2 - p_1 q_2}{q_2^2}\sigma_0.$$

The initial condition $\dot{\varepsilon}^*(t_0)$ is not needed because we are solving the first order ODE. However, one can easily verify that the time derivative of the solution (1.62) at $t = t_0$ is equal to $\dot{\varepsilon}^*(t_0)$.

Note: If we connect Burgers element with additional dashpot with viscosity μ_3 in parallel we obtain a more fluid like model than Burgers model. New element is depicted in Figure 1.35. The difference between the Burgers element and this element is the same as the difference between Maxwell element and Oldroyd element. We will not compute

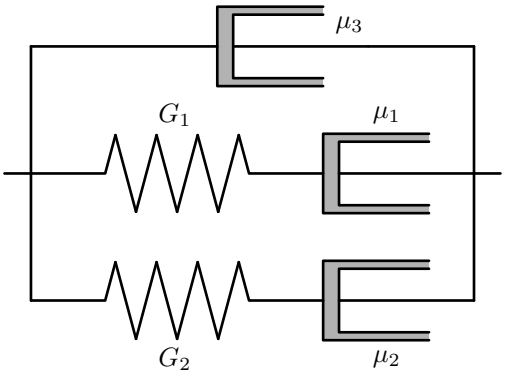

Figure 1.35: Burgers element with additional dashpot connected in parallel.

the stress relaxation test and creep test for this element, just show the stress-strain relation in the alternative form as in case of Oldroyd.

$$\sigma = \sigma_B + \mu_3\dot{\varepsilon}, \tag{1.63a}$$

$$\sigma_B + \left(\frac{\mu_1}{G_1} + \frac{\mu_2}{G_2}\right)\dot{\sigma}_B + \frac{\mu_1\mu_2}{G_1G_2}\ddot{\sigma}_B = (\mu_1 + \mu_2)\dot{\varepsilon} + \left(\frac{\mu_1\mu_2}{G_1} + \frac{\mu_1\mu_2}{G_2}\right)\ddot{\varepsilon}. \tag{1.63b}$$

Chapter 2

Standard viscoelastic models in two- and three-dimensional space

2.1 Generalization of one-dimensional models

In the previous chapter we derived four standard linear one-dimensional viscoelastic models made from mechanical analogs – Maxwell, Oldroyd, Burgers and Burgers model with additional dashpot.

For real computations we need to generalize the models into higher space dimensions. If we replace the stress σ by the extra part of the Cauchy stress $\mathbf{S}$ and the time derivative of the strain $\dot{\varepsilon}$ (the fluid like models do not contain strain ε without any time derivative) by the symmetric part of velocity gradient $2\mathbf{D}$, we do not obtain a proper model. To illustrate it, we apply this generalization procedure to Maxwell model (1.22) and assume the the fluid is incompressible

$$\operatorname{div} \mathbf{v} = 0, \tag{2.1}$$

$$\rho \left(\frac{\partial \mathbf{v}}{\partial t} + \mathbf{v} \cdot \nabla \mathbf{v} \right) = \operatorname{div} \mathbf{T}, \tag{2.2}$$

$$\mathbf{T} = -p\mathbf{I} + \mathbf{S}, \tag{2.3}$$

$$\mathbf{S} + \frac{\mu}{G} \frac{\partial \mathbf{S}}{\partial t} = 2\mu \mathbf{D}. \tag{2.4}$$

One of the problem is that neither the partial time derivative, neither the material time derivative are objective time derivatives, and the appropriate generalizations are not unique. For the definition of the objective tensor, see Appendix C where it is also shown that $\mathbf{D}$ is an objective tensor, but the material time derivative $\dfrac{\partial \mathbf{A}}{\partial t} + \mathbf{v} \cdot \nabla \mathbf{A}$ is not.

The time derivative can be chosen from the family of Gordon-Schowalter objective time derivatives given by

$$\left(\frac{\delta \mathbf{A}}{\delta t} \right)_a = \frac{\partial \mathbf{A}}{\partial t} + (\mathbf{v} \cdot \nabla)\mathbf{A} - (\mathbf{W}\mathbf{A} - \mathbf{A}\mathbf{W}) + a(\mathbf{D}\mathbf{A} + \mathbf{A}\mathbf{D}) \quad a \in [-1, 1]\,.$$

For $a = -1$, it leads to upper convected Oldroyd derivative

$$\overset{\triangledown}{\mathbf{A}} := \frac{\partial \mathbf{A}}{\partial t} + \mathbf{v} \cdot \nabla \mathbf{A} - \mathbf{L}\mathbf{A} - \mathbf{A}\mathbf{L}^{\mathrm{T}}, \tag{2.5}$$

$a = 0$ gives co-rotational (or Jaumann) derivative

$$\overset{\square}{\mathbf{A}} := \frac{\partial \mathbf{A}}{\partial t} + \mathbf{v} \cdot \nabla \mathbf{A} - \mathbf{W}\mathbf{A} + \mathbf{A}\mathbf{W},$$

and for $a = 1$ we get the lower convected Oldroyd derivative

$$\overset{\triangle}{\mathbf{A}} := \frac{\partial \mathbf{A}}{\partial t} + \mathbf{v} \cdot \nabla \mathbf{A} + \mathbf{A}\mathbf{L} + \mathbf{L}^{\mathrm{T}}\mathbf{A}.$$

Oldroyd [46] showed that Oldroyd-B model with upper convected Oldroyd derivative described later in this subsection predicts rod climbing, while Oldroyd-A model predicts opposite effect – the descend. Most of non-Newtonian fluids exhibit rod climbing and that is why we prefer the upper convected Oldroyd derivative.

Maxwell model

We choose the upper convected Oldroyd derivative and generalize Maxwell model (1.22) to

$$\mathbf{T} = -p\mathbf{I} + \mathbf{S}, \tag{2.6a}$$

$$\mathbf{S} + \frac{\mu}{G} \overset{\triangledown}{\mathbf{S}} = 2\mu\mathbf{D}, \tag{2.6b}$$

where the ratio μ/G is relaxation time, usually denoted by τ. If the material is at rest at $t = 0$, then $\mathbf{S}(\mathbf{x}, t = 0) = \mathbf{0}$. This model can be alternatively written in other form with a new tensor $\mathbf{B}$ defined by $\mathbf{S} = G(\mathbf{B} - \mathbf{I})$ (G is the elastic modulus), we obtain

$$\mathbf{T} = -p\mathbf{I} + G(\mathbf{B} - \mathbf{I}), \tag{2.7a}$$

$$\overset{\triangledown}{\mathbf{B}} = \frac{1}{\tau}(\mathbf{I} - \mathbf{B}), \tag{2.7b}$$

and if the material is at rest at $t = 0$ then $\mathbf{B}(0) = \mathbf{I}$.

In the same way as Maxwell model we generalize Oldroyd model (1.40) and Burgers models (1.54) and (1.63).

Oldroyd-B model

Letter B in Oldroyd-B model means that the upper convected Oldroyd derivative is used as the objective time derivative, Oldroyd-A model is the model where lower convected Oldroyd derivative is used. Model (1.40) is transformed to

$$\mathbf{T} = -p\mathbf{I} + \mathbf{S}, \tag{2.8a}$$

$$\mathbf{S} + \frac{\mu_1}{G} \overset{\triangledown}{\mathbf{S}} = 2(\mu_1 + \mu_2)\mathbf{D} + 2\frac{\mu_1\mu_2}{G} \overset{\triangledown}{\mathbf{D}}\,. \tag{2.8b}$$

This model is usually written in the form (which corresponds to (1.42))

$$\mathbf{T} = -p\mathbf{I} + 2\mu_2\mathbf{D} + \mathbf{S}, \tag{2.9a}$$

$$\mathbf{S} + \frac{\mu_1}{G} \overset{\triangledown}{\mathbf{S}} = 2\mu_1\mathbf{D}, \tag{2.9b}$$

and alternatively can be written in the form

$$\mathbf{T} = -p\mathbf{I} + 2\mu_2\mathbf{D} + G(\mathbf{B} - \mathbf{I}), \tag{2.10a}$$

$$\overset{\triangledown}{\mathbf{B}} = \frac{1}{\tau}(\mathbf{I} - \mathbf{B}), \tag{2.10b}$$

where $\tau = \mu_1/G$ is the relaxation time.

Burgers model

Burgers model (1.54) is transformed to

$$\mathbf{T} = -p\mathbf{I} + \mathbf{S}, \tag{2.11a}$$

$$\mathbf{S} + \left(\frac{\mu_1}{G_1} + \frac{\mu_2}{G_2}\right)\overset{\triangledown}{\mathbf{S}} + \frac{\mu_1\mu_2}{G_1G_2}\overset{\triangledown\triangledown}{\mathbf{S}} = 2(\mu_1 + \mu_2)\mathbf{D} + 2\left(\frac{\mu_1\mu_2}{G_1} + \frac{\mu_1\mu_2}{G_2}\right)\overset{\triangledown}{\mathbf{D}} \tag{2.11b}$$

usually written using relaxation times $\tau_1 = \mu_1/G_1$ and $\tau_2 = \mu_2/G_2$

$$\mathbf{T} = -p\mathbf{I} + \mathbf{S}, \tag{2.12a}$$

$$\mathbf{S} + (\tau_1 + \tau_2)\overset{\triangledown}{\mathbf{S}} + \tau_1\tau_2\overset{\triangledown\triangledown}{\mathbf{S}} = 2(\mu_1 + \mu_2)\mathbf{D} + 2(\mu_1\tau_2 + \tau_1\mu_2)\overset{\triangledown}{\mathbf{D}}. \tag{2.12b}$$

Burgers model with additional Newtonian dissipation

Burgers model with additional dashpot (1.63) is transformed to

$$\mathbf{T} = -p\mathbf{I} + 2\mu_3\mathbf{D} + \mathbf{S}, \tag{2.13a}$$

$$\mathbf{S} + \left(\frac{\mu_1}{G_1} + \frac{\mu_2}{G_2}\right)\overset{\triangledown}{\mathbf{S}} + \frac{\mu_1\mu_2}{G_1G_2}\overset{\triangledown\triangledown}{\mathbf{S}} = 2(\mu_1 + \mu_2)\mathbf{D} + 2\left(\frac{\mu_1\mu_2}{G_1} + \frac{\mu_1\mu_2}{G_2}\right)\overset{\triangledown}{\mathbf{D}} \tag{2.13b}$$

usually written using relaxation times $\tau_1 = \mu_1/G_1$ and $\tau_2 = \mu_2/G_2$

$$\mathbf{T} = -p\mathbf{I} + 2\mu_3\mathbf{D} + \mathbf{S}, \tag{2.14a}$$

$$\mathbf{S} + (\tau_1 + \tau_2)\overset{\triangledown}{\mathbf{S}} + \tau_1\tau_2\overset{\triangledown\triangledown}{\mathbf{S}} = 2(\mu_1 + \mu_2)\mathbf{D} + 2(\mu_1\tau_2 + \tau_1\mu_2)\overset{\triangledown}{\mathbf{D}}. \tag{2.14b}$$

2.2 Derivation of Oldroyd-B from microscopical principles – an elastic dumbbell model

Oldroyd-B model can be also derived from microscopical principles in full three dimensional setting.[1] This model was first proposed by Kuhn in [30]. The brief derivation shown in this section is based on the works [48], [6], [50] and [49].

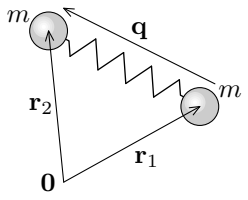

Figure 2.1: Elastic dumbbell model.

Oldroyd-B model is described as a molecular model where polymer chains represented by Hookean dumbbells are diluted in incompressible Newtonian fluid with the viscosity μ_2. Hookean dumbbell consists of two beads with a mass m connected with the Hookean spring (zero mass), $\mathbf{r}_1$ and $\mathbf{r}_2$ are positions of the beads at time t, see Figure 2.1. The elongation vector is denoted by $\mathbf{q} := \mathbf{r}_2 - \mathbf{r}_1$.

The equation of motion for both beads is described by the first Newton's law

$$m\frac{\mathrm{d}^2\mathbf{r}_i}{\mathrm{d}t^2} = -\mathbf{F}_i^d + \mathbf{F}_i^s + \mathbf{B}_i, \quad i = 1, 2, \tag{2.15}$$

where $\mathbf{F}_i^d$ is a drag force exerted on the i-th bead described by Stokes law

$$\mathbf{F}_i^d = \zeta\left(\frac{\mathrm{d}\mathbf{r}_i}{\mathrm{d}t} - \mathbf{v}(\mathbf{r}_i)\right) \text{ with } \zeta = 6\pi\mu_2 a \text{ where } a \text{ is a radius of the bead,}$$

$\mathbf{v}(\mathbf{r}_i)$ is a fluid velocity in $\mathbf{r}_i$ at time t, $\mathbf{F}_i^s$ is the force of spring acting on the i-th bead and in case of Hookean spring they are: $\mathbf{F}_1^s = -\mathbf{F}_2^s = K\mathbf{q}$ where K is stiffness of the spring. Finally, $\mathbf{B}_i$ is the Brownian force caused by molecules of the fluid acting on the $i-$th bead.

Since the mass m is very small and also the inertia effects are much smaller then the elastic and viscous effects we can neglect the left-hand-side of (2.15). Substituting for the forces acting on the beads we reformulate (2.15) as a stochastic differential equation

$$\zeta\,\mathrm{d}\mathbf{r}_i = \zeta\mathbf{v}(\mathbf{r}_i)\,\mathrm{d}t + (-1)^i K\mathbf{q}\,\mathrm{d}t + \mathbf{B}_i\,\mathrm{d}t. \tag{2.16}$$

Brownian force $\mathbf{B}_i$ can be written in the form

$$\mathbf{B}_i\,\mathrm{d}t = \sqrt{2k\theta\zeta}\,\mathrm{d}\mathbf{W}_i,$$

where $\mathbf{W}_i$ is the three-dimensional Wiener process, k is Boltzmann constant and θ thermodynamical temperature. The scaling coefficient $\sqrt{2k\theta\zeta}$ comes from the equipartition principle, for more details see for example [47].

Now we compute the form of the Cauchy stress tensor using the elastic dumbbell model. Since the dumbbells are diluted in the Newtonian fluid, the Cauchy stress tensor consists of three parts: contribution from the Newtonian fluid $\mathbf{T}_N$, the Hookean spring in the dumbbell $\mathbf{T}_s$ and two beads $2\mathbf{T}_b$

$$\mathbf{T} = \mathbf{T}_N + \mathbf{T}_s + 2\mathbf{T}_b, \tag{2.17}$$

[1] The other way how to derive Oldroyd-B model is using the theory of simple fluids with fading memory. We will not discuss it in this thesis, for more details see [11] and [66], the generalization of the notion of simple fluid was studied by [52].

where $\mathbf{T}_N = -p_s\mathbf{I} + 2\mu_2\mathbf{D}$. The contribution of the Hookean spring is computed from the force acting on the imaginary surface S with its normal vector $\mathbf{n}$ that can be seen in Figure 2.2. First we count how many dumbbells with the elongation vector $\mathbf{q}$ are straddling the surface of area S as in Figure 2.2. If N is the number of dumbbells per

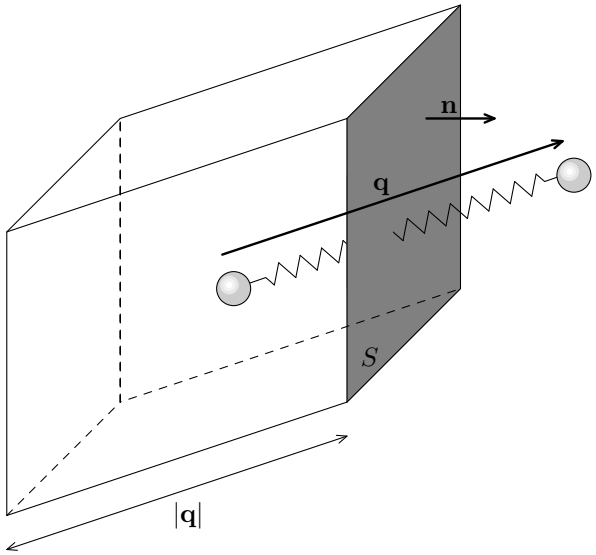

Figure 2.2: Dumbbell straddling the surface S.

unit volume then the number of the dumbbells is equal to $N\mathbf{n}\cdot\mathbf{q}S$ and each of this dumbbell acts on the surface of area S with the force $K\mathbf{q}$. If we define $\psi(\mathbf{q},t)$ the dumbbell probability density function then the total force acting on the surface of area S is equal to

$$\int_{\mathbb{R}^3} N\mathbf{n}\cdot\mathbf{q}SK\mathbf{q}\ \psi(\mathbf{q},t)\,\mathrm{d}\mathbf{q} = NKS\left[\int_{\mathbb{R}^3}\mathbf{q}\otimes\mathbf{q}\ \psi(\mathbf{q},t)\,\mathrm{d}\mathbf{q}\right]\mathbf{n}. \tag{2.18}$$

Since we are interested in the force on a unit surface, we divide the result by S and obtain

$$\mathbf{T}_s\mathbf{n} = NK\int_{\mathbb{R}^3}\mathbf{q}\otimes\mathbf{q}\ \psi(\mathbf{q},t)\,\mathrm{d}\mathbf{q}\mathbf{n} = Nk\theta\mathbf{B}\mathbf{n} \tag{2.19}$$

where we defined the conformation tensor $\mathbf{B}$

$$\mathbf{B} = \frac{K}{k\theta}\langle\mathbf{q}\otimes\mathbf{q}\rangle \tag{2.20}$$

and

$$\langle a(t)\rangle = \int_{\mathbb{R}^3} a(\mathbf{q},t)\psi(\mathbf{q},t)\,\mathrm{d}\mathbf{q} \tag{2.21}$$

is the expected value.

Now, we show the properties of the conformation tensor $\mathbf{B}$. From the equipartition theorem we know that in the thermodynamical equilibrium the mean potential energy of the Hookean springs in 3D is equal to $3k\theta/2$, i.e.,

$$\frac{1}{2}K\langle|\mathbf{q}|^2\rangle = \frac{3}{2}k\theta, \tag{2.22}$$

which gives

$$\operatorname{tr} \mathbf{B}_{\mathrm{eq}} = 3. \tag{2.23}$$

Further, in the thermodynamical equilibrium all dumbbells are randomly rotated with the same probability meaning that the dumbbell probability function is only a function of the size, i.e. $\psi(\mathbf{q}) = \psi(|\mathbf{q}|)$ which together with (2.23) implies that $(B_{ij})_{\mathrm{eq}} = \delta_{ij}$. Hence

$$\mathbf{B}_{\mathrm{eq}} = \mathbf{I}. \tag{2.24}$$

The contribution of the beads is computed from the assumption that the beads are not interacting and so they can be treated as an ideal gas. Hence, using the equation of state for ideal gas we have

$$\mathbf{T}_b = -Nk\theta\mathbf{I}. \tag{2.25}$$

All together we obtain the form of the Cauchy stress

$$\mathbf{T} = -p_s\mathbf{I} + 2\mu_2\mathbf{D} + Nk\theta\mathbf{B} - 2Nk\theta\mathbf{I}. \tag{2.26}$$

If we require that in equilibrium the total pressure p is the mean normal stress $-(\operatorname{tr}\mathbf{T})/3$ we obtain

$$\mathbf{T} = -\underbrace{(p_s + Nk\theta)}_{p}\mathbf{I} + 2\mu_2\mathbf{D} + \underbrace{Nk\theta}_{G}(\mathbf{B} - \mathbf{I}), \tag{2.27}$$

where $G = Nk\theta$ is the elastic modulus.

Now we obtain the evolutionary equation for the conformation tensor $\mathbf{B}$. By subtracting (2.16) for $i = 1$ from (2.16) for $i = 2$ we obtain

$$\mathrm{d}\mathbf{q} = (\mathbf{v}(\mathbf{r}_2) - \mathbf{v}(\mathbf{r}_1))\,\mathrm{d}t + \frac{2K}{\zeta}\mathbf{q}\,\mathrm{d}t + \sqrt{\frac{2k\theta}{\zeta}}(\,\mathrm{d}\mathbf{W}_2 - \,\mathrm{d}\mathbf{W}_1). \tag{2.28}$$

It can be shown that the process $\mathbf{W}_2 - \mathbf{W}_1$ is the same process as $\sqrt{2}\mathbf{W}$. We suppose that the fluid velocity $\mathbf{v}$ is homogeneous, using Taylor expansion we can compute the difference

$$\mathbf{v}(\mathbf{r}_2) - \mathbf{v}(\mathbf{r}_1) = (\nabla_x\mathbf{v})\mathbf{q}$$

and we obtain the final form of stochastic differential equation

$$\mathrm{d}\mathbf{q} = (\nabla_x\mathbf{v})\mathbf{q}\,\mathrm{d}t + \frac{2K}{\zeta}\mathbf{q}\,\mathrm{d}t + 2\sqrt{\frac{k\theta}{\zeta}}\,\mathrm{d}\mathbf{W}. \tag{2.29}$$

The joint Fokker-Planck equation for (2.29) is

$$\frac{\partial\psi}{\partial t} = -\operatorname{div}_{\mathbf{q}}\left(\left((\nabla_x\mathbf{v})\mathbf{q} - \frac{2K}{\zeta}\mathbf{q}\right)\psi\right) + \frac{2k\theta}{\zeta}\Delta_{\mathbf{q}}\psi, \tag{2.30}$$

where $\psi(\mathbf{q}, t)$ is the dumbbell probability density function, for more details on connection between the stochastic differential equation and Fokker-Planck equation; see for example [15].

We multiply (2.30) by $(\mathbf{q}\otimes\mathbf{q})$, integrate over $\mathbf{q}$ and get

$$\frac{\partial}{\partial t}\int_{\mathbb{R}^3}(\mathbf{q}\otimes\mathbf{q})\psi\,\mathrm{d}\mathbf{q} = -\int_{\mathbb{R}^3}\operatorname{div}_{\mathbf{q}}\left(\left((\nabla_x\mathbf{v})\mathbf{q} - \frac{2K}{\zeta}\mathbf{q}\right)\psi\right)(\mathbf{q}\otimes\mathbf{q})\,\mathrm{d}\mathbf{q} + \frac{2k\theta}{\zeta}\int_{\mathbb{R}^3}(\mathbf{q}\otimes\mathbf{q})\Delta_{\mathbf{q}}\psi\,\mathrm{d}\mathbf{q}. \tag{2.31}$$

First, we multiply (2.31) by $K/(k\theta)$ and since ψ vanishes in infinity using Gauss theorem we obtain

$$\frac{K}{k\theta}\frac{\partial}{\partial t}\langle \mathbf{q}\otimes\mathbf{q}\rangle = \frac{K}{k\theta}\left[\nabla_x \mathbf{v}\langle \mathbf{q}\otimes\mathbf{q}\rangle + \langle \mathbf{q}\otimes\mathbf{q}\rangle(\nabla_x\mathbf{v})^{\mathrm{T}}\right] + \frac{4K}{\zeta}\left(\mathbf{I} - \frac{K}{k\theta}\langle \mathbf{q}\otimes\mathbf{q}\rangle\right). \quad (2.32)$$

Specifically, the Gauss theorem for both integrals on the right-hand-side of (2.31) is used in the following way (we suppose that ψ and its gradient vanish in infinity); the first integral:

$$-\int_{\mathbb{R}^3} \operatorname{div}_{\mathbf{q}}\left(\left((\nabla_x\mathbf{v})\mathbf{q} - \frac{2K}{\zeta}\mathbf{q}\right)\psi\right)(\mathbf{q}\otimes\mathbf{q})\,\mathrm{d}\mathbf{q} = -\int_{\mathbb{R}^3}\frac{\partial}{\partial q_k}\left(\left(\frac{\partial v_k}{\partial x_l}q_l - \frac{2K}{\zeta}q_k\right)\psi\right)q_iq_j\,\mathrm{d}\mathbf{q} =$$
$$\int_{\mathbb{R}^3}\left(\left(\frac{\partial v_k}{\partial x_l}q_l - \frac{2K}{\zeta}q_k\right)\psi\right)(\delta_{ik}q_j + q_i\delta_{jk})\,\mathrm{d}\mathbf{q} = \int_{\mathbb{R}^3}\left(\frac{\partial v_i}{\partial x_l}q_lq_j + q_iq_l\frac{\partial v_j}{\partial q_l} - \frac{4K}{\zeta}q_iq_j\right)\psi\,\mathrm{d}\mathbf{q} =$$
$$\int_{\mathbb{R}^3}\left((\nabla_x\mathbf{v})(\mathbf{q}\otimes\mathbf{q}) + (\mathbf{q}\otimes\mathbf{q})(\nabla_x\mathbf{v})^{\mathrm{T}} - \frac{4K}{\zeta}(\mathbf{q}\otimes\mathbf{q})\right)\psi\,\mathrm{d}\mathbf{q},$$

where δ_{ij} is the Kronecker delta. The other integral is done in this way

$$\frac{2k\theta}{\zeta}\int_{\mathbb{R}^3}(\mathbf{q}\otimes\mathbf{q})\Delta_{\mathbf{q}}\psi\,\mathrm{d}\mathbf{q} = \frac{2k\theta}{\zeta}\int_{\mathbb{R}^3}\frac{\partial^2\psi}{\partial q_k^2}q_iq_j\,\mathrm{d}\mathbf{q} = \frac{2k\theta}{\zeta}\int_{\mathbb{R}^3}\psi\ 2\delta_{ik}\delta_{jk}\,\mathrm{d}\mathbf{q} = \frac{4k\theta}{\zeta}\mathbf{I}\int_{\mathbb{R}^3}\psi\,\mathrm{d}\mathbf{q} = \frac{4k\theta}{\zeta}\mathbf{I}.$$

Finally, we insert the definition of $\mathbf{B}$ (2.20) into (2.32) and transform the resulting equation from Langrangian to Eulerian formulation[2]

$$\frac{\partial\mathbf{B}}{\partial t} + (\mathbf{v}\cdot\nabla)\mathbf{B} - \mathbf{L}\mathbf{B} - \mathbf{B}\mathbf{L}^{\mathrm{T}} + \frac{4K}{\zeta}(\mathbf{B}-\mathbf{I}) = 0, \quad (2.33)$$

where $\mathbf{L}$ denotes the velocity gradient and $\tau = \zeta/(4K)$ is the relaxation time. Finally, we obtain Oldroyd-B model (2.10)

$$\mathbf{T} = -p\mathbf{I} + 2\mu_2\mathbf{D} + G(\mathbf{B}-\mathbf{I}),$$
$$\frac{\partial\mathbf{B}}{\partial t} + (\mathbf{v}\cdot\nabla)\mathbf{B} - \mathbf{L}\mathbf{B} - \mathbf{B}\mathbf{L}^{\mathrm{T}} + \frac{1}{\tau}(\mathbf{B}-\mathbf{I}) = 0.$$

2.3 Properties of Oldroyd-B model

Following [7], we investigate several properties of the Oldroyd-B model (2.10). Initially, being at rest $\mathbf{B}(t=0) = \mathbf{I}$ is a symmetric positive definite matrix with $\det\mathbf{B}(t=0) = 1$. We show that it is positive definite for all $t \geq 0$ by contradiction.

From the continuity of $\det\mathbf{B}$ and eigenvalues of $\mathbf{B}$ with respect to time t we know that $\mathbf{B}$ is positive definite and $\det\mathbf{B}(t) > 0$ at least upto some certain time t_0, the symmetry is satisfied for all t because (2.10b) is symmetric. Let us suppose that there is t_0 such that for $t < t_0$ $\mathbf{B}$ is positive definite with $\det\mathbf{B}(t) > 0$ and there is at least one eigenvalue converging to zero for $t \to t_0$, and $\det\mathbf{B}(t=t_0) \leq 0$. Then for $t < t_0$ the matrix $\mathbf{B}$ is symmetric positive definite, and the same holds for its inverse. In a further computation we use Lemma B.1.2 from Appendix saying

$$\operatorname{tr}\mathbf{B}^{-1} \geq d(\det\left(\mathbf{B}^{-1}\right))^{1/d}, \quad (2.35)$$

[2]The only difference is the convective term in Eulerian formulation.

where d is the space dimension. Now we use equation (2.10b) and compute the material time derivative of $\det \mathbf{B}$ using Lemma B.1.1, (its consequence (B.3)) and the incompressibility

$$\frac{\mathrm{d}}{\mathrm{d}t}\left((\det \mathbf{B})^{1/d}\right) = \frac{1}{d}(\det \mathbf{B})^{1/d}\frac{\mathrm{d}}{\mathrm{d}t}(\ln \det \mathbf{B}) \overset{(B.3)}{=} \frac{1}{d}(\det \mathbf{B})^{1/d}\operatorname{tr}\left(\dot{\mathbf{B}}\mathbf{B}^{-1}\right)$$
$$\overset{(2.10b)}{=} \frac{1}{d}(\det \mathbf{B})^{1/d}\frac{1}{\tau}\operatorname{tr}\left(\mathbf{B}^{-1}-\mathbf{I}\right) \overset{(2.35)}{\geq} \frac{1}{\tau}\left(1-(\det \mathbf{B})^{1/d}\right).$$

If we denote $x := (\det \mathbf{B})^{1/d}$ we obtain ODE for x, with $x(0) = 1$

$$\tau\dot{x} + x \geq 1 \Leftrightarrow \tau\dot{x} + x = K(t) \geq 1.$$

The solution of this ODE is

$$x(t) = \left(1 + \frac{1}{\tau}\int_0^t K(s)e^{s/\tau}\,\mathrm{d}s\right)e^{-t/\tau}, 0 \leq t < t_0$$

which is greater or equal than one for $t < t_0$. From the continuity of $\det \mathbf{B}$ w.r.t. time t we also have that $\det \mathbf{B}(t = t_0) > 0$ which is a contradiction with the fact that at least one eigenvalues is zero at $t = t_0$, i.e. $\mathbf{B}$ is still positive definite and so $\det \mathbf{B}(t = t_0) \geq 1$. Thus we found out that $\mathbf{B}$ is positive definite for all t and

$$\det \mathbf{B}(t) \geq 1 \quad \forall t \geq 0. \tag{2.36}$$

Further, together with Lemma B.1.2

$$\operatorname{tr}\mathbf{B} \geq d(\det \mathbf{B})^{1/d} = d + d\left((\det \mathbf{B})^{1/d} - 1\right) \geq d + \ln(\det \mathbf{B}) \tag{2.37}$$

we obtain

$$\operatorname{tr}\mathbf{B} \geq d. \tag{2.38}$$

This important result will be used for getting the apriori estimates for Oldroyd-B model and it also has the following physical meaning. According to (2.20) $\operatorname{tr}\mathbf{B}$ is proportional to the mean square length of the springs (i.e. polymer chains in simplified dumbbell model). Thus (2.38) says that the average length of the polymer chains[3] evolves in the way that it is always bigger than the average length in the equilibrium (2.22).

[3]One particular polymer chain can shorten, but in average all polymer chains has to be longer or equal to the length of polymer chains in equilibrium.

Chapter 3

Thermodynamically compatible viscoelastic rate type fluid models

3.1 A thermodynamic frame work for rate type fluid models

In this chapter we describe a thermodynamic framework for modeling the behavior of inelastic materials, specifically the viscoelastic rate type fluid models. This framework proposed by Rajagopal and Srinivasa is based on the concept of evolving natural configuration and the principle of maximal rate of entropy production. For details see for example [57, 55, 56]. The framework guarantees that the derived models satisfy the second law of thermodynamics.

3.1.1 Natural configuration

The body made from the viscoelastic material is at time t in configuration κ_t, this configuration is called the current configuration. We will compare this configuration with the reference configuration κ_R which is a configuration of the system in rest at the beginning, see Figure 3.1.

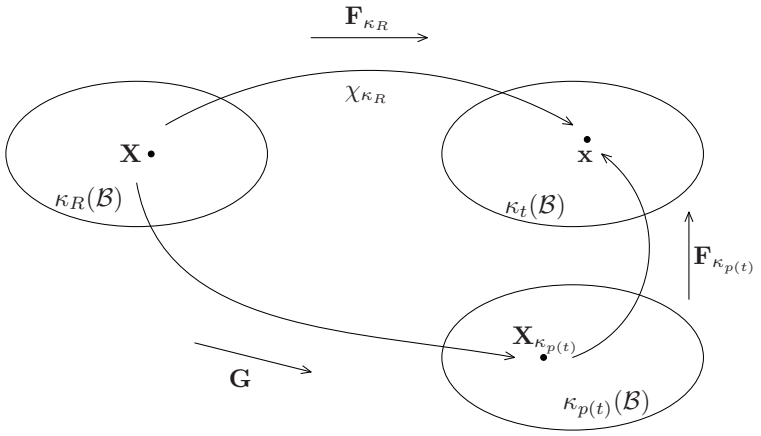

Figure 3.1: Natural configuration.

We define now the natural configuration $\kappa_{p(t)}$. It is a configuration of the body associated with the current configuration κ_t and can be thought of as the configuration that the body in the current configuration κ_t would take if the external stimuli are removed, see Rajagopal [54] and Rajagopal and Srinivasa [58] for a detailed discussion of the notion of natural configuration.

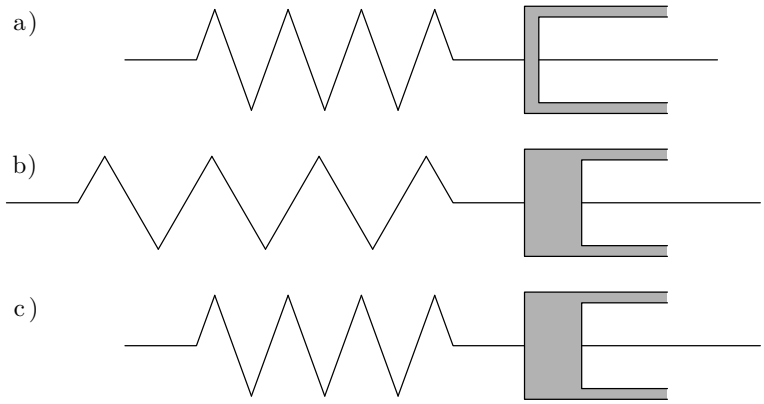

Figure 3.2: Motivational example for the natural configuration.

We motivate the notion of the natural configuration on example of Maxwell element (see Subsection 1.3.2) which consists of of one dashpot and one spring in series. In Figure 3.2a) the element is at the beginning at rest, relaxed, the spring and the dashpot are not stretched. The body is in the reference configuration κ_R. Then we stretch it (Figure 3.2b)) and the body goes to the current configuration κ_t. Now we let the system relax, the spring shrinks to its reference length but the dashpot remains stretched. (Figure 3.2c)). The system is now in the natural configuration $\kappa_{p(t)}$. Because during the relaxation the deformation of the dashpot does not change, we can suppose that the free energy of the system is hidden only in the deformation of the natural configuration.

By defining the natural configuration we split the total deformation into purely elastic part and the dissipative part, the response from the natural configuration $\kappa_{p(t)}$ to the current configuration κ_t is purely elastic.

We define some kinematical quantities. First we remind notation from Section 1.1, $\mathbf{L}$ denotes the velocity gradient and $\mathbf{D}$ its symmetric part

$$\mathbf{L} = \nabla \mathbf{v}, \quad \mathbf{D} = \frac{1}{2}(\mathbf{L} + \mathbf{L}^{\mathrm{T}}). \tag{3.1}$$

Further, the relation between the deformation gradient $\mathbf{F}_{\kappa_R} = \nabla \chi_{\kappa_R}$ and the velocity gradient $\mathbf{L}$ is the following

$$\mathbf{L} = \dot{\mathbf{F}}_{\kappa_R} \mathbf{F}_{\kappa_R}^{-1}, \tag{3.2}$$

the left and right Cauchy-Green tensors $\mathbf{B}_{\kappa_R}$ and $\mathbf{C}_{\kappa_R}$ are defined through

$$\mathbf{B}_{\kappa_R} = \mathbf{F}_{\kappa_R} \mathbf{F}_{\kappa_R}^{\mathrm{T}}, \quad \mathbf{C}_{\kappa_R} = \mathbf{F}_{\kappa_R}^{\mathrm{T}} \mathbf{F}_{\kappa_R}.$$

Finally, we define $\mathbf{F}_{\kappa_{p(t)}}$ as a mapping of the infinitesimal element from $\kappa_{p(t)}$ to κ_t and $\mathbf{G}$ that maps from κ_R to $\kappa_{p(t)}$. The tensors $\mathbf{G}$, $\mathbf{F}_{\kappa_R}$ and $\mathbf{F}_{\kappa_{p(t)}}$ are related through the equation

$$\mathbf{G} = \mathbf{F}_{\kappa_{p(t)}}^{-1} \mathbf{F}_{\kappa_R}. \tag{3.3}$$

We define left and right Cauchy-Green tensor corresponding to $\kappa_{p(t)}$

$$\mathbf{B}_{\kappa_{p(t)}} = \mathbf{F}_{\kappa_{p(t)}}\mathbf{F}^{\mathrm{T}}_{\kappa_{p(t)}}, \quad \mathbf{C}_{\kappa_{p(t)}} = \mathbf{F}^{\mathrm{T}}_{\kappa_{p(t)}}\mathbf{F}_{\kappa_{p(t)}}$$

and motivated by (3.2), we define the quantity related to the rate of the deformation of $\kappa_{p(t)}$, resp. its symmetric part

$$\mathbf{L}_{\kappa_{p(t)}} = \dot{\mathbf{G}}\mathbf{G}^{-1}, \quad \mathbf{D}_{\kappa_{p(t)}} = \frac{\mathbf{L}_{\kappa_{p(t)}} + \mathbf{L}^{\mathrm{T}}_{\kappa_{p(t)}}}{2}.$$

The material time derivative of $\mathbf{B}_{\kappa_{p(t)}}$ is equal to

$$\begin{aligned}\dot{\mathbf{B}}_{\kappa_{p(t)}} &= \dot{\mathbf{F}}_{\kappa_{p(t)}}\mathbf{F}^{\mathrm{T}}_{\kappa_{p(t)}} + \mathbf{F}_{\kappa_{p(t)}}\dot{\mathbf{F}}^{\mathrm{T}}_{\kappa_{p(t)}} = \\ &\dot{\mathbf{F}}_{\kappa_R}\mathbf{G}^{-1}\mathbf{F}^{\mathrm{T}}_{\kappa_{p(t)}} + \mathbf{F}_{\kappa_R}\dot{\overline{\mathbf{G}^{-1}}}\mathbf{F}^{\mathrm{T}}_{\kappa_{p(t)}} + \mathbf{F}_{\kappa_{p(t)}}\dot{\overline{\mathbf{G}^{-\mathrm{T}}}}\mathbf{F}^{\mathrm{T}}_{\kappa_R} + \mathbf{F}_{\kappa_{p(t)}}\mathbf{G}^{-\mathrm{T}}\dot{\mathbf{F}}^{\mathrm{T}}_{\kappa_R} = \\ &\mathbf{L}\mathbf{B}_{\kappa_{p(t)}} + \mathbf{B}_{\kappa_{p(t)}}\mathbf{L}^{\mathrm{T}} - 2\mathbf{F}_{\kappa_{p(t)}}\mathbf{D}_{\kappa_{p(t)}}\mathbf{F}^{\mathrm{T}}_{\kappa_{p(t)}}, \quad (3.4)\end{aligned}$$

where we used

$$\dot{\overline{\mathbf{A}^{-1}}} = -\mathbf{A}^{-1}\dot{\mathbf{A}}\mathbf{A}^{-1}.$$

Using the definition of the upper convected Oldroyd time derivative given by (2.5) we get

$$\overset{\triangledown}{\mathbf{B}}_{\kappa_{p(t)}} = -2\mathbf{F}_{\kappa_{p(t)}}\mathbf{D}_{\kappa_{p(t)}}\mathbf{F}^{\mathrm{T}}_{\kappa_{p(t)}}. \quad (3.5)$$

Note that $\overset{\triangledown}{\mathbf{I}} = -2\mathbf{D}$. It holds that

$$\operatorname{tr}\dot{\mathbf{B}}_{\kappa_{p(t)}} = 2\mathbf{B}_{\kappa_{p(t)}} \cdot \mathbf{D} - 2\mathbf{C}_{\kappa_{p(t)}} \cdot \mathbf{D}_{\kappa_{p(t)}}. \quad (3.6)$$

3.1.2 Incompressibility conditions

By means of the natural configuration we split the total deformation corresponding to deformation gradient $\mathbf{F}_{\kappa_R}$ into purely elastic part given corresponding to $\mathbf{F}_{\kappa_{p(t)}}$ and dissipative part corresponding to $\mathbf{G}$. Material is incompressible if the whole deformation is incompressible, i.e.

$$\det \mathbf{F}_{\kappa_R} = 1, \quad (3.7)$$

which upon differentiation (3.7) with respect to time, see Lemma B.1.1, gives

$$\operatorname{div}\mathbf{v} = \operatorname{tr}\mathbf{D} = 0. \quad (3.8)$$

Material is compressible if (3.7) is not valid. There are more possibilities how to ensure the (in)compressibility of the material using the (in)compressibility of the elastic and the dissipative part of the deformation. We denote the compressibility by ordered triplet of letters 'I' and 'C'. The first letter corresponds to the total deformation, the second to the dissipative part and the third to the elastic part, letter 'I' stands for incompressible, and letter 'C' for compressible.

Material is incompressible in two cases: (III) and (ICC); and compressible in three cases: (CCC), (CIC) and (CCI). We will now discuss all possibilities case by case.

(III) Material is fully incompressible which means that both elastic a dissipative parts of deformation are incompressible, i.e.

$$\det \mathbf{F}_{\kappa_{p(t)}} = 1 \;\Rightarrow\; \det \mathbf{B}_{\kappa_{p(t)}} = 1 \tag{3.9}$$

and

$$\det \mathbf{G} = 1. \tag{3.10}$$

By taking the material time derivative of (3.10), see Lemma B.1.1, we get

$$\operatorname{tr} \mathbf{D}_{\kappa_{p(t)}} = 0. \tag{3.11}$$

Thus, fully incompressible variant (III) satisfies two independent constraints:

$$\operatorname{div} \mathbf{v} = \operatorname{tr} \mathbf{D} = 0, \quad \operatorname{tr} \mathbf{D}_{\kappa_{p(t)}} = 0. \tag{3.12}$$

(ICC) The other possibility for incompressible material is that the elastic and the dissipative part is compressible, such that

$$1 = \det \mathbf{F}_{\kappa_R} = \det \mathbf{G} \det \mathbf{F}_{\kappa_{p(t)}}, \tag{3.13}$$

but $\det \mathbf{F}_{\kappa_{p(t)}} \neq 1$ and $\det \mathbf{G} \neq 1$. Thus, the only restriction for material (ICC) is

$$\operatorname{div} \mathbf{v} = \operatorname{tr} \mathbf{D} = 0. \tag{3.14}$$

(CCC) For the full compressible material determinants of $\mathbf{F}_{\kappa_R}$, $\mathbf{F}_{\kappa_{p(t)}}$, $\mathbf{G}$ are not equal to one and there is no restriction imposed on such material.

(CIC) For the compressible material with incompressible dissipative part of deformation it holds that

$$\det \mathbf{G} = 1 \quad \Rightarrow \quad \operatorname{tr} \mathbf{D}_{\kappa_{p(t)}} = 0. \tag{3.15}$$

(CCI) The last possibility is the compressible material with incompressible elastic part of deformation which satisfies only (3.9).

In this thesis we are mainly interested in models where the total deformation is incompressible – cases (III) and (ICC). For the sake of completeness we however derive for every compressible variant (CCC), (CIC) and (CCI) one model.

3.1.3 Derivation of thermodynamical models

Following the approach developed Rajagopal and Srinivasa [57] two scalar constitutive relations are given in order to derive thermodynamically compatible viscoelastic models. One scalar describes the elastic response (corresponding to the mapping $\mathbf{F}_{\kappa_{p(t)}}$), the other the dissipative response (corresponding to the mapping $\mathbf{G}$). The first scalar constitutive relation is the rate of entropy production $\tilde{\xi}$ that says how the energy in the body dissipates and if it is non-negative the second law of thermodynamics is automatically satisfied. The other scalar that describes the elastic response is a constitutive relation for thermodynamical potential, Helmholtz free energy ψ was used in [57]. In this work we equivalently use a constitutive relation for other thermodynamic potential – the internal energy e – and using it we derive a thermodynamic inequality which gives

a relation between the rate of entropy production and the thermodynamic fluxes and affinities.

We derive the reduced thermodynamic inequalities (we consider constant temperature θ) for two incompressible cases: (III) and (ICC), and thermodynamic inequalities for three compressible cases (CCC), (CIC) and (CCI). In cases where the elastic response is incompressible we assume that is corresponds to that of a incompressible neo-Hookean solid, i.e. the internal energy is in the form

$$e = e_0(\eta, \rho) + \frac{G}{2\rho}\left(\operatorname{tr}\mathbf{B}_{\kappa_{p(t)}} - 3\right). \tag{3.16}$$

In cases where the elastic response is compressible we assume that is corresponds to that of a compressible neo-Hookean solid and the internal energy is in the form (see for example [45])

$$e = e_0(\eta, \rho) + \frac{G}{2\rho}\left(\operatorname{tr}\mathbf{B}_{\kappa_{p(t)}} - 3 - \ln(\det\mathbf{B}_{\kappa_{p(t)}})\right). \tag{3.17}$$

(III) For fully incompressible material it holds that $\operatorname{tr}\mathbf{D} = \operatorname{tr}\mathbf{D}_{\kappa_{p(t)}}$ and we assume internal energy in the form (3.16). Upon differentiation of e we get

$$\rho\dot{e} = \rho\frac{\partial e}{\partial\eta}\dot{\eta} + \rho\frac{\partial e}{\partial\rho}\dot{\rho} + \rho\frac{\partial e}{\partial\mathbf{B}_{\kappa_{p(t)}}}\dot{\mathbf{B}}_{\kappa_{p(t)}} = \rho\theta\dot{\eta} + \frac{G}{2}\operatorname{tr}\dot{\mathbf{B}}_{\kappa_{p(t)}}, \tag{3.18}$$

by comparing (3.18) and balance of energy (1.16) we obtain a balance of entropy

$$\rho\dot{\eta} + \operatorname{div}\left(\frac{\mathbf{q}}{\theta}\right) = \frac{1}{\theta}\underbrace{\left(\mathbf{T}\cdot\mathbf{D} - \frac{\mathbf{q}\cdot\nabla\theta}{\theta} - \frac{G}{2}\operatorname{tr}\dot{\mathbf{B}}_{\kappa_{p(t)}}\right)}_{\xi}, \tag{3.19}$$

where ξ is the rate of entropy production. By inserting (3.6) into balance of entropy (3.19) we obtain

$$0 \le \xi = \mathbf{T}\cdot\mathbf{D} - \frac{\mathbf{q}\cdot\nabla\theta}{\theta} - \frac{G}{2}\operatorname{tr}\dot{\mathbf{B}}_{\kappa_{p(t)}} = \left(\mathbf{T} - G\mathbf{B}_{\kappa_{p(t)}}\right)\cdot\mathbf{D} - \frac{\mathbf{q}\cdot\nabla\theta}{\theta} + G\mathbf{C}_{\kappa_{p(t)}}\cdot\mathbf{D}_{\kappa_{p(t)}}. \tag{3.20}$$

We consider only isothermal processes with constant temperature, i.e. $\nabla\theta = 0$, and we obtain a reduced thermodynamic inequality

$$0 \le \xi = \left(\mathbf{T} - G\mathbf{B}_{\kappa_{p(t)}}\right)\cdot\mathbf{D} + G\mathbf{C}_{\kappa_{p(t)}}\cdot\mathbf{D}_{\kappa_{p(t)}} \tag{3.21}$$

$$= \underbrace{\left(\mathbf{T}^d - G\mathbf{B}^d_{\kappa_{p(t)}}\right)}_{\mathbf{T}^d_{\text{dis}}}\cdot\mathbf{D}^d + G\mathbf{C}^d_{\kappa_{p(t)}}\cdot\mathbf{D}^d_{\kappa_{p(t)}}. \tag{3.22}$$

(ICC) In this incompressible case it holds that $\operatorname{tr}\mathbf{D} = 0$ but $\operatorname{tr}\mathbf{D}_{\kappa_{p(t)}} \neq 0$ and the elastic response is compressible, thus we assume that the internal energy in the form (3.17). Again we derive relation for the rate of entropy production

$$\rho\dot{e} = \rho\frac{\partial e}{\partial\eta}\dot{\eta} + \rho\frac{\partial e}{\partial\rho}\dot{\rho} + \rho\frac{\partial e}{\partial\mathbf{B}_{\kappa_{p(t)}}}\dot{\mathbf{B}}_{\kappa_{p(t)}} = \rho\theta\dot{\eta} + \frac{G}{2}\left(\mathbf{I} - \mathbf{B}^{-1}_{\kappa_{p(t)}}\right)\cdot\dot{\mathbf{B}}_{\kappa_{p(t)}}, \tag{3.23}$$

by comparing (3.23) and balance of energy (1.16) we obtain a balance of entropy

$$\rho\dot{\eta} + \operatorname{div}\left(\frac{\mathbf{q}}{\theta}\right) = \frac{1}{\theta}\underbrace{\left(\mathbf{T}\cdot\mathbf{D} - \frac{\mathbf{q}\cdot\nabla\theta}{\theta} - \frac{G}{2}\left(\operatorname{tr}\dot{\mathbf{B}}_{\kappa_{p(t)}} - \mathbf{B}^{-1}_{\kappa_{p(t)}}\cdot\dot{\mathbf{B}}_{\kappa_{p(t)}}\right)\right)}_{\xi}, \quad (3.24)$$

By inserting (3.6) into balance of entropy (3.24) and considering isothermal processes $\nabla\theta = 0$ we obtain

$$0 \le \xi = \left(\mathbf{T} - G(\mathbf{B}_{\kappa_{p(t)}} - \mathbf{I})\right)\cdot\mathbf{D} + G\left(\mathbf{C}_{\kappa_{p(t)}} - \mathbf{I}\right)\cdot\mathbf{D}_{\kappa_{p(t)}} \quad (3.25)$$

$$= \underbrace{\left(\mathbf{T} - G(\mathbf{B}_{\kappa_{p(t)}} - \mathbf{I})\right)^d}_{\mathbf{T}^d_{\text{dis}}}\cdot\mathbf{D}^d + G(\mathbf{C}_{\kappa_{p(t)}} - \mathbf{I})\cdot\mathbf{D}_{\kappa_{p(t)}}. \quad (3.26)$$

(CCC) In the fully compressible case there is no restriction on $\operatorname{tr}\mathbf{D}$ or $\operatorname{tr}\mathbf{D}_{\kappa_{p(t)}}$, we assume the internal energy e in the form (3.17). Let us take the material time derivative of internal energy e multiplied by ρ

$$\rho\dot{e} = \rho\frac{\partial e}{\partial\rho}\dot{\rho} + \rho\frac{\partial e}{\partial\eta}\dot{\eta} + \rho\frac{\partial e}{\partial\mathbf{B}_{\kappa_{p(t)}}}\dot{\mathbf{B}}_{\kappa_{p(t)}} =$$

$$-\underbrace{\rho^2\frac{\partial e}{\partial\rho}}_{p(\rho,\theta)}\operatorname{div}\mathbf{v} + \rho\theta\dot{\eta} + \frac{G}{2}\left(\operatorname{tr}\dot{\mathbf{B}}_{\kappa_{p(t)}} - \mathbf{B}^{-1}_{\kappa_{p(t)}}\cdot\dot{\mathbf{B}}_{\kappa_{p(t)}}\right). \quad (3.27)$$

Substituting this relation into balance of energy (1.16) and comparing it with balance of entropy (3.19) we obtain the relation for the rate of entropy production

$$\xi = \mathbf{T}\cdot\mathbf{D} + p(\rho,\theta)\operatorname{div}\mathbf{v} - \frac{G}{2}\left(\operatorname{tr}\dot{\mathbf{B}}_{\kappa_{p(t)}} - \mathbf{B}^{-1}_{\kappa_{p(t)}}\cdot\dot{\mathbf{B}}_{\kappa_{p(t)}}\right) - \frac{\mathbf{q}\cdot\nabla\theta}{\theta}. \quad (3.28)$$

Inserting (3.6) into (3.28) we get

$$\xi = (\mathbf{T} - G(\mathbf{B}_{\kappa_{p(t)}} - \mathbf{I}))\cdot\mathbf{D} + p(\rho,\theta)\operatorname{div}\mathbf{v} + G(\mathbf{C}_{\kappa_{p(t)}} - \mathbf{I})\cdot\mathbf{D}_{\kappa_{p(t)}} - \frac{\mathbf{q}\cdot\nabla\theta}{\theta}, \quad (3.29)$$

Now we split the Cauchy stress tensor $\mathbf{T}$ into its deviatoric part $\mathbf{T}^d$ and the spherical part m,

$$\mathbf{T} = m\mathbf{I} + \mathbf{T}^d.$$

we also split the tensor $\mathbf{B}_{\kappa_{p(t)}}$

$$\mathbf{B}_{\kappa_{p(t)}} = \frac{b}{3}\mathbf{I} + \mathbf{B}^d_{\kappa_{p(t)}}, \quad b := \operatorname{tr}\mathbf{B}_{\kappa_{p(t)}} = \operatorname{tr}\mathbf{C}_{\kappa_{p(t)}} \;\Rightarrow\; \mathbf{C}_{\kappa_{p(t)}} - \mathbf{I} = \mathbf{C}^d_{\kappa_{p(t)}} + \left(\frac{b}{3} - 1\right)\mathbf{I}.$$

Then the rate of entropy production ξ can be written in the special form which divides the dissipation into the shear and the bulk part

$$\xi = \underbrace{(\mathbf{T}^d - G\mathbf{B}^d_{\kappa_{p(t)}})}_{\mathbf{T}^d_{\text{dis}}}\cdot\mathbf{D}^d + \underbrace{\left(m + p(\rho,\theta) - G\left(\frac{b}{3} - 1\right)\right)}_{t_{\text{dis}}}\operatorname{div}\mathbf{v} +$$

$$G\mathbf{C}^d_{\kappa_{p(t)}}\cdot\mathbf{D}^d_{\kappa_{p(t)}} + G\left(\frac{b}{3} - 1\right)\operatorname{tr}\mathbf{D}_{\kappa_{p(t)}} - \frac{\mathbf{q}\cdot\nabla\theta}{\theta}. \quad (3.30)$$

As indicated above we denote $\mathbf{T}^d_{\text{dis}}$ the viscous shear thermodynamic flux corresponding to the viscous shear thermodynamic affinity $\mathbf{D}^d$

$$\mathbf{T}^d_{\text{dis}} := \mathbf{T}^d - G\mathbf{B}^d_{\kappa_{p(t)}}$$

and t_{dis} denotes the viscous bulk thermodynamic flux corresponding to the viscous bulk thermodynamic affinity $\operatorname{div}\mathbf{v}$

$$t_{\text{dis}} = m + p(\rho,\theta) - G\left(\frac{b}{3} - 1\right).$$

(CIC) In this case the dissipative part is incompressible, i.e. $\operatorname{tr}\mathbf{D}_{\kappa_{p(t)}} = 0$, and we assume that the internal energy is in the form (3.17). We obtain a similar result as in case (CCC) with the difference that $\operatorname{tr}\mathbf{D}_{\kappa_{p(t)}} = 0$ in (3.30), thus it holds

$$\xi = \underbrace{(\mathbf{T}^d - G\mathbf{B}^d_{\kappa_{p(t)}})}_{\mathbf{T}^d_{\text{dis}}} \cdot \mathbf{D}^d + \underbrace{\left(m + p(\rho,\theta) - G\left(\frac{b}{3} - 1\right)\right)}_{t_{\text{dis}}} \operatorname{div}\mathbf{v} + G\mathbf{C}^d_{\kappa_{p(t)}} \cdot \mathbf{D}^d_{\kappa_{p(t)}} - \frac{\mathbf{q}\cdot\nabla\theta}{\theta}. \quad (3.31)$$

(CCI) In this case we only assume that the elastic response is incompressible and the internal energy is in the form (3.16). Then it holds that

$$\xi = (\mathbf{T} - G\mathbf{B}_{\kappa_{p(t)}}) \cdot \mathbf{D} + p(\rho,\theta)\operatorname{div}\mathbf{v} + G\mathbf{C}_{\kappa_{p(t)}} \cdot \mathbf{D}_{\kappa_{p(t)}} - \frac{\mathbf{q}\cdot\nabla\theta}{\theta} \quad (3.32)$$

$$= (\mathbf{T} - G\mathbf{B}_{\kappa_{p(t)}})^d \cdot \mathbf{D}^d + \left(m + p(\rho,\theta) - G\frac{b}{3}\right)\operatorname{div}\mathbf{v} + G\mathbf{C}^d_{\kappa_{p(t)}} \cdot \mathbf{D}^d_{\kappa_{p(t)}} + G\frac{b}{3}\operatorname{tr}\mathbf{D}_{\kappa_{p(t)}} - \frac{\mathbf{q}\cdot\nabla\theta}{\theta}. \quad (3.33)$$

The methodology for developing constitutive relations for incompressible rate-type fluids is the following: Instead of directly prescribing a constitutive relation for symmetric Cauchy stress tensor $\mathbf{T}$, that in three-dimensional space consists of six elements, we choose constitutive relations for the internal energy (equivalently Helmholtz free energy) and rate of entropy production $\tilde{\xi}$.

In order to obtain a constitutive equation for $\mathbf{T}$, the chosen constitutive relation for the rate of entropy production $\tilde{\xi}$ has to be compared with the thermodynamic inequality for ξ. However, the equation $\xi = \tilde{\xi}$ does not uniquely determines the Cauchy stress tensor $\mathbf{T}$. We assume that from amongst the processes that are possible the body proceeds in such a manner so as to maximize the rate at which entropy is produced. Thus, we maximize the rate of entropy production ξ under the constraint of the thermodynamic inequality ((3.22) for incompressible case (III), (3.25) in case of (ICC), (3.30) in case of (CCC), (3.31) in case of (CIC) and (3.33) in case of (CCI)) and the requirements of incompressibility given in Subsection 3.1.2. For more details on the principle of maximum rate of entropy production see [59].

In the following sections we derive several different viscoelastic models. In their derivation we assume different constitutive relations for the rate of entropy production $\tilde{\xi}$ and according to this section we choose one compressibility variant which gives the restrictions used for the principle of maximum rate of entropy production.

3.2 Derivation of viscoelastic models RaSr2000 and MaRa2007

The model for the fully incompressible material (III) is derived in this section. We choose the same rate of entropy production as in paper by Málek and Rajagopal [36] and similar to the rate of entropy production in the original paper by Rajagopal and Srinivasa [57]

$$\xi = \tilde{\xi}(\mathbf{D}, \mathbf{D}_{\kappa p(t)}, \mathbf{C}_{\kappa_{p(t)}}) = 2\mu_2|\mathbf{D}|^2 + 2\mu_1 \mathbf{D}_{\kappa_{p(t)}} \mathbf{C}_{\kappa_{p(t)}} \cdot \mathbf{D}_{\kappa_{p(t)}}, \quad \mu_2, \mu_1 > 0. \tag{3.34}$$

Note that $\tilde{\xi} \geq 0$ since $\mathbf{D}_{\kappa_{p(t)}} \mathbf{C}_{\kappa_{p(t)}} \cdot \mathbf{D}_{\kappa_{p(t)}} = |\mathbf{F}_{\kappa_{p(t)}} \mathbf{D}_{\kappa_{p(t)}}|^2 \geq 0$ and the second law of thermodynamics is automatically satisfied. The first term in (3.34) corresponds to Newtonian viscous dissipation, the second dissipative mechanism takes into account the mutual interaction of the amorphous phase and macromolecules. The rate of entropy production that was used in [57]

$$\tilde{\xi} = \mathbf{D}_{\kappa_{p(t)}} \mathbf{B}_{\kappa_{p(t)}} \cdot \mathbf{D}_{\kappa_{p(t)}} \tag{3.35}$$

does not contain the Newtonian dissipation and consists only of the second term with the objective tensor $\mathbf{B}_{\kappa_{p(t)}}$. However, the whole rate of entropy production (3.35) is not an objective scalar, while the rate of entropy production (3.34) is. This is shown in Section C in Appendix. Here we derive a model with a rate of entropy production given by (3.34) used in [36].

Now, the assumption of the maximization of the rate of entropy production is used. We maximize $\tilde{\xi}(\mathbf{D}, \mathbf{D}_{\kappa p(t)}, \mathbf{C}_{\kappa_{p(t)}})$ among the values of $\mathbf{D}, \mathbf{D}_{\kappa_{p(t)}}$ fulfilling the equality (3.21) and the constraints of incompressibility (3.12). For this purpose we adopt the method of Lagrange multipliers and we define the Lagrange function

$$\begin{aligned} L(\mathbf{D}, \mathbf{D}_{\kappa_{p(t)}}) = \tilde{\xi}(\mathbf{D}, \mathbf{D}_{\kappa p(t)}, \mathbf{C}_{\kappa_{p(t)}}) - \lambda_2 \operatorname{tr} \mathbf{D} - \lambda_3 \operatorname{tr} \mathbf{D}_{\kappa_{p(t)}} \\ + \lambda_1 \left(\tilde{\xi}(\mathbf{D}, \mathbf{D}_{\kappa p(t)}, \mathbf{C}_{\kappa_{p(t)}}) - \left(\mathbf{T} - G\mathbf{B}_{\kappa_{p(t)}} \right) \cdot \mathbf{D} - G\mathbf{C}_{\kappa_{p(t)}} \cdot \mathbf{D}_{\kappa_{p(t)}} \right). \end{aligned} \tag{3.36}$$

and maximize it. The necessary conditions are

$$\frac{\partial L}{\partial \mathbf{D}} = 0, \quad \frac{\partial L}{\partial \mathbf{D}_{\kappa_{p(t)}}} = 0.$$

We substitute for L and obtain

$$\frac{1+\lambda_1}{\lambda_1} \frac{\partial \tilde{\xi}}{\partial \mathbf{D}} = \mathbf{T} - G\mathbf{B}_{\kappa_{p(t)}} + \frac{\lambda_2}{\lambda_1}\mathbf{I}, \tag{3.37}$$

$$\frac{1+\lambda_1}{\lambda_1} \frac{\partial \tilde{\xi}}{\partial \mathbf{D}_{\kappa_{p(t)}}} = G\mathbf{C}_{\kappa_{p(t)}} + \frac{\lambda_3}{\lambda_1}\mathbf{I}. \tag{3.38}$$

We compute the partial derivatives

$$\frac{\partial \tilde{\xi}}{\partial \mathbf{D}} = 4\mu_2 \mathbf{D}, \quad \frac{\partial \tilde{\xi}}{\partial \mathbf{D}_{\kappa_{p(t)}}} = 4\mu_1 \mathbf{D}_{\kappa_{p(t)}} \mathbf{C}_{\kappa_{p(t)}}. \tag{3.39}$$

and eliminate the Lagrange multipliers. To do this we perform $(3.37)\cdot\mathbf{D}+(3.38)\cdot\mathbf{D}_{\kappa_{p(t)}}$, and use the constraints of incompressibility

$$\frac{1+\lambda_1}{\lambda_1}=\frac{\left(\mathbf{T}-G\mathbf{B}_{\kappa_{p(t)}}\right)\cdot\mathbf{D}+G\mathbf{C}_{\kappa_{p(t)}}\cdot\mathbf{D}_{\kappa_{p(t)}}}{\dfrac{\partial\tilde{\xi}}{\partial\mathbf{D}}\cdot\mathbf{D}+\dfrac{\partial\tilde{\xi}}{\partial\mathbf{D}_{\kappa_{p(t)}}}\cdot\mathbf{D}_{\kappa_{p(t)}}}=\frac{\xi}{2\tilde{\xi}}=\frac{1}{2}. \tag{3.40}$$

Next we take the trace of (3.37) and eliminate λ_2/λ_1 which together with (3.40) gives

$$\frac{\lambda_2}{\lambda_1}=-\frac{1}{3}\operatorname{tr}\left(\mathbf{T}-G\mathbf{B}_{\kappa_{p(t)}}\right). \tag{3.41}$$

We define a pressure p as a mean normal stress

$$p=-\frac{1}{3}\operatorname{tr}\mathbf{T}. \tag{3.42}$$

Substitution of (3.42), (3.41), (3.40) and (3.39) into (3.37) yields

$$\mathbf{T}=-p\mathbf{I}+2\mu_2\mathbf{D}+G\mathbf{B}^d_{\kappa_{p(t)}}. \tag{3.43}$$

Now we insert (3.40) and (3.39) into (3.38) and we get

$$2\mu_1\mathbf{D}_{\kappa_{p(t)}}\mathbf{C}_{\kappa_{p(t)}}=G\mathbf{C}_{\kappa_{p(t)}}+\frac{\lambda_3}{\lambda_1}\mathbf{I} \tag{3.44}$$

The elimination of λ_3/λ_1 can be done in two different ways, one leads to model derived by Rajagopal, Srinivasa (2000) (denoted as RaSr2000), the other to the model due to Málek, Rajagopal (2007) (denoted as MaRa2007).

3.2.1 Derivation of model RaSr2000 due to Rajagopal, Srinivasa (2000)

Rajagopal and Srinivasa [57] eliminate λ_3/λ_1 in the following way. We multiply (3.44) from the left by $\mathbf{C}^{-1}_{\kappa_{p(t)}}$ and take the trace of the result

$$0=3G+\frac{\lambda_3}{\lambda_1}\operatorname{tr}\left(\mathbf{C}^{-1}_{\kappa_{p(t)}}\right),$$

which yields to

$$\frac{\lambda_3}{\lambda_1}=-\frac{3G}{\operatorname{tr}\left(\mathbf{C}^{-1}_{\kappa_{p(t)}}\right)}=-\frac{3G}{\operatorname{tr}\left(\mathbf{B}^{-1}_{\kappa_{p(t)}}\right)}. \tag{3.45}$$

By inserting this result into (3.44) we obtain

$$2\mu_1\mathbf{D}_{\kappa_{p(t)}}\mathbf{C}_{\kappa_{p(t)}}=G\left(\mathbf{C}_{\kappa_{p(t)}}-\frac{3}{\operatorname{tr}\left(\mathbf{B}^{-1}_{\kappa_{p(t)}}\right)}\mathbf{I}\right), \tag{3.46}$$

we multiply it from the left by $\mathbf{F}_{\kappa_{p(t)}}$ and from the right by $\mathbf{F}^{-1}_{\kappa_{p(t)}}$, and get

$$2\mu_1\mathbf{F}_{\kappa_{p(t)}}\mathbf{D}_{\kappa_{p(t)}}\mathbf{F}^{\mathrm{T}}_{\kappa_{p(t)}}=G\left(\mathbf{F}_{\kappa_{p(t)}}\mathbf{F}^{\mathrm{T}}_{\kappa_{p(t)}}-\frac{3}{\operatorname{tr}\left(\mathbf{B}^{-1}_{\kappa_{p(t)}}\right)}\mathbf{I}\right). \tag{3.47}$$

Now we realize that term on the left-hand-side of (3.47) is equal to the upper convected Oldroyd derivative of $\mathbf{B}_{\kappa_{p(t)}}$, using (3.5) we obtain

$$\overset{\triangledown}{\mathbf{B}}_{\kappa_{p(t)}} = -\frac{G}{\mu_1}\left(\mathbf{B}_{\kappa_{p(t)}} - \frac{3}{\operatorname{tr}\left(\mathbf{B}^{-1}_{\kappa_{p(t)}}\right)}\mathbf{I}\right) \tag{3.48}$$

and we obtain viscoelastic model in the form

$$\mathbf{T} = -p\mathbf{I} + 2\mu_2\mathbf{D} + G\mathbf{B}^d_{\kappa_{p(t)}} \tag{3.49a}$$

$$\overset{\triangledown}{\mathbf{B}}_{\kappa_{p(t)}} = -\frac{G}{\mu_1}\left(\mathbf{B}_{\kappa_{p(t)}} - \frac{3}{\operatorname{tr}\left(\mathbf{B}^{-1}_{\kappa_{p(t)}}\right)}\mathbf{I}\right). \tag{3.49b}$$

Properties of the viscoelastic model (3.49)

In this paragraph we show the properties of the model (3.49). First we show some properties of matrix $\mathbf{B}_{\kappa_{p(t)}}$. At the beginning (at rest) $\mathbf{B}_{\kappa_{p(t)}}(t=0) = \mathbf{I}$ is a symmetric positive definite matrix with $\det \mathbf{B}_{\kappa_{p(t)}}(t=0) = 1$. Using (B.3) from the Appendix we get

$$\frac{\mathrm{d}}{\mathrm{d}t}\ln(\det \mathbf{B}_{\kappa_{p(t)}}) = \operatorname{tr}\left(\dot{\mathbf{B}}_{\kappa_{p(t)}}\mathbf{B}^{-1}_{\kappa_{p(t)}}\right) \overset{(3.49b)}{=} 2\operatorname{tr}\mathbf{D} - \frac{G}{\mu_1}(\operatorname{tr}\mathbf{I} - 3) = 0 \tag{3.50}$$

and

$$\det \mathbf{B}_{\kappa_{p(t)}}(t) = 1 \ \forall t \geq 0 \tag{3.51}$$

which means that the evolutionary equation for (3.49b) includes the incompressibility condition of the elastic response (3.9). Further, since eigenvalues are continuous w.r.t time t and $\det \mathbf{B}_{\kappa_{p(t)}} = 1$, all eigenvalues have to be positive. Using Lemma B.1.2 from Appendix we get the relation the trace of $\mathbf{B}_{\kappa_{p(t)}}$

$$\operatorname{tr}\mathbf{B}_{\kappa_{p(t)}} \geq 3 \text{ in a three-dimensional space.} \tag{3.52}$$

Alternative form of model RaSr2000

In model (3.49) there is a term $\operatorname{tr}\mathbf{B}^{-1}_{\kappa_{p(t)}}$ in the equation (3.49b) which is difficult to write in components. Using the observed property that $\det \mathbf{B}_{\kappa_{p(t)}} = 1$ and the Lemma B.1.5 we obtain the model without the inverse of $\mathbf{B}_{\kappa_{p(t)}}$. Using (B.17) we modify the term $3/\operatorname{tr}\left(\mathbf{B}^{-1}_{\kappa_{p(t)}}\right)$

$$\frac{3}{\operatorname{tr}\left(\mathbf{B}^{-1}_{\kappa_{p(t)}}\right)} = \frac{6\det \mathbf{B}_{\kappa_{p(t)}}}{(\operatorname{tr}\mathbf{B}_{\kappa_{p(t)}})^2 - \operatorname{tr}\left(\mathbf{B}^2_{\kappa_{p(t)}}\right)} = \frac{6}{(\operatorname{tr}\mathbf{B}_{\kappa_{p(t)}})^2 - \operatorname{tr}\left(\mathbf{B}^2_{\kappa_{p(t)}}\right)} \tag{3.53}$$

and the model is then in the form

$$\mathbf{T} = -p\mathbf{I} + 2\mu_2\mathbf{D} + G\mathbf{B}^d_{\kappa_{p(t)}}, \tag{3.54a}$$

$$\overset{\triangledown}{\mathbf{B}}_{\kappa_{p(t)}} = -\frac{G}{\mu_1}\left(\mathbf{B}_{\kappa_{p(t)}} - \frac{6}{(\operatorname{tr}\mathbf{B}_{\kappa_{p(t)}})^2 - \operatorname{tr}\left(\mathbf{B}^2_{\kappa_{p(t)}}\right)}\mathbf{I}\right). \tag{3.54b}$$

Linearization of RaSr2000 We show that the model (3.49) reduces to Oldroyd-B model (2.10) when the elastic response is linearized. Suppose that the left Cauchy-Green tensor $\mathbf{B}_{\kappa_{p(t)}}$ is small $\|\mathbf{B}_{\kappa_{p(t)}} - \mathbf{I}\| = \epsilon, \quad 0 < \epsilon \ll 1$. By linearization we understand that we neglect all terms of the order $O(\epsilon^2)$ and higher. We use (3.51) in the Taylor expansion of determinant and obtain

$$1 = \det\left(\mathbf{I} + \mathbf{B}_{\kappa_{p(t)}} - \mathbf{I}\right) = 1 + \operatorname{tr}(\mathbf{B}_{\kappa_{p(t)}} - \mathbf{I}) + O(\epsilon^2) \quad \Rightarrow \quad \operatorname{tr}(\mathbf{B}_{\kappa_{p(t)}}) = 3 + O(\epsilon^2) \tag{3.55}$$

Further, the Taylor expansion of $(\mathbf{I} + \mathbf{B}_{\kappa_{p(t)}} - \mathbf{I})^{-1}$ gives

$$(\mathbf{I} + \mathbf{B}_{\kappa_{p(t)}} - \mathbf{I})^{-1} = \mathbf{I} - (\mathbf{B}_{\kappa_{p(t)}} - \mathbf{I}) + O(\epsilon^2) \quad \Rightarrow \quad \operatorname{tr}\left(\mathbf{B}^{-1}_{\kappa_{p(t)}}\right) = 3 + O(\epsilon^2). \tag{3.56}$$

Now we insert (3.55) and (3.56) into (3.49) and obtain

$$\mathbf{T} = -p\mathbf{I} + 2\mu_2\mathbf{D} + G\left(\mathbf{B}_{\kappa_{p(t)}} - \mathbf{I} + O(\epsilon^2)\mathbf{I}\right), \tag{3.57a}$$

$$\overset{\triangledown}{\mathbf{B}}_{\kappa_{p(t)}} = -\frac{G}{\mu_1}\left(\mathbf{B}_{\kappa_{p(t)}} - \frac{3}{3 + O(\epsilon^2)}\mathbf{I}\right), \tag{3.57b}$$

after neglecting the terms of the order $O(\epsilon^2)$ we obtain Oldroyd-B model (2.10)

$$\mathbf{T} = -p\mathbf{I} + 2\mu_2\mathbf{D} + G\left(\mathbf{B}_{\kappa_{p(t)}} - \mathbf{I}\right), \tag{3.58a}$$

$$\overset{\triangledown}{\mathbf{B}}_{\kappa_{p(t)}} = -\frac{G}{\mu_1}\left(\mathbf{B}_{\kappa_{p(t)}} - \mathbf{I}\right). \tag{3.58b}$$

3.2.2 Derivation of model MaRa2007 due to Málek, Rajagopal (2007)

Málek and Rajagopal [36] eliminate λ_3/λ_1 in the following way. We take the trace of (3.44) and obtain

$$2\mu_1\left(\mathbf{D}_{\kappa_{p(t)}}\mathbf{C}_{\kappa_{p(t)}} - \frac{1}{3}\left(\mathbf{D}_{\kappa_{p(t)}} \cdot \mathbf{C}_{\kappa_{p(t)}}\right)\mathbf{I}\right) = G\left(\mathbf{C}_{\kappa_{p(t)}} - \frac{1}{3}(\operatorname{tr}\mathbf{C}_{\kappa_{p(t)}})\mathbf{I}\right), \tag{3.59}$$

we multiply (3.111) from the left by $\mathbf{F}_{\kappa_{p(t)}}$ and from the right by $\mathbf{F}^{-1}_{\kappa_{p(t)}}$, and get

$$2\mu_1\left(\mathbf{F}_{\kappa_{p(t)}}\mathbf{D}_{\kappa_{p(t)}}\mathbf{F}^{\mathrm{T}}_{\kappa_{p(t)}} - \frac{1}{3}\left(\mathbf{D}_{\kappa_{p(t)}} \cdot \mathbf{C}_{\kappa_{p(t)}}\right)\mathbf{I}\right) = G\left(\mathbf{B}_{\kappa_{p(t)}} - \frac{1}{3}(\operatorname{tr}\mathbf{B}_{\kappa_{p(t)}})\mathbf{I}\right). \tag{3.60}$$

Now we compute the upper convected Oldroyd time derivative of the deviatoric part of $\mathbf{B}_{\kappa_{p(t)}}$ using (3.5)

$$\begin{aligned}
\overset{\triangledown}{\mathbf{B}}^{d}_{\kappa_{p(t)}} &= \overset{\triangledown}{\overline{\left(\mathbf{B}_{\kappa_{p(t)}} - \frac{1}{3}(\operatorname{tr}\mathbf{B}_{\kappa_{p(t)}})\mathbf{I}\right)}} = \overset{\triangledown}{\mathbf{B}}_{\kappa_{p(t)}} - \frac{1}{3}(\operatorname{tr}\dot{\mathbf{B}}_{\kappa_{p(t)}})\mathbf{I} - \frac{1}{3}(\operatorname{tr}\mathbf{B}_{\kappa_{p(t)}})\overset{\triangledown}{\mathbf{I}} = \\
&= -2\mathbf{F}_{\kappa_{p(t)}}\mathbf{D}_{\kappa_{p(t)}}\mathbf{F}^{\mathrm{T}}_{\kappa_{p(t)}} - \frac{1}{3}\operatorname{tr}(\mathbf{L}\mathbf{B}_{\kappa_{p(t)}} + \mathbf{L}^{\mathrm{T}}\mathbf{B}_{\kappa_{p(t)}})\mathbf{I} + \\
&\quad + \frac{2}{3}\operatorname{tr}(\mathbf{F}^{\mathrm{T}}_{\kappa_{p(t)}}\mathbf{F}_{\kappa_{p(t)}}\mathbf{D}_{\kappa_{p(t)}})\mathbf{I} + \frac{2}{3}(\operatorname{tr}\mathbf{B}_{\kappa_{p(t)}})\mathbf{D} = \\
&= -2\mathbf{F}_{\kappa_{p(t)}}\mathbf{D}_{\kappa_{p(t)}}\mathbf{F}^{\mathrm{T}}_{\kappa_{p(t)}} - \frac{2}{3}(\mathbf{D} \cdot \mathbf{B}_{\kappa_{p(t)}})\mathbf{I} + \frac{2}{3}(\mathbf{C}_{\kappa_{p(t)}} \cdot \mathbf{D}_{\kappa_{p(t)}})\mathbf{I} + \frac{2}{3}(\operatorname{tr}\mathbf{B}_{\kappa_{p(t)}})\mathbf{D}.
\end{aligned} \tag{3.61}$$

By comparing (3.61) and (3.60) we get

$$2\mu_1\left(-\frac{1}{2}\overset{\triangledown}{\mathbf{B}}^d_{\kappa_{p(t)}} -\frac{1}{3}(\mathbf{D}\cdot\mathbf{B}^d_{\kappa_{p(t)}})\mathbf{I}+\frac{1}{3}(\operatorname{tr}\mathbf{B}_{\kappa_{p(t)}})\mathbf{D}\right)=G\mathbf{B}^d_{\kappa_{p(t)}}. \tag{3.62}$$

For further use let us denote $b := \operatorname{tr}\mathbf{B}_{\kappa_{p(t)}}$. Note that the trace of both sides of (3.62) is zero, in the three dimensional space it is five scalar equations for six unknowns $\mathbf{B}^d_{\kappa_{p(t)}}, b$. We complete the system of equations with the equation of incompressibility of the elastic response

$$\det\left(\mathbf{B}^d_{\kappa_{p(t)}}+\frac{b}{3}\mathbf{I}\right)=1.$$

We obtain the set of equations for nonlinear viscoelastic rate-type fluid model

$$\mathbf{T}=-p\mathbf{I}+2\mu_2\mathbf{D}+\mu\mathbf{B}^d_{\kappa_{p(t)}}, \tag{3.63a}$$

$$2\mu_1\left(-\frac{1}{2}\overset{\triangledown}{\mathbf{B}}^d_{\kappa_{p(t)}} -\frac{1}{3}(\mathbf{D}\cdot\mathbf{B}^d_{\kappa_{p(t)}})\mathbf{I}+\frac{b}{3}\mathbf{D}\right)=G\mathbf{B}^d_{\kappa_{p(t)}}, \tag{3.63b}$$

$$\det\left(\mathbf{B}^d_{\kappa_{p(t)}}+\frac{b}{3}\mathbf{I}\right)=1. \tag{3.63c}$$

Together with balance of mass and balance of linear momentum we have in threedimensional space a set of 10 PDEs for 10 unknowns $p, \mathbf{v}, \mathbf{B}^d_{\kappa_{p(t)}}, b$.

Linearization of the viscoelastic model MaRa2007

We proceed in the same way as in case of the model (3.49), suppose that the left Cauchy-Green tensor $\mathbf{B}_{\kappa_{p(t)}}$ is small, i.e. $\|\mathbf{B}_{\kappa_{p(t)}}-\mathbf{I}\|=\epsilon,\quad 0<\epsilon\ll 1$. We use the last equation for incompressibility (3.63c) and do the Taylor expansion of determinant. We obtain

$$1=\det\left(\mathbf{I}+\mathbf{B}_{\kappa_{p(t)}}-\mathbf{I}\right)=1+\operatorname{tr}(\mathbf{B}_{\kappa_{p(t)}}-\mathbf{I})+\frac{1}{2}\left((\operatorname{tr}(\mathbf{B}_{\kappa_{p(t)}}-\mathbf{I}))^2-\operatorname{tr}\left((\mathbf{B}_{\kappa_{p(t)}}-\mathbf{I})^2\right)\right)+O(\epsilon^3)\ \Rightarrow$$
$$\operatorname{tr}(\mathbf{B}_{\kappa_{p(t)}})=3+\underbrace{\frac{1}{2}\left(\operatorname{tr}\left((\mathbf{B}_{\kappa_{p(t)}}-\mathbf{I})^2\right)-(\operatorname{tr}(\mathbf{B}_{\kappa_{p(t)}}-\mathbf{I}))^2\right)+O(\epsilon^3)}_{O(\epsilon^2)}. \tag{3.64}$$

We compute the relation for $\mathbf{B}^d_{\kappa_{p(t)}}$,

$$\mathbf{B}^d_{\kappa_{p(t)}}=\mathbf{B}_{\kappa_{p(t)}}-\frac{b}{3}\mathbf{I}=$$
$$\mathbf{B}_{\kappa_{p(t)}}-\mathbf{I}-\frac{1}{6}\left(\operatorname{tr}\left((\mathbf{B}_{\kappa_{p(t)}}-\mathbf{I})^2\right)-(\operatorname{tr}(\mathbf{B}_{\kappa_{p(t)}}-\mathbf{I}))^2\right)\mathbf{I}+O(\epsilon^3)\mathbf{I}. \tag{3.65}$$

Further we need to compute $\overset{\triangledown}{\overline{\mathbf{B}^d_{\kappa_{p(t)}}}}$.

$$\overset{\triangledown}{\overline{\mathbf{B}^d_{\kappa_{p(t)}}}}=\overset{\triangledown}{\mathbf{B}}_{\kappa_{p(t)}}-\frac{1}{3}\dot{b}\mathbf{I}+\frac{2}{3}b\mathbf{D}=$$
$$\overset{\triangledown}{\mathbf{B}}_{\kappa_{p(t)}}-\frac{1}{3}\Big(\dot{\mathbf{B}}_{\kappa_{p(t)}}\cdot(\mathbf{B}_{\kappa_{p(t)}}-\mathbf{I})-\dot{b}\underbrace{\operatorname{tr}\left(\mathbf{B}_{\kappa_{p(t)}}-\mathbf{I}\right)}_{O(\epsilon^2)}\Big)\mathbf{I}+\frac{2}{3}b\mathbf{D}. \tag{3.66}$$

Inserting all into (3.63b) we get

$$2\mu_1\left(-\frac{1}{2}\overset{\triangledown}{\mathbf{B}}_{\kappa_{p(t)}}+\frac{1}{6}\left(\dot{\mathbf{B}}_{\kappa_{p(t)}}-2\mathbf{D}\right)\cdot\left(\mathbf{B}_{\kappa_{p(t)}}-\mathbf{I}\right)\mathbf{I}\right)=G\left(\mathbf{B}_{\kappa_{p(t)}}-\mathbf{I}\right)+O(\epsilon^2). \quad (3.67)$$

This model is very similar to Oldroyd-B model (2.10), the difference is in the second term. We show that this term is of the order $O(\epsilon^2)$, and so we will neglect it. We take the scalar product of (3.67) with $\mathbf{B}_{\kappa_{p(t)}}-\mathbf{I}$, and get

$$\begin{aligned}&\mu_1\Big(\overbrace{-\dot{\mathbf{B}}_{\kappa_{p(t)}}+2\mathbf{D}-\mathbf{L}\left(\mathbf{B}_{\kappa_{p(t)}}-\mathbf{I}\right)-\left(\mathbf{B}_{\kappa_{p(t)}}-\mathbf{I}\right)\mathbf{L}^{\mathrm{T}}}^{\overset{\triangledown}{\mathbf{B}}_{\kappa_{p(t)}}}\Big)\cdot\left(\mathbf{B}_{\kappa_{p(t)}}-\mathbf{I}\right)=\\&-\mu_1\frac{1}{6}\left(\dot{\mathbf{B}}_{\kappa_{p(t)}}-2\mathbf{D}\right)\cdot\left(\mathbf{B}_{\kappa_{p(t)}}-\mathbf{I}\right)\underbrace{\operatorname{tr}\left(\mathbf{B}_{\kappa_{p(t)}}-\mathbf{I}\right)}_{O(\epsilon^2)}+G\underbrace{|\mathbf{B}_{\kappa_{p(t)}}-\mathbf{I}|^2}_{O(\epsilon^2)}+O(\epsilon^2). \quad (3.68)\end{aligned}$$

This implies that

$$\left(2\mathbf{D}-\dot{\mathbf{B}}_{\kappa_{p(t)}}\right)\cdot\left(\mathbf{B}_{\kappa_{p(t)}}-\mathbf{I}\right)=O(\epsilon^2).$$

Thus, we show that the non-linear viscoelastic model linearizes to Oldroyd-B model (2.10).

$$\mathbf{T}=-p\mathbf{I}+2\mu_2\mathbf{D}+G\left(\mathbf{B}_{\kappa_{p(t)}}-\mathbf{I}\right), \quad (3.69a)$$

$$\overset{\triangledown}{\mathbf{B}}_{\kappa_{p(t)}}=-\frac{G}{\mu_1}\left(\mathbf{B}_{\kappa_{p(t)}}-\mathbf{I}\right). \quad (3.69b)$$

To conclude, we observed that the linearization of both thermodynamically compatible non-linear viscoelastic models (3.49) and (3.63) ends up with the standard Oldroyd-B model (2.10). Although the models (3.49) and (3.63) look very different, they should be equivalent because they are derived from the same constitutive relations for the internal energy (3.16) and for the rate of entropy production (3.34). The equivalence of both models is shown next.

3.2.3 On equivalence of the models RaSr2000 and MaRa2007

We show the equivalence of both viscoelastic rate-type fluid models (3.49) derived by Rajagopal and Srinivasa and (3.63) derived by Málek and Rajagopal. For reader's convenience we write these two models below, the first one is (3.49) (the initial condition for $\det\mathbf{B}_{\kappa_{p(t)}}$ is needed), the second one is (3.63):

$$\mathbf{T}=-p\mathbf{I}+2\mu_2\mathbf{D}+G\mathbf{B}^d_{\kappa_{p(t)}}, \quad (3.70a)$$

$$\overset{\triangledown}{\mathbf{B}}_{\kappa_{p(t)}}=-\frac{G}{\mu_1}\left(\mathbf{B}_{\kappa_{p(t)}}-\frac{3}{\operatorname{tr}\left(\mathbf{B}^{-1}_{\kappa_{p(t)}}\right)}\mathbf{I}\right), \quad (3.70b)$$

$$\det\mathbf{B}_{\kappa_{p(t)}}(t=0)=1. \quad (3.70c)$$

$$\mathbf{T} = -p\mathbf{I} + 2\mu_2\mathbf{D} + G\mathbf{B}^d_{\kappa_{p(t)}}, \tag{3.71a}$$

$$2\mu_1\left(-\frac{1}{2}\overset{\triangledown}{\mathbf{B}}^d_{\kappa_{p(t)}} - \frac{1}{3}(\mathbf{D}\cdot\mathbf{B}^d_{\kappa_{p(t)}})\mathbf{I} + \frac{1}{3}b\mathbf{D}\right) = G\mathbf{B}^d_{\kappa_{p(t)}}, \tag{3.71b}$$

$$\det\left(\mathbf{B}^d_{\kappa_{p(t)}} + \frac{1}{3}b\mathbf{I}\right) = 1. \tag{3.71c}$$

First we show how to get (3.71) from (3.70). Let split the tensor $\mathbf{B}_{\kappa_{p(t)}}$ into deviatoric and spherical part

$$\mathbf{B}_{\kappa_{p(t)}} = \mathbf{B}^d_{\kappa_{p(t)}} + \frac{1}{3}b\mathbf{I},$$

Equation (3.51) states that

$$\det(\mathbf{B}_{\kappa_{p(t)}}) = \det\left(\mathbf{B}^d_{\kappa_{p(t)}} + \frac{1}{3}b\mathbf{I}\right) = 1$$

and we get the last equation (3.71c). Now take the trace of the equation (3.70b) and divide by 3

$$\frac{1}{3}\left(\frac{\partial b}{\partial t} + (\mathbf{v}\cdot\nabla)b - 2\mathbf{D}\cdot\mathbf{B}_{\kappa_{p(t)}}\right) = -\frac{G}{\mu_1}\left(\frac{b}{3} - \frac{3}{\operatorname{tr}\left(\mathbf{B}^{-1}_{\kappa_{p(t)}}\right)}\right). \tag{3.72}$$

Now we perform (3.70b) $-$ (3.72)$\mathbf{I}$ and multiply the result by μ_1

$$\mu_1\Bigg[\frac{\partial\mathbf{B}_{\kappa_{p(t)}}}{\partial t} + (\mathbf{v}\cdot\nabla)\mathbf{B}_{\kappa_{p(t)}} - \nabla\mathbf{v}\left(\mathbf{B}^d_{\kappa_{p(t)}} + \frac{1}{3}b\mathbf{I}\right) - \left(\mathbf{B}^d_{\kappa_{p(t)}} + \frac{1}{3}b\mathbf{I}\right)(\nabla\mathbf{v})^{\mathrm{T}} - \left(\frac{1}{3}\frac{\partial b}{\partial t} + \frac{1}{3}(\mathbf{v}\cdot\nabla)b\right)\mathbf{I} + \frac{2}{3}(\mathbf{D}\cdot\mathbf{B}_{\kappa_{p(t)}})\mathbf{I}\Bigg] = -G\left(\mathbf{B}_{\kappa_{p(t)}} - \frac{1}{3}b\mathbf{I}\right), \tag{3.73}$$

which is equivalent to (3.71b)

$$\mu_1\left(-\frac{\partial\mathbf{B}^d_{\kappa_{p(t)}}}{\partial t} - (\mathbf{v}\cdot\nabla)\mathbf{B}^d_{\kappa_{p(t)}} + \nabla\mathbf{v}\mathbf{B}^d_{\kappa_{p(t)}} + \mathbf{B}^d_{\kappa_{p(t)}}(\nabla\mathbf{v})^{\mathrm{T}} - \frac{2}{3}(\mathbf{D}\cdot\mathbf{B}^d_{\kappa_{p(t)}})\mathbf{I} + \frac{2}{3}\left(\operatorname{tr}\mathbf{B}_{\kappa_{p(t)}}\right)\mathbf{D}\right) = G\mathbf{B}^d_{\kappa_{p(t)}}.$$

Further, we show how to get (3.70) from (3.71). We apply a material time derivative on (3.71b) using (B.3) from Appendix

$$0 = \frac{\mathrm{d}\ln(\det\mathbf{B}_{\kappa_{p(t)}})}{\mathrm{d}t} = \operatorname{tr}\left(\frac{\mathrm{d}\mathbf{B}_{\kappa_{p(t)}}}{\mathrm{d}t}\mathbf{B}^{-1}_{\kappa_{p(t)}}\right).$$

Since (3.73) is equivalent to (3.71b), we multiply (3.73) by $\mathbf{B}^{-1}_{\kappa_{p(t)}}$ and take the trace of this product

$$\mu_1\left(\operatorname{tr}\left(\frac{\mathrm{d}\mathbf{B}_{\kappa_{p(t)}}}{\mathrm{d}t}\mathbf{B}^{-1}_{\kappa_{p(t)}}\right) - 2\operatorname{tr}\mathbf{D} - \frac{1}{3}\frac{\mathrm{d}b}{\mathrm{d}t}\operatorname{tr}\left(\mathbf{B}^{-1}_{\kappa_{p(t)}}\right)\right) + \frac{2}{3}\mu_1(\mathbf{D}\cdot\mathbf{B}_{\kappa_{p(t)}})\operatorname{tr}\left(\mathbf{B}^{-1}_{\kappa_{p(t)}}\right) = -G\left(3 - b\frac{\operatorname{tr}\left(\mathbf{B}^{-1}_{\kappa_{p(t)}}\right)}{3}\right). \tag{3.74}$$

The first two terms are equal to zero. We can express $\operatorname{tr}\mathbf{B}^{-1}_{\kappa_{p(t)}}$ from (3.74)

$$\operatorname{tr}\left(\mathbf{B}^{-1}_{\kappa_{p(t)}}\right) = \frac{3G}{\mu_1\left(\frac{1}{3}\frac{\mathrm{d}b}{\mathrm{d}t} - \frac{2}{3}(\mathbf{D}\cdot\mathbf{B}_{\kappa_{p(t)}})\right) + G\frac{b}{3}} \Rightarrow$$

$$\Rightarrow\ \mu_1\left(\frac{1}{3}\frac{\mathrm{d}b}{\mathrm{d}t} - \frac{2}{3}(\mathbf{D}\cdot\mathbf{B}_{\kappa_{p(t)}})\right) + G\frac{b}{3} = \frac{3G}{\operatorname{tr}\left(\mathbf{B}^{-1}_{\kappa_{p(t)}}\right)} \tag{3.75}$$

and substitute it into (3.73)

$$\mu_1\left(\frac{\partial\mathbf{B}_{\kappa_{p(t)}}}{\partial t} + (\mathbf{v}\cdot\nabla)\mathbf{B}_{\kappa_{p(t)}} - \nabla\mathbf{v}\mathbf{B}_{\kappa_{p(t)}} - \mathbf{B}_{\kappa_{p(t)}}(\nabla\mathbf{v})^{\mathrm{T}}\right) = G\left(\frac{3}{\operatorname{tr}\left(\mathbf{B}^{-1}_{\kappa_{p(t)}}\right)}\mathbf{I} - \mathbf{B}_{\kappa_{p(t)}}\right)$$

which is after division by μ_1 equivalent to (3.70).

3.2.4 Models RaSr2000 and MaRa2007 in two-dimensional space

The models (3.49) and (3.63) are derived in a three-dimensional space where $\operatorname{tr}\mathbf{I} = 3$. In two-dimensional space the derivation has to be slightly modified, the constitutive relation for the internal energy (incompressible neo-Hookean) is then in form

$$e = e_0(\eta,\rho) + \frac{G}{2\rho}\left(\operatorname{tr}\mathbf{B}_{\kappa_{p(t)}} - 2\right). \tag{3.76}$$

and it holds that $\operatorname{tr}\mathbf{I} = 2$. Then (3.49) modifies to

$$\mathbf{T} = -p\mathbf{I} + 2\mu_2\mathbf{D} + G\mathbf{B}^d_{\kappa_{p(t)}}, \tag{3.77a}$$

$$\overset{\triangledown}{\mathbf{B}}_{\kappa_{p(t)}} = -\frac{G}{\mu_1}\left(\mathbf{B}_{\kappa_{p(t)}} - \frac{2}{\operatorname{tr}\left(\mathbf{B}^{-1}_{\kappa_{p(t)}}\right)}\mathbf{I}\right) \tag{3.77b}$$

and (3.63) modifies to

$$\mathbf{T} = -p\mathbf{I} + 2\mu_2\mathbf{D} + G\mathbf{B}^d_{\kappa_{p(t)}}, \tag{3.78a}$$

$$\mu_1\left(-\overset{\triangledown}{\mathbf{B}}^d_{\kappa_{p(t)}} - (\mathbf{D}\cdot\mathbf{B}^d_{\kappa_{p(t)}})\mathbf{I} + b\mathbf{D}\right) = G\mathbf{B}^d_{\kappa_{p(t)}}, \tag{3.78b}$$

$$\det\left(\mathbf{B}^d_{\kappa_{p(t)}} + \frac{1}{2}b\mathbf{I}\right) = 1, \tag{3.78c}$$

where $b = \operatorname{tr}\mathbf{B}_{\kappa_{p(t)}}$.

Alternative form of model (3.77) in 2D

Using the derived property $\det\mathbf{B}_{\kappa_{p(t)}} = 1$ and the Lemma B.1.5 we obtain the alternative form of the model (3.77). Using (B.16) we modify the term $2/\operatorname{tr}\left(\mathbf{B}^{-1}_{\kappa_{p(t)}}\right)$

$$\frac{2}{\operatorname{tr}\left(\mathbf{B}^{-1}_{\kappa_{p(t)}}\right)} = \frac{2\det\mathbf{B}_{\kappa_{p(t)}}}{\operatorname{tr}\mathbf{B}_{\kappa_{p(t)}}} = \frac{2}{\operatorname{tr}\mathbf{B}_{\kappa_{p(t)}}} \tag{3.79}$$

and the model is then described by

$$\mathbf{T} = -p\mathbf{I} + 2\mu_2\mathbf{D} + G\mathbf{B}^d_{\kappa_{p(t)}}, \tag{3.80a}$$

$$\overset{\triangledown}{\mathbf{B}}_{\kappa_{p(t)}} = -\frac{G}{\mu_1}\left(\mathbf{B}_{\kappa_{p(t)}} - \frac{2}{\operatorname{tr}\mathbf{B}_{\kappa_{p(t)}}}\mathbf{I}\right). \tag{3.80b}$$

3.3 Power-law like viscoelastic model PL2012

We derive a power law like viscoelastic model, we suppose that the model is fully incompressible (III) and the constitutive relation for the rate of entropy production $\tilde{\xi}$ is in the form

$$\tilde{\xi} = \epsilon_1\left(\epsilon_0 + |\mathbf{D}|^2\right)^{\alpha-1}|\mathbf{D}|^2 + \epsilon_2\left(\mathbf{D}_{\kappa_{p(t)}}\mathbf{C}_{\kappa_{p(t)}}\cdot\mathbf{D}_{\kappa_{p(t)}}\right)^{\beta} \tag{3.81}$$

for $\epsilon_0 > 0$, $\epsilon_1 > 0$, $\epsilon_2 > 0$, $\alpha \in \mathbb{R}$, $\beta > 0.5$. Note that

$$\mathbf{D}_{\kappa_{p(t)}}\mathbf{C}_{\kappa_{p(t)}}\cdot\mathbf{D}_{\kappa_{p(t)}} = |\mathbf{F}_{\kappa_{p(t)}}\mathbf{D}_{\kappa_{p(t)}}|^2 \geq 0.$$

The reason why we consider $\beta > 0.5$ comes from the analogy related to the standard power-law fluid model with dissipation in the form $|\mathbf{D}|^{2\beta}$. In order to give a clear meaning to the term $|\mathbf{D}|^{2(\beta-1)}\mathbf{D}$ that occurs in the formula for the Cauchy stress (in standard power-law model) we need that $2(\beta-1) \geq -1$. Here, we require the strict inequality that leads to $\beta > 0.5$.

Similar model was proposed by Anand, Rajagopal [1] (see also [36]) where they used

$$\tilde{\xi} = \epsilon_1\mathbf{D}\cdot\mathbf{D} + \epsilon_2\left(\mathbf{D}_{\kappa_{p(t)}}\mathbf{B}_{\kappa_{p(t)}}\cdot\mathbf{D}_{\kappa_{p(t)}}\right)^{\beta}.$$

The main difference was that they did not maximize ξ among all values of $\mathbf{D}$ and $\mathbf{D}_{\kappa_{p(t)}}$, but they maximized separately the term $\epsilon_1\mathbf{D}\cdot\mathbf{D}$ over $\mathbf{D}$ and $\epsilon_2\left(\mathbf{D}_{\kappa_{p(t)}}\mathbf{B}_{\kappa_{p(t)}}\cdot\mathbf{D}_{\kappa_{p(t)}}\right)^{\beta}$ over $\mathbf{D}_{\kappa_{p(t)}}$ which is much simpler than maximizing $\tilde{\xi}$ among $\mathbf{D}$ and $\mathbf{D}_{\kappa_{p(t)}}$.

We now maximize $\tilde{\xi}(\mathbf{D}, \mathbf{D}_{\kappa_{p(t)}}, \mathbf{C}_{\kappa_{p(t)}})$ among the values of $\mathbf{D}$ and $\mathbf{D}_{\kappa_{p(t)}}$ fulfilling the reduced thermodynamic inequality (3.21) and the constraints of incompressibility $\operatorname{tr}\mathbf{D} = \operatorname{tr}\mathbf{D}_{\kappa_{p(t)}} = 0$. For this purpose we adopt the method of Lagrange multipliers. Let us define the Lagrange function

$$\begin{aligned} L(\mathbf{D}, \mathbf{D}_{\kappa_{p(t)}}) :=& \tilde{\xi}(\mathbf{D}, \mathbf{D}_{\kappa_{p(t)}}, \mathbf{C}_{\kappa_{p(t)}}) - \lambda_2\operatorname{tr}\mathbf{D} - \lambda_3\operatorname{tr}\mathbf{D}_{\kappa_{p(t)}} + \\ & \lambda_1\left(\tilde{\xi}(\mathbf{D}, \mathbf{D}_{\kappa_{p(t)}}, \mathbf{C}_{\kappa_{p(t)}}) - (\mathbf{T} - G\mathbf{B}_{\kappa_{p(t)}})\cdot\mathbf{D} - G\mathbf{C}_{\kappa_{p(t)}}\cdot\mathbf{D}_{\kappa_{p(t)}}\right) \end{aligned}$$

and maximize it

$$\frac{1+\lambda_1}{\lambda_1}2\epsilon_1\left(\epsilon_0 + |\mathbf{D}|^2\right)^{\alpha-2}\left(\epsilon_0 + \alpha|\mathbf{D}|^2\right)\mathbf{D} = \mathbf{T} - G\mathbf{B}_{\kappa_{p(t)}} + \frac{\lambda_2}{\lambda_1}\mathbf{I}, \tag{3.82}$$

$$\frac{1+\lambda_1}{\lambda_1}2\beta\epsilon_2\left(\mathbf{D}_{\kappa_{p(t)}}\mathbf{C}_{\kappa_{p(t)}}\cdot\mathbf{D}_{\kappa_{p(t)}}\right)^{\beta-1}\mathbf{D}_{\kappa_{p(t)}}\mathbf{C}_{\kappa_{p(t)}} = G\mathbf{C}_{\kappa_{p(t)}} + \frac{\lambda_3}{\lambda_1}\mathbf{I}, \tag{3.83}$$

where the Lagrange multipliers λ_1, λ_2 and λ_3 have to be determined. To accomplish this we first take the scalar product of (3.82) with $\mathbf{D}$ and (3.83) with $\mathbf{D}_{\kappa_{p(t)}}$ and sum these products. With help of (3.81) and (3.22) we conclude that

$$2\frac{1+\lambda_1}{\lambda_1} = \frac{\epsilon_1\left(\epsilon_0+|\mathbf{D}|^2\right)^{\alpha-1}|\mathbf{D}|^2+\epsilon_2\left(\mathbf{D}_{\kappa_{p(t)}}\mathbf{C}_{\kappa_{p(t)}}\cdot\mathbf{D}_{\kappa_{p(t)}}\right)^{\beta}}{\epsilon_1\left(\epsilon_0+|\mathbf{D}|^2\right)^{\alpha-2}\left(\epsilon_0+\alpha|\mathbf{D}|^2\right)|\mathbf{D}|^2+\beta\epsilon_2\left(\mathbf{D}_{\kappa_{p(t)}}\mathbf{C}_{\kappa_{p(t)}}\cdot\mathbf{D}_{\kappa_{p(t)}}\right)^{\beta}}. \tag{3.84}$$

Let Y denote the right hand side of (3.84). Obviously, $Y \geq 0$. Next we take the trace of (3.82), which delivers

$$\frac{\lambda_2}{\lambda_1} = -\frac{1}{3}\operatorname{tr}(\mathbf{T}-G\mathbf{B}_{\kappa_{p(t)}}). \tag{3.85}$$

We define a quantity p through

$$p = -\frac{1}{3}\operatorname{tr}\mathbf{T}. \tag{3.86}$$

Substitution of (3.86) and (3.85) into (3.82) yields

$$\mathbf{T} = -p\mathbf{I}+Y\epsilon_1\left(\epsilon_0+|\mathbf{D}|^2\right)^{\alpha-2}\left(\epsilon_0+\alpha|\mathbf{D}|^2\right)\mathbf{D}+G\mathbf{B}^d_{\kappa_{p(t)}}. \tag{3.87}$$

Multiplying the equation (3.83) by $\mathbf{C}^{-1}_{\kappa_{p(t)}}$ from the right and taking its trace we obtain (using incompressibility constraint (3.12))

$$\frac{\lambda_3}{\lambda_1} = -\frac{3G}{\operatorname{tr}(\mathbf{C}^{-1}_{\kappa_{p(t)}})} =: -\lambda G. \tag{3.88}$$

Rewriting the equation (3.83) using the variable Y we have

$$Y\beta\epsilon_2\left(\mathbf{D}_{\kappa_{p(t)}}\mathbf{C}_{\kappa_{p(t)}}\cdot\mathbf{D}_{\kappa_{p(t)}}\right)^{\beta-1}\mathbf{D}_{\kappa_{p(t)}}\mathbf{C}_{\kappa_{p(t)}} = G\left(\mathbf{C}_{\kappa_{p(t)}}-\lambda\mathbf{I}\right). \tag{3.89}$$

Our aim is to get an equation only for $\mathbf{C}_{\kappa_{p(t)}}$, that is why $\mathbf{D}_{\kappa_{p(t)}}$ has to be eliminated out of (3.89). This is done in the following way. Taking the trace of (3.89) we get

$$Y\beta\epsilon_2\left(\mathbf{D}_{\kappa_{p(t)}}\mathbf{C}_{\kappa_{p(t)}}\cdot\mathbf{D}_{\kappa_{p(t)}}\right)^{\beta-1}\mathbf{D}_{\kappa_{p(t)}}\cdot\mathbf{C}_{\kappa_{p(t)}} = G\left(\operatorname{tr}\mathbf{C}_{\kappa_{p(t)}}-3\lambda\right) \tag{3.90}$$

and multiplying (3.89) by $\mathbf{D}_{\kappa_{p(t)}}$ we obtain

$$Y\beta\epsilon_2\left(\mathbf{D}_{\kappa_{p(t)}}\mathbf{C}_{\kappa_{p(t)}}\cdot\mathbf{D}_{\kappa_{p(t)}}\right)^{\beta} = G\mathbf{C}_{\kappa_{p(t)}}\cdot\mathbf{D}_{\kappa_{p(t)}}. \tag{3.91}$$

Inserting (3.91) into (3.90) we get the equation for $\mathbf{D}_{\kappa_{p(t)}}\mathbf{C}_{\kappa_{p(t)}}\cdot\mathbf{D}_{\kappa_{p(t)}}$:

$$Y^2\beta^2\epsilon_2^2\left(\mathbf{D}_{\kappa_{p(t)}}\mathbf{C}_{\kappa_{p(t)}}\cdot\mathbf{D}_{\kappa_{p(t)}}\right)^{2\beta-1} = G^2\left(\operatorname{tr}\mathbf{C}_{\kappa_{p(t)}}-3\lambda\right), \tag{3.92}$$

which implies that

$$\operatorname{tr}\mathbf{C}_{\kappa_{p(t)}}-3\lambda \geq 0.$$

Now on taking the square root of (3.92) we find that

$$Y\beta\epsilon_2\left(\mathbf{D}_{\kappa_{p(t)}}\mathbf{C}_{\kappa_{p(t)}}\cdot\mathbf{D}_{\kappa_{p(t)}}\right)^{\beta-1}\sqrt{\mathbf{D}_{\kappa_{p(t)}}\mathbf{C}_{\kappa_{p(t)}}\cdot\mathbf{D}_{\kappa_{p(t)}}} = G\sqrt{\operatorname{tr}\mathbf{C}_{\kappa_{p(t)}}-3\lambda}. \tag{3.93}$$

To prevent dividing by zero, β has to be greater than 0.5. Multiplying (3.89) by $\mathbf{F}_{\kappa_{p(t)}}$ from the left and by $\mathbf{F}^{-1}_{\kappa_{p(t)}}$ from the right, using (3.5) and (3.93) we arrive at

$$\sqrt{\operatorname{tr}\mathbf{B}_{\kappa_{p(t)}} - 3\lambda}\ \overset{\triangledown}{\mathbf{B}}_{\kappa_{p(t)}} = -2\sqrt{\mathbf{D}_{\kappa_{p(t)}}\mathbf{C}_{\kappa_{p(t)}}\cdot\mathbf{D}_{\kappa_{p(t)}}}\left(\mathbf{B}_{\kappa_{p(t)}} - \lambda\mathbf{I}\right). \tag{3.94}$$

If we denote the last term

$$X = \mathbf{D}_{\kappa_{p(t)}}\mathbf{C}_{\kappa_{p(t)}}\cdot\mathbf{D}_{\kappa_{p(t)}},$$

we can obtain an expression for it from the equation (3.92), i.e.,

$$\beta^2\epsilon_2^2 Y^2 X^{2\beta-1} = G^2\left(\operatorname{tr}\mathbf{B}_{\kappa_{p(t)}} - 3\lambda\right), \tag{3.95}$$

where by (3.84)

$$Y = \frac{\frac{\epsilon_1}{\epsilon_2}\left(\epsilon_0 + |\mathbf{D}|^2\right)^{\alpha-1}|\mathbf{D}|^2 + X^\beta}{\frac{\epsilon_1}{\epsilon_2}\left(\epsilon_0 + |\mathbf{D}|^2\right)^{\alpha-2}\left(\epsilon_0 + \alpha|\mathbf{D}|^2\right)|\mathbf{D}|^2 + \beta X^\beta}. \tag{3.96}$$

Then, we obtain the following model

$$\mathbf{T} + p\mathbf{I} = Y\epsilon_1\left(\epsilon_0 + |\mathbf{D}|^2\right)^{\alpha-2}\left(\epsilon_0 + \alpha|\mathbf{D}|^2\right)\mathbf{D} + G\mathbf{B}^d_{\kappa_{p(t)}}, \tag{3.97a}$$

$$\sqrt{\operatorname{tr}\mathbf{B}_{\kappa_{p(t)}} - 3\lambda}\ \overset{\triangledown}{\mathbf{B}}_{\kappa_{p(t)}} = -2\sqrt{X}\left(\mathbf{B}_{\kappa_{p(t)}} - \lambda\mathbf{I}\right), \tag{3.97b}$$

where Y is defined through (3.96), X is the solution of (3.95) and λ is defined through (3.88). Using (B.17) we can modify λ

$$\lambda = \frac{3}{\operatorname{tr}\left(\mathbf{B}^{-1}_{\kappa_{p(t)}}\right)} = \frac{6\det\mathbf{B}_{\kappa_{p(t)}}}{(\operatorname{tr}\mathbf{B}_{\kappa_{p(t)}})^2 - \operatorname{tr}\left(\mathbf{B}^2_{\kappa_{p(t)}}\right)} = \frac{6}{(\operatorname{tr}\mathbf{B}_{\kappa_{p(t)}})^2 - \operatorname{tr}\left(\mathbf{B}^2_{\kappa_{p(t)}}\right)}. \tag{3.98}$$

Notice that for $\alpha < 1$ one gets shear thinning and for $\alpha > 1$ shear thickening model.

For $\alpha = \beta = 1$ this model reduces to the RaSr2000 model (3.49)

$$\mathbf{T} = -p\mathbf{I} + \epsilon_1\mathbf{D} + G\mathbf{B}^d_{\kappa_{p(t)}}, \tag{3.99a}$$

$$\overset{\triangledown}{\mathbf{B}}_{\kappa_{p(t)}} = -2\frac{G}{\epsilon_2}\left(\mathbf{B}_{\kappa_{p(t)}} - \lambda\mathbf{I}\right). \tag{3.99b}$$

3.4 Incompressible viscoelastic model with purely quadratic dissipation Quad1

Further model that is derived is again fully incompressible (III) with purely quadratic form of the constitutive relation for the rate of entropy production

$$\tilde{\xi}(\mathbf{D}, \mathbf{D}_{\kappa_{p(t)}}) = 2\mu_2\mathbf{D}\cdot\mathbf{D} + 2\mu_1\mathbf{D}_{\kappa_{p(t)}}\cdot\mathbf{D}_{\kappa_{p(t)}}, \tag{3.100}$$

where $\mu_1, \mu_2 > 0$ and thus $\tilde{\xi} \geq 0$ – the second law of thermodynamics is automatically satisfied.

In order to use the principle of maximization of the rate of entropy production, we maximize $\tilde{\xi}(\mathbf{D}, \mathbf{D}_{\kappa_{p(t)}})$ among the values of $\mathbf{D}, \mathbf{D}_{\kappa_{p(t)}}$ fulfilling the equality (3.21) and

the constraints of incompressibility (3.12).

We define the Lagrange function

$$L(\mathbf{D},\mathbf{D}_{\kappa_{p(t)}}) = \tilde{\xi}(\mathbf{D},\mathbf{D}_{\kappa p(t)},\mathbf{C}_{\kappa_{p(t)}}) - \lambda_2 \operatorname{tr}\mathbf{D} - \lambda_3 \operatorname{tr}\mathbf{D}_{\kappa_{p(t)}} + \lambda_1\left(\tilde{\xi}(\mathbf{D},\mathbf{D}_{\kappa p(t)}) - \left(\mathbf{T} - G\mathbf{B}_{\kappa_{p(t)}}\right)\cdot\mathbf{D} - G\mathbf{C}_{\kappa_{p(t)}}\cdot\mathbf{D}_{\kappa_{p(t)}}\right) \tag{3.101}$$

and find the extremes of $\mathbf{L}$. The necessary conditions are

$$\frac{\partial L}{\partial \mathbf{D}} = 0, \quad \frac{\partial L}{\partial \mathbf{D}_{\kappa_{p(t)}}} = 0.$$

We substitute for L and $\tilde{\xi}$ and obtain

$$\frac{1+\lambda_1}{\lambda_1}4\mu_2\mathbf{D} = \mathbf{T} - G\mathbf{B}_{\kappa_{p(t)}} + \frac{\lambda_2}{\lambda_1}\mathbf{I}, \tag{3.102}$$

$$\frac{1+\lambda_1}{\lambda_1}4\mu_1\mathbf{D}_{\kappa_{p(t)}} = G\mathbf{C}_{\kappa_{p(t)}} + \frac{\lambda_3}{\lambda_1}\mathbf{I}. \tag{3.103}$$

Further we eliminate the Lagrange multipliers, we perform (3.102) $\cdot\,\mathbf{D}$ + (3.103) $\cdot\,\mathbf{D}_{\kappa_{p(t)}}$, and use the constraints of incompressibility

$$\frac{1+\lambda_1}{\lambda_1} = \frac{\left(\mathbf{T} - G\mathbf{B}_{\kappa_{p(t)}}\right)\cdot\mathbf{D} + G\mathbf{C}_{\kappa_{p(t)}}\cdot\mathbf{D}_{\kappa_{p(t)}}}{4\mu_2\mathbf{D}\cdot\mathbf{D} + 4\mu_1\mathbf{D}_{\kappa_{p(t)}}\cdot\mathbf{D}_{\kappa_{p(t)}}} = \frac{\xi}{2\tilde{\xi}} = \frac{1}{2}. \tag{3.104}$$

Next we take the trace of (3.102) and eliminate λ_2/λ_1 which together with (3.104) gives

$$\frac{\lambda_2}{\lambda_1} = -\frac{1}{3}\operatorname{tr}\left(\mathbf{T} - G\mathbf{B}_{\kappa_{p(t)}}\right). \tag{3.105}$$

We define a pressure p as mean normal stress

$$p = -\frac{1}{3}\operatorname{tr}\mathbf{T}. \tag{3.106}$$

Substitution of (3.106), (3.105), (3.104) into (3.102) gives

$$\mathbf{T} = -p\mathbf{I} + 2\mu_2\mathbf{D} + G\mathbf{B}^d_{\kappa_{p(t)}}. \tag{3.107}$$

Now we insert (3.104) into (3.103)

$$2\mu_1\mathbf{D}_{\kappa_{p(t)}} = G\mathbf{C}_{\kappa_{p(t)}} + \frac{\lambda_3}{\lambda_1}\mathbf{I}, \tag{3.108}$$

and by taking trace of (3.108) we eliminate λ_3/λ_1

$$\frac{\lambda_3}{\lambda_1} = -\frac{G}{3}(\operatorname{tr}\mathbf{C}_{\kappa_{p(t)}})\mathbf{I}. \tag{3.109}$$

Multiplying (3.108) from the left by $\mathbf{F}_{\kappa_{p(t)}}$ and from the right by $\mathbf{F}^{\mathrm{T}}_{\kappa_{p(t)}}$, and using (3.109) we obtain

$$2\mu_1\mathbf{F}_{\kappa_{p(t)}}\mathbf{D}_{\kappa_{p(t)}}\mathbf{F}^{\mathrm{T}}_{\kappa_{p(t)}} = G\mathbf{B}_{\kappa_{p(t)}}\left(\mathbf{B}_{\kappa_{p(t)}} - \frac{1}{3}(\operatorname{tr}\mathbf{B}_{\kappa_{p(t)}})\mathbf{I}\right). \tag{3.110}$$

By comparing the left-hand-side of (3.110) with (3.5) we get

$$\overset{\triangledown}{\mathbf{B}}_{\kappa_{p(t)}} = -\frac{G}{\mu_1}\mathbf{B}_{\kappa_{p(t)}}\mathbf{B}^d_{\kappa_{p(t)}}. \tag{3.111}$$

We obtain

$$\mathbf{T} = -p\mathbf{I} + 2\mu_2\mathbf{D} + G\mathbf{B}^d_{\kappa_{p(t)}}, \tag{3.112a}$$

$$\overset{\triangledown}{\mathbf{B}}_{\kappa_{p(t)}} = -\frac{G}{\mu_1}\mathbf{B}_{\kappa_{p(t)}}\mathbf{B}^d_{\kappa_{p(t)}}. \tag{3.112b}$$

We call this model Quad1.

Note: Incompressible model with purely quadratic dissipation (3.112) can be simply modified in order to obtain model with pressure dependent (typically pressure thickening) viscosities μ_1 and μ_2. If we assume the constitutive relation for the rate of entropy production in the form

$$\tilde{\xi}(\mathbf{D}, \mathbf{D}_{\kappa_{p(t)}}) = 2\mu_2(p)\mathbf{D}\cdot\mathbf{D} + 2\mu_1(p)\mathbf{D}_{\kappa_{p(t)}}\cdot\mathbf{D}_{\kappa_{p(t)}}, \tag{3.113}$$

where μ_1 and μ_2 are positive functions of the pressure p, we obtain model

$$\mathbf{T} = -p\mathbf{I} + 2\mu_2(p)\mathbf{D} + G\mathbf{B}^d_{\kappa_{p(t)}} \tag{3.114a}$$

$$\overset{\triangledown}{\mathbf{B}}_{\kappa_{p(t)}} = -\frac{G}{\mu_1(p)}\mathbf{B}_{\kappa_{p(t)}}\mathbf{B}^d_{\kappa_{p(t)}}. \tag{3.114b}$$

3.4.1 Alternative derivation of the model Quad1

Model (3.112) can be also achieved if we start with the assumption that

$$\tilde{\xi}(\mathbf{T}^d_{\text{dis}}, \mathbf{C}^d_{\kappa_{p(t)}}) = \frac{1}{2\mu_2}|\mathbf{T}^d_{\text{dis}}|^2 + \frac{G^2}{2\mu_1}|\mathbf{C}^d_{\kappa_{p(t)}}|^2, \tag{3.115}$$

where thermodynamic fluxes $\mathbf{T}^d_{\text{dis}}, \mathbf{C}^d_{\kappa_{p(t)}}$ are preferred to thermodynamic affinities $\mathbf{D}$, $\mathbf{D}_{\kappa_{p(t)}}$, similarly as in [37] where this idea was used for derivation of generalized Newtonian models, $\mathbf{T}^d_{\text{dis}} = \mathbf{T}^d - G\mathbf{B}^d_{\kappa_{p(t)}}$. We use reduced thermodynamic inequality (3.22) which assumes incompressibility conditions (3.12). Let us denote

$$L(\mathbf{T}^d_{\text{dis}}, \mathbf{C}^d_{\kappa_{p(t)}}) := \mathbf{T}^d_{\text{dis}}\cdot\mathbf{D}^d + G\mathbf{C}^d_{\kappa_{p(t)}}\cdot\mathbf{D}^d_{\kappa_{p(t)}} - \tilde{\xi}(\mathbf{T}^d_{\text{dis}}, \mathbf{C}^d_{\kappa_{p(t)}}) \tag{3.116}$$

and maximize $\tilde{\xi}(\mathbf{T}^d_{\text{dis}}, \mathbf{C}^d_{\kappa_{p(t)}})$ among the values of $\mathbf{T}^d_{\text{dis}}$ and $\mathbf{C}^d_{\kappa_{p(t)}}$ fulfilling the reduced thermodynamic inequality

$$0 = L(\mathbf{T}^d_{\text{dis}}, \mathbf{C}^d_{\kappa_{p(t)}}). \tag{3.117}$$

We use Lagrange multipliers which delivers the following set of equations

$$\frac{\partial\tilde{\xi}}{\partial\mathbf{T}\text{dis}^d} = \lambda_1\frac{\partial L}{\partial\mathbf{T}^d_{\text{dis}}}, \tag{3.118}$$

$$\frac{\partial\tilde{\xi}}{\partial\mathbf{C}^d_{\kappa_{p(t)}}} = \lambda_1\frac{\partial L}{\partial\mathbf{C}^d_{\kappa_{p(t)}}}, \tag{3.119}$$

that can be simplified to

$$\frac{1+\lambda_1}{\lambda_1}\frac{1}{\mu_2}\mathbf{T}^d_{\text{dis}} = \mathbf{D}^d, \tag{3.120}$$

$$\frac{1+\lambda_1}{\lambda_1}\frac{G^2}{\mu_1}\mathbf{C}^d_{\kappa_{p(t)}} = G\mathbf{D}^d_{\kappa_{p(t)}}. \tag{3.121}$$

We determine λ_1 by taking the scalar product of (3.120) with $\mathbf{T}^d_{\text{dis}}$ and (3.121) with $\mathbf{C}^d_{\kappa_{p(t)}}$ and sum these products. With help of (3.22) we conclude that

$$2\frac{1+\lambda_1}{\lambda_1} = 1$$

and get

$$\mathbf{T}^d_{\text{dis}} = 2\mu_2\mathbf{D}^d \Rightarrow \mathbf{T} = -p\mathbf{I} + 2\mu_2\mathbf{D}^d + G\mathbf{B}^d_{\kappa_{p(t)}}, \text{ where } p = -\frac{1}{3}\operatorname{tr}\mathbf{T}\,, \tag{3.122}$$

$$2\mathbf{D}_{\kappa_{p(t)}} = \frac{G}{\mu_1}\mathbf{C}^d_{\kappa_{p(t)}}\,. \tag{3.123}$$

Multiplying (3.123) by $\mathbf{F}_{\kappa_{p(t)}}$ from the left and by $\mathbf{F}^{\mathrm{T}}_{\kappa_{p(t)}}$ from the right, using (3.5) we arrive at

$$\overset{\triangledown}{\mathbf{B}}_{\kappa_{p(t)}} = -\frac{G}{\mu_1}\mathbf{B}_{\kappa_{p(t)}}\mathbf{B}^d_{\kappa_{p(t)}}\,. \tag{3.124}$$

which together with (3.122) fives again model Quad1, see (3.112).

3.4.2 Properties of model Quad1

Model (3.112) has similar properties as model (3.49), we show some properties of matrix $\mathbf{B}_{\kappa_{p(t)}}$. At the beginning (at rest) $\mathbf{B}_{\kappa_{p(t)}}(t=0) = \mathbf{I}$ is a symmetric positive definite matrix with $\det\mathbf{B}_{\kappa_{p(t)}}(t=0) = 1$. Using (B.3) from the Appendix we get

$$\frac{\mathrm{d}}{\mathrm{d}t}\ln(\det\mathbf{B}_{\kappa_{p(t)}}) = \operatorname{tr}\left(\dot{\mathbf{B}}_{\kappa_{p(t)}}\mathbf{B}^{-1}_{\kappa_{p(t)}}\right) \overset{(3.112\text{b})}{=} 2\operatorname{tr}\mathbf{D} - \frac{G}{\mu_1}\operatorname{tr}\mathbf{B}^d_{\kappa_{p(t)}} = 0 \tag{3.125}$$

and

$$\det\mathbf{B}_{\kappa_{p(t)}}(t) = 1 \ \forall t \geq 0 \tag{3.126}$$

which means that the evolutionary equation (3.112b) includes the incompressibility condition of the elastic response (3.9). Further, using Lemma B.1.2 from Appendix we get the relation the trace of $\mathbf{B}_{\kappa_{p(t)}}$

$$\operatorname{tr}\mathbf{B}_{\kappa_{p(t)}} \geq d \text{ where } d \text{ is space dimension.} \tag{3.127}$$

3.4.3 Linearization of model Quad1

We show that the model Quad1 reduces to Oldroyd-B model (2.10) when the elastic response is linearized. Again, suppose that the left Cauchy-Green tensor is small $\|\mathbf{B}_{\kappa_{p(t)}} - \mathbf{I}\| = \epsilon, \quad 0 < \epsilon \ll 1$. We use (3.126) in the Taylor expansion of determinant and obtain

$$1 = \det\left(\mathbf{I} + \mathbf{B}_{\kappa_{p(t)}} - \mathbf{I}\right) = 1 + \operatorname{tr}(\mathbf{B}_{\kappa_{p(t)}} - \mathbf{I}) + O(\epsilon^2) \quad \Rightarrow \quad \operatorname{tr}(\mathbf{B}_{\kappa_{p(t)}}) = 3 + O(\epsilon^2). \tag{3.128}$$

Now we insert (3.55) into (3.112) and obtain

$$\mathbf{T} = -p\mathbf{I} + 2\mu_2\mathbf{D} + G\left(\mathbf{B}_{\kappa_{p(t)}} - \mathbf{I} + O(\epsilon^2)\mathbf{I}\right), \tag{3.129a}$$

$$\overset{\triangledown}{\mathbf{B}}_{\kappa_{p(t)}} = -\frac{G}{\mu_1}\frac{\left(\mathbf{B}_{\kappa_{p(t)}} - \mathbf{I} + \mathbf{I}\right)\underbrace{\left(\mathbf{B}_{\kappa_{p(t)}} - (1+O(\epsilon^2))\mathbf{I}\right)}}{\underbrace{(\mathbf{B}_{\kappa_{p(t)}} - \mathbf{I})^2}_{O(\epsilon^2)} + \left(\mathbf{B}_{\kappa_{p(t)}} - \mathbf{I} + O(\epsilon^2)\right)}, \tag{3.129b}$$

after neglecting the terms of the order $O(\epsilon^2)$ we obtain Oldroyd-B model (2.10)

$$\mathbf{T} = -p\mathbf{I} + 2\mu_2\mathbf{D} + G\left(\mathbf{B}_{\kappa_{p(t)}} - \mathbf{I}\right), \tag{3.130a}$$

$$\overset{\triangledown}{\mathbf{B}}_{\kappa_{p(t)}} = -\frac{G}{\mu_1}\left(\mathbf{B}_{\kappa_{p(t)}} - \mathbf{I}\right). \tag{3.130b}$$

Alternative form of model with purely quadratic dissipation in 2D

Using the derived property $\det \mathbf{B}_{\kappa_{p(t)}} = 1$ and the Lemma B.1.6 we obtain the alternative form of the model (3.112) in two-dimensional space

$$\mathbf{T} = -p\mathbf{I} + 2\mu_2\mathbf{D} + G\mathbf{B}^d_{\kappa_{p(t)}}, \tag{3.131a}$$

$$\overset{\triangledown}{\mathbf{B}}_{\kappa_{p(t)}} = -\frac{G}{\mu_1}\left(\frac{\operatorname{tr}\mathbf{B}_{\kappa_{p(t)}}}{2}\mathbf{B}_{\kappa_{p(t)}} - \mathbf{I}\right). \tag{3.131b}$$

By comparing this alternative form with alternative form of RaSr2000 (3.80) we find out that both models are very similar in two-dimensional space.

3.5 Incompressible mixed power-law like model

Using the maximization with respect to thermodynamic fluxes as in previous two sections we derive an incompressible power-law like model with the Cauchy stress tensor that is similar to the Cauchy stress tensor of model PL2012. The advantage of preferring the thermodynamic fluxes to thermodynamic affinities is that we can maximize a quadratic functional with respect to the fluxes and the material parameters depending on the affinities can be simply prescribed, see (3.132).

We make the following choice for the rate of entropy production $\xi = \tilde{\xi}(\mathbf{T}^d_{\mathrm{dis}}, \mathbf{C}^d_{\kappa_{p(t)}})$

$$\tilde{\xi} = \frac{1}{\epsilon_1\left(\epsilon_0 + |\mathbf{D}|^2\right)^{\alpha-1}}|\mathbf{T}^d_{\mathrm{dis}}|^2 + \left(\frac{G}{\epsilon_2}\right)^{2\beta-1}\frac{G}{|\mathbf{D}_{\kappa_{p(t)}}|^{2\beta-2}}|\mathbf{C}_{\kappa_{p(t)}}|^2 \tag{3.132}$$

for $\epsilon_0 > 0$, $\epsilon_1 > 0$, $\epsilon_2 > 0$, $\alpha \in \mathbb{R}$, $\beta > 0.5$. The reduced thermodynamical equality remains in the form (3.22).

Let us denote

$$L(\mathbf{T}^d_{\mathrm{dis}}, \mathbf{B}_{\kappa_{p(t)}}) := \mathbf{T}^d_{\mathrm{dis}} \cdot \mathbf{D}^d + G\mathbf{C}^d_{\kappa_{p(t)}} \cdot \mathbf{D}^d_{\kappa_{p(t)}} - \tilde{\xi}(\mathbf{T}^d_{\mathrm{dis}}, \mathbf{C}_{\kappa_{p(t)}}). \tag{3.133}$$

We now maximize $\tilde{\xi}(\mathbf{T}^d_{\mathrm{dis}}, \mathbf{C}^d_{\kappa_{p(t)}})$ among the values of $\mathbf{T}^d_{\mathrm{dis}}$ and $\mathbf{C}^d_{\kappa_{p(t)}}$ fulfilling the reduced thermodynamic equality

$$0 = L(\mathbf{T}^d_{\mathrm{dis}}, \mathbf{C}_{\kappa_{p(t)}}). \tag{3.134}$$

For this purpose we adopt the method of Lagrange multipliers which delivers the following set of equations

$$\frac{\partial\tilde{\xi}}{\partial\mathbf{T}^d_{\mathrm{dis}}} = \lambda_1\frac{\partial L}{\partial\mathbf{T}^d_{\mathrm{dis}}}, \tag{3.135}$$

$$\frac{\partial\tilde{\xi}}{\partial\mathbf{C}^d_{\kappa_{p(t)}}} = \lambda_1\frac{\partial L}{\partial\mathbf{C}^d_{\kappa_{p(t)}}}, \tag{3.136}$$

that can be simplified to

$$\frac{1+\lambda_1}{\lambda_1}2\frac{1}{\epsilon_1\left(\epsilon_0+|\mathbf{D}|^2\right)^{\alpha-1}}\mathbf{T}^d_{\mathrm{dis}}=\mathbf{D}^d, \tag{3.137}$$

$$\frac{1+\lambda_1}{\lambda_1}2\left(\frac{G}{\epsilon_2}\right)^{2\beta-1}\frac{G}{|\mathbf{D}_{\kappa_{p(t)}}|^{2\beta-2}}\mathbf{C}^d_{\kappa_{p(t)}}=G\mathbf{D}^d_{\kappa_{p(t)}}. \tag{3.138}$$

We take the scalar product of (3.137) with $\mathbf{T}^d_{\mathrm{dis}}$ and (3.138) with $\mathbf{C}^d_{\kappa_{p(t)}}$, sum these products and with help of reduced thermodynamical equality we conclude that

$$2\frac{1+\lambda_1}{\lambda_1}=1$$

and get

$$\mathbf{T}^d_{\mathrm{dis}}=\epsilon_1\left(\epsilon_0+|\mathbf{D}|^2\right)^{\alpha-1}\mathbf{D}^d\Rightarrow\mathbf{T}=-p\mathbf{I}+\epsilon_1\left(\epsilon_0+|\mathbf{D}|^2\right)^{\alpha-1}\mathbf{D}^d+G\mathbf{B}^d_{\kappa_{p(t)}},$$

$$\text{where } p=-\frac{1}{3}\operatorname{tr}\mathbf{T}, \tag{3.139}$$

$$|\mathbf{D}_{\kappa_{p(t)}}|^{2\beta-2}\mathbf{D}_{\kappa_{p(t)}}=\left(\frac{G}{\epsilon_2}\right)^{2\beta-1}\mathbf{B}_{\kappa_{p(t)}}. \tag{3.140}$$

Now we take the absolute value of (3.140)

$$|\mathbf{D}_{\kappa_{p(t)}}|^{2\beta-1}=\left(\frac{G}{\epsilon_2}\right)^{2\beta-1}|\mathbf{B}_{\kappa_{p(t)}}|\Rightarrow|\mathbf{D}_{\kappa_{p(t)}}|^{2\beta-2}=\left(\frac{G}{\epsilon_2}\right)^{2\beta-2}\left(|\mathbf{B}_{\kappa_{p(t)}}|\right)^{\frac{2\beta-2}{2\beta-1}}.$$

Multiplying (3.140) by $\mathbf{F}_{\kappa_{p(t)}}$ from the left and by $\mathbf{F}^{\mathrm{T}}_{\kappa_{p(t)}}$ from the right, using (3.5) we arrive at

$$\overset{\triangledown}{\mathbf{B}}_{\kappa_{p(t)}}=-2\frac{G}{\epsilon_2}|\mathbf{B}_{\kappa_{p(t)}}|^{\frac{2-2\beta}{2\beta-1}}\mathbf{B}_{\kappa_{p(t)}}\mathbf{B}^d_{\kappa_{p(t)}}. \tag{3.141}$$

We obtain a model with the Cauchy stress tensor similar to Cauchy stress tensor of model PL2012 (3.97)

$$\mathbf{T}=-p\mathbf{I}+\epsilon_1\left(\epsilon_0+|\mathbf{D}|^2\right)^{\alpha-1}\mathbf{D}^d+G\mathbf{B}^d_{\kappa_{p(t)}}, \tag{3.142a}$$

$$\overset{\triangledown}{\mathbf{B}}_{\kappa_{p(t)}}=-2\frac{G}{\epsilon_2}|\mathbf{B}_{\kappa_{p(t)}}|^{\frac{2-2\beta}{2\beta-1}}\mathbf{B}_{\kappa_{p(t)}}\mathbf{B}^d_{\kappa_{p(t)}}. \tag{3.142b}$$

The derivation of this model is much simpler than derivation of model PL2012 (3.97). For $\alpha=\beta=1$ this model reduces to incompressible model with purely quadratic dissipation (3.112).

3.6 Incompressible viscoelastic model with purely quadratic dissipation and compressible elastic response

In this section we derive a compressible variant (ICC) of model Quad1 (3.112). The same constitutive relation for the rate of entropy production (3.100) as in case of fully incompressible model Quad1 is used, i.e.

$$\tilde{\xi}=2\mu_2|\mathbf{D}|^2+2\mu_1|\mathbf{D}_{\kappa_{p(t)}}|^2. \tag{3.143}$$

Now we use the principle of maximization of the rate of entropy production.

We maximize $\tilde{\xi}(\mathbf{D},\mathbf{D}_{\kappa_{p(t)}})$ among the values of $\mathbf{D},\mathbf{D}_{\kappa_{p(t)}}$ fulfilling the equality (3.25) and the constraint of incompressibility $\operatorname{tr}\mathbf{D}=0$. We define the Lagrange function

$$\begin{aligned}L(\mathbf{D},\mathbf{D}_{\kappa_{p(t)}})=\tilde{\xi}(\mathbf{D},\mathbf{D}_{\kappa p(t)},\mathbf{C}_{\kappa_{p(t)}})-\lambda_2\operatorname{tr}\mathbf{D}\\+\lambda_1\left(\tilde{\xi}(\mathbf{D},\mathbf{D}_{\kappa p(t)})-\left(\mathbf{T}-G(\mathbf{B}_{\kappa_{p(t)}}-\mathbf{I})\right)\cdot\mathbf{D}-G(\mathbf{C}_{\kappa_{p(t)}}-\mathbf{I})\cdot\mathbf{D}_{\kappa_{p(t)}}\right)\end{aligned} \tag{3.144}$$

and find the extremes of $\mathbf{L}$. The necessary conditions are

$$\frac{\partial L}{\partial \mathbf{D}} = 0, \quad \frac{\partial L}{\partial \mathbf{D}_{\kappa_{p(t)}}} = 0.$$

We substitute for L and $\tilde{\xi}$ and obtain

$$\frac{1+\lambda_1}{\lambda_1} 4\mu_2 \mathbf{D} = \mathbf{T} - G(\mathbf{B}_{\kappa_{p(t)}} - \mathbf{I}) + \frac{\lambda_2}{\lambda_1}\mathbf{I}, \tag{3.145}$$

$$\frac{1+\lambda_1}{\lambda_1} 4\mu_1 \mathbf{D}_{\kappa_{p(t)}} = G(\mathbf{C}_{\kappa_{p(t)}} - \mathbf{I}). \tag{3.146}$$

Further we eliminate the Lagrange multipliers, we perform (3.145) $\cdot\, \mathbf{D}$ + (3.146) $\cdot\, \mathbf{D}_{\kappa_{p(t)}}$, and use the constraint of incompressibility

$$\frac{1+\lambda_1}{\lambda_1} = \frac{\left(\mathbf{T} - G(\mathbf{B}_{\kappa_{p(t)}} - \mathbf{I})\right) \cdot \mathbf{D} + G(\mathbf{C}_{\kappa_{p(t)}} - \mathbf{I}) \cdot \mathbf{D}_{\kappa_{p(t)}}}{4\mu_2 \mathbf{D} \cdot \mathbf{D} + 4\mu_1 \mathbf{D}_{\kappa_{p(t)}} \cdot \mathbf{D}_{\kappa_{p(t)}}} = \frac{\xi}{2\tilde{\xi}} = \frac{1}{2}. \tag{3.147}$$

Next we take the trace of (3.102) and eliminate λ_2/λ_1 which together with (3.147) gives

$$\frac{\lambda_2}{\lambda_1} = -\frac{1}{3}\operatorname{tr}\left(\mathbf{T} - G\mathbf{B}_{\kappa_{p(t)}}\right) - G. \tag{3.148}$$

We define a pressure p as mean normal stress

$$p = -\frac{1}{3}\operatorname{tr}\mathbf{T}. \tag{3.149}$$

Substitution of (3.149), (3.148), (3.147) into (3.145) gives

$$\mathbf{T} = -p\mathbf{I} + 2\mu_2\mathbf{D} + G\mathbf{B}^d_{\kappa_{p(t)}}. \tag{3.150}$$

Now we insert (3.147) into (3.146)

$$2\mu_1 \mathbf{D}_{\kappa_{p(t)}} = G(\mathbf{C}_{\kappa_{p(t)}} - \mathbf{I}), \tag{3.151}$$

Multiplying (3.151) from the left by $\mathbf{F}_{\kappa_{p(t)}}$ and from the right by $\mathbf{F}^{\mathrm{T}}_{\kappa_{p(t)}}$ we obtain

$$2\mu_1 \mathbf{F}_{\kappa_{p(t)}} \mathbf{D}_{\kappa_{p(t)}} \mathbf{F}^{\mathrm{T}}_{\kappa_{p(t)}} = G\mathbf{B}_{\kappa_{p(t)}}\left(\mathbf{B}_{\kappa_{p(t)}} - \mathbf{I}\right). \tag{3.152}$$

By comparing the left-hand-side of (3.152) with (3.5) we get

$$\overset{\triangledown}{\mathbf{B}}_{\kappa_{p(t)}} = -\frac{G}{\mu_1}\mathbf{B}_{\kappa_{p(t)}}(\mathbf{B}_{\kappa_{p(t)}} - \mathbf{I}). \tag{3.153}$$

We obtain

$$\mathbf{T} = -p\mathbf{I} + 2\mu_2\mathbf{D} + G\mathbf{B}^d_{\kappa_{p(t)}}, \tag{3.154a}$$

$$\overset{\triangledown}{\mathbf{B}}_{\kappa_{p(t)}} = -\frac{G}{\mu_1}\mathbf{B}_{\kappa_{p(t)}}(\mathbf{B}_{\kappa_{p(t)}} - \mathbf{I}). \tag{3.154b}$$

It can be shown that this model reduces to standard Oldroyd-B model (2.10) if the elastic part of response is linearized.

Model (3.154) can be also obtained by preferring the thermodynamic fluxes $\mathbf{T}^d_{\mathrm{dis}}$ and $\mathbf{C}_{\kappa_{p(t)}}$. We suppose the constitutive relation in the form

$$\tilde{\xi}(\mathbf{T}^d_{\mathrm{dis}}, \mathbf{C}_{\kappa_{p(t)}}) = \frac{1}{2\mu_2}|\mathbf{T}^d_{\mathrm{dis}}|^2 + \frac{G^2}{2\mu_1}|\mathbf{C}_{\kappa_{p(t)}} - \mathbf{I}|^2, \tag{3.155}$$

and the reduced thermodynamic equality is equal to (3.26). The model is obtained by maximization of rate of entropy production (3.155) among the values of $\mathbf{T}^d_{\mathrm{dis}} = \mathbf{T}^d - G\mathbf{B}^d_{\kappa_{p(t)}}$ and $\mathbf{C}_{\kappa_{p(t)}} - \mathbf{I}$ fulfilling the equality (3.26) and the constraint of incompressibility $\operatorname{tr}\mathbf{D} = 0$.

3.7 Oldroyd-B model

The model (3.154) is very similar to Oldroyd-B model, we show how to derive Oldroyd-B (2.10) from the thermodynamical principles. As in the previous section we use a compressible variant (ICC). For the rate of entropy production we use the entropy production (3.34)

$$\xi = \tilde{\xi}(\mathbf{D}, \mathbf{D}_{\kappa p(t)}, \mathbf{C}_{\kappa_{p(t)}}) = 2\mu_2|\mathbf{D}|^2 + 2\mu_1 \mathbf{D}_{\kappa_{p(t)}} \mathbf{C}_{\kappa_{p(t)}} \cdot \mathbf{D}_{\kappa_{p(t)}}, \quad \mu_2, \mu_1 > 0. \tag{3.156}$$

Now we again use the principle of maximization of the rate of entropy production.

We maximize $\tilde{\xi}(\mathbf{D}, \mathbf{D}_{\kappa_{p(t)}})$ among the values of $\mathbf{D}, \mathbf{D}_{\kappa_{p(t)}}$ fulfilling the equality (3.25) and the constraint of incompressibility $\operatorname{tr} \mathbf{D} = 0$. We define the Lagrange function

$$\begin{aligned} L(\mathbf{D}, \mathbf{D}_{\kappa_{p(t)}}) = \tilde{\xi}(\mathbf{D}, \mathbf{D}_{\kappa p(t)}, \mathbf{C}_{\kappa_{p(t)}}) - \lambda_2 \operatorname{tr} \mathbf{D} \\ + \lambda_1 \left(\tilde{\xi}(\mathbf{D}, \mathbf{D}_{\kappa p(t)}) - \left(\mathbf{T} - G(\mathbf{B}_{\kappa_{p(t)}} - \mathbf{I}) \right) \cdot \mathbf{D} - G(\mathbf{C}_{\kappa_{p(t)}} - \mathbf{I}) \cdot \mathbf{D}_{\kappa_{p(t)}} \right) \end{aligned} \tag{3.157}$$

and find the extremes of $\mathbf{L}$. The necessary conditions are

$$\frac{\partial L}{\partial \mathbf{D}} = 0, \quad \frac{\partial L}{\partial \mathbf{D}_{\kappa_{p(t)}}} = 0.$$

We substitute for L and $\tilde{\xi}$ and obtain

$$\frac{1+\lambda_1}{\lambda_1} 4\mu_2 \mathbf{D} = \mathbf{T} - G(\mathbf{B}_{\kappa_{p(t)}} - \mathbf{I}) + \frac{\lambda_2}{\lambda_1} \mathbf{I}, \tag{3.158}$$

$$\frac{1+\lambda_1}{\lambda_1} 4\mu_1 \mathbf{D}_{\kappa_{p(t)}} \mathbf{C}_{\kappa_{p(t)}} = G(\mathbf{C}_{\kappa_{p(t)}} - \mathbf{I}). \tag{3.159}$$

Further we eliminate the Lagrange multipliers, we perform (3.158) $\cdot\, \mathbf{D}$ + (3.159) $\cdot\, \mathbf{D}_{\kappa_{p(t)}}$, and use the constraint of incompressibility

$$\frac{1+\lambda_1}{\lambda_1} = \frac{\left(\mathbf{T} - G(\mathbf{B}_{\kappa_{p(t)}} - \mathbf{I}) \right) \cdot \mathbf{D} + G(\mathbf{C}_{\kappa_{p(t)}} - \mathbf{I}) \cdot \mathbf{D}_{\kappa_{p(t)}}}{4\mu_2 \mathbf{D} \cdot \mathbf{D} + 4\mu_1 \mathbf{D}_{\kappa_{p(t)}} \mathbf{C}_{\kappa_{p(t)}} \cdot \mathbf{D}_{\kappa_{p(t)}}} = \frac{\xi}{2\tilde{\xi}} = \frac{1}{2}. \tag{3.160}$$

Multiplier λ_2/λ_1 has to be eliminated in (3.158), we define a pressure p as

$$p = -\lambda_2/\lambda_1 \tag{3.161}$$

and using (3.158) we get

$$\mathbf{T} = -p\mathbf{I} + 2\mu_2 \mathbf{D} + G(\mathbf{B}_{\kappa_{p(t)}} - \mathbf{I}). \tag{3.162}$$

Now we insert (3.160) into (3.159)

$$2\mu_1 \mathbf{D}_{\kappa_{p(t)}} \mathbf{C}_{\kappa_{p(t)}} = G(\mathbf{C}_{\kappa_{p(t)}} - \mathbf{I}), \tag{3.163}$$

Multiplying (3.163) from the left by $\mathbf{F}_{\kappa_{p(t)}}$ and from the right by $\mathbf{F}^{-1}_{\kappa_{p(t)}}$ we obtain

$$2\mu_1 \mathbf{F}_{\kappa_{p(t)}} \mathbf{D}_{\kappa_{p(t)}} \mathbf{F}^{\mathrm{T}}_{\kappa_{p(t)}} = G\left(\mathbf{B}_{\kappa_{p(t)}} - \mathbf{I} \right). \tag{3.164}$$

By comparing the left-hand-side of (3.164) with (3.5) we get

$$\overset{\triangledown}{\mathbf{B}}_{\kappa_{p(t)}} = -\frac{G}{\mu_1} (\mathbf{B}_{\kappa_{p(t)}} - \mathbf{I}). \tag{3.165}$$

We obtain standard Oldroyd-B model

$$\mathbf{T} = -p\mathbf{I} + 2\mu_2 \mathbf{D} + G(\mathbf{B}_{\kappa_{p(t)}} - \mathbf{I}), \tag{3.166a}$$

$$\overset{\triangledown}{\mathbf{B}}_{\kappa_{p(t)}} = -\frac{G}{\mu_1} (\mathbf{B}_{\kappa_{p(t)}} - \mathbf{I}). \tag{3.166b}$$

Since we defined pressure p as a Lagrange multiplier through (3.161), pressure p is not equal to a mean normal stress.[1] Hence, we showed that Oldroyd-B model (2.10) can be derived from the thermodynamical principles, and thus it satisfies the second law of thermodynamics. Moreover we showed that the elastic response between the natural and the current configuration corresponds to that of compressible neo-Hookean solid.

Note: Maxwell model (2.7) is obtained in the compressible variant (ICC), where the elastic response corresponds to that of compressible neo-Hookean solid, and if we assume that the rate of entropy production is in the form

$$\tilde{\xi}(\mathbf{D}_{\kappa p(t)}, \mathbf{C}_{\kappa_{p(t)}}) = 2\mu \mathbf{D}_{\kappa_{p(t)}} \mathbf{C}_{\kappa_{p(t)}} \cdot \mathbf{D}_{\kappa_{p(t)}}, \quad \mu > 0. \tag{3.167}$$

3.8 Fully compressible model with purely quadratic dissipation

In this section we derive a fully compressible viscoelastic model (CCC) with thermodynamic inequality in the form (3.30). We make the following choice for the rate of dissipation $\xi = \tilde{\xi}(\mathbf{T}^d_{\rm dis}, t_{\rm dis}, \mathbf{C}^d_{\kappa_{p(t)}}, b/3-1, \mathbf{q})$

$$\tilde{\xi} = \frac{1}{2\mu_2}|\mathbf{T}^d_{\rm dis}|^2 + \frac{3}{2\mu_2+3\lambda}|t_{\rm dis}|^2 + \frac{G^2}{2\mu_1}|\mathbf{C}^d_{\kappa_{p(t)}}|^2 + \frac{3G^2}{2\mu_1}\left|\frac{b}{3}-1\right|^2 + \frac{1}{k}\frac{|\mathbf{q}|^2}{\theta} \tag{3.168}$$

for $G>0$, $\mu_2>0$, $2\mu_2+3\lambda>0$, $\mu_1>0$ and $k>0$ and

$$\mathbf{T}^d_{\rm dis} = \mathbf{T}^d - G\mathbf{B}^d_{\kappa_{p(t)}}, \quad t_{\rm dis} = m + p(\rho,\theta) - G\left(\frac{b}{3}-1\right), \quad b = \operatorname{tr}\mathbf{C}_{\kappa_{p(t)}}.$$

We now use the principle of maximization of the rate of entropy production.

Let us denote

$$L(\mathbf{T}^d_{\rm dis}, t_{\rm dis}, \mathbf{C}^d_{\kappa_{p(t)}}, b, \mathbf{q}) := \tilde{\xi} + \lambda_1\Big(\tilde{\xi} - \mathbf{T}^d_{\rm dis}\cdot\mathbf{D}^d - t_{\rm dis}\operatorname{div}\mathbf{v} - G\mathbf{C}^d_{\kappa_{p(t)}}\cdot\mathbf{D}^d_{\kappa_{p(t)}} - G\left(\frac{b}{3}-1\right)\operatorname{tr}\mathbf{D}_{\kappa_{p(t)}} + \frac{\mathbf{q}\cdot\nabla\theta}{\theta}\Big). \tag{3.169}$$

We now maximize $\tilde{\xi}(\mathbf{T}^d_{\rm dis}, t_{\rm dis}, \mathbf{C}^d_{\kappa_{p(t)}}, b/3-1, \mathbf{q})$ among the values of $\mathbf{T}^d_{\rm dis}$, $t_{\rm dis}$, $\mathbf{C}^d_{\kappa_{p(t)}}$, $(b/3-1)$, $\mathbf{q}$ fulfilling the reduced thermodynamic inequality (3.30). For this purpose we adopt the method of Lagrange multipliers which delivers the following set of equations

$$\frac{\partial L}{\partial \mathbf{T}^d_{\rm dis}} = 0, \quad \frac{\partial L}{\partial t_{\rm dis}} = 0, \quad \frac{\partial L}{\partial \mathbf{C}^d_{\kappa_{p(t)}}} = 0, \quad \frac{\partial L}{\partial (b/3-1)} = 0, \quad \frac{\partial L}{\partial \mathbf{q}} = 0 \tag{3.170}$$

[1] We could have defined pressure as $p = -(\operatorname{tr}\mathbf{T})/3$ and obtain the Cauchy stress tensor in the form

$$\mathbf{T} = -p\mathbf{I} + 2\mu_2\mathbf{D} + G\mathbf{B}^d.$$

However, we aimed to obtain the model in the standard form (2.10) with the Cauchy stress tensor in the form (3.166a) where pressure is not a mean normal stress.

that can be simplified to

$$\frac{1+\lambda_1}{\lambda_1}2\frac{1}{2\mu_2}\mathbf{T}^d_{\text{dis}} = \mathbf{D}^d, \tag{3.171}$$

$$\frac{1+\lambda_1}{\lambda_1}2\frac{3}{2\mu_2+3\lambda}t_{\text{dis}} = \operatorname{div}\mathbf{v}, \tag{3.172}$$

$$\frac{1+\lambda_1}{\lambda_1}2\frac{G^2}{2\mu_1}\mathbf{C}^d_{\kappa_{p(t)}} = G\mathbf{D}^d_{\kappa_{p(t)}}, \tag{3.173}$$

$$\frac{1+\lambda_1}{\lambda_1}2\frac{3G^2}{2\mu_1}\left(\frac{b}{3}-1\right) = G\operatorname{tr}\mathbf{D}_{\kappa_{p(t)}}, \tag{3.174}$$

$$\frac{1+\lambda_1}{\lambda_1}2\frac{1}{k}\frac{\mathbf{q}}{\theta} = -\frac{\nabla\theta}{\theta}, \tag{3.175}$$

where the Lagrange multiplier λ_1 has to be determined. To accomplish this we take the scalar product of (3.171) with $\mathbf{T}^d_{\text{dis}}$, (3.172) with t_{dis}, (3.173) with $\mathbf{C}^d_{\kappa_{p(t)}}$, (3.174) with $b/3-1$ and (3.175) with $\mathbf{q}$ and sum these products. With help of (3.30) we conclude that

$$2\frac{1+\lambda_1}{\lambda_1} = 1$$

and get

$$\mathbf{T}^d = 2\mu_2\mathbf{D}^d + G\mathbf{B}^d_{\kappa_{p(t)}}, \tag{3.176}$$

$$m = -p(\rho,\theta) + G\left(\frac{b}{3}-1\right) + \left(\lambda+\frac{2\mu_2}{3}\right)\operatorname{div}\mathbf{v}, \tag{3.177}$$

$$\frac{G}{2\mu_1}\mathbf{C}^d_{\kappa_{p(t)}} = \mathbf{D}^d_{\kappa_{p(t)}}, \tag{3.178}$$

$$\frac{G}{2\mu_1}\left(\frac{b}{3}-1\right) = \frac{1}{3}\operatorname{tr}\mathbf{D}_{\kappa_{p(t)}}, \tag{3.179}$$

$$\mathbf{q} = -k\nabla\theta. \tag{3.180}$$

From equations (3.176) and (3.177) one can read

$$\mathbf{T} = m\mathbf{I} + \mathbf{T}^d = \left(-p(\rho,\theta) + G\left(\frac{b}{3}-1\right) + \left(\lambda+\frac{2\mu_2}{3}\right)\operatorname{div}\mathbf{v}\right)\mathbf{I} + 2\mu_2\mathbf{D}^d + G\mathbf{B}^d_{\kappa_{p(t)}}.$$

Adding (3.178) and (3.179)$\mathbf{I}$ one gets

$$\frac{G}{2\mu_1}(\mathbf{C}_{\kappa_{p(t)}} - \mathbf{I}) = \mathbf{D}_{\kappa_{p(t)}},$$

multiplying this equation by $\mathbf{F}_{\kappa_{p(t)}}$ from the left and by $\mathbf{F}^{\mathrm{T}}_{\kappa_{p(t)}}$ from the right, using (3.5) we arrive at

$$\overset{\triangledown}{\mathbf{B}}_{\kappa_{p(t)}} = -\frac{G}{\mu_1}\mathbf{B}_{\kappa_{p(t)}}(\mathbf{B}_{\kappa_{p(t)}} - \mathbf{I}). \tag{3.181}$$

We obtain the following set of partial differential equations

$$\dot\rho + \rho\operatorname{div}\mathbf{v} = 0, \tag{3.182a}$$

$$\rho\dot{\mathbf{v}} = \operatorname{div}\mathbf{T}, \tag{3.182b}$$

$$\mathbf{T} = (-p(\rho,\theta) - G + \lambda\operatorname{div}\mathbf{v})\,\mathbf{I} + 2\mu_2\mathbf{D} + G\mathbf{B}_{\kappa_{p(t)}}, \tag{3.182c}$$

$$\overset{\triangledown}{\mathbf{B}}_{\kappa_{p(t)}} = -\frac{G}{\mu_1}\mathbf{B}_{\kappa_{p(t)}}(\mathbf{B}_{\kappa_{p(t)}} - \mathbf{I}), \tag{3.182d}$$

$$\mathbf{q} = -k\nabla\theta. \tag{3.182e}$$

If we assumed in the constitutive relation for the rate of entropy production $\tilde\xi$ (3.168) that the viscosities depend on shear rate $\mathbf{D}$ and temperature θ we would obtain even more general model. As in case of compressible Navier-Stokes equations, additional constitutive equation for pressure $p = p(\rho)$ (e.g. equation of state) is needed, the set of equation can be closed with the balance of energy and relation between internal energy e and temperature θ.

3.9 Compressible variant (CIC) of model with purely quadratic dissipation

In this section we derive compressible variant (CIC) of viscoelastic model with thermodynamic inequality in the form (3.31). We make the following choice for the rate of dissipation $\xi = \tilde{\xi}(\mathbf{T}^d_{\rm dis}, t_{\rm dis}, \mathbf{C}^d_{\kappa_{p(t)}}, \mathbf{q})$

$$\tilde{\xi} = \frac{1}{2\mu_2}|\mathbf{T}^d_{\rm dis}|^2 + \frac{3}{2\mu_2+3\lambda}|t_{\rm dis}|^2 + \frac{G^2}{2\mu_1}|\mathbf{C}^d_{\kappa_{p(t)}}|^2 + \frac{1}{k}\frac{|\mathbf{q}|^2}{\theta} \tag{3.183}$$

for $G>0$, $\mu_2>0$, $2\mu_2+3\lambda>0$, $\mu_1>0$ and $k>0$ and

$$\mathbf{T}^d_{\rm dis} = \mathbf{T}^d - G\mathbf{B}^d_{\kappa_{p(t)}}, \quad t_{\rm dis} = m + p(\rho,\theta) - G\left(\frac{b}{3}-1\right), \quad b = \operatorname{tr}\mathbf{C}_{\kappa_{p(t)}}.$$

We now use the principle of maximization of the rate of entropy production.

Let us denote

$$L(\mathbf{T}^d_{\rm dis}, t_{\rm dis}, \mathbf{C}^d_{\kappa_{p(t)}}, b, \mathbf{q}) := \tilde{\xi} + \lambda_1\Big(\tilde{\xi} - \mathbf{T}^d_{\rm dis}\cdot\mathbf{D}^d - t_{\rm dis}\operatorname{div}\mathbf{v} - G\mathbf{C}^d_{\kappa_{p(t)}}\cdot\mathbf{D}^d_{\kappa_{p(t)}} + \frac{\mathbf{q}\cdot\nabla\theta}{\theta}\Big). \tag{3.184}$$

We maximize $\tilde{\xi}(\mathbf{T}^d_{\rm dis}, t_{\rm dis}, \mathbf{C}^d_{\kappa_{p(t)}}, b/3-1, \mathbf{q})$ among the values of $\mathbf{T}^d_{\rm dis}$, $t_{\rm dis}$, $\mathbf{C}^d_{\kappa_{p(t)}}$, $\mathbf{q}$ fulfilling the reduced thermodynamic inequality (3.31). For this purpose we adopt the method of Lagrange multipliers which delivers the following set of equations

$$\frac{\partial L}{\partial \mathbf{T}^d_{\rm dis}} = 0, \quad \frac{\partial L}{\partial t_{\rm dis}} = 0, \quad \frac{\partial L}{\partial \mathbf{q}} = 0 \tag{3.185}$$

that can be simplified to

$$\frac{1+\lambda_1}{\lambda_1}2\frac{1}{2\mu_2}\mathbf{T}^d_{\rm dis} = \mathbf{D}^d, \tag{3.186}$$

$$\frac{1+\lambda_1}{\lambda_1}2\frac{3}{2\mu_2+3\lambda}t_{\rm dis} = \operatorname{div}\mathbf{v}, \tag{3.187}$$

$$\frac{1+\lambda_1}{\lambda_1}2\frac{G^2}{2\mu_1}\mathbf{C}^d_{\kappa_{p(t)}} = G\mathbf{D}^d_{\kappa_{p(t)}}, \tag{3.188}$$

$$\frac{1+\lambda_1}{\lambda_1}2\frac{1}{k}\frac{\mathbf{q}}{\theta} = -\frac{\nabla\theta}{\theta}, \tag{3.189}$$

where the Lagrange multiplier λ_1 has to be determined. To accomplish this we take the scalar product of (3.186) with $\mathbf{T}^d_{\rm dis}$, (3.187) with $t_{\rm dis}$, (3.188) with $\mathbf{C}^d_{\kappa_{p(t)}}$, and (3.189) with $\mathbf{q}$ and sum these products. With help of (3.31) we conclude that

$$2\frac{1+\lambda_1}{\lambda_1} = 1$$

and get

$$\mathbf{T}^d = 2\mu_2\mathbf{D}^d + G\mathbf{B}^d_{\kappa_{p(t)}}, \tag{3.190}$$

$$m = -p(\rho,\theta) + G(b-1) + \left(\lambda + \frac{2\mu_2}{3}\right)\operatorname{div}\mathbf{v}, \tag{3.191}$$

$$\frac{G}{2\mu_1}\mathbf{C}^d_{\kappa_{p(t)}} = \mathbf{D}^d_{\kappa_{p(t)}}, \tag{3.192}$$

$$\mathbf{q} = -k\nabla\theta. \tag{3.193}$$

From equations (3.190) and (3.191) one can read

$$\mathbf{T} = m\mathbf{I} + \mathbf{T}^d = \left(-p(\rho,\theta) + G\left(\frac{b}{3}-1\right) + \left(\lambda+\frac{2\mu_2}{3}\right)\operatorname{div}\mathbf{v}\right)\mathbf{I} + 2\mu_2\mathbf{D}^d + G\mathbf{B}^d_{\kappa_{p(t)}}.$$

Since $\operatorname{tr}\mathbf{D}_{\kappa_{p(t)}}=0$ (3.192) gives

$$\frac{G}{2\mu_1}\mathbf{C}^d_{\kappa_{p(t)}}=\mathbf{D}_{\kappa_{p(t)}}\,,$$

multiplying this equation by $\mathbf{F}_{\kappa_{p(t)}}$ from the left and by $\mathbf{F}^{\mathrm{T}}_{\kappa_{p(t)}}$ from the right, using (3.5) we arrive at

$$\overset{\triangledown}{\mathbf{B}}_{\kappa_{p(t)}}=-\frac{G}{\mu_1}\mathbf{B}_{\kappa_{p(t)}}\mathbf{B}^d_{\kappa_{p(t)}}\,. \tag{3.194}$$

We obtain the following set of partial differential equations

$$\dot\rho+\rho\operatorname{div}\mathbf{v}=0\,, \tag{3.195a}$$
$$\rho\dot{\mathbf{v}}=\operatorname{div}\mathbf{T}\,, \tag{3.195b}$$
$$\mathbf{T}=(-p(\rho,\theta)-G+\lambda\operatorname{div}\mathbf{v})\,\mathbf{I}+2\mu_2\mathbf{D}+G\mathbf{B}_{\kappa_{p(t)}}\,, \tag{3.195c}$$
$$\overset{\triangledown}{\mathbf{B}}_{\kappa_{p(t)}}=-\frac{G}{\mu_1}\mathbf{B}_{\kappa_{p(t)}}\mathbf{B}^d_{\kappa_{p(t)}}\,, \tag{3.195d}$$
$$\mathbf{q}=-k\nabla\theta\,. \tag{3.195e}$$

3.10 Compressible variant (CCI) of model with purely quadratic dissipation

In this section we derive a fully compressible viscoelastic model (CCI) with thermodynamic inequality in the form (3.33). We make the following choice for the rate of dissipation $\xi=\tilde\xi(\mathbf{T}^d_{\mathrm{dis}},t_{\mathrm{dis}_1},\mathbf{C}^d_{\kappa_{p(t)}},b/3,\mathbf{q})$

$$\tilde\xi=\frac{1}{2\mu_2}|\mathbf{T}^d_{\mathrm{dis}}|^2+\frac{3}{2\mu_2+3\lambda}|t_{\mathrm{dis}_1}|^2+\frac{G^2}{2\mu_1}|\mathbf{C}^d_{\kappa_{p(t)}}|^2+\frac{3G^2}{2\mu_1}\left|\frac{b}{3}\right|^2+\frac{1}{k}\frac{|\mathbf{q}|^2}{\theta} \tag{3.196}$$

for $G>0$, $\mu_2>0$, $2\mu_2+3\lambda>0$, $\mu_1>0$ and $k>0$ and

$$\mathbf{T}^d_{\mathrm{dis}}=\mathbf{T}^d-G\mathbf{B}^d_{\kappa_{p(t)}},\quad t_{\mathrm{dis}_1}=m+p(\rho,\theta)-G\frac{b}{3},\quad b=\operatorname{tr}\mathbf{C}_{\kappa_{p(t)}}.$$

We now use the principle of maximization of the rate of entropy production.

Let us denote

$$L(\mathbf{T}^d_{\mathrm{dis}},t_{\mathrm{dis}_1},\mathbf{C}^d_{\kappa_{p(t)}},b,\mathbf{q}):=\tilde\xi+\lambda_1\Big(\tilde\xi-\mathbf{T}^d_{\mathrm{dis}}\cdot\mathbf{D}^d-t_{\mathrm{dis}_1}\operatorname{div}\mathbf{v} - G\mathbf{C}^d_{\kappa_{p(t)}}\cdot\mathbf{D}^d_{\kappa_{p(t)}}-G\frac{b}{3}\operatorname{tr}\mathbf{D}_{\kappa_{p(t)}}+\frac{\mathbf{q}\cdot\nabla\theta}{\theta}\Big). \tag{3.197}$$

We maximize $\tilde\xi(\mathbf{T}^d_{\mathrm{dis}},t_{\mathrm{dis}_1},\mathbf{C}^d_{\kappa_{p(t)}},b/3,\mathbf{q})$ among the values of $\mathbf{T}^d_{\mathrm{dis}}$, t_{dis_1}, $\mathbf{C}^d_{\kappa_{p(t)}}$, $\mathbf{q}$ fulfilling the reduced thermodynamic inequality (3.31). For this purpose we adopt the method of Lagrange multipliers which delivers the following set of equations

$$\frac{\partial L}{\partial\mathbf{T}^d_{\mathrm{dis}}}=0,\quad\frac{\partial L}{\partial t_{\mathrm{dis}_1}}=0,\quad\frac{\partial L}{\partial\mathbf{C}^d_{\kappa_{p(t)}}}=0,\quad\frac{\partial L}{\partial(b/3)}=0,\quad\frac{\partial L}{\partial\mathbf{q}}=0 \tag{3.198}$$

that can be simplified to

$$\frac{1+\lambda_1}{\lambda_1}2\frac{1}{2\mu_2}\mathbf{T}^d_{\mathrm{dis}} = \mathbf{D}^d, \tag{3.199}$$

$$\frac{1+\lambda_1}{\lambda_1}2\frac{3}{2\mu_2+3\lambda}t_{\mathrm{dis}_1} = \operatorname{div}\mathbf{v}, \tag{3.200}$$

$$\frac{1+\lambda_1}{\lambda_1}2\frac{G^2}{2\mu_1}\mathbf{C}^d_{\kappa_{p(t)}} = G\mathbf{D}^d_{\kappa_{p(t)}}, \tag{3.201}$$

$$\frac{1+\lambda_1}{\lambda_1}2\frac{3G^2}{2\mu_1}\left(\frac{b}{3}\right) = G\operatorname{tr}\mathbf{D}_{\kappa_{p(t)}}, \tag{3.202}$$

$$\frac{1+\lambda_1}{\lambda_1}2\frac{1}{k}\frac{\mathbf{q}}{\theta} = -\frac{\nabla\theta}{\theta}, \tag{3.203}$$

where the Lagrange multiplier λ_1 has to be determined. To accomplish this we take the scalar product of (3.199) with $\mathbf{T}^d_{\mathrm{dis}}$, (3.200) with t_{dis_1}, (3.201) with $\mathbf{C}^d_{\kappa_{p(t)}}$, (3.202) with $b/3$, and (3.203) with $\mathbf{q}$ and sum these products. With help of (3.31) we conclude that

$$2\frac{1+\lambda_1}{\lambda_1} = 1$$

and get

$$\mathbf{T}^d = 2\mu_2\mathbf{D}^d + G\mathbf{B}^d_{\kappa_{p(t)}}\,, \tag{3.204}$$

$$m = -p(\rho,\theta) + G\frac{b}{3} + \left(\lambda + \frac{2\mu_2}{3}\right)\operatorname{div}\mathbf{v}\,, \tag{3.205}$$

$$\frac{G}{2\mu_1}\mathbf{C}^d_{\kappa_{p(t)}} = \mathbf{D}^d_{\kappa_{p(t)}}\,, \tag{3.206}$$

$$\frac{G}{2\mu_1}\frac{b}{3} = \frac{1}{3}\operatorname{tr}\mathbf{D}_{\kappa_{p(t)}}\,, \tag{3.207}$$

$$\mathbf{q} = -k\nabla\theta\,. \tag{3.208}$$

From equations (3.204) and (3.205) one can read

$$\mathbf{T} = m\mathbf{I} + \mathbf{T}^d = \left(-p(\rho,\theta) + G\frac{b}{3} + \left(\lambda + \frac{2\mu_2}{3}\right)\operatorname{div}\mathbf{v}\right)\mathbf{I} + 2\mu_2\mathbf{D}^d + G\mathbf{B}^d_{\kappa_{p(t)}}\,.$$

Performing (3.206)+(3.207)$\mathbf{I}$ one gets

$$\frac{G}{2\mu_1}\mathbf{C}_{\kappa_{p(t)}} = \mathbf{D}_{\kappa_{p(t)}}\,,$$

multiplying this equation by $\mathbf{F}_{\kappa_{p(t)}}$ from the left and by $\mathbf{F}^{\mathrm{T}}_{\kappa_{p(t)}}$ from the right, using (3.5) we arrive at

$$\overset{\triangledown}{\mathbf{B}}_{\kappa_{p(t)}} = -\frac{G}{\mu_1}\mathbf{B}^2_{\kappa_{p(t)}}\,. \tag{3.209}$$

We obtain the following set of partial differential equations

$$\dot\rho + \rho\operatorname{div}\mathbf{v} = 0\,, \tag{3.210a}$$

$$\rho\dot{\mathbf{v}} = \operatorname{div}\mathbf{T}\,, \tag{3.210b}$$

$$\mathbf{T} = \left(-p(\rho,\theta) + \lambda\operatorname{div}\mathbf{v}\right)\mathbf{I} + 2\mu_2\mathbf{D} + G\mathbf{B}_{\kappa_{p(t)}}\,, \tag{3.210c}$$

$$\overset{\triangledown}{\mathbf{B}}_{\kappa_{p(t)}} = -\frac{G}{\mu_1}\mathbf{B}^2_{\kappa_{p(t)}}\,, \tag{3.210d}$$

$$\mathbf{q} = -k\nabla\theta\,. \tag{3.210e}$$

3.11 Viscoelastic models with two natural configurations

Our aim is to model asphalt binder, a complex material consisting of many constituent hydrocarbons. Since it is a material that exhibits two different relaxation mechanisms we need model that would be able to describe them. We incorporate the complex response of material by assuming the co-existence of two natural configurations (giving us the possibility to describe two different relaxation mechanisms). In fact, by considering two natural configurations we are able to model the fact that asphalt binder is a mixture. Thus two natural configurations as described in Section 3.1.1 are used, see Figure 3.3.

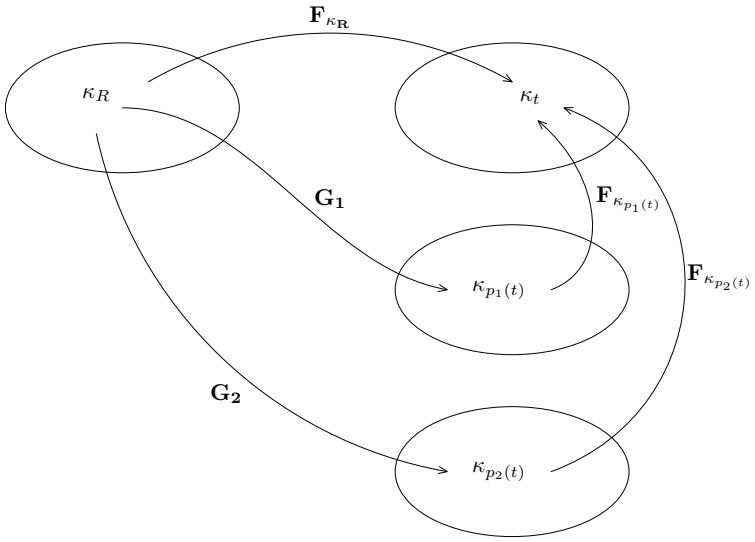

Figure 3.3: Two natural configurations.

We define kinematical quantities. Tensors $\mathbf{F}_{\kappa_{p_i(t)}}$ map the infinitesimal element from $\kappa_{p_i(t)}$ to κ_t and $\mathbf{G}_i$ map from κ_R to $\kappa_{p_i(t)}$ for $i = 1, 2$. They are related through the deformation gradient

$$\mathbf{G}_i = \mathbf{F}^{-1}_{\kappa_{p_i(t)}} \mathbf{F}_{\kappa_R}. \tag{3.211}$$

The left and right Cauchy-Green tensors corresponding to $\kappa_{p_i(t)}$ are defined through

$$\mathbf{B}_{\kappa_{p_i(t)}} = \mathbf{F}_{\kappa_{p_i(t)}} \mathbf{F}^{\mathrm{T}}_{\kappa_{p_i(t)}}, \quad \mathbf{C}_{\kappa_{p_i(t)}} = \mathbf{F}^{\mathrm{T}}_{\kappa_{p_i(t)}} \mathbf{F}_{\kappa_{p_i(t)}}, i = 1, 2,$$

and the rates of the deformation of $\kappa(p_i(t))$, resp. its symmetric part

$$\mathbf{L}_{\kappa_{p_i(t)}} = \dot{\mathbf{G}}_i \mathbf{G}_i^{-1}, \quad \mathbf{D}_{\kappa_{p_i(t)}} = \frac{\mathbf{L}_{\kappa_{p_i(t)}} + \mathbf{L}^{\mathrm{T}}_{\kappa_{p_i(t)}}}{2}, i = 1, 2,$$

Upon differentiation $\mathbf{B}_{\kappa_{p_1(t)}}$ we obtain

$$\overset{\triangledown}{\mathbf{B}}_{\kappa_{(p_i(t))}} = -2\mathbf{F}_{\kappa_{p_i(t)}} \mathbf{D}_{\kappa_{p_i(t)}} \mathbf{F}^{\mathrm{T}}_{\kappa_{p_i(t)}}, i = 1, 2. \tag{3.212}$$

and

$$\operatorname{tr} \dot{\mathbf{B}}_{\kappa_{p_i(t)}} = 2\mathbf{B}_{\kappa_{p_1(t)}} \cdot \mathbf{D} - 2\mathbf{F}_{\kappa_{p_i(t)}} \mathbf{D}_{\kappa_{p_i(t)}} \cdot \mathbf{F}_{\kappa_{p_i(t)}}, i = 1, 2. \tag{3.213}$$

3.11.1 Incompressibility conditions

According to Subsection 3.1.2 we can consider several compressible/incompressible variants in case of two natural configurations.

For example one natural configuration can be fully incompressible (III) and the other incompressible with compressible viscous and elastic response (ICC), or simply both can be fully incompressible (III)/(III) or we can consider a compressible variant (ICC)/(ICC).

Since the natural configurations are symmetric, we can consider a compressible total deformation with six possible combinations:

(CCC)/(CCC), (CCC)/(CIC), (CCC)/(CCI), (CIC)/(CIC), (CIC)/(CCI), (CCI)/(CCI).

For the brevity, in this work we present only two variants of compressibility (III)/(III) and (ICC)/(ICC).

(III)/(III) In case of (III)/(III) it holds that

$$\operatorname{tr}\mathbf{D} = \operatorname{tr}\mathbf{D}_{\kappa_{p_1(t)}} = \operatorname{tr}\mathbf{D}_{\kappa_{p_2(t)}} = 0 \tag{3.214}$$

and the internal energy describing the elastic responses that correspond to that of incompressible neo-Hookean solids is in the form

$$e = e_0(\eta,\rho) + \frac{G_1}{2\rho}(\operatorname{tr}\mathbf{B}_{\kappa_{p_1(t)}} - 3) + \frac{G_2}{2\rho}(\operatorname{tr}\mathbf{B}_{\kappa_{p_2(t)}} - 3) \quad (\mu_1 > 0, \mu_2 > 0) \tag{3.215}$$

where G_1, G_2 are two elastic moduli each corresponding to elastic response of individual natural configuration. It follows from (3.215) that

$$\rho\dot{e} = \rho\frac{\partial e}{\partial\eta}\dot{\eta} + \rho\frac{\partial e}{\partial\rho}\dot{\rho} + \rho\frac{\partial e}{\partial\mathbf{B}_{\kappa_{p_1(t)}}}\cdot\dot{\mathbf{B}}_{\kappa_{p_1(t)}} + \rho\frac{\partial e}{\partial\mathbf{B}_{\kappa_{p_2(t)}}}\cdot\dot{\mathbf{B}}_{\kappa_{p_2(t)}} \tag{3.216}$$

$$\overset{(3.215)}{=} \rho\theta\dot{\eta} + \frac{G_1}{2}\operatorname{tr}\dot{\mathbf{B}}_{\kappa_{p_1(t)}} + \frac{G_2}{2}\operatorname{tr}\dot{\mathbf{B}}_{\kappa_{p_2(t)}}. \tag{3.217}$$

which on using (3.213) leads to

$$\rho\dot{e} = \rho\theta\dot{\eta} + (\mu_1\mathbf{B}_{\kappa_{p_1(t)}} + \mu_2\mathbf{B}_{\kappa_{p_2(t)}})\cdot\mathbf{D} - G_1\mathbf{C}_{\kappa_{p_1(t)}}\cdot\mathbf{D}_{\kappa_{p_1(t)}} - G_2\mathbf{C}_{\kappa_{p_2(t)}}\cdot\mathbf{D}_{\kappa_{p_2(t)}}. \tag{3.218}$$

By inserting this result into balance of internal energy (1.16) we obtain balance of entropy

$$\rho\dot{\eta} + \operatorname{div}\left(\frac{\mathbf{q}}{\theta}\right) = \rho\frac{r}{\theta} + \frac{\xi}{\theta} \tag{3.219}$$

where

$$\xi = (\mathbf{T} - G_1\mathbf{B}_{\kappa_{p_1(t)}} - G_2\mathbf{B}_{\kappa_{p_2(t)}})\cdot\mathbf{D} + G_1\mathbf{C}_{\kappa_{p_1(t)}}\cdot\mathbf{D}_{\kappa_{p_1(t)}} + G_2\mathbf{C}_{\kappa_{p_2(t)}}\cdot\mathbf{D}_{\kappa_{p_2(t)}} - \frac{\mathbf{q}\cdot\nabla\theta}{\theta} \tag{3.220}$$

is the rate of entropy production. Because we only consider processes wherein the temperature of the body is constant, the last term disappears and we arrive at the reduced thermodynamic equality

$$\xi = (\mathbf{T} - G_1\mathbf{B}_{\kappa_{p_1(t)}} - G_2\mathbf{B}_{\kappa_{p_2(t)}})\cdot\mathbf{D} + G_1\mathbf{C}_{\kappa_{p_1(t)}}\cdot\mathbf{D}_{\kappa_{p_1(t)}} + G_2\mathbf{C}_{\kappa_{p_2(t)}}\cdot\mathbf{D}_{\kappa_{p_2(t)}}. \tag{3.221}$$

(ICC)/(ICC) In case of (ICC)/(ICC) there is only one incompressibility condition $\operatorname{tr}\mathbf{D}=0$. The constitutive relation for the elastic response is given by the internal energy

$$e = e_0(\eta,\rho) + \frac{G_1}{2\rho}\left(\operatorname{tr}\mathbf{B}_{\kappa_{p_1(t)}} - 3 - \ln(\det\mathbf{B}_{\kappa_{p_1(t)}})\right) + \frac{G_2}{2\rho}\left(\operatorname{tr}\mathbf{B}_{\kappa_{p_2(t)}} - 3 - \ln(\det\mathbf{B}_{\kappa_{p_2(t)}})\right), \quad (3.222)$$

which corresponds to two compressible neo-Hookean solids. Then the reduced thermodynamic inequality is in the form

$$0 \le \xi = \left(\mathbf{T} - G_1(\mathbf{B}_{\kappa_{p_1(t)}} - \mathbf{I}) - G_2(\mathbf{B}_{\kappa_{p_2(t)}} - \mathbf{I})\right)\cdot\mathbf{D} + G_1\left(\mathbf{C}_{\kappa_{p_1(t)}} - \mathbf{I}\right)\cdot\mathbf{D}_{\kappa_{p_1(t)}} + G_2\left(\mathbf{C}_{\kappa_{p_2(t)}} - \mathbf{I}\right)\cdot\mathbf{D}_{\kappa_{p_2(t)}}. \quad (3.223)$$

3.12 Incompressible model with two natural configurations and purely quadratic dissipation Quad2

First we derive a fully incompressible viscoelastic model (III)/(III) with thermodynamic inequality in the form (3.221). We choose a purely quadratic constitutive relation for the rate of entropy production

$$0 \le \tilde{\xi} = \tilde{\xi}(\mathbf{D},\mathbf{D}_{\kappa_{p_1(t)}},\mathbf{D}_{\kappa_{p_2(t)}}) = 2\mu_3|\mathbf{D}|^2 + 2\mu_1|\mathbf{D}_{\kappa_{p_1(t)}}|^2 + \mu_2|\mathbf{D}_{\kappa_{p_2(t)}}|^2, \quad (3.224)$$

where $\mu_3>0$, $\mu_1>0$, $\mu_2>0$. Now, the principle of the maximization of the rate of entropy production is used under the restrictions of reduced thermodynamic inequality (3.221) and incompressibility conditions $\operatorname{tr}\mathbf{D} = \operatorname{tr}\mathbf{D}_{\kappa_{p_1(t)}} = \operatorname{tr}\mathbf{D}_{\kappa_{p_2(t)}} = 0$.

Let us define

$$L(\mathbf{D},\mathbf{D}_{\kappa_{p_1(t)}},\mathbf{D}_{\kappa_{p_2(t)}}) := \tilde{\xi}(\mathbf{D},\mathbf{D}_{\kappa_{p_1(t)}},\mathbf{D}_{\kappa_{p_2(t)}}) + \lambda_1\Big(\tilde{\xi}(\mathbf{D},\mathbf{D}_{\kappa_{p_1(t)}},\mathbf{D}_{\kappa_{p_2(t)}}) - (\mathbf{T} - G_1\mathbf{B}_{\kappa_{p_1(t)}} - G_2\mathbf{B}_{\kappa_{p_2(t)}})\cdot\mathbf{D} - G_1\mathbf{C}_{\kappa_{p_1(t)}}\cdot\mathbf{D}_{\kappa_{p_1(t)}} - G_2\mathbf{C}_{\kappa_{p_2(t)}}\cdot\mathbf{D}_{\kappa_{p_2(t)}}\Big) - \lambda_2\operatorname{tr}\mathbf{D} - \lambda_3\operatorname{tr}\mathbf{D}_{\kappa_{p_1(t)}} - \lambda_4\operatorname{tr}\mathbf{D}_{\kappa_{p_2(t)}}. \quad (3.225)$$

We use Lagrange multipliers which delivers the following set of equations

$$\frac{\partial L}{\partial\mathbf{D}} = \mathbf{0}, \quad (3.226)$$

$$\frac{\partial L}{\partial\mathbf{D}_{\kappa_{p_1(t)}}} = \mathbf{0}, \quad (3.227)$$

$$\frac{\partial L}{\partial\mathbf{D}_{\kappa_{p_2(t)}}} = \mathbf{0}, \quad (3.228)$$

that can be simplified to

$$\frac{1+\lambda_1}{\lambda_1}4\mu_3\mathbf{D} = \mathbf{T} - G_1\mathbf{B}_{\kappa_{p_1(t)}} - G_2\mathbf{B}_{\kappa_{p_2(t)}} + \frac{\lambda_2}{\lambda_1}\mathbf{I}, \quad (3.229)$$

$$\frac{1+\lambda_1}{\lambda_1}4\mu_1\mathbf{D}_{\kappa_{p_1(t)}} = G_1\mathbf{C}_{\kappa_{p_1(t)}} + \frac{\lambda_3}{\lambda_1}\mathbf{I}, \quad (3.230)$$

$$\frac{1+\lambda_1}{\lambda_1}4\mu_2\mathbf{D}_{\kappa_{p_2(t)}} = G_2\mathbf{C}_{\kappa_{p_2(t)}} + \frac{\lambda_4}{\lambda_1}\mathbf{I}. \quad (3.231)$$

We first take the scalar product of (3.229) with $\mathbf{D}$, (3.230) with $\mathbf{D}_{\kappa_{p_1(t)}}$ and (3.231) with $\mathbf{D}_{\kappa_{p_2(t)}}$ and sum these products. With help of (3.224) and (3.221) we conclude that

$$\frac{1+\lambda_1}{\lambda_1} = \frac{1}{2}\,. \tag{3.232}$$

Next we take the trace of (3.229), which together with (3.214) delivers

$$\frac{\lambda_2}{\lambda_1} = -\frac{1}{3}\,\mathrm{tr}(\mathbf{T} - G_1\mathbf{B}_{\kappa_{p_1(t)}} - G_2\mathbf{B}_{\kappa_{p_2(t)}})\,. \tag{3.233}$$

We define a quantity p through

$$p = -\frac{1}{3}\,\mathrm{tr}\,\mathbf{T}\,. \tag{3.234}$$

Substitution of (3.234), (3.233) and (3.232) into (3.229) yields

$$\mathbf{T} = -p\mathbf{I} + 2\mu_3\mathbf{D} + G_1\mathbf{B}^d_{\kappa_{p_1(t)}} + G_2\mathbf{B}^d_{\kappa_{p_2(t)}}\,. \tag{3.235}$$

Further, taking the trace of (3.230) and (3.231) we obtain (using incompressibility (3.214))

$$\frac{\lambda_3}{\lambda_1} = -\frac{1}{3}G_1\,\mathrm{tr}\,\mathbf{C}_{\kappa_{p_1(t)}}, \quad \frac{\lambda_4}{\lambda_1} = -\frac{1}{3}G_2\,\mathrm{tr}\,\mathbf{C}_{\kappa_{p_2(t)}}\,, \tag{3.236}$$

which after substitution into (3.230) and (3.231) yields

$$2\mu_i\mathbf{D}_{\kappa_{p_i(t)}} = G_i\mathbf{C}^d_{\kappa_{p_i(t)}}, \quad i=1,2. \tag{3.237}$$

Multiplying these equations by $\mathbf{F}_{\kappa_{p_i(t)}}$ from the left and $\mathbf{F}^{\mathrm{T}}_{\kappa_{p_i(t)}}$ from the right and using (3.212) we obtain

$$\overset{\triangledown}{\mathbf{B}}_{\kappa_{p_i(t)}} = -\frac{G_i}{\mu_i}\mathbf{B}_{\kappa_{p_i(t)}}\mathbf{B}^d_{\kappa_{p_i(t)}}, \quad i=1,2. \tag{3.238}$$

We obtain the model with two relaxation mechanisms

$$\mathbf{T} = -p\mathbf{I} + 2\mu_3\mathbf{D} + G_1\mathbf{B}^d_{\kappa_{p_1(t)}} + G_2\mathbf{B}^d_{\kappa_{p_2(t)}}\,, \tag{3.239a}$$

$$\overset{\triangledown}{\mathbf{B}}_{\kappa_{p_1(t)}} = -\frac{G_1}{\mu_1}\mathbf{B}_{\kappa_{p_1(t)}}\mathbf{B}^d_{\kappa_{p_1(t)}}\,, \tag{3.239b}$$

$$\overset{\triangledown}{\mathbf{B}}_{\kappa_{p_2(t)}} = -\frac{G_2}{\mu_2}\mathbf{B}_{\kappa_{p_2(t)}}\mathbf{B}^d_{\kappa_{p_2(t)}}\,. \tag{3.239c}$$

This model can be also obtained by preferring the thermodynamic fluxes $\mathbf{T}^d_{\mathrm{dis}}$, $\mathbf{C}^d_{\kappa_{p_1(t)}}$ and $\mathbf{C}^d_{\kappa_{p_2(t)}}$. We suppose the constitutive relation in the form

$$\tilde{\xi}(\mathbf{T}^d_{\mathrm{dis}}, \mathbf{C}^d_{\kappa_{p_1(t)}}, \mathbf{C}^d_{\kappa_{p_2(t)}}) = \frac{1}{2\mu_3}|\mathbf{T}^d_{\mathrm{dis}}|^2 + \frac{G_1^2}{2\mu_1}|\mathbf{C}^d_{\kappa_{p_1(t)}}|^2 + \frac{G_2^2}{2\mu_2}|\mathbf{C}^d_{\kappa_{p_2(t)}}|^2, \tag{3.240}$$

and the reduced thermodynamic equality is equal to

$$0 \le \xi = \underbrace{\left(\mathbf{T} - G_1\mathbf{B}_{\kappa_{p_1(t)}} - G_2\mathbf{B}_{\kappa_{p_2(t)}}\right)^d}_{\mathbf{T}^d_{\mathrm{dis}}}\cdot\mathbf{D}^d + G_1(\mathbf{C}_{\kappa_{p_1(t)}} - \mathbf{I})\cdot\mathbf{D}_{\kappa_{p_1(t)}} + G_2(\mathbf{C}_{\kappa_{p_2(t)}} - \mathbf{I})\cdot\mathbf{D}_{\kappa_{p_2(t)}}. \tag{3.241}$$

The model is obtained by maximization of the rate of entropy production (3.240) among the values of $\mathbf{T}^d_{\mathrm{dis}}$, $\mathbf{C}^d_{\kappa_{p_1(t)}}$ and $\mathbf{C}^d_{\kappa_{p_2(t)}}$ fulfilling the equality (3.241).

3.12.1 Properties of model Quad2

Model (3.239) has similar properties as model (3.112), the properties of both matrices $\mathbf{B}_{\kappa_{p_1(t)}}$ and $\mathbf{B}_{\kappa_{p_2(t)}}$ in model (3.239) are the same as the property of $\mathbf{B}_{\kappa_{p(t)}}$ for model (3.112). At the beginning (at rest) $\mathbf{B}_{\kappa_{p_i(t)}}(t=0)=\mathbf{I}$ are positive definite matrices with $\det \mathbf{B}_{\kappa_{p_i(t)}}(t=0)=1$. Using (B.3) from the Appendix we get

$$\frac{\mathrm{d}}{\mathrm{d}t}\ln(\det \mathbf{B}_{\kappa_{p_i(t)}}) = \operatorname{tr}\left(\dot{\mathbf{B}}_{\kappa_{p_i(t)}}\mathbf{B}^{-1}_{\kappa_{p_i(t)}}\right) \overset{(3.239)(bc)}{=} 2\operatorname{tr}\mathbf{D} - \frac{G}{\mu_i}\operatorname{tr}\mathbf{B}^{d}_{\kappa_{p_i(t)}} = 0, \quad i=1,2 \tag{3.242}$$

and

$$\det \mathbf{B}_{\kappa_{p_i(t)}}(t) = 1 \ \forall t \geq 0, \quad i=1,2, \tag{3.243}$$

which means that the evolutionary equations (3.239b) and (3.239c) include the incompressibility conditions of the elastic responses (3.214). Further, using Lemma B.1.2 from Appendix we get the relation the trace of $\mathbf{B}_{\kappa_{p_i(t)}}$

$$\operatorname{tr}\mathbf{B}_{\kappa_{p_i(t)}} \geq d, \ i=1,2, \text{ where } d \text{ is the space dimension.} \tag{3.244}$$

3.12.2 Linearization of model Quad2

We show that the model with purely quadratic dissipation and two relaxation mechanisms (3.239) reduces to Burgers model with additional Newtonian dissipation (2.13) when the elastic response is linearized. We showed this reduction in [38]. If we suppose that the left Cauchy-Green tensors are small $\|\mathbf{B}_{\kappa_{p_i(t)}}-\mathbf{I}\|=\epsilon_i, \quad 0<\epsilon_i \ll 1, \quad i=1,2$, then (3.239) reduces to

$$\mathbf{T} = -p\mathbf{I} + 2\mu_3\mathbf{D} + G_1(\mathbf{B}_{\kappa_{p_1(t)}}-\mathbf{I}) + G_2(\mathbf{B}_{\kappa_{p_2(t)}}-\mathbf{I}), \tag{3.245a}$$

$$\overset{\triangledown}{\mathbf{B}}_{\kappa_{p_1(t)}} = -\frac{G_1}{\mu_1}(\mathbf{B}_{\kappa_{p_1(t)}}-\mathbf{I}), \tag{3.245b}$$

$$\overset{\triangledown}{\mathbf{B}}_{\kappa_{p_2(t)}} = -\frac{G_2}{\mu_2}(\mathbf{B}_{\kappa_{p_2(t)}}-\mathbf{I}). \tag{3.245c}$$

Linearization is done in the same way as linearization of model (3.112). Let us denote two relaxation times $\tau_1=\mu_1/G_1$ and $\tau_2=\mu_2/G_2$ and let us define

$$\mathbf{S}_1 = G_1(\mathbf{B}_{\kappa_{p_1(t)}}-\mathbf{I}), \quad \mathbf{S}_2 = G_2(\mathbf{B}_{\kappa_{p_2(t)}}-\mathbf{I}), \quad \mathbf{S}=\mathbf{S}_1+\mathbf{S}_2, \tag{3.246}$$

then the system (3.245a) – (3.245c) reduces to

$$\mathbf{T} = -p\mathbf{I} + 2\mu_3\mathbf{D} + \mathbf{S}, \tag{3.247a}$$

$$\overset{\triangledown}{\mathbf{S}}_1 = -\frac{1}{\tau_1}\mathbf{S}_1 + 2G_1\mathbf{D}, \tag{3.247b}$$

$$\overset{\triangledown}{\mathbf{S}}_2 = -\frac{1}{\tau_2}\mathbf{S}_2 + 2G_2\mathbf{D}. \tag{3.247c}$$

Using (3.247b) and (3.247c) repeatedly we calculate $\overset{\triangledown}{\mathbf{S}}$ and $\overset{\triangledown\triangledown}{\mathbf{S}}$. We obtain

$$\overset{\triangledown}{\mathbf{S}} = \overset{\triangledown}{\mathbf{S}}_1 + \overset{\triangledown}{\mathbf{S}}_2 = -\frac{1}{\tau_1}\mathbf{S}_1 - \frac{1}{\tau_2}\mathbf{S}_2 + 2(G_1+G_2)\mathbf{D}, \tag{3.248}$$

$$\begin{aligned}\overset{\triangledown\triangledown}{\mathbf{S}} &= -\frac{1}{\tau_1}\overset{\triangledown}{\mathbf{S}}_1 - \frac{1}{\tau_2}\overset{\triangledown}{\mathbf{S}}_2 + 2(G_1+G_2)\overset{\triangledown}{\mathbf{D}} \\ &= \frac{1}{\tau_1^2}\mathbf{S}_1 + \frac{1}{\tau_2^2}\mathbf{S}_2 - 2\left(\frac{G_1}{\tau_1}+\frac{G_2}{\tau_2}\right)\mathbf{D} + 2(G_1+G_2)\overset{\triangledown}{\mathbf{D}}.\end{aligned} \tag{3.249}$$

Adding then the $(\tau_1+\tau_2)\times(3.248)+\tau_1\tau_2\times(3.249)$ we arrive at

$$(\tau_1+\tau_2)\overset{\triangledown}{\mathbf{S}}+\tau_1\tau_2\overset{\triangledown\triangledown}{\mathbf{S}}=-(\mathbf{S}_1+\mathbf{S}_2)+(2\tau_1G_1+2\tau_2G_2)\mathbf{D}+ 2\tau_1\tau_2(G_1+G_2)\overset{\triangledown}{\mathbf{D}}, \tag{3.250}$$

which is Burgers model with additional Newtonian dissipation (2.13)

$$\mathbf{T}=-p\mathbf{I}+2\mu_3\mathbf{D}+\mathbf{S}, \tag{3.251}$$

$$\mathbf{S}+(\tau_1+\tau_2)\overset{\triangledown}{\mathbf{S}}+\tau_1\tau_2\overset{\triangledown\triangledown}{\mathbf{S}}=2(\mu_1+\mu_2)\mathbf{D}+2(\mu_1\tau_2+\tau_1\mu_2)\overset{\triangledown}{\mathbf{D}}\ . \tag{3.252}$$

Since the model with purely quadratic dissipation and two relaxation mechanisms (3.239) reduces to Burgers model we call this model 'non-linear Burgers.

3.13 Burgers model with additional Newtonian dissipation

Burgers model can be obtained in a similar way as Oldroyd-B model. We assume that both elastic responses are compressible corresponding to that of compressible neo-Hookean solids with the internal energy given by (3.222). The total deformation is incompressible and we assume a compressible variant (ICC)/(ICC) with the thermodynamic inequality in the form (3.223).

The constitutive relation for the rate of entropy production is in the form

$$\tilde{\xi}(\mathbf{D},\mathbf{D}_{\kappa p_1(t)},\mathbf{D}_{\kappa p_2(t)},\mathbf{C}_{\kappa_{p_1(t)}},\mathbf{C}_{\kappa_{p_2(t)}})=2\mu_3|\mathbf{D}|^2+ 2\mu_1\mathbf{D}_{\kappa_{p_1(t)}}\mathbf{C}_{\kappa_{p_1(t)}}\cdot\mathbf{D}_{\kappa_{p_1(t)}}+2\mu_2\mathbf{D}_{\kappa_{p_2(t)}}\mathbf{C}_{\kappa_{p_2(t)}}\cdot\mathbf{D}_{\kappa_{p_2(t)}},\quad \mu_3,\mu_2,\mu_1>0. \tag{3.253}$$

By maximization of the rate of entropy production $\tilde{\xi}$ among the values of $\mathbf{D}$, $\mathbf{D}_{\kappa_{p_1(t)}}$ and $\mathbf{D}_{\kappa_{p_2(t)}}$ fulfilling the equality (3.223) and the constraint of incompressibility $\operatorname{tr}\mathbf{D}=0$ we obtain the Burgers model

$$\mathbf{T}=-p\mathbf{I}+2\mu_3\mathbf{D}+G_1(\mathbf{B}_{\kappa_{p_1(t)}}-\mathbf{I})+G_2(\mathbf{B}_{\kappa_{p_2(t)}}-\mathbf{I}), \tag{3.254a}$$

$$\overset{\triangledown}{\mathbf{B}}_{\kappa_{p_1(t)}}=-\frac{G_1}{\mu_1}(\mathbf{B}_{\kappa_{p_1(t)}}-\mathbf{I}), \tag{3.254b}$$

$$\overset{\triangledown}{\mathbf{B}}_{\kappa_{p_2(t)}}=-\frac{G_2}{\mu_2}(\mathbf{B}_{\kappa_{p_2(t)}}-\mathbf{I}). \tag{3.254c}$$

In the previous subsection we showed that this model is equivalent to Burgers models with additional Newtonian dissipation (2.13), tensors $\mathbf{B}_i$ are used instead of tensors $\mathbf{B}_{\kappa_{p_i(t)}}$. Ratios $\mu_1/G_1=\tau_1$ and $\mu_2/G_2=\tau_2$ are called relaxation times and the model is written in this work in the form

$$\mathbf{T}=-p\mathbf{I}+2\mu_3\mathbf{D}+G_1(\mathbf{B}_1-\mathbf{I})+G_2(\mathbf{B}_2-\mathbf{I}), \tag{3.255a}$$

$$\overset{\triangledown}{\mathbf{B}}_1=-\frac{1}{\tau_1}(\mathbf{B}_1-\mathbf{I}), \tag{3.255b}$$

$$\overset{\triangledown}{\mathbf{B}}_2=-\frac{1}{\tau_2}(\mathbf{B}_2-\mathbf{I}). \tag{3.255c}$$

3.13.1 Properties of Burgers model

Upon applying the same procedure as in Section 2.3 the following property can be proved. If $\mathbf{B}_i, i = 1, 2$ is symmetric positive at the beginning (at rest) $t = 0$, then $B_i, i = 1, 2$ remains to be symmetric positive definite for all $t \geq 0$ and it holds that

$$\det \mathbf{B}_i \geq 1 \quad \forall t \geq 0, \quad i = 1, 2. \tag{3.256}$$

and

$$\operatorname{tr} \mathbf{B}_i \geq d, \quad i = 1, 2. \tag{3.257}$$

Chapter 4

Fitting of the experimental data with derived models

"It doesn't matter how beautiful your theory is, it doesn't matter how smart you are. If it doesn't agree with experiment, it's wrong."

Richard P. Feynman, 1964[1]

In this chapter we present three different sets of experiments concerning asphalt concrete or asphalt binder and use them to corroborate the models derived in the previous chapter.

Most of experimental results reported in literature present the data in which some model is assumed, usually the linear viscoelastic model, rather than the raw data that can then be used to corroborate models. Raw experimental data are provided in the experimental studies of Monismith and Secor [41, 42], and other papers by Monismith and his co-workers. We use standard stress relaxation and creep test experiment performed by Monismith, Secor (1962) in [41].

Furthermore, we use raw experimental data obtained by Krishnan and Narayan [27] that exhibit a very interesting phenomenon of the torque overshoot due to the specimen in the torsional rheometer, under constant shear-rate. This set of experiments is very useful with regard to the corroboration of models because the torque overshoot can not be captured by linear models like Oldroyd-B or Burgers.

The last experiment is a stress relaxation experiment performed by Narayan et al. [43]. They measured the torque and normal force in a torsional rheometer and showed that the material exhibits markedly different relaxation times with regards to the torque and normal force which can not be predicted by model with one relaxation time.

The last two sets of experiments were performed with different types of asphalt binder. In [38] we used the model Quad2 Quad2 for fitting these two experiments. The experiment by Monismith and Secor was performed with asphalt concrete. Although the density of such material is not constant (compared to asphalt binder that is almost incompressible), mainly due to the air voids reduction of asphalt concrete (see [62]), we

[1] According to [14].

suppose for simplicity that the material is incompressible. This experiment is used in this work to corroborate the model Quad2.

The experiment by Narayan et al. [43] that documents the torque overshoot was also used to corroborate PL2012 and RaSr2000 model, we published this result in [21].

4.1 Experimental data

In this section we present experimental data by Monismith, Secor (1962), Krishnan and Narayan (2007) and Narayan et al. (2012). We start from the oldest one.

4.1.1 Monismith, Secor (1962) – stress relaxation and creep test experiment

Monismith and Secor (1962) performed an experiment with a cylindrical piece of asphalt concrete. The height of the cylinder is 6.5 in, the radius is 1.4 in. This experiment was performed at three different constant temperatures T: 40°F (cca 4.4°C), 77°F (=25°C) and 140°F (=60°C). The lateral pressure on the cylinder is equal to zero. Monismith and Secor tried to fit this experiment with standard Burgers model, and the fit was quite satisfactory. Later, this experiment was better fitted for example by Krishnan and Rajagopal, see [29], where a model with eight parameters was used.

Stress relaxation experiment

In this experiment a cylindrical piece of asphalt was at time $t = 0$s suddenly deformed with a constant strain, this deformation was kept for all time and the corresponding stress (T_{zz} component) was measured.

Temp [°F]	Strain s [%]	Stretch ratio $\lambda = 1 - s$
40	0.75%	0.9925
	0.52%	0.9948
	0.29%	0.9971
77	0.30%	0.9970
	0.21%	0.9979
	0.10%	0.9990
140	0.28%	0.9972
	0.18%	0.9982
	0.09%	0.9991

Table 4.1: Experiment setting for the stress relaxation Monismith, Secor (1962).

In the Table 4.1 you can see the settings of the experiment. The experimental data are depicted in the Figure 4.1.

Creep test experiment

In this experiment the cylinder was pushed in the $z-$axis with a constant pressure between the time 0 s and 12 000 s (200 min) and after that the pressure (T_{zz} component) was released and the evolution of the strain was recorded. Like in the stress relaxation experiment, this experiment was performed for three different temperatures: 40°F, 77°F and 140°F.

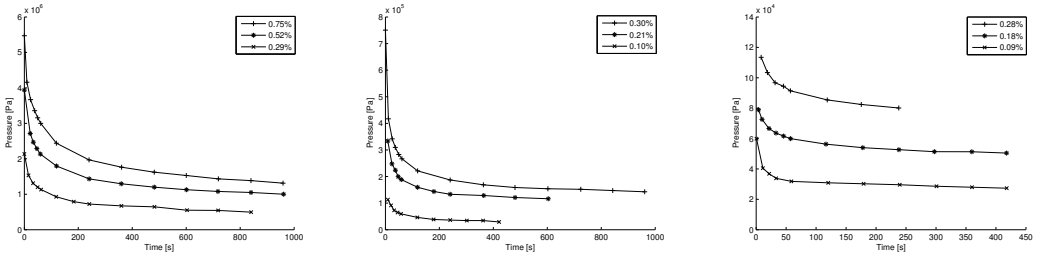

a) 40°F b) 77°F c) 140°F

Figure 4.1: Experimental data for the stress relaxation, Monismith, Secor (1962).

In the Table 4.2 you can see the settings of the experiment and the experimental data are depicted in the Figure 4.2.

Temp [°F]	Pressure [psi]	Pressure [kPa]
40	85.50	589.5
	68.40	471.6
	51.30	353.7
77	25.60	176.5
	16.10	111.0
	8.55	59.0
140	4.27	29.4
	2.56	17.7
	1.71	11.8

Table 4.2: Experiment setting for the creep test Monismith, Secor (1962).

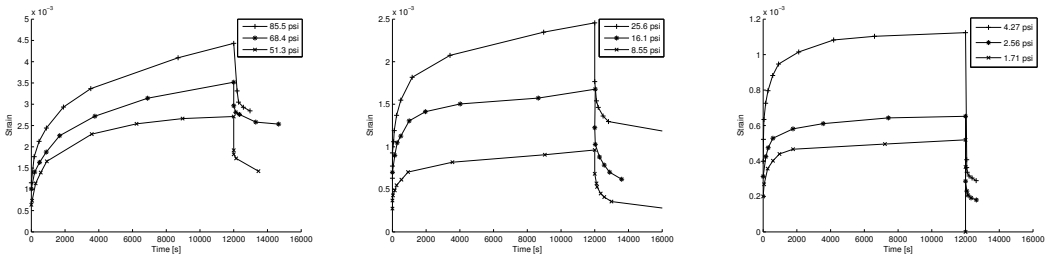

a) 40°F b) 77°F c) 140°F

Figure 4.2: Experimental data for the creep test, Monismith, Secor (1962).

4.1.2 Narayan et al. (2012) – torsional experiment

This experiment studies relaxation torque and normal force in torsion. In this experiment and the other experiment from 2007 the torsional rheometer is used. It consists of two plates, the lower is fixed and does not move, the upper one can rotate, the radius of the plates is $R = 4$mm. The experiment was performed with several different asphalt

binders: unaged base binder and aged base binder, unaged polymer modified binder and aged polymer modified binder[2].

At the beginning a sample of asphalt was placed between the plates and it was squeezed to the height $h = 1$mm. The excess material was trimmed off. Then the specimen was allowed to relax and settle at the given temperature. Finally, at time $t = 0$ the upper plate started to rotate with an angular velocity 0.5 rad s^{-1} and at $t = 0.5$s it stopped rotating and the corresponding torque and normal force was recorded up to the time $t = 2$s. The angular velocity ω is equal to

$$\omega = \begin{cases} 0.5\text{rad s}^{-1} & 0\text{s} \leq t \leq 0.5\text{s} \\ 0\text{rad s}^{-1} & 0.5\text{s} < t \leq 2.0\text{s}. \end{cases} \tag{4.1}$$

The experiments with four types of asphalt binder were performed at four different constant temperatures: 25°C, 30°C, 35°C and 40°C. Experimental data are depicted in the Figures 4.3a), 4.3b) – 4.6a), 4.6b). The error measurement is 0.02 N for the Normal force data and 0.05 mNm for the torque.

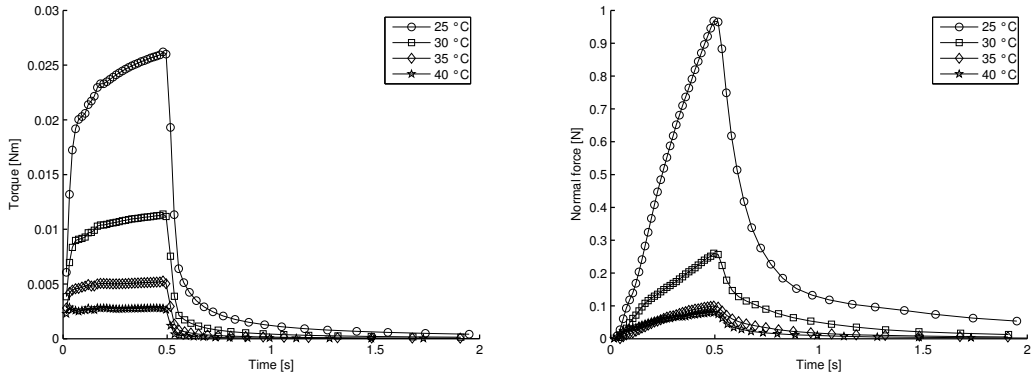

a) Experimental data for the torque b) Experimental data for the normal force

Figure 4.3: Experimental data, unaged base asphalt binder.

It is clear from the experimental data that at least two different relaxation mechanisms are present in all materials. The relaxation time in the normal force data is significantly higher than the relaxation time in the torque data. That is why we have to use the model that is able to describe these two mechanisms.

4.1.3 Krishnan and Narayan (2007) – torque overshoot experiment

In 2007 Krishnan and Narayan performed a similar experiment like the one described in the previous subsection. The difference is that they used different material and they did not stop rotation of the upper plate like in the year 2012, so the angular velocity was constant.

They performed the experiment at a constant temperature 35°C with three different angular velocities 0.5 rad.s^{-1}, 0.25 rad.s^{-1} and 0.125 rad.s^{-1}. They measured only the torque needed to achieve the constant angular velocity and not the normal force,

[2]Asphalt binder is modified in order to improve the engineering performance of the resulting asphalt cement when it is used in asphalt concrete.

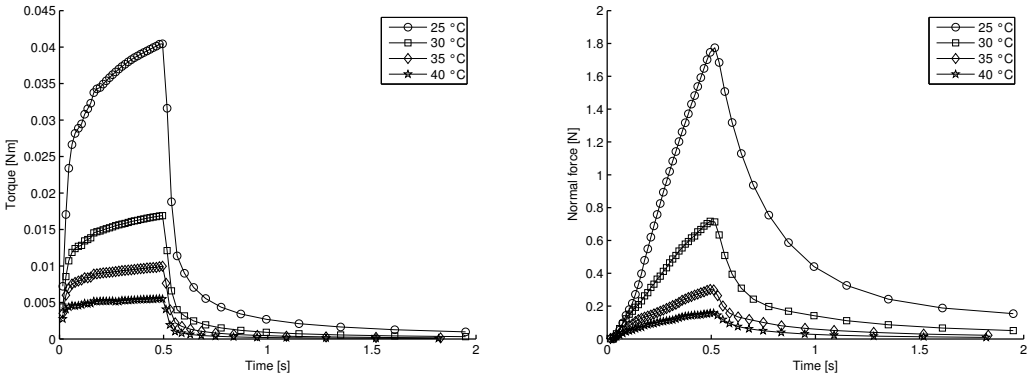

a) Experimental data for the torque b) Experimental data for the normal force

Figure 4.4: Experimental data, aged base asphalt binder.

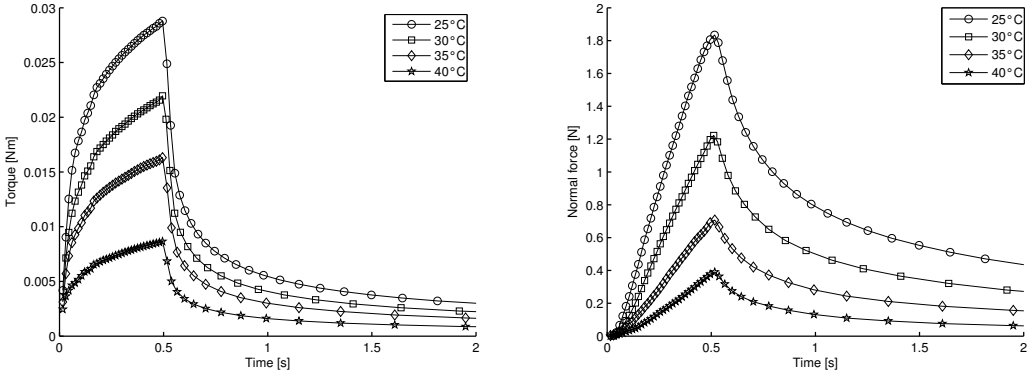

a) Experimental data for the torque b) Experimental data for the normal force

Figure 4.5: Experimental data, unaged polymer modified asphalt binder.

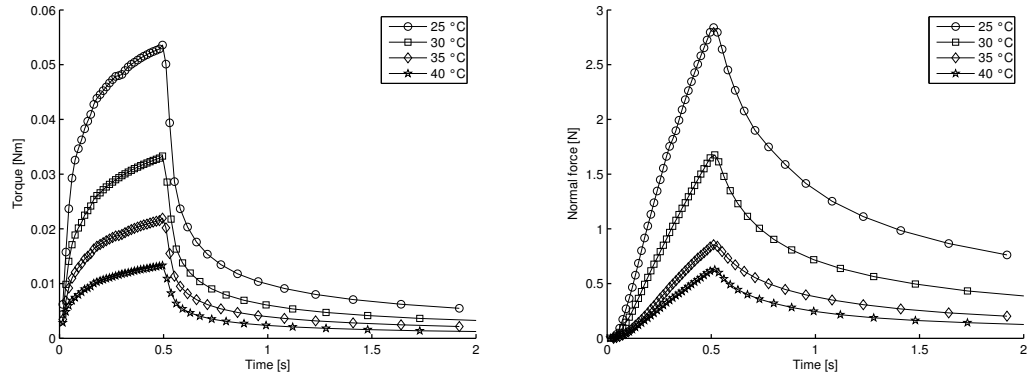

a) Experimental data for the torque b) Experimental data for the normal force

Figure 4.6: Experimental data, aged polymer modified asphalt binder.

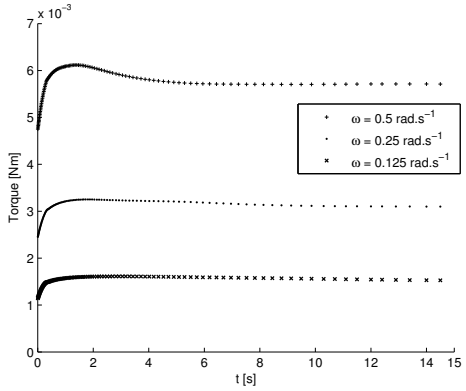

Figure 4.7: Experimental data, Krishnan and Narayan (2007).

measured data are depicted in Figure 4.7. The overshoot of the torque (that can be mainly seen for $\omega = 0.35$ rad s^{-1}) at the beginning of the measurement is very interesting because linear viscoelastic models like Oldroyd-B or Burgers can not capture it.

4.2 Fitting of the experiments

Fitting of the experiments was done with the following models: Oldroyd-B (2.10), Burgers (3.255), RaSr2000 (3.49), PL2012 (3.97), Quad1 (3.112) and Quad2 (3.239). All these models were used for fitting the experiment with the torque overshoot by Krishnan and Narayan (2007). Sets of experiments by Monismith and Secor and Narayan et al. (2012) were fitted only with the model Quad2.

All models contain some set of material parameters. Our aim is to find for each set of experiments a set of material parameters for which the model describes the experimental data best.

Let $\{E_i\}_{i=1}^n$ be a set of experimental data consisting of n experiments $E_i : [0, T] \to R$. For example, in case of Monismith and Secor (1962) $n = 6$, $E_i, i = 1, 2, 3$ is the measured pressure in the stress relaxation experiment at three different strains and $E_i, i = 4, 5, 6$ is the measured strain in the creep test at three different pressures, while in case of Krishnan and Narayan (2007) $n = 3$ and E_i, $i = 1, 2, 3$ stand for three measured torques for three different angular velocities and in case of Narayan et al. (2012) $n = 2$, E_1 is the measured torque and E_2 is the measured normal force. The values of $E_i(t)$ are measured only at discrete times t^j, $j = 1, \ldots, k$. Since all used models are isothermal, different temperature of the experiment defines a new material.

Further, let $C_i(\text{parms}, t)$ be the theoretical values predicted for the experiment E_i by a given model, where *parms* are the material parameters (for example for model Quad2 *parms* are μ_1, μ_2, μ_3, G_1, G_2) corresponding to the given model. For $i = 1, \ldots, n$ we define the absolute error g^i_{abs} and the relative error g^i_{rel} of one experiment E^i through

$$g^i_{\text{abs}}(parms) = \frac{1}{T}\int_0^T |C^i(parms, t) - E^i(t)|\,\mathrm{d}t, \tag{4.2}$$

$$g^i_{\text{rel}}(parms) = \frac{1}{T}\int_0^T \left|\frac{C^i(parms, t) - E^i(t)}{E^i(t)}\right|\,\mathrm{d}t, \tag{4.3}$$

where the integral over time is a mean value of k discrete experimental data points measured at times $t^1, \dots, t^k$

$$\frac{1}{T}\int_0^T f(t)\,\mathrm{d}t := \frac{1}{k}\sum_{j=1}^{k} f(t^j), \quad 0 = t^1 < t^2 < \cdots < t^{k-1} < t^k = T.$$

In [21] we fitted the experiment with model PL2012 using the relative errors g_{rel}. We were fitting three experiments at once by one set of material parameters, in such case it seemed that the relative error is a good measure because it is enough to sum individual relative errors to obtain the global error

$$g_{\mathrm{rel}} = \sum_{i=1}^{n} g^i_{\mathrm{rel}}. \tag{4.4}$$

Later in [38] we preferred the absolute error g_{abs} over the relative error g_{rel} as a proper measure of the error because the relative error at times when the values of experimental data are close to zero, fits the such almost perfectly to the detriment of the times when values of data from the experiment are large. However, in case of absolute error, the global error can not be obtained as a simple sum of individual errors. We aim to fit the set of experiments $\{E_i(t)\}_{i=1}^n$ with different corresponding characteristic values N_i. For example in case of the experiment by [43] $N_2/N_1 \approx 50$. In case of the absolute errors, we have to weight individual experiments by these characteristic values of the experimental data, i.e. our global error is defined through

$$g = \sum_{i=1}^{n} \frac{1}{N_i} g^i_{\mathrm{abs}}, \tag{4.5}$$

where n is the number of experiments in the set, g^i_{abs} is the absolute error of the experiment E_i defined by (4.2) and N_i is a characteristic value associated with the experiment E_i that is being considered.

We use the functional g introduced in (4.5) also to quantify how well one particular set of experiments is fitted with different models. If $g = 0$ the set of experiments is fitted perfectly.

The minimization of the scalar function g described by (4.5) or (4.4) is carried out using Matlab function `fminsearch` with the Nelder-Mead simplex algorithm, see [44]. It is known that this algorithm converges less often to local minima than for example the Newton method. However, there is no universal algorithm for finding the global minima for a general non-convex function, therefore the solution depends strongly on the initial guess. We improved the way of finding the minimum in the following manner. The same algorithm is still used, but after it converges to a (local) minimum, we round the minimizing parameters, use them as a new initial guess and run the minimization again. We repeat it until the cost function g of the solution decreases. The reason that this helps is due to the fact that at the beginning of the algorithm the neighborhood where the method tries other values of the parameters, is greater than in later runs of the algorithm. In virtue of this the algorithm is able to converge to a new lower (local) minimum.

4.2.1 Fitting of Monismith and Secor (1962)

The set of experiments performed by Monismith, Secor in [41] is described in Subsection 4.1.1 and it consists of two parts: stress relaxation test and creep test. It was fitted with model Quad2.

The initial-boundary value problem that is corroborated

For the simplicity we suppose that all variables depend only on time t and not on the coordinates. Since the deformation for both experiments is uniaxial it holds that all non-diagonal components of the stress tensor and its elastic part are zero

$$\mathbf{T} = \begin{pmatrix} T_{rr} & 0 & 0 \\ 0 & T_{\varphi\varphi} & 0 \\ 0 & 0 & T_{zz} \end{pmatrix}, \ \mathbf{B}_{\kappa_{p_1(t)}} = \begin{pmatrix} B_{1rr} & 0 & 0 \\ 0 & B_{1\varphi\varphi} & 0 \\ 0 & 0 & B_{1zz} \end{pmatrix}, \ \mathbf{B}_{\kappa_{p_2(t)}} = \begin{pmatrix} B_{2rr} & 0 & 0 \\ 0 & B_{2\varphi\varphi} & 0 \\ 0 & 0 & B_{2zz} \end{pmatrix}.$$

Due to the incompressibility the deformation in the cylindrical coordinates is described by $r = R/\sqrt{\lambda}, \varphi = \Phi, z = \lambda Z$, where capital letters correspond to undeformed coordinates and small letters to deformed coordinates, λ is the stretch ratio meaning how the height of the cylinder decreases. The deformation gradient and the left Cauchy-Green tensor are in the form

$$\mathbf{F} = \begin{pmatrix} \frac{1}{\sqrt{\lambda}} & 0 & 0 \\ 0 & \frac{1}{\sqrt{\lambda}} & 0 \\ 0 & 0 & \lambda \end{pmatrix}, \quad \nabla\mathbf{v} = \mathbf{L} = \dot{\mathbf{F}}\mathbf{F}^{-1} = \begin{pmatrix} -\frac{\dot{\lambda}}{2\lambda} & 0 & 0 \\ 0 & -\frac{\dot{\lambda}}{2\lambda} & 0 \\ 0 & 0 & \frac{\dot{\lambda}}{\lambda} \end{pmatrix}, \quad \mathbf{B} = \mathbf{F}\mathbf{F}^{\mathrm{T}} = \begin{pmatrix} \frac{1}{\lambda} & 0 & 0 \\ 0 & \frac{1}{\lambda} & 0 \\ 0 & 0 & \lambda^2 \end{pmatrix}.$$

The initial conditions are different in the stress relaxation and the creep test. Due to the instantaneous application in both cases we can suppose that the response is elastic and we can read the initial condition from it, i.e. $\mathbf{B}_{\kappa_{p_1(t)}}(0) = \mathbf{B}_{\kappa_{p_2(t)}}(0) = \mathbf{B}(0)$:

$$B_{1rr}(0) = B_{2rr}(0) = B_{1\varphi\varphi}(0) = B_{2\varphi\varphi}(0) = \frac{1}{\lambda(0)}, \quad B_{1zz} = B_{2zz} = \lambda(0)^2. \tag{4.6}$$

Now, we will write the components of the model (3.239) that are valid for both experiments

$$T_{rr} = -p - \mu_3\dot{\lambda}\lambda^{-1} + \frac{G_1}{3}\left(2B_{1rr} - B_{1\varphi\varphi} - B_{1zz}\right) + \frac{G_2}{3}\left(2B_{2rr} - B_{2\varphi\varphi} - B_{2zz}\right) \tag{4.7}$$

$$T_{\varphi\varphi} = -p - \mu_3\dot{\lambda}\lambda^{-1} + \frac{G_1}{3}\left(2B_{1\varphi\varphi} - B_{1rr} - B_{1zz}\right) + \frac{G_2}{3}\left(2B_{2\varphi\varphi} - B_{2rr} - B_{2zz}\right) \tag{4.8}$$

$$T_{zz} = -p + 2\mu_3\dot{\lambda}\lambda^{-1} + \frac{G_1}{3}\left(2B_{1zz} - B_{1\varphi\varphi} - B_{1rr}\right) + \frac{G_2}{3}\left(2B_{2zz} - B_{2\varphi\varphi} - B_{2rr}\right) \tag{4.9}$$

Because the lateral pressure is equal to zero, i.e. $T_{rr} = T_{\varphi\varphi} = 0$, subtracting (4.8) from (4.7) we get $G_1B_{1rr} + G_2B_{2rr} = G_1B_{1\varphi\varphi} + G_2B_{2\varphi\varphi}$ which is generally valid if $B_{1rr} = B_{1\varphi\varphi}$ and $B_{2rr} = B_{2\varphi\varphi}$. From (4.7) we get

$$-p - \mu_3\dot{\lambda}\lambda^{-1} = \frac{G_1}{3}(B_{1zz} - B_{1rr}) + \frac{G_2}{3}(B_{2zz} - B_{2rr}).$$

Inserting this into (4.9) we get

$$T_{zz} = 3\mu_3\dot{\lambda}\lambda^{-1} + G_1(B_{1zz} - B_{1rr}) + G_2(B_{2zz} - B_{2rr}). \tag{4.10}$$

The governing equations for $B_{1rr}, B_{2rr}, B_{1zz}$ and B_{2zz} are

$$\frac{\partial B_{1rr}}{\partial t} + \dot{\lambda}\lambda^{-1}B_{1rr} = -\frac{G_1}{3\mu_1}B_{1rr}(B_{1rr} - B_{1zz}), \tag{4.11}$$

$$\frac{\partial B_{1zz}}{\partial t} - 2\dot{\lambda}\lambda^{-1}B_{1zz} = -\frac{2G_1}{3\mu_1}B_{1rr}(B_{1zz} - B_{1rr}), \tag{4.12}$$

$$\frac{\partial B_{2rr}}{\partial t} + \dot{\lambda}\lambda^{-1}B_{2rr} = -\frac{G_2}{3\mu_2}B_{2rr}(B_{2rr} - B_{2zz}), \tag{4.13}$$

$$\frac{\partial B_{2zz}}{\partial t} - 2\dot{\lambda}\lambda^{-1}B_{2zz} = -\frac{2G_2}{3\mu_2}B_{2rr}(B_{2zz} - B_{2rr}). \tag{4.14}$$

Our aim is to use the equations (4.11) – (4.14) and the equation (4.10) to compute T_{zz} in case of the stress relaxation experiment and λ in case of the creep test.

Stress relaxation

In the stress relaxation experiment the cylinder is suddenly deformed with constant strain, that is why we suppose that $\dot{\lambda} = 0$ and the initial condition for λ is given by the Table 4.1. Then we obtain T_{zz} in the following way. First we solve the set of ODE

$$\frac{\partial B_{1rr}}{\partial t} = -\frac{G_1}{3\mu_1}B_{1rr}(B_{1rr} - B_{1zz}), \tag{4.15}$$

$$\frac{\partial B_{1zz}}{\partial t} = -\frac{2G_1}{3\mu_1}B_{1rr}(B_{1zz} - B_{1rr}), \tag{4.16}$$

$$\frac{\partial B_{2rr}}{\partial t} = -\frac{G_2}{3\mu_2}B_{2rr}(B_{2rr} - B_{2zz}), \tag{4.17}$$

$$\frac{\partial B_{2zz}}{\partial t} = -\frac{2G_2}{3\mu_2}B_{2rr}(B_{2zz} - B_{2rr}) \tag{4.18}$$

with the initial conditions (4.6) and then we compute

$$T_{zz} = G_1(B_{1zz} - B_{1rr}) + G_2(B_{2zz} - B_{2rr}).$$

Note that parameter μ_3 is not present in any of the equations and so we can not fit it using stress relaxation experiment. To solve the set of ODE, Runge-Kutta method of the fifth order is used, concretely Matlab function `ode45`.

Creep test

In the creep test experiment we press the top of the cylinder with the pressure P given by the Table 4.2 and after 200 minutes we release it

$$T_{zz} = \begin{cases} P & 0 \text{ s} \le t \le 12\,000 \text{ s} \\ 0 & t > 12\,000 \text{ s}. \end{cases}$$

The initial condition is that the cylinder is undeformed at $t = 0$, i.e. $\lambda(0) = 0$, and corresponding initial conditions for $\mathbf{B}_{\kappa_{p_1(t)}}$ and $\mathbf{B}_{\kappa_{p_2(t)}}$ are given by (4.6). We use the equation (4.10) and we express $\dot{\lambda}\lambda^{-1}$ in terms of T_{zz}, B_{1rr}, B_{2rr}, B_{1zz}, B_{2zz}

$$\dot{\lambda}\lambda^{-1} = \frac{1}{3\mu_3}\left(T_{zz} - G_1(B_{1zz} - B_{1rr}) - G_2(B_{2zz} - B_{2rr})\right). \tag{4.19}$$

Further, we substitute it into (4.11) – (4.14) and adding $\lambda \times$ (4.19) we obtain

$$\frac{\partial B_{1rr}}{\partial t} + \frac{1}{3\mu_3}\left(T_{zz} - G_1(B_{1zz} - B_{1rr}) - G_2(B_{2zz} - B_{2rr})\right) B_{1rr} = -\frac{G_1}{3\mu_1} B_{1rr}(B_{1rr} - B_{1zz}), \quad (4.20)$$

$$\frac{\partial B_{1zz}}{\partial t} - \frac{2}{3\mu_3}\left(T_{zz} - G_1(B_{1zz} - B_{1rr}) - G_2(B_{2zz} - B_{2rr})\right) B_{1zz} = -\frac{2G_1}{3\mu_1} B_{1rr}(B_{1zz} - B_{1rr}), \quad (4.21)$$

$$\frac{\partial B_{2rr}}{\partial t} + \frac{1}{3\mu_3}\left(T_{zz} - G_1(B_{1zz} - B_{1rr}) - G_2(B_{2zz} - B_{2rr})\right) B_{2rr} = -\frac{G_2}{3\mu_2} B_{2rr}(B_{2rr} - B_{2zz}), \quad (4.22)$$

$$\frac{\partial B_{2zz}}{\partial t} - \frac{2}{3\mu_3}\left(T_{zz} - G_1(B_{1zz} - B_{1rr}) - G_2(B_{2zz} - B_{2rr})\right) B_{2zz} = -\frac{2G_2}{3\mu_2} B_{2rr}(B_{2zz} - B_{2rr}), \quad (4.23)$$

$$\frac{\partial \lambda}{\partial t} = \frac{1}{3\mu_3}\left(T_{zz} - G_1(B_{1zz} - B_{1rr}) - G_2(B_{2zz} - B_{2rr})\right) \lambda. \quad (4.24)$$

For fitting this experiment we minimize absolute error g given by (4.5), i.e.

$$g = \sum_{i=1}^{6} \frac{1}{N_i} g^i_{\text{abs}}, \quad (4.25)$$

where $N_i = N_s$ for $i = 1, 2, 3$ in the stress relaxation test and $N_i = N_c$ for $i = 4, 5, 6$ in the creep test are given in Table 4.3 together with fitted material parameters for each temperature T.

T [°F]	G_1 [MPa]	G_2 [MPa]	G_1/μ_1 [1/s]	G_2/μ_2 [1/s]	μ_3 [GPa s]	N_s [10^{-4}]	N_c [10^5]
40	73.36	108.85	7.50×10^{-5}	8.50×10^{-3}	3.44	25.0	20.0
77	21.95	37.22	2.72×10^{-5}	2.88×10^{-2}	0.82	16.0	1.5
140	10.07	5.86	1.43×10^{-5}	3.96×10^{-2}	1.85	8.0	0.8

Table 4.3: Fitted parameters for the stress relaxation experiment and the creep test.

The result for 40°F is depicted in Figure 4.8, for 77°F in Figure 4.9 and for 140°F in Figure 4.10. The results for the lowest and the highest temperature are very reasonable, the fit for 77°F is not too much satisfactory. This is strange because we are able to fit quite well the lowest and also the highest temperature and the parameters in the Table 4.3 depend monotonically on the temperature. Is it possible that the experiment was not performed perfectly? Monismith, Secor tried to fit the experiments with the linear Burgers model and they had also problems with fitting the middle-temperature experiment, see [41].

If we compare our result obtained with the model Quad2 (five parameters, extra solvent viscosity μ_3) and their result obtained with the linear Burgers model without additional Newtonian dissipation (i.e. $\mu_3 = 0$, model consists four parameters), we find out that though our result is better, the difference is not enormous. However, there is a reason to use non-linear models like we did. This will be seen in the Subsection 4.2.3.

4.2.2 Fitting of torsional experiment by Narayan et al. (2012)

The set of experiments performed by Narayan et al. in [43] is described in Subsection 4.1.2 and it is fitted with the model Quad2 (3.239).

The initial-boundary value problem that is corroborated

The initial conditions for the tensors $\mathbf{B}_{\kappa_{p_1(t)}}$ and $\mathbf{B}_{\kappa_{p_2(t)}}$ that appear in the model (3.239) are $\mathbf{B}_{\kappa_{p_1(t)}} = \mathbf{B}_{\kappa_{p_2(t)}} = \mathbf{I}$, which means that at the beginning the material is relaxed.

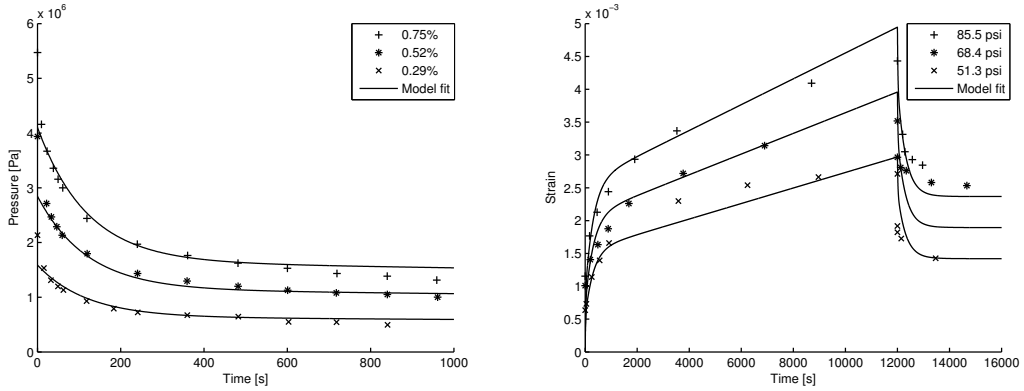

a) Stress relaxation b) Creep test

Figure 4.8: Data fit, Monismith, Secor (1962), 40°F.

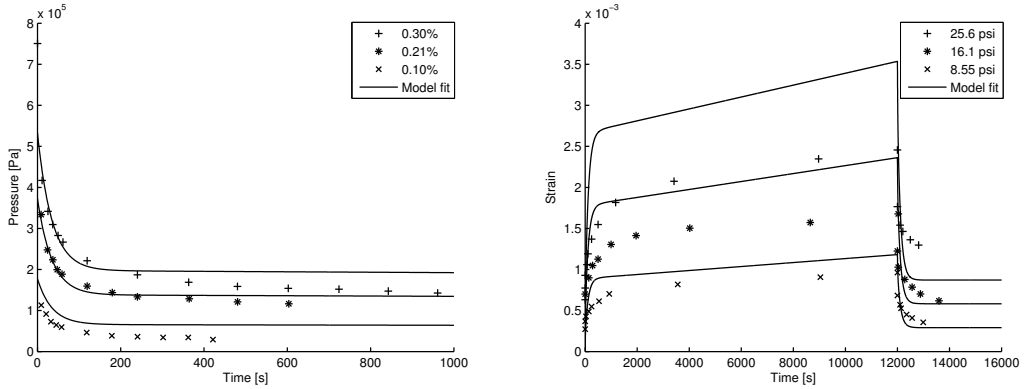

a) Stress relaxation b) Creep test

Figure 4.9: Data fit, Monismith, Secor (1962), 77°F.

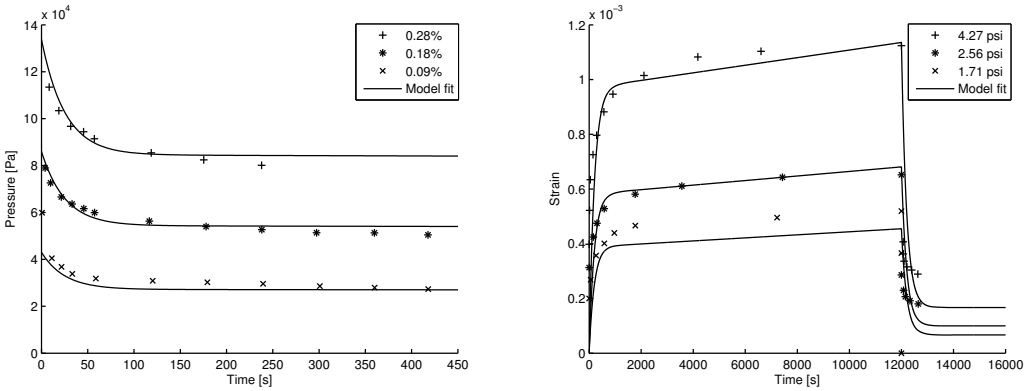

a) Stress relaxation b) Creep test

Figure 4.10: Data fit, Monismith, Secor (1962), 140°F.

We compute the problem in cylindrical coordinates (r, φ, z), see Figure 4.11. Due to the symmetry all the unknowns are assumed to not depend on the variable φ. The unknowns of the equations are

$$p = p(r,z), \quad \mathbf{B}_{\kappa_{p_1(t)}} = \begin{pmatrix} B_{1rr} & B_{1r\varphi} & B_{1rz} \\ B_{1r\varphi} & B_{1\varphi\varphi} & B_{1\varphi z} \\ B_{1rz} & B_{1\varphi z} & B_{1zz} \end{pmatrix}(r,z), \quad \mathbf{B}_{\kappa_{p_2(t)}} = \begin{pmatrix} B_{2rr} & B_{2r\varphi} & B_{2rz} \\ B_{2r\varphi} & B_{2\varphi\varphi} & B_{2\varphi z} \\ B_{2rz} & B_{2\varphi z} & B_{2zz} \end{pmatrix}(r,z).$$

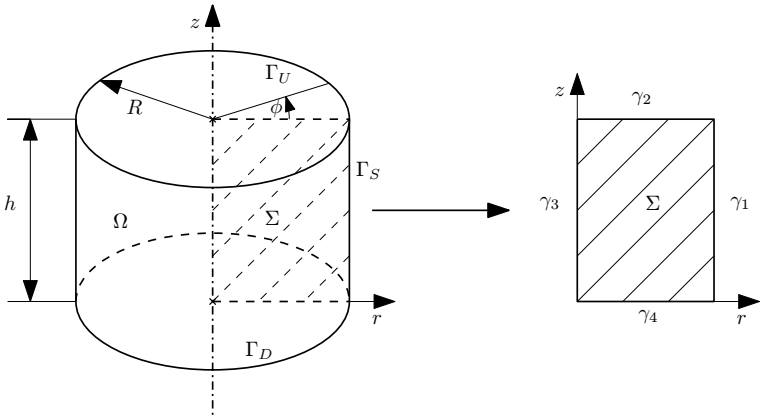

Figure 4.11: The geometry of the axially symmetric flow in a cylinder.

In this experiment we suppose that the material flows only in the direction of rotation, i.e. the $\varphi-$direction, satisfying the no-slip boundary conditions on the bottom and the top plate, that is

$$\mathbf{v} = \left(0, \frac{\omega r z}{h}, 0\right),$$

which automatically satisfies the constraint of incompressibility i.e. $\operatorname{div} \mathbf{v} = 0$.

We are interested in computing the torque M and the normal force F on the upper plate:

$$M = \int_{\Gamma_U} r T_{\varphi z} \, \mathrm{d}S = 2\pi \int_0^R r^2 T_{\varphi z} \, \mathrm{d}r, \tag{4.26}$$

$$F = \int_{\Gamma_U} T_{zz} \, \mathrm{d}S = 2\pi \int_0^R r T_{zz} \, \mathrm{d}r. \tag{4.27}$$

Using cylindrical coordinates[3] and supposing that the inertial effects can be neglected since the flow is slow (we neglect time derivative of ω), we can express the balance

[3]For details on differential operators in cylindrical coordinates, see Appendix A.2.

of linear momentum and the constitutive relations

$$0 = \frac{\partial T_{rr}}{\partial r} + \frac{T_{rr} - T_{\varphi\varphi}}{r} + \frac{\partial T_{rz}}{\partial z}, \tag{4.28}$$

$$0 = \frac{\partial T_{r\varphi}}{\partial r} + 2\frac{T_{r\varphi}}{r} + \frac{\partial T_{\varphi z}}{\partial z}, \tag{4.29}$$

$$0 = \frac{\partial T_{rz}}{\partial r} + \frac{T_{rz}}{r} + \frac{\partial T_{zz}}{\partial z}, \tag{4.30}$$

$$T_{rr} = -p + \frac{G_1}{3}(2B_{1rr} - B_{1\varphi\varphi} - B_{1zz}) + \frac{G_2}{3}(2B_{2rr} - B_{2\varphi\varphi} - B_{2zz}), \tag{4.31}$$

$$T_{r\varphi} = G_1 B_{1r\varphi} + G_2 B_{2r\varphi}, \quad T_{rz} = G_1 B_{1rz} + G_2 B_{2rz}, \tag{4.32}$$

$$T_{\varphi\varphi} = -p + \frac{G_1}{3}(2B_{1\varphi\varphi} - B_{1rr} - B_{1zz}) + \frac{G_2}{3}(2B_{2\varphi\varphi} - B_{2rr} - B_{2zz}), \tag{4.33}$$

$$T_{\varphi z} = \mu_3 \frac{r\omega}{h} + G_1 B_{1\varphi z} + G_2 B_{2\varphi z}, \tag{4.34}$$

$$T_{zz} = -p + \frac{G_1}{3}(2B_{1zz} - B_{1\varphi\varphi} - B_{1rr}) + \frac{G_2}{3}(2B_{2zz} - B_{2\varphi\varphi} - B_{2rr}), \tag{4.35}$$

$$\frac{\partial B_{irr}}{\partial t} = -\frac{G_i}{\mu_i}\left(B_{ir\varphi}^2 + B_{irz}^2\right) + \frac{G_i}{3\mu_i} B_{irr}\left(-2B_{irr} + B_{i\varphi\varphi} + B_{izz}\right), \tag{4.36}$$

$$\frac{\partial B_{ir\varphi}}{\partial t} = \frac{r\omega}{h} B_{irz} - \frac{G_i}{\mu_i} B_{irz} B_{i\varphi z} + \frac{G_i}{3\mu_i} B_{ir\varphi}\left(-2B_{irr} - 2B_{i\varphi\varphi} + B_{izz}\right), \tag{4.37}$$

$$\frac{\partial B_{irz}}{\partial t} = -\frac{G_i}{\mu_i} B_{ir\varphi} B_{i\varphi z} + \frac{G_i}{3\mu_i} B_{irz}\left(-2B_{irr} + B_{i\varphi\varphi} - 2B_{izz}\right), \tag{4.38}$$

$$\frac{\partial B_{i\varphi\varphi}}{\partial t} = 2\frac{r\omega}{h} B_{i\varphi z} - \frac{G_i}{\mu_i}\left(B_{ir\varphi}^2 + B_{i\varphi z}^2\right) + \frac{G_i}{3\mu_i} B_{i\varphi\varphi}\left(B_{irr} - 2B_{i\varphi\varphi} + B_{izz}\right), \tag{4.39}$$

$$\frac{\partial B_{i\varphi z}}{\partial t} = \frac{r\omega}{h} B_{izz} - \frac{G_i}{\mu_i} B_{ir\varphi} B_{irz} + \frac{G_i}{3\mu_i} B_{i\varphi z}\left(B_{irr} - 2B_{i\varphi\varphi} - 2B_{izz}\right), \tag{4.40}$$

$$\frac{\partial B_{izz}}{\partial t} = -\frac{G_i}{\mu_i}\left(B_{irz}^2 + B_{i\varphi z}^2\right) + \frac{G_i}{3\mu_i} B_{izz}\left(B_{irr} + B_{i\varphi\varphi} - 2B_{izz}\right). \tag{4.41}$$

Equations (4.36) – (4.41) are valid for $i = 1, 2$. The set of equations does not seem to have an analytical solution. They can be simplified considerably in the following manner. First, we observe that none of the initial conditions as well as none of the equations (4.36) – (4.41) depend on z and therefore also the components of $\mathbf{B}_{\kappa_{p_1(t)}}$ and $\mathbf{B}_{\kappa_{p_2(t)}}$ do not depend on this coordinate. Further, the zero initial conditions for $B_{1r\varphi}, B_{2r\varphi}, B_{1rz}$ and B_{2rz} together with the equations (4.37) – (4.38) imply that $B_{1r\varphi} = B_{2r\varphi} = B_{1rz} = B_{2rz} = 0$. In view of this result and from equations (4.30) and (4.35) we determine that also p does not depend on z and so, all the components of the

stress tensor $\mathbf{T}$ does not depend on z and the equations simplify to $(i = 1, 2)$

$$0 = \frac{\partial T_{rr}}{\partial r} + \frac{T_{rr} - T_{\varphi\varphi}}{r}, \tag{4.42}$$

$$\frac{\partial B_{irr}}{\partial t} = \frac{G_i}{3\mu_i} B_{irr} \left(-2B_{irr} + B_{i\varphi\varphi} + B_{izz}\right), \tag{4.43}$$

$$\frac{\partial B_{i\varphi\varphi}}{\partial t} = 2\frac{r\omega}{h} B_{i\varphi z} - \frac{G_i}{\mu_i} B_{i\varphi z}^2 + \frac{G_i}{3\mu_i} B_{i\varphi\varphi} \left(B_{irr} - 2B_{i\varphi\varphi} + B_{izz}\right), \tag{4.44}$$

$$\frac{\partial B_{i\varphi z}}{\partial t} = \frac{r\omega}{h} B_{izz} + \frac{G_i}{3\mu_i} B_{i\varphi z} \left(B_{irr} - 2B_{i\varphi\varphi} - 2B_{izz}\right), \tag{4.45}$$

$$\frac{\partial B_{izz}}{\partial t} = -\frac{G_i}{\mu_i} B_{i\varphi z}^2 + \frac{G_i}{3\mu_i} B_{izz} \left(B_{irr} + B_{i\varphi\varphi} - 2B_{izz}\right). \tag{4.46}$$

Our aim is to compute the torque (5.141) and the normal force (5.142) on the upper plate.

Torque The case of the torque is simple, we solve the set of ODEs (4.43) – (4.46) for fixed r and compute

$$M = 2\pi \int_0^R r^2 T_{\varphi z}(r)\,\mathrm{d}r \overset{(4.34)}{=} \frac{\mu_3 \pi \omega}{2h} R^4 + 2\pi \int_0^R r^2 (G_1 B_{1\varphi z}(r) + G_2 B_{2\varphi z}(r))\,\mathrm{d}r. \tag{4.47}$$

To solve the set of ODEs Runge-Kutta method of the fifth order is used, namely Matlab function `ode45`. For the numerical integration the composed Simpson's rule with five nodes is used.

Normal force The case of the normal force is more difficult because in order to compute it using (4.35) we need to know the solution for the pressure p. In order to avoid it, we compute the normal force using the first and the second normal stress differences in the following manner.

We express the term T_{zz} in the form

$$T_{zz}(r) = T_{rr}(r) + (T_{zz}(r) - T_{rr}(r)) = \int_R^r \frac{\partial T_{rr}(r')}{\partial r'}\,\mathrm{d}r' + (T_{zz}(r) - T_{rr}(r)), \tag{4.48}$$

and use (4.42) to get the information for the partial derivative

$$\frac{\partial T_{rr}}{\partial r} = \frac{T_{\varphi\varphi} - T_{rr}}{r},$$

substituting it back into (4.48) we obtain

$$T_{zz} = \int_R^r \frac{T_{\varphi\varphi} - T_{rr}}{r'}\,\mathrm{d}r' + (T_{zz} - T_{rr}). \tag{4.49}$$

Now, this can be inserted into the formula for the normal force

$$F = 2\pi \int_0^R r T_{zz}\,\mathrm{d}r = 2\pi \int_0^R r \int_R^r \frac{T_{\varphi\varphi} - T_{rr}}{r'}\,\mathrm{d}r'\,\mathrm{d}r + 2\pi \int_0^R r (T_{zz} - T_{rr})\,\mathrm{d}r.$$

The first term can be computed by applying integration by parts on the first integral (the boundary terms are zero)

$$2\pi \int_0^R r \int_R^r \frac{T_{\varphi\varphi} - T_{rr}}{r'} \,\mathrm{d}r' \,\mathrm{d}r = \pi \int_0^R r(T_{rr} - T_{\varphi\varphi}) \,\mathrm{d}r$$

and so

$$F = \pi \int_0^R r(T_{rr} - T_{\varphi\varphi}) \,\mathrm{d}r + 2\pi \int_0^R r(T_{zz} - T_{rr}) \,\mathrm{d}r. \tag{4.50}$$

Using equations (4.31), (4.33) and (4.35) we get

$$F = \pi \int_0^R r(G_1(B_{1rr}(r) - B_{1\varphi\varphi}(r)) + G_2(B_{2rr}(r) - B_{2\varphi\varphi}(r))) \,\mathrm{d}r + 2\pi \int_0^R r(G_1(B_{1zz}(r) - B_{1rr}(r)) + G_2(B_{2zz}(r) - B_{2rr}(r))) \,\mathrm{d}r.$$

This integral is computed as in the case of the torque using the composed Simpson's rule where $B_{irr}(r), B_{i\varphi\varphi}(r)$ and $B_{izz}(r)$ are obtained as the solution of the set of ODEs (4.43) – (4.46).

Results

We find, for each type of binder and for each temperature, one set of parameters for which the computed torque M and the computed normal force F best fits the experimental data. The fitting is done by minimizing absolute error (4.5), here N_1 is the maximum of the measured torque and N_2 is the maximum of the normal force, both values and the measure g are in the Tables.

Unaged polymer modified binder Fitted parameters for unaged polymer modified binder are shown in the Table 4.4.

Temp °C	G_1 [kPa]	G_2 [kPa]	G_1/μ_1 [1/s]	G_2/μ_2 [1/s]	μ_3 [kPa]	N_1	N_2	g
25	543.7	105.8	9.37	0.90	46.3	0.029	1.83	0.033
30	273.8	541.7	7.12	0.69	47.2	0.022	1.22	0.059
35	130.4	27.7	5.96	0.66	45.3	0.016	0.71	0.087
40	58.7	8.04	4.10	0.35	25.0	0.009	0.39	0.096

Table 4.4: One set of fitted parameters for the torque and the normal force for unaged polymer modified binder.

The Figures 4.12a) and 4.12b) depict the experimental data and the computations based on the model for the above values of the material parameters.

Aged polymer modified binder Fitted parameters for aged polymer modified binder are shown in the Table 4.5.

The Figures 4.13a) and 4.13b) depict the experimental data and the computations based on the model for the above values of the material parameters.

For both polymer modified binders one can see that the material parameters depend monotonically on the temperature and that with the higher temperature the asphalt binder behaves more like a fluid. Experiments with both polymer modified binders are fitted very well.

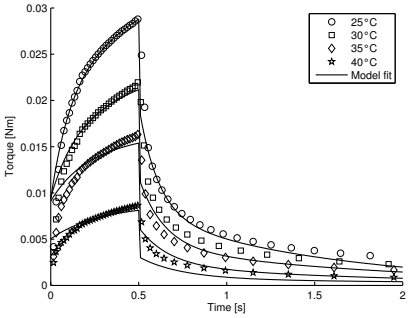

a) Fitted torque

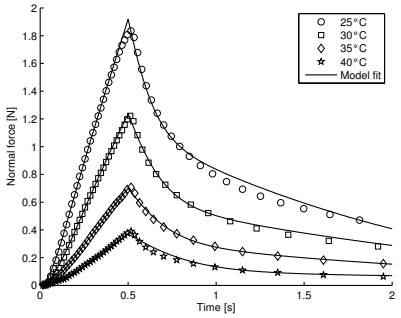

b) Fitted normal force

Figure 4.12: Fitted experiment for unaged polymer modified binder.

Temp °C	G_1 [kPa]	G_2 [kPa]	G_1/μ_1 [1/s]	G_2/μ_2 [1/s]	μ_3 [kPa]	N_1	N_2	g
25	934.2	190.6	9.01	0.92	110.3	0.054	2.84	0.062
30	398.1	86.7	7.80	0.80	78.8	0.033	1.68	0.071
35	143.0	41.0	5.90	0.78	63.7	0.022	0.85	0.106
40	124.0	26.9	6.42	0.77	34.4	0.013	0.63	0.078

Table 4.5: One set of fitted parameters for the torque and the normal force for aged polymer modified binder.

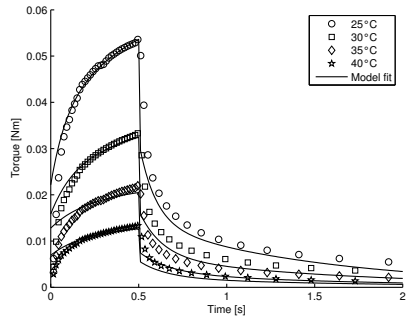

a) Fitted torque

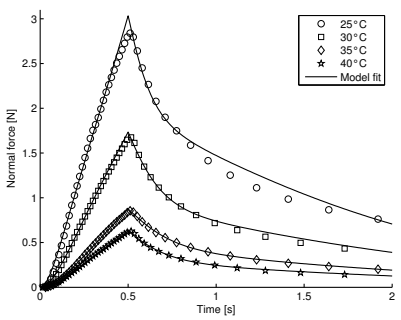

b) Fitted normal force

Figure 4.13: Fitted experiment for aged polymer modified binder.

Unaged base binder Fitted parameters for unaged base binder are shown in the Table 4.6.

Temp °C	μ_1 [kPa]	μ_2 [kPa]	μ_1/ϵ_1 [1/s]	μ_2/ϵ_2 [1/s]	μ_3 [kPa]	N_1	N_2	g
25	333.5	7.48	6.81	0.23	78.8	0.026	0.968	0.046
30	185.3	19.1	15.14	2.51	37.6	0.011	0.260	0.055
35	50.2	3.45	9.80	1.68	19.7	0.005	0.099	0.033
40	125.3	4.46	19.03	2.82	6.33	0.003	0.080	0.062

Table 4.6: One set of fitted parameters for the torque and the normal force for unaged base binder.

The Figures 4.14a) and 4.14b) depict the experimental data and the model prediction

for the material parameters given by Table 4.6.

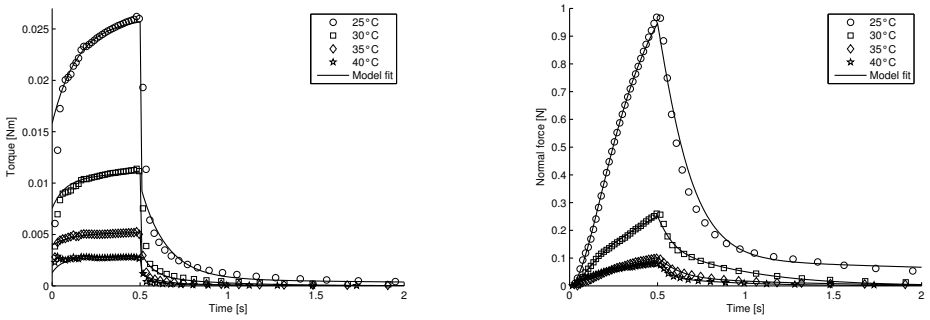

a) Fitted torque b) Fitted normal force

Figure 4.14: Fitted experiment for unaged base binder.

Aged base binder Fitted parameters for aged base binder are shown in the Table 4.7.

Temp °C	G_1 [kPa]	G_2 [kPa]	G_1/μ_1 [1/s]	G_2/μ_2 [1/s]	μ_3 [kPa]	N_1	N_2	g
25	397.7	25.4	5.07	0.55	118.7	0.041	1.77	0.048
30	280.5	18.6	4.34	1.17	43.6	0.017	0.72	0.044
35	280.8	28.9	18.95	2.77	26.0	0.010	0.30	0.050
40	196.8	13.3	19.78	2.81	13.9	0.006	0.16	0.038

Table 4.7: One set of fitted parameters for the torque and the normal force for aged base binder.

The Figures 4.15a) and 4.15b) depict the experimental data and the computations based on the model for the above values of the material parameters.

According to value of the measure g, both fits of base binder are good. Contrary to polymer modified binder, except the viscosity μ_3 other parameters do not depend monotonically on temperature. This may be one of the reasons for adding the polymer, so as to not have such a behavior.

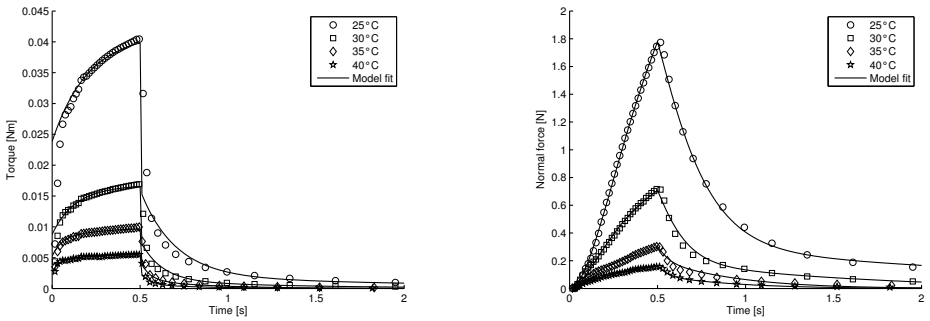

a) Fitted torque b) Fitted normal force

Figure 4.15: Fitted experiment for aged base binder.

4.2.3 Fitting of torsional experiment with torque overshoot by Krishnan and Narayan (2007)

Experiment performed by Krishnan and Narayan in [27] is described in Subsection 4.1.3 and it was fitted with all models: Oldroyd-B, Burgers, PL2012, RaSr2000, Quad1 and Quad2. We solve this problem in the same way as in case of experiment by Narayan et al. (2012) described in the previous subsection.

The initial-boundary value problem

The initial conditions that are appropriate for the initial-boundary value problem that corresponds to the experiment are:

$$\mathbf{B}_{\kappa_{p_1(t)}} = \mathbf{B}_{\kappa_{p_2(t)}} = \mathbf{I} \quad \text{for Quad2 model,} \tag{4.51}$$
$$\mathbf{B}_{\kappa_{p(t)}} = \mathbf{I} \quad \text{for Quad1 model,} \tag{4.52}$$
$$\mathbf{B}_{\kappa_{p(t)}} = \mathbf{I} \quad \text{for the model PL2012,} \tag{4.53}$$
$$\mathbf{B}_{\kappa_{p(t)}} = \mathbf{I} \quad \text{for RaSr2000 model,} \tag{4.54}$$
$$\mathbf{B} = \mathbf{I} \quad \text{for Oldroyd-B model,} \tag{4.55}$$
$$\mathbf{B}_1 = \mathbf{B}_2 = \mathbf{I} \quad \text{for Burgers model,} \tag{4.56}$$

which means that the material is at rest and relaxed at $t = 0$. We use the same ansatz for the velocity $\mathbf{v}$ satisfying boundary conditions on the lower and upper plate

$$\mathbf{v} = \left(0, \frac{\omega r z}{h}, 0\right).$$

First we show that the torque overshoot can not be captured by linear models Oldroyd-B (2.10) and Burgers (3.255).

Oldroyd-B model The governing equations for (2.10) after neglecting time derivative of ω are

$$T_{\varphi z} = \mu_2 \frac{r\omega}{h} + G B_{\varphi z}, \tag{4.57}$$
$$\frac{\partial B_{rr}}{\partial t} = \frac{1}{\tau}(1 - B_{rr}), \tag{4.58}$$
$$\frac{\partial B_{\varphi\varphi}}{\partial t} = 2\frac{r\omega}{h} B_{\varphi z} + \frac{1}{\tau}(1 - B_{\varphi\varphi}), \tag{4.59}$$
$$\frac{\partial B_{\varphi z}}{\partial t} = \frac{r\omega}{h} B_{zz} - \frac{1}{\tau} B_{\varphi z}, \tag{4.60}$$
$$\frac{\partial B_{zz}}{\partial t} = \frac{1}{\tau}(1 - B_{zz}). \tag{4.61}$$

Together with the initial conditions $B_{rr}(0) = B_{\varphi\varphi}(0) = B_{zz}(0) = 1$ this gives $B_{zz} = B_{rr} = 1$. The solution of (4.60) together with the initial condition $B_{\varphi z}(0) = 0$ gives

$$B_{\varphi z} = \frac{\tau r\omega}{h}\left(1 - e^{-t/\tau}\right) \Rightarrow T_{\varphi z} = \frac{\omega r}{h}\left(\mu_2 + G\tau\left(1 - e^{-t/\tau}\right)\right)$$
$$\Rightarrow M = \frac{\pi\omega R^4}{2h}\left(\mu_2 + G\tau\left(1 - e^{-t/\tau}\right)\right).$$

From this formula one can immediately see that this model is incapable of describing the overshoot of the torque towards the beginning of the experiment. The time derivative of $M(t)$ with respect to time t

$$\frac{\mathrm{d}M}{\mathrm{d}t} = \frac{\pi\omega R^4}{2h} G e^{-t/\tau} > 0$$

is always greater than zero. Thus the torque M is monotonically increasing and for times much longer than the relaxation time, i.e. $t \gg \tau$, the torque is almost constant.

Burgers model The governing equations for (3.255) after neglecting time derivative of ω are

$$T_{\varphi z} = \mu_3 \frac{r\omega}{h} + G_1 B_{1\varphi z} + G_2 B_{2\varphi z}, \tag{4.62}$$

$$\frac{\partial B_{irr}}{\partial t} = \frac{1}{\tau_i}(1 - B_{irr}), \tag{4.63}$$

$$\frac{\partial B_{i\varphi\varphi}}{\partial t} = 2\frac{r\omega}{h} B_{i\varphi z} + \frac{1}{\tau_i}(1 - B_{i\varphi\varphi}), \tag{4.64}$$

$$\frac{\partial B_{i\varphi z}}{\partial t} = \frac{r\omega}{h} B_{izz} - \frac{1}{\tau_i} B_{i\varphi z}, \tag{4.65}$$

$$\frac{\partial B_{izz}}{\partial t} = \frac{1}{\tau_i}(1 - B_{zz}), \tag{4.66}$$

for $i = 1, 2$. As in case of Oldroyd-B model we get

$$B_{i\varphi z} = \frac{\tau r\omega}{h}\left(1 - e^{-t/\tau_i}\right) \Rightarrow T_{i\varphi z} = \frac{\omega r}{h}\left(\mu_3 + G_1\tau_1\left(1 - e^{-t/\tau_1}\right) + G_2\tau_2\left(1 - e^{-t/\tau_1}\right)\right)$$
$$\Rightarrow M = \frac{\pi\omega R^4}{2h}\left(\mu_2 + G_1\tau_1\left(1 - e^{-t/\tau_1}\right) + G_2\tau_2\left(1 - e^{-t/\tau_2}\right)\right).$$

The time derivative of $M(t)$ with respect to time t

$$\frac{\mathrm{d}M}{\mathrm{d}t} = \frac{\pi\omega R^4}{2h}\left(G_1 e^{-t/\tau_1} + G_2 e^{-t/\tau_2}\right) > 0$$

is always greater than zero. Thus the torque M is monotonically increasing, for times much longer than the relaxation time, i.e. $t \gg \tau_1 + \tau_2$, the torque is almost constant.

Further, we use four non-linear models – PL2012, RaSr2000, Quad1 and Quad2 – and compare their abilities to capture the experiment by Krishnan and Narayan (2007).

Power law like model PL2012

Using the power law like model PL2012 we fitted the experiment by Krishnan and Narayan (2007) in [21]. Upon substituting the ansatz

$$p = p(t, r, z), \quad \mathbf{v} = \left(0, \frac{\omega r z}{h}, 0\right), \tag{4.67}$$

$$\mathbf{B}_{\kappa_{p(t)}} = \begin{pmatrix} B_{rr}(t,r,z) & B_{r\varphi}(t,r,z) & B_{rz}(t,r,z) \\ B_{r\varphi}(t,r,z) & B_{\varphi\varphi}(t,r,z) & B_{\varphi z}(t,r,z) \\ B_{rz}(t,r,z) & B_{\varphi z}(t,r,z) & B_{zz}(t,r,z) \end{pmatrix}. \tag{4.68}$$

into the governing equations (3.97) we get

$$0 = -\frac{\partial p}{\partial r} + G\left(\frac{\partial B_{rr}}{\partial r} + \frac{B_{rr}}{r} - \frac{B_{\varphi\varphi}}{r} + \frac{\partial B_{rz}}{\partial z}\right), \tag{4.69a}$$

$$\rho\frac{rz}{h}\frac{\mathrm{d}\omega}{\mathrm{d}t} = G\left(\frac{\partial B_{r\varphi}}{\partial r} + \frac{2B_{r\varphi}}{r} + \frac{\partial B_{\varphi z}}{\partial z}\right) + \frac{\epsilon_1 r\omega}{2h}\frac{\partial}{\partial z}\left[Y\left(\epsilon_0 + \frac{r^2\omega^2}{2h^2}\right)^{\alpha-2}\left(\epsilon_0 + \alpha\frac{r^2\omega^2}{2h^2}\right)\right], \tag{4.69b}$$

$$0 = -\frac{\partial p}{\partial z} + G\left(\frac{\partial B_{rz}}{\partial r} + \frac{B_{rz}}{r} + \frac{\partial B_{zz}}{\partial z}\right), \tag{4.69c}$$

$$\sqrt{\operatorname{tr}\mathbf{B}_{\kappa_{p(t)}} - 3\lambda}\frac{\partial B_{rr}}{\partial t} = -2\sqrt{X}B_{rr} + 2\sqrt{X}\lambda, \tag{4.69d}$$

$$\sqrt{\operatorname{tr}\mathbf{B}_{\kappa_{p(t)}} - 3\lambda}\frac{\partial B_{r\varphi}}{\partial t} = -2\sqrt{X}B_{r\varphi} + \sqrt{\operatorname{tr}\mathbf{B}_{\kappa_{p(t)}} - 3\lambda}\frac{r\omega}{h}B_{rz}, \tag{4.69e}$$

$$\sqrt{\operatorname{tr}\mathbf{B}_{\kappa_{p(t)}} - 3\lambda}\frac{\partial B_{rz}}{\partial t} = -2\sqrt{X}B_{rz}, \tag{4.69f}$$

$$\sqrt{\operatorname{tr}\mathbf{B}_{\kappa_{p(t)}} - 3\lambda}\frac{\partial B_{\varphi\varphi}}{\partial t} = -2\sqrt{X}B_{\varphi\varphi} + \sqrt{\operatorname{tr}\mathbf{B}_{\kappa_{p(t)}} - 3\lambda}\frac{2r\omega}{h}B_{\varphi z} + 2\sqrt{X}\lambda, \tag{4.69g}$$

$$\sqrt{\operatorname{tr}\mathbf{B}_{\kappa_{p(t)}} - 3\lambda}\frac{\partial B_{\varphi z}}{\partial t} = -2\sqrt{X}B_{\varphi z} + \sqrt{\operatorname{tr}\mathbf{B}_{\kappa_{p(t)}} - 3\lambda}\frac{r\omega}{h}B_{zz}, \tag{4.69h}$$

$$\sqrt{\operatorname{tr}\mathbf{B}_{\kappa_{p(t)}} - 3\lambda}\frac{\partial B_{zz}}{\partial t} = -2\sqrt{X}B_{zz} + 2\sqrt{X}\lambda, \tag{4.69i}$$

where Y is defined through (3.96), X is the solution of (3.95) and

$$\lambda = \frac{3}{\operatorname{tr}\mathbf{B}^{-1}_{\kappa_{p(t)}}} \overset{(\mathrm{B}.17)}{=} \frac{3}{B_{\varphi\varphi}B_{zz} - B^2_{\varphi z} - B^2_{rz} + B_{rr}B_{zz} - B^2_{r\varphi} + B_{rr}B_{\varphi\varphi}}. \tag{4.70}$$

We neglect time derivative of ω and observe that none of the initial conditions as well as none of the equations (4.69d) – (4.69i) depend on z and therefore the components of $\mathbf{B}_{\kappa_{p(t)}}$ do not depend on this coordinate. We are interested in

$$T_{\varphi z} = \frac{1}{2}Y\epsilon_1\left(\epsilon_0 + \frac{r^2\omega^2}{2h^2}\right)^{\alpha-2}\left(\epsilon_0 + \alpha\frac{r^2\omega^2}{2h^2}\right)\frac{r\omega}{h} + GB_{\varphi z}. \tag{4.71}$$

We solve these equations in the same way as in the previous subsection. For fixed r we solve the system of ODEs in time and one algebraic equation and once we know $B_{\varphi z}(\epsilon_0, \epsilon_1, \epsilon_2, G, \alpha, \beta)$ we can compute the component of the stress tensor (4.71). Torque is computed with the composite Simpson's rule with five nodes

$$M(\epsilon_0, \epsilon_1, \epsilon_2, G, \alpha, \beta, t) = \int_0^R 2\pi r^2 T_{\varphi z}(\epsilon_0, \epsilon_1, \epsilon_2, G, \alpha, \beta, r, t)\,\mathrm{d}r.$$

First we fit only the experiment with the angular velocity $\omega = 0.5$ rad s^{-1}, this is done by minimizing absolute error

$$g(\epsilon_0, \epsilon_1, \epsilon_2, G, \alpha, \beta,) = \frac{1}{N}\frac{1}{T}\int_0^T |E(t) - M(\epsilon_0, \epsilon_1, \epsilon_2, G, \alpha, \beta, t)|\,\mathrm{d}t.$$

G [kPa]	ϵ_0 [10^{-3} s^{-2}]	ϵ_1 [kPa s$^{2\alpha-1}$]	ϵ_2 [kPa s]	α	β	N	g
29.8	0.24	52.8	8.9	0.16	2.88	0.0061	0.0065

Table 4.8: Fitted parameters for the torque overshot experiment using power law like model PL2012 for $\omega = 0.5$ rad s^{-1}.

Obtained material parameters, maximum N and the value of minimizing functional g are given in Table 4.8. Note that we obtained $\alpha < 1$ which means that asphalt binder is a shear thinning material. The graph of the fitted torque is plotted and compared with all non-linear models in Figure 4.16.

In [21] we also fitted all three angular velocities ω at once by minimizing L^2 norm of relative errors

$$g_{\text{rel}} = \left(\left(g^1_{\text{rel}}\right)^2 + \left(g^2_{\text{rel}}\right)^2 + \left(g^3_{\text{rel}}\right)^2 \right)^{1/2}. \tag{4.72}$$

By minimizing g_{rel} we get material parameters given in Table 4.9, the graph of the obtained result is plotted and compared with all other non-linear models in 4.19.

G [kPa]	ϵ_0 [10^{-3} s^{-2}]	ϵ_1 [kPa.s$^{2\alpha-1}$]	ϵ_2 [kPa.s]	α	β
5.9	0.27	52.1	13.3	0.95	1.44

Table 4.9: Fitted parameters for the torque overshot experiment using power law like model PL2012 for all three angular velocities ω.

RaSr2000 model

In [21] we also used model RaSr2000 to fit the experiment by Krishnan and Narayan (2007). Upon substituting the ansatz

$$p = p(t, r, z), \quad \mathbf{v} = \left(0, \frac{\omega(t) r z}{h}, 0\right), \tag{4.73}$$

$$\mathbf{B}_{\kappa_{p(t)}} = \begin{pmatrix} B_{rr}(t,r,z) & B_{r\varphi}(t,r,z) & B_{rz}(t,r,z) \\ B_{r\varphi}(t,r,z) & B_{\varphi\varphi}(t,r,z) & B_{\varphi z}(t,r,z) \\ B_{rz}(t,r,z) & B_{\varphi z}(t,r,z) & B_{zz}(t,r,z) \end{pmatrix} \tag{4.74}$$

into the governing equations for nonlinear model RaSr2000 (3.49) we get

$$0 = -\frac{\partial p}{\partial r} + G\left(\frac{\partial B_{rr}}{\partial r} + \frac{B_{rr}}{r} - \frac{B_{\varphi\varphi}}{r} + \frac{\partial B_{rz}}{\partial z}\right), \tag{4.75a}$$

$$\rho \frac{rz}{h} \frac{\mathrm{d}\omega}{\mathrm{d}t} = G\left(\frac{\partial B_{r\varphi}}{\partial r} + \frac{2B_{r\varphi}}{r} + \frac{\partial B_{\varphi z}}{\partial z}\right), \tag{4.75b}$$

$$0 = -\frac{\partial p}{\partial z} + G\left(\frac{\partial B_{rz}}{\partial r} + \frac{B_{rz}}{r} + \frac{\partial B_{zz}}{\partial z}\right), \tag{4.75c}$$

$$\frac{\partial B_{rr}}{\partial t} = -\frac{G}{\mu_1} B_{rr} + \frac{G}{\mu_1}\lambda, \tag{4.75d}$$

$$\frac{\partial B_{r\varphi}}{\partial t} = -\frac{G}{\mu_1} B_{r\varphi} + \frac{r\omega}{h} B_{rz}, \tag{4.75e}$$

$$\frac{\partial B_{rz}}{\partial t} = -\frac{G}{\mu_1} B_{rz}, \tag{4.75f}$$

$$\frac{\partial B_{\varphi\varphi}}{\partial t} = -\frac{G}{\mu_1}B_{\varphi\varphi} + \frac{2r\omega}{h}B_{\varphi z} + \frac{G}{\mu_1}\lambda, \tag{4.75g}$$

$$\frac{\partial B_{\varphi z}}{\partial t} = -\frac{G}{\mu_1}B_{\varphi z} + \frac{r\omega}{h}B_{zz}, \tag{4.75h}$$

$$\frac{\partial B_{zz}}{\partial t} = -\frac{G}{\mu_1}B_{zz} + \frac{G}{\mu_1}\lambda, \tag{4.75i}$$

where

$$\lambda \overset{(B.17)}{=} \frac{3}{2B_{\varphi\varphi}B_{zz} - B_{\varphi z}^2 + B_{zz}^2}\,. \tag{4.76}$$

These equations do not seem to have an analytical solution. They can be noticeably simplified in the following way. First, equations (4.75e) – (4.75f) have together with the initial condition (4.54) the solution

$$B_{r\varphi} = B_{rz} = 0\,. \tag{4.77}$$

Next, from equations (4.75d) and (4.75i) together with the initial condition (4.54) yields

$$B_{rr} = B_{zz}\,. \tag{4.78}$$

Furthermore, we observe that none of the initial conditions as well as none of the equations (4.75d) – (4.75i) depends on z and therefore also the components of $\mathbf{B}_{\kappa_{p(t)}}$ do not depend on this coordinate. In view of these results, equations (4.75) simplify to

$$\frac{\partial p}{\partial r} = G\left(\frac{\partial B_{zz}}{\partial r} + \frac{B_{zz}}{r} - \frac{B_{\varphi\varphi}}{r}\right), \tag{4.79a}$$

$$\frac{\partial p}{\partial z} = G\frac{\partial B_{zz}}{\partial z}, \tag{4.79b}$$

$$\frac{\partial B_{\varphi\varphi}}{\partial t} = -\frac{G}{\mu_1}B_{\varphi\varphi} + \frac{2r\omega}{h}B_{\varphi z} + \frac{2\mu}{\mu_1}\lambda, \tag{4.79c}$$

$$\frac{\partial B_{\varphi z}}{\partial t} = -\frac{G}{\mu_1}B_{\varphi z} + \frac{r\omega}{h}B_{zz}, \tag{4.79d}$$

$$\frac{\partial B_{zz}}{\partial t} = -\frac{G}{\mu_1}B_{zz} + \frac{2\mu}{\mu_1}\lambda\,. \tag{4.79e}$$

Since we are interested only in $B_{\varphi z}$ we need to solve only the last three equations (4.79c) – (4.79e) for the three unknowns $B_{\varphi\varphi}, B_{\varphi z}, B_{zz}$ that depend on r and t.

The torque is obtained from the knowledge of $T_{\varphi z}$

$$T_{\varphi z}(\mu_2, \mu_1, G, r, t) = \frac{\mu_2 r\omega}{2h} + GB_{\varphi z}\left(\frac{G}{\mu_1}, r, t\right).$$

Torque is computed with the composite Simpson's rule with five nodes

$$M(\mu_2, \mu_1, G, t) = \int_0^R 2\pi r^2 T_{\varphi z}(\mu_2, \mu_1, G, r, t)\,\mathrm{d}r\,.$$

First only the experiment with the angular velocity $\omega = 0.5$ rad s^{-1} is fitted which is done by minimizing absolute error g_{abs} Obtained material parameters, maximum N and minimizing functional g are given in Table 4.10. The graph is plotted and compared with all non-linear models in Figure 4.16.

G [kPa]	G/μ_1 [1/s]	μ_2 [kPa s]	N	g
5.7	0.81	24.2	0.0061	0.0227

Table 4.10: Fitted parameters for the torque overshot experiment using RaSr2000 model for $\omega = 0.5$ rad s^{-1}.

In [21] we also fitted all three angular velocities ω by minimizing L^2 norm of relative errors

$$g_{\text{rel}} = \left(\left(g^1_{\text{rel}}\right)^2 + \left(g^2_{\text{rel}}\right)^2 + \left(g^3_{\text{rel}}\right)^2 \right)^{1/2}. \tag{4.80}$$

By minimizing g_{rel} we get material parameters given in Table 4.11, the graph is plotted and compared with all non-linear models in Figure 4.16.

G [kPa]	G/μ_1 [1/s]	μ_2 [kPa s]
7.4	1.09	24.8

Table 4.11: Fitted parameters for the torque overshot experiment using RaSr2000 model for all three angular velocities ω.

Models Quad1 and Quad2

We fitted the experiment by Krishnan and Narayan (2007) using both models Quad1 and Quad2 in [38]. The governing equations for model Quad2 for the problem under consideration are the same as in the previous subsection, namely the equations (4.43) – (4.46) (the only difference is that angular velocity ω is now constant). The torque is computed by (4.47). The governing equations for the model Quad1 are

$$T_{\varphi z} = \mu_2 \frac{r\omega}{h} + \mu B_{\varphi z}, \tag{4.81}$$

$$\frac{\partial B_{rr}}{\partial t} = \frac{G}{3\mu_1} B_{rr} \left(-2B_{rr} + B_{\varphi\varphi} + B_{zz}\right), \tag{4.82}$$

$$\frac{\partial B_{\varphi\varphi}}{\partial t} = 2\frac{r\omega}{h} B_{\varphi z} - \frac{G}{\mu_1} B^2_{\varphi z} + \frac{2\mu}{3\epsilon_1} B_{\varphi\varphi} \left(B_{rr} - 2B_{\varphi\varphi} + B_{zz}\right), \tag{4.83}$$

$$\frac{\partial B_{\varphi z}}{\partial t} = \frac{r\omega}{h} B_{zz} + \frac{G}{3\mu_1} B_{\varphi z} \left(B_{rr} - 2B_{\varphi\varphi} - 2B_{zz}\right), \tag{4.84}$$

$$\frac{\partial B_{zz}}{\partial t} = -\frac{G}{\mu_1} B^2_{\varphi z} + \frac{G}{3\mu_1} B_{zz} \left(B_{rr} + B_{\varphi\varphi} - 2B_{zz}\right) \tag{4.85}$$

and the torque is computed using (5.141).

First we start with fitting the data for one angular velocity $\omega = 0.5$ rad s^{-1}. It turns out that the model Quad2 with two natural configurations as well as the one natural configuration Quad1 model provide equally good results. However, this should not lead one to the erroneous conclusion that the simpler model Quad1 is as good as the more complicated model Quad2. In fact, it is not. The model Quad1 is incapable of capturing the previous experiment where one has different relaxation times associated with the normal force and torque. Model Quad1 has only one relaxation time associated with. It is just in this particular experiment, Krishnan and Narayan (2007) did not measure the normal force and we have to deal with only one relaxation mechanism associated with torque.

The parameter values that were obtained in fitting the model Quad2 and model Quad1 are provided in the Table 4.12 (G_1 means G for Quad1 and μ_3 is used instead of μ_2 for Quad1). The graphs of the result are almost the same for both models Quad1 and Quad2 and they are depicted in the Figure 4.16 together with the other two non-linear models.

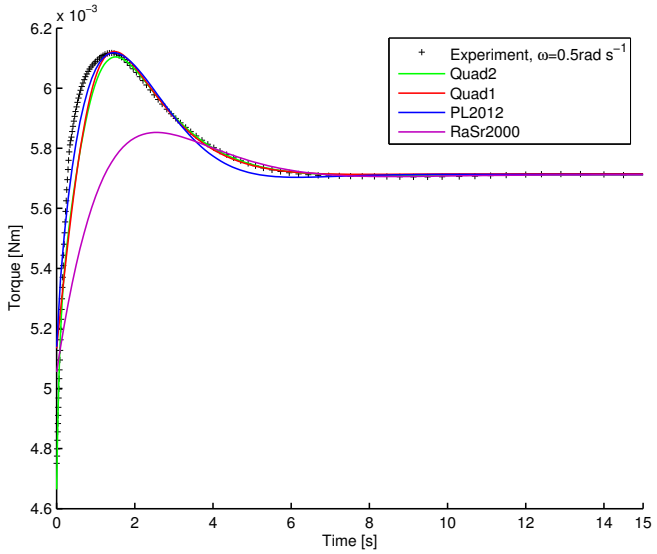

Figure 4.16: Fitted torque, $\omega = 0.5$ rad.s^{-1}.

	G_1 [kPa]	G_2 [kPa]	G_1/μ_1 [1/s]	G_2/μ_2 [1/s]	μ_3 [kPa]	N	g
Quad2	5.6	37.4	0.38	13.70	23.2	0.0061	0.0045
Quad1	6.4	–	0.42	–	25.5	0.0061	0.0064

Table 4.12: Fitted parameters for models Quad1 and Quad2, $\omega = 0.5$rad.s^{-1}.

For comparison, power law like model PL2012 with 6 material parameters has $g = 0.0065$ which is comparable to the fit of the model Quad1 with only three material parameters. However, model RaSr2000 model with three material parameters has $g = 0.0227$ (more than three times larger).

If we try to use model Quad2 with the parameters obtained during fitting the angular velocity $\omega = 0.5$ rad s^{-1} (see Table 4.12) for prediction of the experiment with the two lower angular velocities we get the result depicted in the Figure 4.17. We can see that the prediction is quite satisfactory, to be more precise the measure g defined by (4.5), where N_i are the maximums of individual experiments, is equal to 0.0996. Thus, using material parameters obtained by fitting the experimental data for $\omega = 0.5$ rad s^{-1} we can predict experimental data for lower angular velocities $\omega = 0.25$ rad s^{-1} and $\omega = 0.125$ rad s^{-1}.

Further, we fit all three angular velocities with one set of parameters. For fitting we prefer the experiment with $\omega = 0.5$ rad s^{-1} because two other experimental data are too flat. Let us define a new functional

$$g_{\text{pref}_1} = \frac{3}{N_1} g^1_{\text{abs}} + \frac{1}{N_2} g^2_{\text{abs}} + \frac{1}{N_3} g^3_{\text{abs}}$$

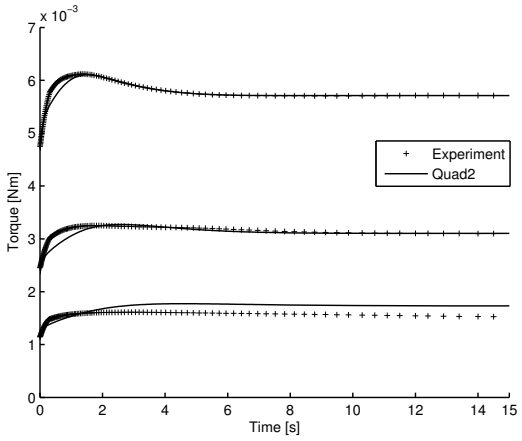

Figure 4.17: Model Quad2, parameters from Table 4.12.

that is minimized.

The material parameters are given in Table 4.13, $N_1 = 0.0061$ is the maximum of torque for $\omega = 0.5$ rad s^{-1}, $N_2 = 0.0033$ is maximum of torque for $\omega = 0.25$ rad s^{-1} and $N_3 = 0.0016$ is maximum of torque for $\omega = 0.125$ rad s^{-1}. However, we also computed the functional g given by (4.5) in order to make a comparison with predictions of the models PL2012 and RaSr2000.

	G_1 [kPa]	G_2 [kPa]	G_1/μ_1 [1/s]	G_2/μ_2 [1/s]	μ_3 [kPa]	g	g_{pref_1}
Quad2	3.7	35.5	0.46	8.2	23.1	0.071	0.096
Quad1	5.0	–	0.37	–	26.2	0.091	0.107

Table 4.13: Fitted parameters for model Quad2 for all three angular velocities ω.

In [21] we fitted this experiment using model PL2012 with six material parameters with $g = 0.088$ and $g_{\text{pref}_1} = 0.139$ and using model RaSr2000 $g = 0.101$ and $g_{\text{pref}_1} = 0.156$.[4]

The graphs of all non-linear models are plotted in Figure 4.19, zoom to $t = [0, 1]$ is plotted in Figure 4.18. According to the absolute error g the best fit gives model Quad2. Model PL2012 with 6 material parameters is comparable to Quad1 with only three material parameters and the worst is model RaSr2000. Further, in Figure 4.18 it can be seen that model Quad2 is for all angular velocities much better at the beginning of the experiment than the other models.

Note on comparison of the material parameters for Quad2 model obtained for different experiments Model Quad2 was used to fit all three sets of experiments – Monismith, Secor (1962), Narayan et al. (2012) and Krishnan and Narayan (2007). Experiment by Monismith and Secor was performed with asphalt concrete which is very

[4] It is important to remind that the fit of all three angular velocities using PL2012 and RaSr2000 models was obtained by minimizing relative errors which is a handicap for these two models when comparing absolute errors. However, the fit was done in order to obtain the best looking fit using power law like model PL2012 and one can compare both fits visually. Moreover, when fitting only one angular velocity $\omega = 0.5$ rad s^{-1}, the absolute error was used for all non-linear models and models Quad2 and Quad1 have lower errors than models PL2012 and RaSr2000.

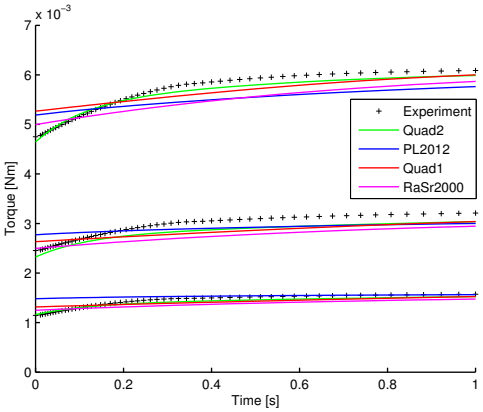

Figure 4.18: Fit of all angular velocities using all non-linear models, zoom to $t = [0, 1]$.

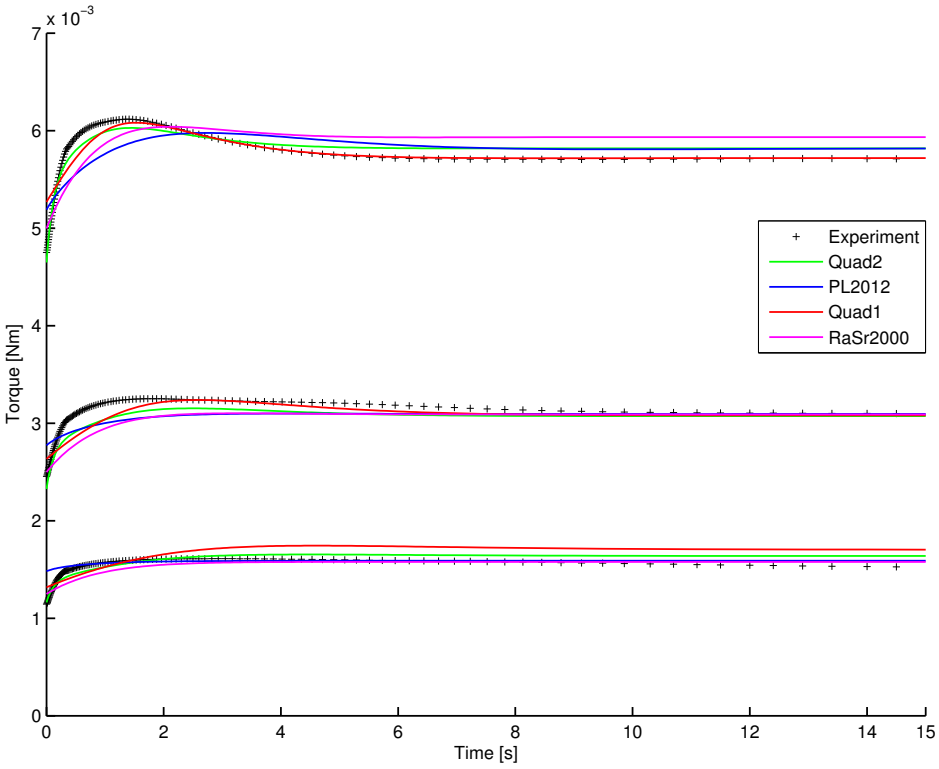

Figure 4.19: Fit of all angular velocities using all non-linear models.

different from asphalt binder used in remaining two experiments. Asphalt binder used by Krishnan and Narayan (2007) at temperature 35 °C is quite similar to unaged base binder at temperature 35 °C used by Narayan et al. (2012). In Figure 4.20 we can compare the torques for $\omega = 0.5$ rad s^{-1} (for $t \leq 0.5$, after that $\omega = 0$ in experiment by Narayan et al. (2012)) and we find out that the difference is approximately 15%.

In Table 4.14 we can compare obtained material parameters (due to the symmetry

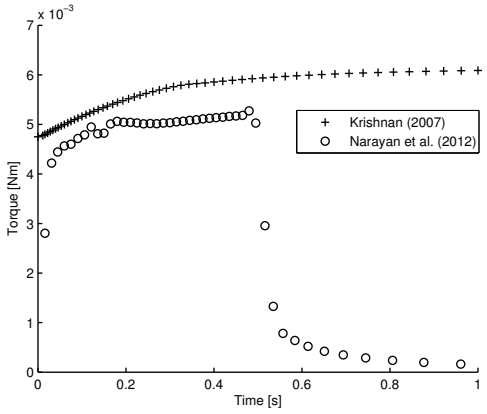

Figure 4.20: Comparison of experimental data for the torque from Krishnan (2007) and Narayan (2012).

of the natural configurations in model Quad2 we can swap (G_1, μ_1) and (G_2, μ_2)), three of five parameters are similar (15% and lower), two parameters are different (30% and 70%). According to the fact that different materials were used in both experiment, the similarity of the material parameters is reasonable.

	G_1 [kPa]	G_2 [kPa]	G_1/μ_1 [1/s]	G_2/μ_2 [1/s]	μ_3 [kPa]
Narayan (2012)	50.2	3.45	9.80	1.68	19.7
Krishan (2007)	35.5	3.70	8.20	0.46	23.1

Table 4.14: Comparison of material parameters for similar materials used from two sets of experiments: Krishnan and Narayan (2007), and Narayan et al. (2012).

Chapter 5

Numerical solution of initial and boundary value problems for selected rate-type fluid models

In this chapter we define weak formulations for two standard viscoelastic models Oldroyd-B and Burgers, and for two new viscoelastic models Quad1 and Quad2. Furthermore, we introduce finite element method based on these weak formulations for the numerical computation of different problems in fixed and deforming domains.

At first we compute two benchmark tests using Oldroyd-B model and model Quad1 for proving abilities of our numerical method. As the next step, we perform full simulation of the experiment using the fitted experiment parameters with the model Quad2 and verify that the solution of our full simulation agrees with the assumption for the simplified computation used for the fitting.

Finally, we introduce the Arbitrary Lagrangian-Eulerian (ALE) formulation which enables us to compute the problems in time-varying domains. We use this approach to simulate real life problems, for example "rutting" of roadways or rolling of the asphalt with our new models.

We abbreviate "the initial and boundary value problem" by IBVP, and "the boundary value problem" by BVP.

5.1 Weak formulation for BVP and IBVP involving Oldroyd-B, Burgers, Quad1 and Quad2 models

In this section we derive formal apriori estimates for unsteady Oldroyd-B model (2.10) and Burgers model (3.255) and also apriori estimates for models Quad1 (3.154) and Quad2 (3.239). Furthermore, we define a weak formulation for all these models.

Initial and boundary conditions For time-dependent problems we assume that the material is at rest at $t = 0$, i.e. the initial conditions are the following: $\mathbf{v}(t = 0) = \mathbf{0}$,

$p(t=0)=0$ and

$$\mathbf{B}_{\kappa_{p_1(t)}}(t=0)=\mathbf{B}_{\kappa_{p_2(t)}}(t=0)=\mathbf{I} \quad \text{for Quad2 model,} \tag{5.1}$$

$$\mathbf{B}_{\kappa_{p(t)}}(t=0)=\mathbf{I} \quad \text{for Quad1 model,} \tag{5.2}$$

$$\mathbf{B}(t=0)=\mathbf{I} \quad \text{for Oldroyd-B model,} \tag{5.3}$$

$$\mathbf{B}_1(t=0)=\mathbf{B}_2(t=0)=\mathbf{I} \quad \text{for Burgers model.} \tag{5.4}$$

The problems are solved in domain Ω. For the boundary conditions we assume that the boundary $\partial\Omega$ consists of two parts Γ_N and Γ_D such that $\Gamma_N \cup \Gamma_D = \partial\Omega$ and $\Gamma_N \cap \Gamma_D = \emptyset$. We suppose that Dirichlet boundary condition $\mathbf{v}=\mathbf{v}_D$ is prescribed on Γ_D and the normal traction $\mathbf{Tn}=\mathbf{t}$ is given on Γ_N. For the tensors $\mathbf{B}_i$ in case of Oldroyd-B and Burgers model, and $\mathbf{B}_{\kappa_{p_i(t)}}$ in case of models Quad1 and Quad2 no boundary condition is prescribed.

In derivation of apriori estimates, for simplicity, we suppose that $\mathbf{v}=0$ on whole boundary $\partial\Omega$.

5.1.1 Apriori estimates for unsteady Oldroyd-B and Burgers model

We show the apriori estimates only for Burgers model because in case of Oldroyd-B model the transport equation for the second tensor $\mathbf{B}_2$ is missing and the estimates are the same as in case of Burgers.

In order to obtain the apriori estimates for Burgers model we use the property (3.257) saying that

$$\operatorname{tr}\mathbf{B}_i - d \geq 0, i=1,2, \tag{5.5}$$

where d is the space dimension.

First, we multiply balance of linear momentum (1.13) by $\mathbf{v}$, integrate over Ω and use Gauss theorem

$$\frac{\rho}{2}\frac{\mathrm{d}}{\mathrm{d}t}\int_\Omega |\mathbf{v}|^2 \,\mathrm{d}x = -\int_\Omega \mathbf{T}\cdot\mathbf{D}\,\mathrm{d}x, \tag{5.6}$$

where the Cauchy stress tensor $\mathbf{T}$ is defined through (3.255a). Then we take the trace of (3.255b) and (3.255c) and integrate the result over Ω

$$\frac{\mathrm{d}}{\mathrm{d}t}\int_\Omega \operatorname{tr}(\mathbf{B}_1-\mathbf{I})\,\mathrm{d}x + \frac{1}{\tau_1}\int_\Omega \operatorname{tr}(\mathbf{B}_1-\mathbf{I})\,\mathrm{d}x = 2\int_\Omega \mathbf{B}_1\cdot\mathbf{D}\,\mathrm{d}x\,, \tag{5.7}$$

$$\frac{\mathrm{d}}{\mathrm{d}t}\int_\Omega \operatorname{tr}(\mathbf{B}_2-\mathbf{I})\,\mathrm{d}x + \frac{1}{\tau_2}\int_\Omega \operatorname{tr}(\mathbf{B}_2-\mathbf{I})\,\mathrm{d}x = 2\int_\Omega \mathbf{B}_2\cdot\mathbf{D}\,\mathrm{d}x \tag{5.8}$$

and we perform (5.6) + $G_1/2\times$ (5.7) + $G_2/2\times$ (5.8)

$$\frac{\rho}{2}\frac{\mathrm{d}}{\mathrm{d}t}\int_\Omega |\mathbf{v}|^2\,\mathrm{d}x + \mu_3\int_\Omega |\nabla\mathbf{v}|^2\,\mathrm{d}x + \frac{G_1}{2}\frac{\mathrm{d}}{\mathrm{d}t}\int_\Omega \operatorname{tr}(\mathbf{B}_1-\mathbf{I})\,\mathrm{d}x + \frac{G_1}{2\tau_1}\int_\Omega \operatorname{tr}(\mathbf{B}_1-\mathbf{I})\,\mathrm{d}x$$
$$+\frac{G_2}{2}\frac{\mathrm{d}}{\mathrm{d}t}\int_\Omega \operatorname{tr}(\mathbf{B}_2-\mathbf{I})\,\mathrm{d}x + \frac{G_2}{2\tau_2}\int_\Omega \operatorname{tr}(\mathbf{B}_2-\mathbf{I})\,\mathrm{d}x = 0. \tag{5.9}$$

Relation (5.5) guarantees that all terms are non-negative. Using Lemma B.1.4 we obtain that all components of $\mathbf{B}_i$ are bounded in the same space as $\operatorname{tr}\mathbf{B}_i$. Hence, see Temam [63] for example,

$$\|\mathbf{v}\|_V \leq C, \quad \|\mathbf{B}_1\|_{L^\infty(0,T;L^1(\Omega))^{d\times d}} \leq C, \quad \|\mathbf{B}_2\|_{L^\infty(0,T;L^1(\Omega))^{d\times d}} \leq C, \tag{5.10}$$

where $V = L^\infty(0,T;L^2(\Omega))^d \cap L^2(0,T;W^{1,2}(\Omega))^d$. Hence

$$\|\mathbf{v}\|_{L^4((0,T)\times\Omega)^d} \leq C \text{ for } d=2, \tag{5.11}$$

$$\|\mathbf{v}\|_{L^{10/3}((0,T)\times\Omega)^d} \leq C \text{ for } d=3. \tag{5.12}$$

The estimate for pressure is obtained from the balance of linear momentum, we apply divergence on balance of linear momentum (1.13) and get

$$-\Delta p = \operatorname{div}\operatorname{div}\left(\mathbf{v}\otimes\mathbf{v} - 2\mu_3\mathbf{D} - G_1(\mathbf{B}_1-\mathbf{I}) - G_2(\mathbf{B}_2-\mathbf{I})\right) \tag{5.13}$$

which suggests that pressure p can at most satisfy the following estimate

$$\|p\|_{V_{p_O}} \leq C, \tag{5.14}$$

where

$$V_{p_O} = \begin{cases} L^2(0,T;L^1(\Omega)) & \text{for } d=2, \\ L^{5/3}(0,T;L^1(\Omega)) & \text{for } d=3. \end{cases} \tag{5.15}$$

Note on apriori estimate corresponding to reduced thermodynamic inequality

If ψ denotes the Helmholtz free energy corresponding to (3.222) and it is given by[1]

$$\psi = \frac{G_1}{2\rho}\left(\operatorname{tr}\mathbf{B}_{\kappa_{p_1(t)}} - d - \ln(\det\mathbf{B}_{\kappa_{p_1(t)}})\right) + \frac{G_2}{2\rho}\left(\operatorname{tr}\mathbf{B}_{\kappa_{p_2(t)}} - d - \ln(\det\mathbf{B}_{\kappa_{p_2(t)}})\right) \tag{5.16}$$

and the rate of entropy production ξ is given by (3.223)

$$\xi = 2\mu_3|\mathbf{D}|^2 + 2\mu_1\mathbf{D}_{\kappa_{p_1(t)}}\mathbf{C}_{\kappa_{p_1(t)}}\cdot\mathbf{D}_{\kappa_{p_1(t)}} + 2\mu_2\mathbf{D}_{\kappa_{p_2(t)}}\mathbf{C}_{\kappa_{p_2(t)}}\cdot\mathbf{D}_{\kappa_{p_2(t)}}, \tag{5.17}$$

then the reduced thermodynamic inequality (1.18) in the form

$$\frac{\mathrm{d}}{\mathrm{d}t}\int_\Omega \rho\psi\,\mathrm{d}x + \int_\Omega \xi = \int_\Omega \mathbf{T}\cdot\mathbf{D} \tag{5.18}$$

can be obtained in the following way: We start as in the previous apriori estimate (5.9); we perform $G_1/2\times(5.7) + G_2/2\times(5.8)$ an obtain

$$\frac{G_1}{2}\frac{\mathrm{d}}{\mathrm{d}t}\int_\Omega \operatorname{tr}(\mathbf{B}_1-\mathbf{I})\,\mathrm{d}x + \frac{G_1}{2\tau_1}\int_\Omega \operatorname{tr}(\mathbf{B}_1-\mathbf{I})\,\mathrm{d}x + \frac{G_2}{2}\frac{\mathrm{d}}{\mathrm{d}t}\int_\Omega \operatorname{tr}(\mathbf{B}_2-\mathbf{I})\,\mathrm{d}x + \frac{G_2}{2\tau_2}\int_\Omega \operatorname{tr}(\mathbf{B}_2-\mathbf{I})\,\mathrm{d}x = \underbrace{G_1\int_\Omega \mathbf{B}_1\cdot\mathbf{D}\,\mathrm{d}x + G_2\int_\Omega \mathbf{B}_2\cdot\mathbf{D}\,\mathrm{d}x}_{\int_\Omega \mathbf{T}\cdot\mathbf{D}\,\mathrm{d}x - 2\mu_3\int_\Omega|\mathbf{D}|^2\,\mathrm{d}x}. \tag{5.19}$$

Further, we compute the following $G_1/2\times(3.255\text{b})\cdot\mathbf{B}_1^{-1} + G_2/2\times(3.255\text{c})\cdot\mathbf{B}_2^{-1}$, integrate over Ω and obtain

$$\frac{G_1}{2}\int_\Omega \dot{\mathbf{B}}_1\cdot\mathbf{B}_1^{-1}\,\mathrm{d}x + \frac{G_1}{2\tau_1}\int_\Omega \operatorname{tr}\left(\mathbf{I}-\mathbf{B}_1^{-1}\right)\,\mathrm{d}x + \frac{G_2}{2}\int_\Omega \dot{\mathbf{B}}_2\cdot\mathbf{B}_2^{-1}\,\mathrm{d}x + \frac{G_2}{2\tau_2}\int_\Omega \operatorname{tr}\left(\mathbf{I}-\mathbf{B}_2^{-1}\right)\,\mathrm{d}x = 0. \tag{5.20}$$

[1] Note that tensors $\mathbf{B}_1$ and $\mathbf{B}_2$ for Burgers model in our thermodynamical approach correspond to tensors $\mathbf{B}_{\kappa_{p_1(t)}}$ and $\mathbf{B}_{\kappa_{p_2(t)}}$.

Now, we subtract relations (5.19) and (5.20) and get another form of apriori estimate

$$\begin{aligned}\frac{G_1}{2}\left[\frac{\mathrm{d}}{\mathrm{d}t}\int_\Omega \mathrm{tr}\,(\mathbf{B}_1-\mathbf{I})\,\mathrm{d}x-\int_\Omega \dot{\mathbf{B}}_1\cdot\mathbf{B}_1^{-1}\,\mathrm{d}x\right]\\ +\frac{G_2}{2}\left[\frac{\mathrm{d}}{\mathrm{d}t}\int_\Omega \mathrm{tr}\,(\mathbf{B}_2-\mathbf{I})\,\mathrm{d}x-\int_\Omega \dot{\mathbf{B}}_2\cdot\mathbf{B}_2^{-1}\,\mathrm{d}x\right]+2\mu_3\int_\Omega|\mathbf{D}|^2\,\mathrm{d}x\\ +\frac{G_1}{2\tau_1}\int_\Omega \mathrm{tr}\left(\mathbf{B}_1-2\mathbf{I}+\mathbf{B}_1^{-1}\right)\,\mathrm{d}x+\frac{G_2}{2\tau_2}\int_\Omega \mathrm{tr}\left(\mathbf{B}_2-2\mathbf{I}+\mathbf{B}_2^{-1}\right)\,\mathrm{d}x=\int_\Omega \mathbf{T}\cdot\mathbf{D}\,\mathrm{d}x.\end{aligned} \tag{5.21}$$

Note that according to (5.5) $\mathrm{tr}\,\mathbf{B}_i \geq d$ and also $\mathrm{tr}\,\mathbf{B}_i^{-1} \geq d$ for $i=1,2$, and thus $\mathrm{tr}\left(\mathbf{B}_1-2\mathbf{I}+\mathbf{B}_1^{-1}\right)$ is non-negative. In order to show that (5.21) is equivalent to (5.18) we have to show that

$$\frac{\mathrm{d}}{\mathrm{d}t}(\rho\psi)=\frac{G_1}{2}\left[\frac{\mathrm{d}}{\mathrm{d}t}\,\mathrm{tr}(\mathbf{B}_1-\mathbf{I})-\dot{\mathbf{B}}_1\cdot\mathbf{B}_1^{-1}\right]+\frac{G_2}{2}\left[\frac{\mathrm{d}}{\mathrm{d}t}\,\mathrm{tr}(\mathbf{B}_2-\mathbf{I})-\dot{\mathbf{B}}_2\cdot\mathbf{B}_2^{-1}\right], \tag{5.22}$$

$$\xi=2\mu_3|\mathbf{D}|^2+\frac{G_1}{2\tau_1}\,\mathrm{tr}\left(\mathbf{B}_1-2\mathbf{I}+\mathbf{B}_1^{-1}\right)+\frac{G_2}{2\tau_2}\,\mathrm{tr}\left(\mathbf{B}_2-2\mathbf{I}+\mathbf{B}_2^{-1}\right). \tag{5.23}$$

Since

$$\frac{\mathrm{d}}{\mathrm{d}t}\ln(\det\mathbf{B})=\dot{\mathbf{B}}\cdot\mathbf{B}^{-1}$$

relation (5.22) holds and first two terms in (5.21) can be written in the form

$$\frac{\mathrm{d}}{\mathrm{d}t}\int_\Omega \rho\psi.$$

The integrand $\rho\psi$ is non-negative according to (2.37). In order to prove (5.23) we have to show that

$$2\mu_1\mathbf{D}_{\kappa_{p(t)}}\mathbf{C}_{\kappa_{p(t)}}\cdot\mathbf{D}_{\kappa_{p(t)}}=\frac{G_1}{2\tau_1}\,\mathrm{tr}\left(\mathbf{B}_{\kappa_{p(t)}}-2\mathbf{I}+\mathbf{B}^{-1}_{\kappa_{p(t)}}\right), \tag{5.24}$$

where $\tau_1=\mu_1/G_1$. Relation (5.24) is shown by using (3.163):

$$2\mu_1\mathbf{D}_{\kappa_{p(t)}}\mathbf{C}_{\kappa_{p(t)}}=G_1(\mathbf{C}_{\kappa_{p(t)}}-\mathbf{I}). \tag{5.25}$$

We take the scalar product of (5.25) by $\mathbf{D}_{\kappa_{p(t)}}$ and we obtain

$$2\mu_1\mathbf{D}_{\kappa_{p(t)}}\mathbf{C}_{\kappa_{p(t)}}\cdot\mathbf{D}_{\kappa_{p(t)}}=G_1(\mathbf{C}_{\kappa_{p(t)}}-\mathbf{I})\cdot\mathbf{D}_{\kappa_{p(t)}}, \tag{5.26}$$

then we take the trace of (5.25) and multiply the result by $G_1/(2\mu_1)$

$$G_1\mathbf{D}_{\kappa_{p(t)}}\cdot\mathbf{C}_{\kappa_{p(t)}}=\frac{G_1^2}{2\mu_1}\,\mathrm{tr}\left(\mathbf{C}_{\kappa_{p(t)}}-\mathbf{I}\right). \tag{5.27}$$

Further, we take the scalar product of (5.25) with $\mathbf{C}^{-1}_{\kappa_{p(t)}}$ and multiply the result by $G_1/(2\mu_1)$

$$G_1\,\mathrm{tr}\,\mathbf{D}_{\kappa_{p(t)}}=\frac{G_1^2}{2\mu_1}\,\mathrm{tr}\left(\mathbf{I}-\mathbf{C}^{-1}_{\kappa_{p(t)}}\right). \tag{5.28}$$

Finally, by combining (5.26), (5.27) and (5.28) we obtain

$$2\mu_1\mathbf{D}_{\kappa_{p(t)}}\mathbf{C}_{\kappa_{p(t)}}\cdot\mathbf{D}_{\kappa_{p(t)}}=\frac{G_1}{2\tau_1}\,\mathrm{tr}\left(\mathbf{C}_{\kappa_{p(t)}}-2\mathbf{I}+\mathbf{C}^{-1}_{\kappa_{p(t)}}\right) \tag{5.29}$$

which is equivalent to (5.24) because $\mathrm{tr}\,\mathbf{B}_{\kappa_{p(t)}}=\mathrm{tr}\,\mathbf{C}_{\kappa_{p(t)}}$ and $\mathrm{tr}\left(\mathbf{B}^{-1}_{\kappa_{p(t)}}\right)=\left(\mathbf{C}^{-1}_{\kappa_{p(t)}}\right)$.

5.1.2 Weak formulation for IBVP involving Oldroyd-B and Burgers model

Since $\mathbf{B}_i$ is bounded only in $L^\infty(0,T;L^1(\Omega))^{d\times d}$ we derive a weak renormalized formulation which is obtained by taking the Hadamard product of (3.255b), resp. (3.255c) with $(\mathbf{R}^L)_1'(\mathbf{B}_1)$, resp. $(\mathbf{R}^L)_2'(\mathbf{B}_2)$. We define the Hadamard product of two matrices as (in the three-dimensional setting the definition is similar)

$$\mathbf{A}\circ\mathbf{B}=\begin{pmatrix}A_{11}B_{11} & A_{12}B_{12}\\ A_{21}B_{21} & A_{22}B_{22}\end{pmatrix}. \tag{5.30}$$

Further, we define $\mathbf{R}^L(\mathbf{B})\in\mathcal{R}$ as a set of continuously differentiable matrix functions in the form

$$\mathbf{R}^L(\mathbf{B})=\begin{pmatrix}R^L_{11}(B_{11}) & R^L_{12}(B_{12})\\ R^L_{21}(B_{21}) & R^L_{22}(B_{22})\end{pmatrix},\quad (\mathbf{R}^L)'(\mathbf{B})=\begin{pmatrix}\dfrac{\partial R^L_{11}}{\partial B_{11}} & \dfrac{\partial R^L_{12}}{\partial B_{12}}\\ \dfrac{\partial R^L_{21}}{\partial B_{21}} & \dfrac{\partial R^L_{22}}{\partial B_{22}}\end{pmatrix}, \tag{5.31}$$

where

$$\mathcal{R}=\big\{(R^L_{ij})_{i,j=1}^d \text{ continuously differentiable matrix function of } B_{ij}, R^L_{ij}(B_{ij})=B_{ij}\\ \text{for } |B_{ij}|\le L \text{ and } R^L_{ij}(B_{ij})=L+1 \text{ for } |B_{ij}|>L+1,\ L=2,\dots,\infty\big\}.$$

Then the renormalizations of the transport equations (3.255b) and (3.255c) are equal to

$$\frac{\partial\mathbf{R}^L_i(\mathbf{B}_i)}{\partial t}+\mathbf{v}\cdot\nabla\mathbf{R}^L_i(\mathbf{B}_i)+\left(-(\nabla\mathbf{v})\mathbf{B}_i-\mathbf{B}_i(\nabla\mathbf{v})^{\mathrm{T}}+\frac{1}{\tau_i}(\mathbf{B}_i-\mathbf{I})\right)\circ(\mathbf{R}^L_i)'(\mathbf{B}_i)=0,\quad i=1,2. \tag{5.32}$$

Note that $(\mathbf{R}^L_i)'(\mathbf{B}_i)=\mathbf{0}$ for $|\mathbf{B}_i|>L+1$, and thus the last term in (5.32) is integrable. The weak renormalized solution is obtained by multiplying balance of mass (1.11) by test function q, balance of linear momentum (1.13) by test function $\mathbf{q}$ and renormalized equations (5.32) by test functions $\mathbf{Q}_1$ and $\mathbf{Q}_2$. The Gauss theorem is applied on the convective terms in (1.11) and (5.32).

The weak renormalized solution is the following: The quadruple $(\mathbf{v},p,\mathbf{B}_1,\mathbf{B}_2)\in V\times V_{pO}\times L^\infty(0,T;L^1(\Omega))^{d\times d}\times L^\infty(0,T;L^1(\Omega))^{d\times d}$, such that $\mathbf{v}-\tilde{\mathbf{v}}\in L^2(0,T;W^{1,2}_{0,\Gamma_D}(\Omega))^d$ is a weak renormalized solution of the Burgers model (3.255) in $\Omega\subset\mathbb{R}^d$ if

$$\int_\Omega \mathrm{tr}(\nabla\mathbf{v})q\,\mathrm{d}x=0, \tag{5.33a}$$

$$\int_\Omega\rho\left[\frac{\partial\mathbf{v}}{\partial t}+(\nabla\mathbf{v})\mathbf{v}\right]\cdot\mathbf{q}\,\mathrm{d}x-\int_\Omega\mathbf{T}\cdot\nabla\mathbf{q}\,\mathrm{d}x+\int_{\Gamma_N}\mathbf{t}\cdot\mathbf{q}\,\mathrm{d}S=0, \tag{5.33b}$$

$$\mathbf{T}=-p\mathbf{I}+\mu_3\left((\nabla\mathbf{v})+(\nabla\mathbf{v})^{\mathrm{T}}\right)+G_1(\mathbf{B}_1-\mathbf{I})+G_2(\mathbf{B}_2-\mathbf{I}), \tag{5.33c}$$

$$\int_\Omega\left[\frac{\partial\mathbf{R}^L_1(\mathbf{B}_1)}{\partial t}+\left(-(\nabla\mathbf{v})\mathbf{B}_1-\mathbf{B}_1(\nabla\mathbf{v})^{\mathrm{T}}+\frac{1}{\tau_1}(\mathbf{B}_1-\mathbf{I})\right)\circ(\mathbf{R}^L_1)'(\mathbf{B}_1)\right]\cdot\mathbf{Q}_1\,\mathrm{d}x\\ -\int_\Omega\mathbf{R}^L_1(\mathbf{B}_1)\otimes\mathbf{v}\cdot\nabla\mathbf{Q}_1\,\mathrm{d}x+\int_{\partial\Omega}(\mathbf{v}\cdot\mathbf{n})\,\mathbf{R}^L_1(\mathbf{B}_1)\cdot\mathbf{Q}_1\,\mathrm{d}S=0, \tag{5.33d}$$

$$\int_\Omega\left[\frac{\partial\mathbf{R}^L_2(\mathbf{B}_2)}{\partial t}+\left(-(\nabla\mathbf{v})\mathbf{B}_2-\mathbf{B}_2(\nabla\mathbf{v})^{\mathrm{T}}+\frac{1}{\tau_2}(\mathbf{B}_2-\mathbf{I})\right)\circ(\mathbf{R}^L_2)'(\mathbf{B}_2)\right]\cdot\mathbf{Q}_2\,\mathrm{d}x\\ -\int_\Omega\mathbf{R}^L_2(\mathbf{B}_2)\otimes\mathbf{v}\cdot\nabla\mathbf{Q}_2\,\mathrm{d}x+\int_{\partial\Omega}(\mathbf{v}\cdot\mathbf{n})\,\mathbf{R}^L_2(\mathbf{B}_2)\cdot\mathbf{Q}_2\,\mathrm{d}S=0 \tag{5.33e}$$

is satisfied for all $(q, \mathbf{q}, \mathbf{Q}_1, \mathbf{Q}_2) \in C^1(\Omega) \times V_1 \times C^1(\Omega)^{d\times d} \times C^1(\Omega)^{d\times d}$, all $\mathbf{R}_i^L \in \mathcal{R}$ and a.a. $t \in (0,T)$, where $V_1 = \{\mathbf{v} \in C^1(\Omega)^2, \mathbf{v} = \mathbf{0} \text{ on } \Gamma_D\}$ and $\tilde{\mathbf{v}}|_{\Gamma_D} = \mathbf{v}_D$.

For numerical implementation all computations are done for $R_{ij}(B_{ij}) = B_{ij}$ with the original convective term in the transport equations for $\mathbf{B}_i$, then the weak formulation is in the form

$$\int_\Omega \operatorname{tr}(\nabla \mathbf{v}) q \,\mathrm{d}x = 0, \tag{5.34a}$$

$$\int_\Omega \rho \left[\frac{\partial \mathbf{v}}{\partial t} + (\nabla \mathbf{v})\mathbf{v}\right] \cdot \mathbf{q} \,\mathrm{d}x - \int_\Omega \mathbf{T} \cdot \nabla \mathbf{q} \,\mathrm{d}x + \int_{\Gamma_N} \mathbf{t} \cdot \mathbf{q} \,\mathrm{d}S = 0, \tag{5.34b}$$

$$\mathbf{T} = -p\mathbf{I} + \mu_3 \left((\nabla \mathbf{v}) + (\nabla \mathbf{v})^{\mathrm{T}}\right) + G_1(\mathbf{B}_1 - \mathbf{I}) + G_2(\mathbf{B}_2 - \mathbf{I}), \tag{5.34c}$$

$$\int_\Omega \left[\frac{\partial \mathbf{B}_1}{\partial t} + (\nabla \mathbf{B}_1)\mathbf{v} - (\nabla \mathbf{v})\mathbf{B}_1 - \mathbf{B}_1(\nabla \mathbf{v})^{\mathrm{T}} + \frac{1}{\tau_1}(\mathbf{B}_1 - \mathbf{I})\right] \cdot \mathbf{Q}_1 \,\mathrm{d}x = 0, \tag{5.34d}$$

$$\int_\Omega \left[\frac{\partial \mathbf{B}_2}{\partial t} + (\nabla \mathbf{B}_2)\mathbf{v} - (\nabla \mathbf{v})\mathbf{B}_2 - \mathbf{B}_2(\nabla \mathbf{v})^{\mathrm{T}} + \frac{1}{\tau_2}(\mathbf{B}_2 - \mathbf{I})\right] \cdot \mathbf{Q}_2 \,\mathrm{d}x = 0. \tag{5.34e}$$

5.1.3 Apriori estimates for unsteady models Quad1 and Quad2

We show the apriori estimates only for model Quad2 because in case of model Quad1 the transport equation for the second tensor $\mathbf{B}_{\kappa_{p_2(t)}}$ is missing and the estimates are the same as in case of model Quad2. In order to obtain the apriori estimates for model Quad2 we use the property (3.244) saying that $\operatorname{tr} \mathbf{B}_{\kappa_{p_i(t)}} - d \geq 0, i = 1,2$, where d is the space dimension.

First, we multiply balance of linear momentum (1.13) by $\mathbf{v}$, integrate over Ω and use Gauss theorem

$$\frac{\rho}{2}\frac{\mathrm{d}}{\mathrm{d}t}\int_\Omega |\mathbf{v}|^2 \,\mathrm{d}x = -\int_\Omega \mathbf{T} \cdot \mathbf{D} \,\mathrm{d}x, \tag{5.35}$$

then we integrate the trace of (3.239b) and (3.239b) over Ω

$$\frac{\mathrm{d}}{\mathrm{d}t}\int_\Omega \operatorname{tr}\left(\mathbf{B}_{\kappa_{p_1(t)}}\right) \,\mathrm{d}x + \frac{G_1}{\mu_1}\int_\Omega |\mathbf{B}^d_{\kappa_{p_1(t)}}|^2 \,\mathrm{d}x = 2\int_\Omega \mathbf{B}^d_{\kappa_{p_1(t)}} \cdot \mathbf{D} \,\mathrm{d}x\,, \tag{5.36}$$

$$\frac{\mathrm{d}}{\mathrm{d}t}\int_\Omega \operatorname{tr}\left(\mathbf{B}_{\kappa_{p_2(t)}}\right) \,\mathrm{d}x + \frac{G_2}{\mu_2}\int_\Omega |\mathbf{B}^d_{\kappa_{p_2(t)}}|^2 \,\mathrm{d}x = 2\int_\Omega \mathbf{B}^d_{\kappa_{p_2(t)}} \cdot \mathbf{D} \,\mathrm{d}x \tag{5.37}$$

and from (5.35) + $G_1/2 \times$ (5.36) + $G_2/2 \times$ (5.37) we get

$$\begin{aligned}\frac{\rho}{2}\frac{\mathrm{d}}{\mathrm{d}t}\int_\Omega |\mathbf{v}|^2 \,\mathrm{d}x + \mu_3 \int_\Omega |\nabla \mathbf{v}|^2 \,\mathrm{d}x + \frac{G_1}{2}\frac{\mathrm{d}}{\mathrm{d}t}\int_\Omega \operatorname{tr}\left(\mathbf{B}_{\kappa_{p_1(t)}}\right) \,\mathrm{d}x + \frac{G_1^2}{2\mu_1}\int_\Omega |\mathbf{B}^d_{\kappa_{p_1(t)}}|^2 \,\mathrm{d}x \\ + \frac{G_2}{2}\frac{\mathrm{d}}{\mathrm{d}t}\int_\Omega \operatorname{tr}\left(\mathbf{B}_{\kappa_{p_2(t)}}\right) \,\mathrm{d}x + \frac{G_2^2}{2\mu_2}\int_\Omega |\mathbf{B}^d_{\kappa_{p_2(t)}}|^2 \,\mathrm{d}x = 0.\end{aligned} \tag{5.38}$$

Equation (3.244) guarantees that all terms are non-negative. Thus, we obtain the following apriori estimates (using Lemma B.1.4 we obtain that not only $\operatorname{tr} \mathbf{B}_{\kappa_{p_i(t)}}$ is bounded in $L^\infty(L^1)$ but the whole tensor $\mathbf{B}_{\kappa_{p_i(t)}}$)

$$\|\mathbf{v}\|_V \leq C, \quad \|\mathbf{B}_{\kappa_{p_i(t)}}\|_{L^\infty(0,T;L^1(\Omega))^{d\times d}} \leq C, \quad \|\mathbf{B}^d_{\kappa_{p_i(t)}}\|_{L^2(0,T;L^2(\Omega))^{d\times d}} \leq C, i = 1,2, \tag{5.39}$$

where $V = L^\infty(0,T;L^2(\Omega))^d \cap L^2(0,T;W^{1,2}(\Omega))^d$. Hence

$$\|\mathbf{v}\|_{L^4((0,T)\times\Omega)^d} \leq C \text{ for } d = 2, \tag{5.40}$$

$$\|\mathbf{v}\|_{L^{10/3}((0,T)\times\Omega)^d} \leq C \text{ for } d = 3. \tag{5.41}$$

Note that by summing $G_1/2 \times (5.36) + G_2/2 \times (5.37)$ we obtain the reduced thermodynamical inequality (1.18) in the form

$$\frac{\mathrm{d}}{\mathrm{d}t}\int_\Omega \rho\psi \,\mathrm{d}x + \int_\Omega \xi = \int_\Omega \mathbf{T}\cdot\mathbf{D}, \tag{5.42}$$

where

$$\psi = \frac{G_1}{2\rho}\left(\operatorname{tr}\mathbf{B}_{\kappa_{p_1(t)}} - d\right) + \frac{G_2}{2\rho}\left(\operatorname{tr}\mathbf{B}_{\kappa_{p_2(t)}} - d\right) \tag{5.43}$$

is the Helmholtz free energy corresponding to the internal energy (3.215) used in the derivation of model Quad2 and

$$\xi = 2\mu_3|\mathbf{D}|^2 + \frac{G_1^2}{2\mu_1}|\mathbf{B}^d_{\kappa_{p_1(t)}}|^2 + \frac{G_2^2}{2\mu_2}|\mathbf{B}^d_{\kappa_{p_2(t)}}|^2 \tag{5.44}$$

is the mixed alternative form of the rate of entropy production that could have been used in the derivation of model Quad2 (compare the standard form (3.100) and the alternative form (3.115) used in the derivation of model Quad1).

We would like to show that whole tensor $\mathbf{B}_{\kappa_{p_i(t)}}$ is bounded in $L^2(0,T;L^2(\Omega))^{d\times d}$ and not only its deviatoric part $\mathbf{B}^d_{\kappa_{p_i(t)}}$. It holds that

$$|\mathbf{B}_{\kappa_{p_i(t)}}|^2 = |\mathbf{B}^d_{\kappa_{p_i(t)}}|^2 + \frac{1}{d}(\operatorname{tr}\mathbf{B}_{\kappa_{p_i(t)}})^2. \tag{5.45}$$

Thus, we add $\displaystyle\int_\Omega \left(\frac{G_1^2}{2d\mu_1}(\operatorname{tr}\mathbf{B}_{\kappa_{p_1(t)}})^2 + \frac{G_2^2}{2d\mu_2}(\operatorname{tr}\mathbf{B}_{\kappa_{p_2(t)}})^2\right)\mathrm{d}x$ to (5.38)

$$\begin{aligned}\frac{\rho}{2}\frac{\mathrm{d}}{\mathrm{d}t}\int_\Omega|\mathbf{v}|^2\,\mathrm{d}x + \mu_3\int_\Omega|\nabla\mathbf{v}|^2\,\mathrm{d}x + \frac{G_1}{2}\frac{\mathrm{d}}{\mathrm{d}t}\int_\Omega\operatorname{tr}\left(\mathbf{B}_{\kappa_{p_1(t)}}\right)\mathrm{d}x + \frac{G_1^2}{2\mu_1}\int_\Omega|\mathbf{B}_{\kappa_{p_1(t)}}|^2\,\mathrm{d}x \\ + \frac{G_2}{2}\frac{\mathrm{d}}{\mathrm{d}t}\int_\Omega\operatorname{tr}\left(\mathbf{B}_{\kappa_{p_2(t)}}\right)\mathrm{d}x + \frac{G_2^2}{2\mu_2}\int_\Omega|\mathbf{B}_{\kappa_{p_2(t)}}|^2\,\mathrm{d}x = \\ \int_\Omega\Big(\frac{G_1^2}{2d\mu_1}\underbrace{(\operatorname{tr}\mathbf{B}_{\kappa_{p_1(t)}})^2}_{(\operatorname{tr}\mathbf{B}_{\kappa_{p_1(t)}})(\operatorname{tr}\mathbf{B}_{\kappa_{p_1(t)}})} + \frac{G_2^2}{2d\mu_2}\underbrace{(\operatorname{tr}\mathbf{B}_{\kappa_{p_2(t)}})^2}_{(\operatorname{tr}\mathbf{B}_{\kappa_{p_2(t)}})(\operatorname{tr}\mathbf{B}_{\kappa_{p_2(t)}})}\Big)\mathrm{d}x.\end{aligned} \tag{5.46}$$

Since we know that $\operatorname{tr}\mathbf{B}_{\kappa_{p_i(t)}}$ is bounded in $L^1(0,T;L^1(\Omega))$ we can apply Gronwall inequality on the term $\operatorname{tr}\mathbf{B}_{\kappa_{p_i(t)}}$ and finally we obtain

$$\|\mathbf{B}_{\kappa_{p_i(t)}}\|_{V_B} \leq C, i = 1,2, \tag{5.47}$$

where $V_B = L^\infty(0,T;L^1(\Omega))^{d\times d} \cap L^2(0,T;L^2(\Omega))^{d\times d}$. The estimate for pressure is obtained from the balance of linear momentum, again we apply divergence on balance of linear momentum (1.13) and get

$$-\Delta p = \operatorname{div}\operatorname{div}\left(\mathbf{v}\otimes\mathbf{v} - 2\mu_3\mathbf{D} - G_1\mathbf{B}^d_{\kappa_{p_1(t)}} - G_2\mathbf{B}^d_{\kappa_{p_2(t)}}\right) \tag{5.48}$$

which suggests that pressure p can at most satisfy the following estimate

$$\|p\|_{V_{pQ}} \leq C, \tag{5.49}$$

where

$$V_{pQ} = \begin{cases} L^2(0,T;L^2(\Omega)) & \text{for } d=2, \\ L^{5/3}(0,T;L^{5/3}(\Omega)) & \text{for } d=3. \end{cases} \tag{5.50}$$

5.1.4 Weak formulation for IBVP involving models Quad1 and Quad2

In case of model Quad2 (and also Quad1) no renormalized solution is needed. The weak solution is the following: The quadruple $(\mathbf{v}, p, \mathbf{B}_1, \mathbf{B}_2) \in V \times V_{pQ} \times V_B \times V_B$, such that $\mathbf{v} - \tilde{\mathbf{v}} \in L^2(0,T;W^{1,2}_{0,\Gamma_D}(\Omega_x))^d$ is a weak solution of the model Quad2 (3.239) in $\Omega \subset \mathbb{R}^d$ if

$$\int_\Omega \operatorname{tr}(\nabla \mathbf{v}) q \,\mathrm{d}x = 0, \tag{5.51a}$$

$$\int_\Omega \rho \left[\frac{\partial \mathbf{v}}{\partial t} + (\nabla \mathbf{v})\mathbf{v} \right] \cdot \mathbf{q} \,\mathrm{d}x - \int_\Omega \mathbf{T} \cdot \nabla \mathbf{q} \,\mathrm{d}x + \int_{\Gamma_N} \mathbf{t} \cdot \mathbf{q} \,\mathrm{d}S = 0, \tag{5.51b}$$

$$\mathbf{T} = -p\mathbf{I} + \mu_3 \left((\nabla \mathbf{v}) + (\nabla \mathbf{v})^{\mathrm{T}} \right) + G_1 \mathbf{B}^d_{\kappa_{p_1(t)}} + G_2 \mathbf{B}^d_{\kappa_{p_2(t)}}, \tag{5.51c}$$

$$\int_\Omega \left[\frac{\partial \mathbf{B}_{\kappa_{p_1(t)}}}{\partial t} - (\nabla \mathbf{v}) \mathbf{B}_{\kappa_{p_1(t)}} - \mathbf{B}_{\kappa_{p_1(t)}} (\nabla \mathbf{v})^{\mathrm{T}} + \frac{G_1}{\mu_1} \mathbf{B}_{\kappa_{p_1(t)}} \mathbf{B}^d_{\kappa_{p_1(t)}} \right] \cdot \mathbf{Q}_1 \,\mathrm{d}x$$
$$- \int_\Omega \mathbf{B}_{\kappa_{p_1(t)}} \otimes \mathbf{v} \cdot \nabla \mathbf{Q}_1 \,\mathrm{d}x + \int_{\partial\Omega} (\mathbf{v} \cdot \mathbf{n}) \, \mathbf{B}_{\kappa_{p_1(t)}} \cdot \mathbf{Q}_1 \,\mathrm{d}S = 0, \tag{5.51d}$$

$$\int_\Omega \left[\frac{\partial \mathbf{B}_{\kappa_{p_2(t)}}}{\partial t} - (\nabla \mathbf{v}) \mathbf{B}_{\kappa_{p_2(t)}} - \mathbf{B}_{\kappa_{p_2(t)}} (\nabla \mathbf{v})^{\mathrm{T}} + \frac{G_2}{\mu_2} \mathbf{B}_{\kappa_{p_2(t)}} \mathbf{B}^d_{\kappa_{p_2(t)}} \right] \cdot \mathbf{Q}_2 \,\mathrm{d}x$$
$$- \int_\Omega \mathbf{B}_{\kappa_{p_2(t)}} \otimes \mathbf{v} \cdot \nabla \mathbf{Q}_2 \,\mathrm{d}x + \int_{\partial\Omega} (\mathbf{v} \cdot \mathbf{n}) \, \mathbf{B}_{\kappa_{p_2(t)}} \cdot \mathbf{Q}_2 \,\mathrm{d}S = 0, \tag{5.51e}$$

is satisfied for all $(q, \mathbf{q}, \mathbf{Q}_1, \mathbf{Q}_2) \in C^1(\Omega) \times V_1 \times C^1(\Omega)^{d\times d} \times C^1(\Omega)^{d\times d}$ and a.a. $t \in (0,T)$, where $V_1 = \{\mathbf{v} \in C^1(\Omega)^2, \mathbf{v} = \mathbf{0} \text{ on } \Gamma_D\}$ and $\tilde{\mathbf{v}}|_{\Gamma_D} = \mathbf{v}_D$. Since the last two equations are transport equations for $\mathbf{B}_{\kappa_{p_i(t)}}, i = 1,2$, boundary conditions for $\mathbf{B}_{\kappa_{p_1(t)}}$ and $\mathbf{B}_{\kappa_{p_2(t)}}$ have to be prescribed on the inlet.

For numerical implementation all computations are done using the weak formulation with the original convective term in the transport equations for $\mathbf{B}_{\kappa_{p_i(t)}}$ (we do not prescribe any boundary condition for tensors $\mathbf{B}_{\kappa_{p_i(t)}}$), so the weak formulation is in the form

$$\int_\Omega \operatorname{tr}(\nabla \mathbf{v}) q \,\mathrm{d}x = 0, \tag{5.52a}$$

$$\int_\Omega \rho \left[\frac{\partial \mathbf{v}}{\partial t} + (\nabla \mathbf{v})\mathbf{v} \right] \cdot \mathbf{q} \,\mathrm{d}x - \int_\Omega \mathbf{T} \cdot \nabla \mathbf{q} \,\mathrm{d}x + \int_{\Gamma_N} \mathbf{t} \cdot \mathbf{q} \,\mathrm{d}S = 0, \tag{5.52b}$$

$$\mathbf{T} = -p\mathbf{I} + \mu_3 \left((\nabla \mathbf{v}) + (\nabla \mathbf{v})^{\mathrm{T}} \right) + G_1 \mathbf{B}^d_{\kappa_{p_1(t)}} + G_2 \mathbf{B}^d_{\kappa_{p_2(t)}}, \tag{5.52c}$$

$$\int_\Omega \left[\frac{\partial \mathbf{B}_{\kappa_{p_1(t)}}}{\partial t} + (\nabla \mathbf{B}_{\kappa_{p_1(t)}})\mathbf{v} - (\nabla \mathbf{v}) \mathbf{B}_{\kappa_{p_1(t)}} - \mathbf{B}_{\kappa_{p_1(t)}} (\nabla \mathbf{v})^{\mathrm{T}} + \frac{1}{\tau_1} \mathbf{B}_{\kappa_{p_1(t)}} \mathbf{B}^d_{\kappa_{p_1(t)}} \right] \cdot \mathbf{Q}_1 \,\mathrm{d}x = 0, \tag{5.52d}$$

$$\int_\Omega \left[\frac{\partial \mathbf{B}_{\kappa_{p_2(t)}}}{\partial t} + (\nabla \mathbf{B}_{\kappa_{p_2(t)}})\mathbf{v} - (\nabla \mathbf{v}) \mathbf{B}_{\kappa_{p_2(t)}} - \mathbf{B}_{\kappa_{p_2(t)}} (\nabla \mathbf{v})^{\mathrm{T}} + \frac{1}{\tau_2} \mathbf{B}_{\kappa_{p_2(t)}} \mathbf{B}^d_{\kappa_{p_2(t)}} \right] \cdot \mathbf{Q}_2 \,\mathrm{d}x = 0. \tag{5.52e}$$

A short overview of mathematical results. In the previous section we derived formal apriori estimates for both standard models Oldroyd-B and Burgers and the new non-linear models Quad1 and Quad2. We have not studied other mathematical results concerning the existence of solution for models Quad1 and Quad2.

It is necessary to recognize that even in the analysis of standard Oldroyd type models there are several open problems concerning long time and large data existence. Lions, Masmoudi [33] and Bejaoui, Majdoub [4] proved the global in time existence of the weak solutions for large data of the viscoelastic Oldroyd model with the corrotational (Jaumann) derivative. In case of standard Oldroyd-B model this seems to be an open problem. Short time results or long time results for small data were proved in [18] by Guillope and Saut. Further interesting results concerning the local well posedness of the initial boundary value problem for the Oldroyd type fluids have been done in several other studies, see [26, 31, 32].

5.1.5 Weak formulation for BVP involving models Oldroyd-B, Burgers, Quad1 and Quad2

In the previous Subsections we derived apriori estimates and possible weak formulation for evolutionary Oldroyd-B and Burgers models and models Quad1 and Quad2. In this subsection we write the weak formulation for steady models.

Weak formulation for BVP involving Oldroyd-B and Burgers model

Inspired by the weak renormalized solution for Burgers model (therefore also Oldroyd-B model) it can be expectedthat the weak formulation of steady Burgers model is the following: The quadruple $(\mathbf{v}, p, \mathbf{B}_1, \mathbf{B}_2) \in W^{1,2}(\Omega)^d \times L^1(\Omega) \times L^1(\Omega)^{d\times d} \times L^1(\Omega)^{d\times d}$, such that $\mathbf{v} - \mathbf{v}_D \in W^{1,2}_{0,\Gamma_D}(\Omega)^d$ is a weak renormalized solution of the Burgers model (3.255) in $\Omega \subset \mathbb{R}^d$ if

$$\int_\Omega \operatorname{tr}(\nabla\mathbf{v}) q \,\mathrm{d}x = 0, \tag{5.53a}$$

$$\int_\Omega \rho\,[(\nabla\mathbf{v})\mathbf{v}]\cdot\mathbf{q}\,\mathrm{d}x - \int_\Omega \mathbf{T}\cdot\nabla\mathbf{q}\,\mathrm{d}x + \int_{\Gamma_N} \mathbf{t}\cdot\mathbf{q}\,\mathrm{d}S = 0, \tag{5.53b}$$

$$\mathbf{T} = -p\mathbf{I} + \mu_3\left((\nabla\mathbf{v}) + (\nabla\mathbf{v})^{\mathrm{T}}\right) + G_1(\mathbf{B}_1 - \mathbf{I}) + G_2(\mathbf{B}_2 - \mathbf{I}), \tag{5.53c}$$

$$\int_\Omega \left[\left(-(\nabla\mathbf{v})\mathbf{B}_1 - \mathbf{B}_1(\nabla\mathbf{v})^{\mathrm{T}} + \frac{1}{\tau_1}(\mathbf{B}_1 - \mathbf{I})\right) \circ (\mathbf{R}_1^L)'(\mathbf{B}_1)\right]\cdot\mathbf{Q}_1 - \mathbf{R}_1^L(\mathbf{B}_1)\otimes\mathbf{v}\cdot\nabla\mathbf{Q}_1\,\mathrm{d}x + \int_{\partial\Omega}(\mathbf{v}\cdot\mathbf{n})\,\mathbf{R}_1^L(\mathbf{B}_1)\cdot\mathbf{Q}_1\,\mathrm{d}S = 0, \tag{5.53d}$$

$$\int_\Omega \left[\left(-(\nabla\mathbf{v})\mathbf{B}_2 - \mathbf{B}_2(\nabla\mathbf{v})^{\mathrm{T}} + \frac{1}{\tau_2}(\mathbf{B}_2 - \mathbf{I})\right) \circ (\mathbf{R}_2^L)'(\mathbf{B}_2)\right]\cdot\mathbf{Q}_2 - \mathbf{R}_2^L(\mathbf{B}_2)\otimes\mathbf{v}\cdot\nabla\mathbf{Q}_2\,\mathrm{d}x + \int_{\partial\Omega}(\mathbf{v}\cdot\mathbf{n})\,\mathbf{R}_2^L(\mathbf{B}_2)\cdot\mathbf{Q}_2\,\mathrm{d}S = 0 \tag{5.53e}$$

is satisfied for all $(q, \mathbf{q}, \mathbf{Q}_1, \mathbf{Q}_2) \in C^1(\Omega) \times V_1 \times C^1(\Omega)^{d\times d} \times C^1(\Omega)^{d\times d}$, all $\mathbf{R}_i^L \in \mathcal{R}$, where $V_1 = \{\mathbf{v} \in C^1(\Omega)^2, \mathbf{v} = \mathbf{0} \text{ on } \Gamma_D\}$, $\circ$ is the Hadamard product defined by (5.30) and $R(\mathbf{B})$ is defined by (5.31).

For numerical implementation all computations are done for $R_{ij}(B_{ij}) = B_{ij}$ with the original convective term in the transport equations for $\mathbf{B}_i$, then the weak formulation

is in the form

$$\int_\Omega \operatorname{tr}(\nabla \mathbf{v}) q \,\mathrm{d}x = 0, \tag{5.54a}$$

$$\int_\Omega \rho\left[(\nabla \mathbf{v})\mathbf{v}\right] \cdot \mathbf{q} \,\mathrm{d}x - \int_\Omega \mathbf{T} \cdot \nabla \mathbf{q} \,\mathrm{d}x + \int_{\Gamma_N} \mathbf{t} \cdot \mathbf{q} \,\mathrm{d}S = 0, \tag{5.54b}$$

$$\mathbf{T} = -p\mathbf{I} + \mu_3 \left((\nabla \mathbf{v}) + (\nabla \mathbf{v})^{\mathrm{T}}\right) + G_1(\mathbf{B}_1 - \mathbf{I}) + G_2(\mathbf{B}_2 - \mathbf{I}), \tag{5.54c}$$

$$\int_\Omega \left[(\nabla \mathbf{B}_1)\mathbf{v} - (\nabla \mathbf{v})\mathbf{B}_1 - \mathbf{B}_1(\nabla \mathbf{v})^{\mathrm{T}} + \frac{1}{\tau_1}(\mathbf{B}_1 - \mathbf{I})\right] \cdot \mathbf{Q}_1 \,\mathrm{d}x = 0, \tag{5.54d}$$

$$\int_\Omega \left[(\nabla \mathbf{B}_2)\mathbf{v} - (\nabla \mathbf{v})\mathbf{B}_2 - \mathbf{B}_2(\nabla \mathbf{v})^{\mathrm{T}} + \frac{1}{\tau_2}(\mathbf{B}_2 - \mathbf{I})\right] \cdot \mathbf{Q}_2 \,\mathrm{d}x = 0. \tag{5.54e}$$

Weak formulation for BVP involving models Quad1 and Quad2

Inspired by the weak solution for model Quad2 (and also model Quad1) it can be expectedthat the weak formulation of steady model Quad2 is the following: The quadruple $(\mathbf{v}, p, \mathbf{B}_{\kappa_{p_1(t)}}, \mathbf{B}_{\kappa_{p_2(t)}}) \in W^{1,2}(\Omega)^d \times L^2(\Omega) \times L^2(\Omega)^{d\times d} \times L^2(\Omega)^{d\times d}$, such that $\mathbf{v} - \mathbf{v}_D \in W^{1,2}_{0,\Gamma_D}(\Omega)^d$ is a weak solution of the model Quad2 (3.239) in $\Omega \subset \mathbb{R}^d$ if

$$\int_\Omega \operatorname{tr}(\nabla \mathbf{v}) q \,\mathrm{d}x = 0, \tag{5.55a}$$

$$\int_\Omega \rho\left[+(\nabla \mathbf{v})\mathbf{v}\right] \cdot \mathbf{q} \,\mathrm{d}x - \int_\Omega \mathbf{T} \cdot \nabla \mathbf{q} \,\mathrm{d}x + \int_{\Gamma_N} \mathbf{t} \cdot \mathbf{q} \,\mathrm{d}S = 0, \tag{5.55b}$$

$$\mathbf{T} = -p\mathbf{I} + \mu_3 \left((\nabla \mathbf{v}) + (\nabla \mathbf{v})^{\mathrm{T}}\right) + G_1 \mathbf{B}^d_{\kappa_{p_1(t)}} + G_2 \mathbf{B}^d_{\kappa_{p_2(t)}}, \tag{5.55c}$$

$$\int_\Omega \left[- (\nabla \mathbf{v})\mathbf{B}_{\kappa_{p_1(t)}} - \mathbf{B}_{\kappa_{p_1(t)}}(\nabla \mathbf{v})^{\mathrm{T}} + \frac{G_1}{\mu_1}\mathbf{B}_{\kappa_{p_1(t)}}\mathbf{B}^d_{\kappa_{p_1(t)}}\right] \cdot \mathbf{Q}_1 - \mathbf{B}_{\kappa_{p_1(t)}} \otimes \mathbf{v} \cdot \nabla \mathbf{Q}_1 \,\mathrm{d}x + \int_{\partial\Omega} (\mathbf{v} \cdot \mathbf{n})\, \mathbf{B}_{\kappa_{p_1(t)}} \cdot \mathbf{Q}_1 \,\mathrm{d}S = 0, \tag{5.55d}$$

$$\int_\Omega \left[- (\nabla \mathbf{v})\mathbf{B}_{\kappa_{p_2(t)}} - \mathbf{B}_{\kappa_{p_2(t)}}(\nabla \mathbf{v})^{\mathrm{T}} + \frac{G_2}{\mu_2}\mathbf{B}_{\kappa_{p_2(t)}}\mathbf{B}^d_{\kappa_{p_2(t)}}\right] \cdot \mathbf{Q}_2 - \mathbf{B}_{\kappa_{p_2(t)}} \otimes \mathbf{v} \cdot \nabla \mathbf{Q}_2 \,\mathrm{d}x + \int_{\partial\Omega} (\mathbf{v} \cdot \mathbf{n})\, \mathbf{B}_{\kappa_{p_2(t)}} \cdot \mathbf{Q}_2 \,\mathrm{d}S = 0, \tag{5.55e}$$

is satisfied for all $(q, \mathbf{q}, \mathbf{Q}_1, \mathbf{Q}_2) \in C^1(\Omega) \times V_1 \times C^1(\Omega)^{d\times d} \times C^1(\Omega)^{d\times d}$, where $V_1 = \{\mathbf{v} \in C^1(\Omega)^2, \mathbf{v} = \mathbf{0} \text{ on } \Gamma_D\}$.

For the numerical implementation all computations are done using the weak formulation with the original convective term in the transport equations for $\mathbf{B}_{\kappa_{p_i(t)}}$, the steady weak formulation is in the form

$$\int_\Omega \operatorname{tr}(\nabla \mathbf{v}) q \,\mathrm{d}x = 0, \tag{5.56a}$$

$$\int_\Omega \rho\left[\frac{\partial \mathbf{v}}{\partial t} + (\nabla \mathbf{v})\mathbf{v}\right] \cdot \mathbf{q} \,\mathrm{d}x - \int_\Omega \mathbf{T} \cdot \nabla \mathbf{q} \,\mathrm{d}x + \int_{\Gamma_N} \mathbf{t} \cdot \mathbf{q} \,\mathrm{d}S = 0, \tag{5.56b}$$

$$\mathbf{T} = -p\mathbf{I} + \mu_3 \left((\nabla \mathbf{v}) + (\nabla \mathbf{v})^{\mathrm{T}}\right) + G_1 \mathbf{B}^d_{\kappa_{p_1(t)}} + G_2 \mathbf{B}^d_{\kappa_{p_2(t)}}, \tag{5.56c}$$

$$\int_\Omega \left[(\nabla \mathbf{B}_{\kappa_{p_1(t)}})\mathbf{v} - (\nabla \mathbf{v})\mathbf{B}_{\kappa_{p_1(t)}} - \mathbf{B}_{\kappa_{p_1(t)}}(\nabla \mathbf{v})^{\mathrm{T}} + \frac{1}{\tau_1}\mathbf{B}_{\kappa_{p_1(t)}}\mathbf{B}^d_{\kappa_{p_1(t)}}\right] \cdot \mathbf{Q}_1 \,\mathrm{d}x = 0, \tag{5.56d}$$

$$\int_\Omega \left[(\nabla \mathbf{B}_{\kappa_{p_2(t)}})\mathbf{v} - (\nabla \mathbf{v})\mathbf{B}_{\kappa_{p_2(t)}} - \mathbf{B}_{\kappa_{p_2(t)}}(\nabla \mathbf{v})^{\mathrm{T}} + \frac{1}{\tau_2}\mathbf{B}_{\kappa_{p_2(t)}}\mathbf{B}^d_{\kappa_{p_2(t)}}\right] \cdot \mathbf{Q}_2 \,\mathrm{d}x = 0. \tag{5.56e}$$

5.2 Finite element method

In this section we show how the Finite element method works on an example viscoelastic model Quad1[2] in two dimensional space. In the first Subsection we describe how the steady solution is found, in the second Subsection we show how the evolutionary problem is solved and describe four different time discretizations.

5.2.1 Steady solution of model Quad1

Let us remind that the strong formulation of model Quad1 is (for simplicity we denote Cauchy-Green tensor $\mathbf{B}_{\kappa_{p(t)}}$ by $\mathbf{B}$)

$$\begin{aligned} \operatorname{div}\mathbf{v} &= 0, \\ \rho(\mathbf{v}\cdot\nabla\mathbf{v}) &= \operatorname{div}\mathbf{T}, \\ \mathbf{T} &= -p\mathbf{I} + \mu_2\left(\nabla\mathbf{v} + (\nabla\mathbf{v})^{\mathrm{T}}\right) + G\mathbf{B}^d, \\ \mathbf{v}\cdot\nabla\mathbf{B} - (\nabla\mathbf{v})\mathbf{B} - \mathbf{B}(\nabla\mathbf{v})^{\mathrm{T}} &= -\frac{1}{\tau}\mathbf{B}\mathbf{B}^d. \end{aligned} \tag{5.57}$$

These equations has to be satisfied inside Ω, on the boundary $\partial\Omega$ consisting of two non-intersecting parts Γ_D and Γ_N it holds that $\mathbf{v} = \tilde{\mathbf{v}}$ on Γ_D and $\mathbf{T}\mathbf{n} = \mathbf{t}$ on Γ_N.

Finite element method is based on the weak formulation. The weak formulation for model Quad2 is described by (5.56), in case of model Quad1 the equation for $\mathbf{B}_2$ is missing. Here we define the Galerkin system. The problem is to find $(\mathbf{v}_h, p_h, \mathbf{B}_h)$ such that

$$\begin{aligned} p_h &\in P_h, \\ \mathbf{v}_h - \tilde{\mathbf{v}}_h &\in V_h, \text{ where } \tilde{\mathbf{v}}_h = \mathbf{v}_{\mathbf{D}} \text{ on } \Gamma_D, \\ \mathbf{B}_h &\in B_h \end{aligned}$$

satisfying

$$\begin{aligned} \int_{\Omega_h} (\operatorname{div}\mathbf{v}_h)\psi_h \,\mathrm{d}x = 0, \quad \forall\psi_h \in P_h, \\ \int_{\Omega_h} \rho(\mathbf{v}_h\cdot\nabla\mathbf{v}_h)\cdot\boldsymbol{\varphi}_h \,\mathrm{d}x + \int_{\Omega_h} \mathbf{T}_h\cdot\nabla\boldsymbol{\varphi}_h \,\mathrm{d}x = \int_{\Gamma_N} \mathbf{t}_h\cdot\boldsymbol{\varphi}_h \,\mathrm{d}S, \quad \forall\boldsymbol{\varphi}_h \in V_h, \\ \int_{\Omega_h} \left(\mathbf{v}_h\cdot\nabla\mathbf{B}_h - (\nabla\mathbf{v})\mathbf{B}_h - \mathbf{B}_h(\nabla\mathbf{v}_h)^{\mathrm{T}}\right)\cdot\mathbf{Q}_h \,\mathrm{d}x = -\frac{1}{\tau}\int_{\Omega_h} (\mathbf{B}_h\mathbf{B}_h^d)\cdot\mathbf{Q}_h \,\mathrm{d}x, \quad \forall\mathbf{Q}_h \in B_h, \end{aligned}$$

where

$$\mathbf{T}_h = -p_h\mathbf{I} + \mu_2\left(\nabla\mathbf{v}_h + (\nabla\mathbf{v}_h)^{\mathrm{T}}\right) + G\mathbf{B}_h^d$$

and the finite dimensional spaces are following

$$P_h = \left\{q_h \in L^2(\Omega_h), q_h|_T \in P_1^{\mathrm{disc}}(T)\ \forall T \in \mathcal{T}_h\right\}, \tag{5.58a}$$

$$V_h = \left\{\mathbf{w}_h \in (C(\Omega_h))^2, \mathbf{w}_h|_T \in Q_2(T)\ \forall T \in \mathcal{T}_h\right\}, \tag{5.58b}$$

$$B_h = \left\{\mathbf{K}_h \in (C(\Omega_h))^{2\times 2}, \mathbf{K}_h|_T \in Q_2(T)\ \forall T \in \mathcal{T}_h\right\}. \tag{5.58c}$$

[2] In case of another viscoelastic model the only difference is in the transport equation for tensor $\mathbf{B}$, this tensor is always approximated by biquadratic finite element that is defined later.

The domain Ω_h has a polygonal boundary and it is an approximation of the domain Ω. By $\mathcal{T}_h$ we denote a set of quadrilateral elements T covering the domain Ω_h. We assume that $\mathcal{T}_h$ is regular which means that any two quadrilaterals are disjoint or have one common edge or a common vertex.

The combination of Q_2 (standard continuous biquadratic with nine degrees of freedom per quadrilateral, see Fig. 5.1b)) for the velocity and P_1^{disc} (discontinuous linear with three degrees of freedom per quadrilateral given by the value and two derivatives in the middle, see Fig. 5.1a)) for the pressure is a stable pair for velocity and pressure satisfying Babuška-Brezi condition. Extra stress part $\mathbf{B}$ is also approximated by Q2 elements.

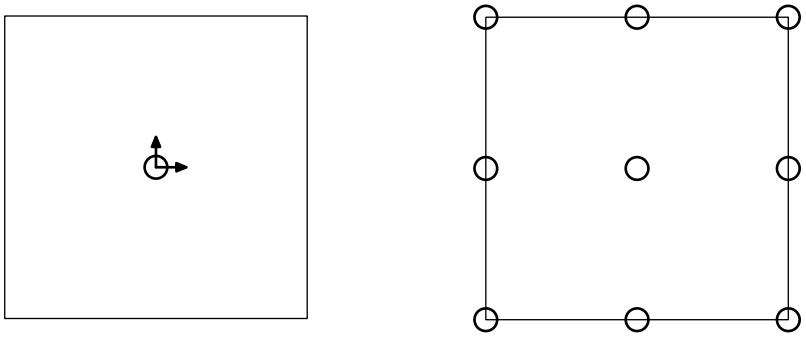

a)P_1^{disc} element for the pressure p

b) Q_2 element for the velocity $\mathbf{v}$ and extra stress tensor $\mathbf{B}$

Figure 5.1: Location of degrees of freedom on the reference quadrilateral

Now, let us denote $\{q_i\}_{i=1}^{l}$ a usual Finite element basis of the finite dimensional space P_h, $\{\mathbf{w}_i\}_{i=1}^{m}$ a basis of the finite dimensional space V_h and $\{\mathbf{K}_i\}_{i=1}^{n}$ a basis of the finite dimensional space B_h. Then we can express the approximate solution in the form

$$p_h = \sum_{i=1}^{l} P_i q_i, \tag{5.59a}$$

$$\mathbf{v}_h = \tilde{\mathbf{v}}_h + \sum_{i=1}^{m} V_i \mathbf{w}_i, \tag{5.59b}$$

$$\mathbf{B}_h = \sum_{i=1}^{n} B_i \mathbf{K}_i, \tag{5.59c}$$

where l is equal to three times number of all quadrilaterals and m and n is equal to the number of all vertices + number of all edges + number of all quadrilaterals. We use the following test functions in the Galerkin system

$$\psi_h = q_j, \quad j = 1, \ldots, l, \tag{5.60a}$$

$$\boldsymbol{\varphi}_h = \mathbf{w}_j, \quad j = 1, \ldots, m, \tag{5.60b}$$

$$\mathbf{Q}_h = \mathbf{K}_j, \quad j = 1, \ldots, n, \tag{5.60c}$$

after substitution of (5.59) and (5.60) into (5.58) we get

$$\underbrace{\varrho \int_{\Omega_h} \left[\left(\tilde{\mathbf{v}}_h + \sum_{i=1}^{m} V_i \mathbf{w}_i \right) \cdot \left(\nabla \tilde{\mathbf{v}}_h + \sum_{k=1}^{m} V_k \mathbf{w}_k \right) \right] \cdot \nabla \mathbf{w}_j}_{N_1(\mathbf{V})_j} + \underbrace{\eta \int_{\Omega_h} \nabla \tilde{\mathbf{v}}_h \cdot \nabla \mathbf{w}_j - \int_{\Gamma_N} \mathbf{t}_h \cdot \mathbf{w}_j}_{F_j} +$$
$$+ \sum_{i=1}^{m} V_i \underbrace{\eta \int_{\Omega_h} \nabla \mathbf{w}_i \cdot \nabla \mathbf{w}_j}_{A_{ji}} - \sum_{i=1}^{m} P_i \underbrace{\int_{\Omega_h} q_i \operatorname{div} \mathbf{w}_j}_{-C_{ji}} +$$
$$+ \sum_{i=1}^{n} B_i \underbrace{G \int_{\Omega_h} \mathbf{K}_i \cdot \nabla \mathbf{w}_j - \frac{1}{2} (\operatorname{tr} \mathbf{K}_i) \operatorname{div} \mathbf{w}_j}_{E_{ji}} = 0, \quad j = 1, \ldots, m$$

$$\underbrace{\int_{\Omega_h} \sum_{k=1}^{n} \left(\left(\tilde{\mathbf{v}}_h + \sum_{i=1}^{m} V_i \mathbf{w}_i \right) \cdot (B_k \nabla \mathbf{K}_k) - \left(\nabla \tilde{\mathbf{v}}_h + \sum_{i=1}^{m} V_i \nabla \mathbf{w}_i \right) (B_k \mathbf{K}_k) - (B_k \mathbf{K}_k) \left(\nabla \tilde{\mathbf{v}}_h^{\mathrm{T}} + \sum_{i=1}^{m} V_i \nabla \mathbf{w}_i^{\mathrm{T}} \right) \right) \cdot \mathbf{K}_j}_{N_2(\mathbf{V},\mathbf{B})_j}$$
$$+ \underbrace{\int_{\Omega_h} \frac{1}{\tau} \sum_{i=1}^{n} B_i \mathbf{K}_i \left(\sum_{k=1}^{n} B_k \left(\mathbf{K}_k - \frac{1}{2} (\operatorname{tr} \mathbf{K}_k) \mathbf{I} \right) \right) \cdot \mathbf{K}_j}_{N_3(\mathbf{B})_j} = 0, \quad j = 1, \ldots, n$$
$$\sum_{i=1}^{m} V_i \underbrace{\int_{\Omega_h} (\operatorname{div} \mathbf{w}_i) q_j \, \mathrm{d}x}_{-C_{ij}} + \underbrace{\int_{\Omega_h} (\operatorname{div} \tilde{\mathbf{v}}_h) q_j}_{G_j} = 0, \quad j = 1, \ldots, l$$

which can be rewritten into the set of $(l + m + n)$ nonlinear algebraic equations

$$\Phi \begin{pmatrix} \mathbf{V} \\ \mathbf{B} \\ \mathbf{P} \end{pmatrix} := \begin{pmatrix} \mathbf{AV} + \mathbf{N}_1(\mathbf{V}) + \mathbf{CP} + \mathbf{EB} + \mathbf{F} \\ \mathbf{N}_2(\mathbf{V}, \mathbf{B}) + \mathbf{N}_3(\mathbf{B}) \\ -\mathbf{C}^{\mathrm{T}} \mathbf{V} + \mathbf{G} \end{pmatrix} = \mathbf{0},$$

where vector $\mathbf{V}$ contains components V_i, vector $\mathbf{B}$ components B_i and vector $\mathbf{P}$ components P_i. We solve it by the Newton method

$$\mathbf{J}\boldsymbol{\delta} = \mathbf{R}, \tag{5.61}$$

where the Jacobian $\mathbf{J}$ is computed by finite differences

$$\mathbf{J} = \frac{D\Phi \begin{pmatrix} \mathbf{V}^k \\ \mathbf{B}^k \\ \mathbf{P}^k \end{pmatrix}}{D \begin{pmatrix} \mathbf{V} \\ \mathbf{B} \\ \mathbf{P} \end{pmatrix}} \quad \text{and} \quad \boldsymbol{\delta} = \begin{pmatrix} \mathbf{V}^{k+1} \\ \mathbf{B}^{k+1} \\ \mathbf{P}^{k+1} \end{pmatrix} - \begin{pmatrix} \mathbf{V}^k \\ \mathbf{B}^k \\ \mathbf{P}^k \end{pmatrix}, \quad \mathbf{R} = -\Phi \begin{pmatrix} \mathbf{V}^k \\ \mathbf{B}^k \\ \mathbf{P}^k \end{pmatrix}.$$

We iterate in the Newton method in this sense

$$\begin{pmatrix} \mathbf{V}^{k+1} \\ \mathbf{B}^{k+1} \\ \mathbf{P}^{k+1} \end{pmatrix} = \begin{pmatrix} \mathbf{V}^k \\ \mathbf{B}^k \\ \mathbf{P}^k \end{pmatrix} + \omega \boldsymbol{\delta}, \quad \omega \in (0, 1],$$

where ω is adaptively chosen to improve the convergence. Stopping criterion are the L^2 norm and the energy-like norm of the residuum. The set of linear algebraic equations

(5.61) for the unknown $\boldsymbol{\delta}$ is computed by the direct solver UMFPACK (see [12]) for small problems, for larger problems iterative solver GMRES with ILU1 preconditioning from the package SPLIB by [8] is used. The implementation is based on the code developed in [20].

5.2.2 Time discretization for IBVP involving the model Quad1

In the previous subsection we described spatial discretization of the problem. In this section we focus on time discretization of the evolutionary problem described by

$$\begin{aligned} \operatorname{div} \mathbf{v} &= 0, \\ \rho \frac{\partial \mathbf{v}}{\partial t} + \rho(\mathbf{v} \cdot \nabla \mathbf{v}) &= \operatorname{div} \mathbf{T}, \\ \mathbf{T} &= -p\mathbf{I} + \mu_2 \left(\nabla \mathbf{v} + (\nabla \mathbf{v})^{\mathrm{T}}\right) + G\mathbf{B}^d, \\ \frac{\partial \mathbf{B}}{\partial t} + \mathbf{v} \cdot \nabla \mathbf{B} - (\nabla \mathbf{v})\mathbf{B} - \mathbf{B}(\nabla \mathbf{v})^{\mathrm{T}} &= -\frac{1}{\tau}\mathbf{B}\mathbf{B}^d, \end{aligned} \tag{5.62}$$

which is solved in $\Omega \times [0, T]$. We split the time interval $[0, T]$ into N subintervals using $N + 1$ times $t^n : 0 = t^0 < t^1 < \cdots < t^N = T$, where $\Delta t^n := t^{n+1} - t^n$ is the $n-$th time step, $n = 0, \ldots, N - 1$. We use four different one-step time schemes[3] in order to solve (5.62) which is generally in the form

$$\frac{\partial u(x,t)}{\partial t} + f\left(u(x,t)\right) = 0 \text{ in } \Omega \times [0,T]. \tag{5.63}$$

At every time level t^{n+1} we have to find solution for $u^{n+1}(x) := u(x, t_0 + \sum_{i=0}^{n} \Delta t^i)$. All time schemes are implicit, thus on every $(n + 1)$-th time level the space problem is solved using FEM described in the previous Subsection. The time derivatives are discretized by four different time schemes:

(1) Implicit backward Euler scheme (BE):

$$\frac{u^{n+1}(x) - u^n(x)}{\Delta t^n} + f\left(u^{n+1}(x)\right) = 0 \tag{5.64}$$

which is the first order unconditionally stable time scheme.

(2) Crank-Nicolson scheme (CR):

$$\frac{u^{n+1}(x) - u^n(x)}{\Delta t^n} + \frac{1}{2}\left(f\left(u^n(x)\right) + f\left(u^{n+1}(x)\right)\right) = 0, \tag{5.65}$$

which is the second order conditionally stable time scheme.

(3) Implicit three-step θ-scheme (TH): For $\theta = 1 - \sqrt{2}/2$, $\alpha = (1 - 2\theta)/(1 - \theta)$, the time derivative is approximated in three steps (requires three times more CPU

[3] By one-step time scheme we mean that it is enough to remember the solution on the last time level but the time scheme can consists of more than one step.

time compared to BE time scheme):

$$\begin{aligned}
&1. \quad \frac{u^{n+\frac{1}{3}}(x) - u^n(x)}{\theta \Delta t^n} = \alpha f(u^{n+\frac{1}{3}}(x)) + (1-\alpha) f(u^n(x)),\\
&2. \quad \frac{u^{n+\frac{2}{3}}(x) - u^{n+\frac{1}{3}}(x)}{(1-2\theta) \Delta t^n} = (1-\alpha) f(u^{n+\frac{2}{3}}(x)) + \alpha f(u^{n+\frac{1}{3}}(x)),\\
&3. \quad \frac{u^{n+1}(x) - u^{n+\frac{2}{3}}(x)}{\theta \Delta t^n} = \alpha f(u^{n+1}(x)) + (1-\alpha) f(u^{n+\frac{2}{3}}(x)).
\end{aligned}$$

This is the second order unconditionally stable time scheme (see for example [16]).

(4) Implicit Glowinski three-step scheme (GL): For $\theta := 1 - 1/\sqrt{2}$, it consists of two implicit Euler steps and one explicit Euler step (requires two times more CPU time than BE time scheme)

$$\begin{aligned}
&1. \quad \frac{u^{n+\theta}(x) - u^n(x)}{\theta \Delta t^n} = f\left(u^{n+\theta}(x))\right),\\
&2. \quad u^{n+1-\theta} = \frac{1-\theta}{\theta} u^{n+\theta} + \frac{2\theta - 1}{\theta} u^n,\\
&3. \quad \frac{u^{n+1}(x) - u^{n+1-\theta}(x)}{\theta \Delta t^n} = f\left(u^{n+1}(x))\right).
\end{aligned}$$

This time scheme is better that the second order (almost the third order according to [17]) conditionally stable time scheme. This time scheme was proposed by Glowinski [17] and tested in [64].

Since f in ALE formulation instead of (5.63) includes time derivative of u, i.e.

$$\frac{\partial u(x,t)}{\partial t} + f\left(u(x,t), \frac{\partial u(x,t)}{\partial t}\right) = 0 \text{ in } \Omega \times [0,T], \tag{5.66}$$

it is not clear how for example the Crank-Nicolson time scheme or three-step θ-scheme should be implemented in case of (5.66) with fully mixed time derivatives. For this purpose BE time scheme and GL time scheme are used.

For reader's convenience we provide time discretization scheme of (5.62) where BE scheme is used. It leads to

$$\operatorname{div} \mathbf{v}^{n+1} = 0, \tag{5.67a}$$

$$\rho \frac{\mathbf{v}^{n+1} - \mathbf{v}^n}{\Delta t^n} + \rho(\mathbf{v}^{n+1} \cdot \nabla \mathbf{v}^{n+1}) = \operatorname{div} \mathbf{T}^{n+1}, \tag{5.67b}$$

$$\mathbf{T}^{n+1} = -p^{n+1}\mathbf{I} + \mu_2 \left(\nabla \mathbf{v}^{n+1} + (\nabla \mathbf{v}^{n+1})^{\mathrm{T}}\right) +, G\left(\mathbf{B}^{n+1}\right)^d \tag{5.67c}$$

$$\frac{\mathbf{B}^{n+1} - \mathbf{B}^n}{\Delta t^n} + \mathbf{v}^{n+1} \cdot \nabla \mathbf{B}^{n+1} - (\nabla \mathbf{v}^{n+1}) \mathbf{B}^{n+1} - \mathbf{B}^{n+1} (\nabla \mathbf{v}^{n+1})^{\mathrm{T}} = -\frac{1}{\tau} \mathbf{B}^{n+1} \left(\mathbf{B}^{n+1}\right)^d, \tag{5.67d}$$

$p^0, \mathbf{v}^0, \mathbf{B}^0$ are known from the initial conditions. On the $(n+1)$-th time level the space problem is solved using FEM as described in a previous subsection, values with index n are known from the previous time step.

5.3 Poiseuille flow

In this section we compare the numerical and analytical solution for steady Poiseuille flow problem concerning the Oldroyd-B model (2.10) and the model Quad1 (3.112). The viscoelastic fluid is pushed from the left into the planar channel whose length is 4 m and height is 1 m. The fluid freely leaves the channel on the right. The boundary condition on the inlet and the outlet are the following:

$$T_{xx}(x=0) = -4 + G(B_{11} - B_{22}),\ T_{xx}(x=4) = -G(B_{11} - B_{22}). \tag{5.68}$$

The problem is depicted in Figure 5.2.

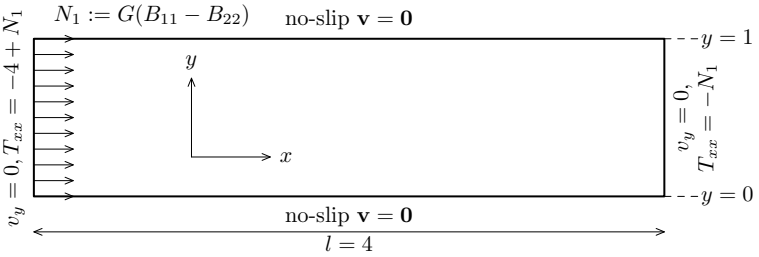

Figure 5.2: Poiseuille flow, problem description.

For the analytical solution we suppose that the fluid velocity is in the form

$$\mathbf{v} = (u(y), 0) \tag{5.69}$$

which automatically satisfies the balance of mass $\operatorname{div}\mathbf{v} = 0$. The convective term in the balance of linear momentum for this steady problem

$$\rho\mathbf{v}\cdot\nabla\mathbf{v} = \operatorname{div}\mathbf{T}, \tag{5.70}$$

is with help of (5.69) equal to zero. Hence, we are solving the following problem

$$\operatorname{div}\mathbf{T} = 0, \tag{5.71}$$

$$T_{xx}(x=0) = -4 + G(B_{11} - B_{22}),\ T_{xx}(x=4) = -G(B_{11} - B_{22}), \tag{5.72}$$

$$u(0) = u(1) = 0, \tag{5.73}$$

where the Cauchy stress tensor $\mathbf{T}$ is given by (2.10) for Oldroyd-B model and by (3.112) for quadratic model. For later use we compute the velocity gradient $\mathbf{L}$ and its symmetric part $\mathbf{D}$

$$\mathbf{L} = \begin{pmatrix} 0 & u' \\ 0 & 0 \end{pmatrix}, \quad \mathbf{D} = \frac{1}{2}\begin{pmatrix} 0 & u' \\ u' & 0 \end{pmatrix}, \text{ where } u' := \frac{\partial u}{\partial y}. \tag{5.74}$$

5.3.1 Oldroyd-B model

In case of the Oldroyd-B model (2.10) the Cauchy stress tensor $\mathbf{T}$ is in the form

$$\mathbf{T} = p\mathbf{I} + 2\mu_2\mathbf{D} + G(\mathbf{B} - \mathbf{I}). \tag{5.75}$$

Assuming that $\mathbf{B} = \mathbf{B}(y)$ is only a function of y, i.e.,

$$\mathbf{B} = \begin{pmatrix} B_{11}(y) & B_{12}(y) \\ B_{12}(y) & B_{22}(y) \end{pmatrix}, \tag{5.76}$$

the balance of linear momentum leads to

$$-\frac{\partial p}{\partial x} + \mu_2 \frac{\partial^2 u}{\partial y^2} + G\frac{\partial B_{12}}{\partial y} = 0, \tag{5.77}$$

$$-\frac{\partial p}{\partial y} + G\frac{\partial (B_{22} - 1)}{\partial y} = 0. \tag{5.78}$$

From (5.78) we get that $p = C(x) + G(B_{22}(y) - 1)$, inserting this into (5.77) we obtain

$$\frac{\partial C}{\partial x} = \mu_2 \frac{\partial^2 u}{\partial y^2} + G\frac{\partial B_{12}}{\partial y}. \tag{5.79}$$

Since the left-hand side of (5.79) is only a function of x and the right-hand side is only of function of y, both sides have to be equal to some constant K. Then

$$p(x) = Kx + \tilde{C} + G(B_{22} - 1). \tag{5.80}$$

Now we use the boundary conditions (5.72) with $T_{xx} = -p + G(B_{11} - 1)$. Using (5.80) and (5.72) we conclude that

$$p(x) = 4 - x + G(B_{22} - 1). \tag{5.81}$$

Now we rewrite the transport equation for $\mathbf{B}$

$$\mathbf{v} \cdot \nabla \mathbf{B} - \mathbf{L}\mathbf{B} - \mathbf{B}\mathbf{L}^{\mathrm{T}} + \frac{1}{\tau}(\mathbf{B} - \mathbf{I}) = 0$$

into components. Since $\mathbf{B}$ is only a function of y and $\mathbf{v} = (u(y), 0)$ the term $\mathbf{v} \cdot \nabla \mathbf{B}$ vanishes. Using (5.74) we obtain

$$\begin{aligned} B_{22} &= 1, \\ B_{12} &= \tau u' B_{22}, \\ B_{11} - 1 &= 2\tau u' B_{12}. \end{aligned}$$

The solution is

$$B_{22} = 1, \quad B_{12} = \tau u', \quad B_{11} = 1 + 2\tau^2 (u')^2. \tag{5.82}$$

By inserting (5.82) into (5.79) and using (5.81) we obtain

$$1 + (\mu_2 + G\tau)\frac{\partial^2 u}{\partial y^2} = 0.$$

Now solving this ODE by integrating it twice with respect to y, we get

$$\frac{1}{2}y^2 + C_1 y + C_2 + (\mu_2 + G\tau)\, u = 0.$$

Using no-slip boundary conditions $u(0) = u(1) = 0$, we eliminate C_1 and C_2 and get the solution

$$u = \frac{1}{2(\mu_2 + G\tau)}\left(y - y^2\right). \tag{5.83}$$

By inserting (5.83) into (5.82) we obtain

$$B_{22} = 1, \quad B_{12} = \frac{\tau}{2(\mu_2 + G\tau)}(1-2y), \quad B_{11} = 1 + 2\left[\frac{\tau}{2(\mu_2 + G\tau)}(1-2y)\right]^2. \quad (5.84)$$

Since $B_{22} = 1$, pressure $p = 4 - x$ and it does not depend on y.

We compare this analytical solution with the numerical solution and compute the full problem with $\rho = \mu_2 = G = \tau = 1$. We use Finite element method as described in Section 5.2. The mesh is regular (128×32, $\approx 96\,000$ DOFS). The full simulations of pressure p and x-component of velocity u are depicted in Figure 5.3.

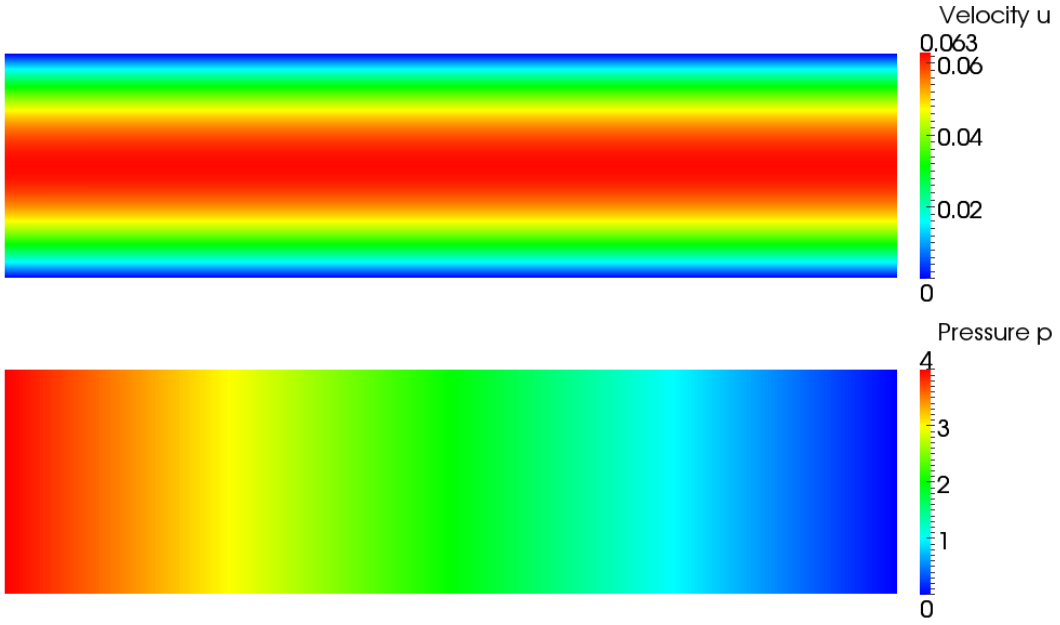

Figure 5.3: Full simulation of Poiseuille flow of Oldroyd-B model for u and p.

We plot the solution of $u, p, B_{11}, B_{12}, B_{22}$ and also $\operatorname{tr}\mathbf{B}$ and $\det\mathbf{B}$ at $x = 2$, red solid line is the solution of FEM, green dashed line is the analytical solution. The graphs are plotted in Figure 5.4.

The numerical solution corresponds very well with the analytical solution. However, there is a little difference near no-slip boundary ($y = 0$ and $y = 1$).

5.3.2 Model Quad1

In case of model Quad1 (3.112) the Cauchy stress tensor $\mathbf{T}$ is in the form

$$\mathbf{T} = p\mathbf{I} + 2\mu\mathbf{D} + G\mathbf{B}^d, \quad (5.85)$$

again we suppose that $\mathbf{B} = \mathbf{B}(y)$ is only a function of y with the components

$$\mathbf{B} = \begin{pmatrix} B_{11}(y) & B_{12}(y) \\ B_{12}(y) & B_{22}(y) \end{pmatrix}. \quad (5.86)$$

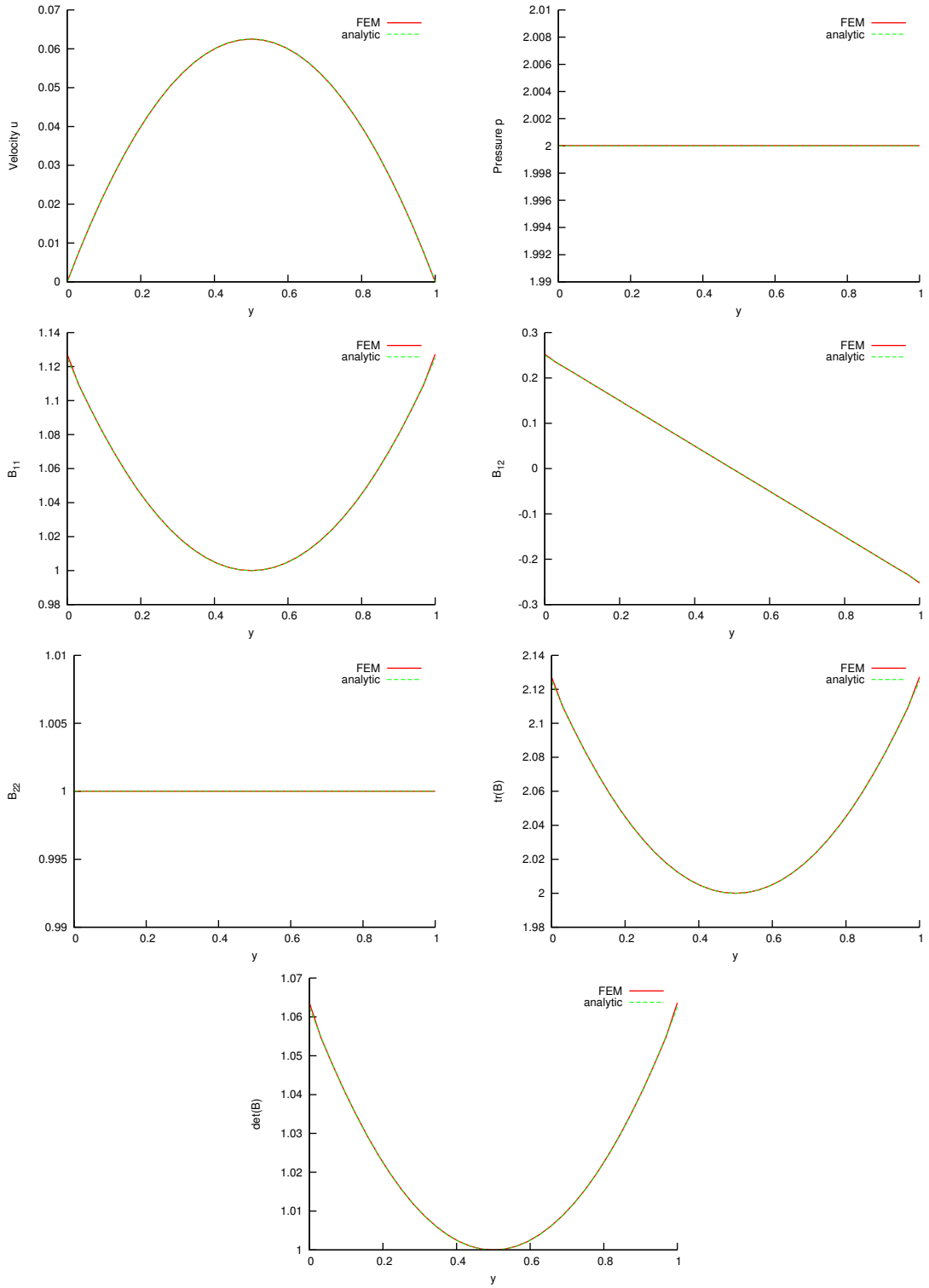

Figure 5.4: Comparison of analytical solution with full simulation using FEM for Poiseuille flow of Oldroyd-B model, for $u, p, B_{11}, B_{12}, B_{22}, \mathrm{tr}(\mathbf{B}), \det(\mathbf{B})$ at $x = 2$.

Then the balance of linear momentum is in the form

$$-\frac{\partial p}{\partial x}+\mu_2\frac{\partial^2 u}{\partial y^2}+G\frac{\partial B_{12}}{\partial y}=0, \tag{5.87}$$

$$-\frac{\partial p}{\partial y}+\frac{G}{2}\left(\frac{\partial B_{22}}{\partial y}-\frac{\partial B_{11}}{\partial y}\right)=0. \tag{5.88}$$

From (5.88) we get that $p=C(x)+G(B_{22}(y)-B_{11}(y))/2$, inserting this into (5.87) we obtain

$$\frac{\partial C}{\partial x}=\mu_2\frac{\partial^2 u}{\partial y^2}+G\frac{\partial B_{12}}{\partial y}. \tag{5.89}$$

Since the left-hand side of (5.89) is only a function of x and the right-hand side is only of function of y, both sides have to be equal to some constant K. Then

$$p(x,y)=Kx+\tilde{C}+\frac{G}{2}\left(B_{22}-B_{11}\right). \tag{5.90}$$

Now we use the boundary conditions (5.72) with $T_{xx}=-p+\frac{G}{2}(B_{11}-B_{22})$. Using (5.90) and (5.72) we conclude that

$$p\left(x,y\right)=4-x+\frac{G}{2}\left(B_{22}-B_{11}\right). \tag{5.91}$$

Further we use the alternative form of the transport equation for $\mathbf{B}$ (3.131)

$$\mathbf{v}\cdot\nabla\mathbf{B}-\mathbf{L}\mathbf{B}-\mathbf{B}\mathbf{L}^{\mathrm{T}}+\frac{1}{\tau}\left(\frac{\operatorname{tr}\mathbf{B}}{2}\mathbf{B}-\mathbf{I}\right)=0$$

and rewrite it into components. Since $\mathbf{B}$ is only a function of y and $\mathbf{v}=(u(y),0)$ the term $\mathbf{v}\cdot\nabla\mathbf{B}$ is equal to zero. Using (5.74) we obtain

$$B_{22}(B_{11}+B_{22})=2, \tag{5.92}$$

$$(B_{11}+B_{22})B_{12}=2\tau u' B_{22}, \tag{5.93}$$

$$\frac{1}{2}(B_{11}+B_{22})B_{11}-1=2\tau u' B_{12}. \tag{5.94}$$

Note that $\operatorname{tr}\mathbf{B}=B_{11}+B_{22}\geq 2$ due to (3.127). Let us denote

$$0\leq X:=\frac{\sqrt{1+4\tau^2(u')^2}-1}{2\tau^2(u')^2}, \tag{5.95}$$

then the solution is

$$B_{22}=\sqrt{X},\quad B_{12}=\tau u' X=\frac{\sqrt{1+4\tau^2(u')^2}-1}{2\tau u'},\quad B_{11}=\frac{2-B_{22}^2}{B_{22}}=\frac{2-X}{\sqrt{X}}. \tag{5.96}$$

Note that

$$\lim_{u'\to 0}X=1\ \Rightarrow\ \lim_{u'\to 0}B_{22}=1,\quad \lim_{u'\to 0}B_{11}=1 \tag{5.97}$$

and also it holds

$$\lim_{u'\to 0}B_{12}=0. \tag{5.98}$$

By inserting (5.96) into (5.87) and using (5.91) we obtain

$$1 + \mu_2 \frac{\partial^2 u}{\partial y^2} + G \frac{\partial}{\partial y} \left[\frac{\sqrt{1 + 4\tau^2 (u')^2} - 1}{2\tau u'} \right] = 0. \tag{5.99}$$

This ODE can not be solved analytically. First, we integrate this equation with respect to y and we get

$$y + C_1 + \mu_2 u' + G \frac{\sqrt{1 + 4\tau^2 (u')^2} - 1}{2\tau u'} = 0, \tag{5.100}$$

using the symmetry of the problem and no-slip boundary conditions $u(0) = u(1) = 0$ we suppose that u' in the middle of the channel is equal to zero, thus $u'(y = 1/2) = 0$. Using (5.98) we obtain that $C_1 = -1/2$ and get the algebraical equation for u'

$$y - \frac{1}{2} + \mu_2 u' + G \frac{\sqrt{1 + 4\tau^2 (u')^2} - 1}{2\tau u'} = 0. \tag{5.101}$$

Using Newton method equation (5.101) with the material parameters $\rho = \mu_2 = G = \tau = 1$ is solved numerically and thus u' is found. Velocity u is obtained by

$$u(y) = \int_0^y u'(a)\,\mathrm{d}a + u(0), \tag{5.102}$$

where $u(0) = 0$. Five-point Newton-Cotes integration formula is used for the integration. We obtained numerically a solution for u' and u, solutions for $p, B_{11}, B_{12}, B_{22}$ are described by formulae (5.91) and (5.96).

We compare this semi-analytical solution with the numerical solution of the full problem with material parameters $\rho = \mu_2 = G = \tau = 1$. Again Finite element method as described in Section 5.2 is used. The mesh is regular (128×32, $\approx 96\,000$ DOFS). The full simulations of pressure p and x-component of velocity u are depicted in Figure 5.5.

We plot the solution of $u, p, B_{11}, B_{12}, B_{22}$ and also $\operatorname{tr}\mathbf{B}$ and $\det\mathbf{B}$ at $x = 2$, red solid line is the solution of FEM, green dashed line is the semi-analytical solution. The graphs are plotted in Figure 5.6. They show that the numerical solution almost merges the semi-analytical solution, but there is a little difference near no-slip boundary ($y = 0$ and $y = 1$). This can be seen very well in the plot of $\det\mathbf{B}$ where FEM does not preserve $\det\mathbf{B} = 1$.

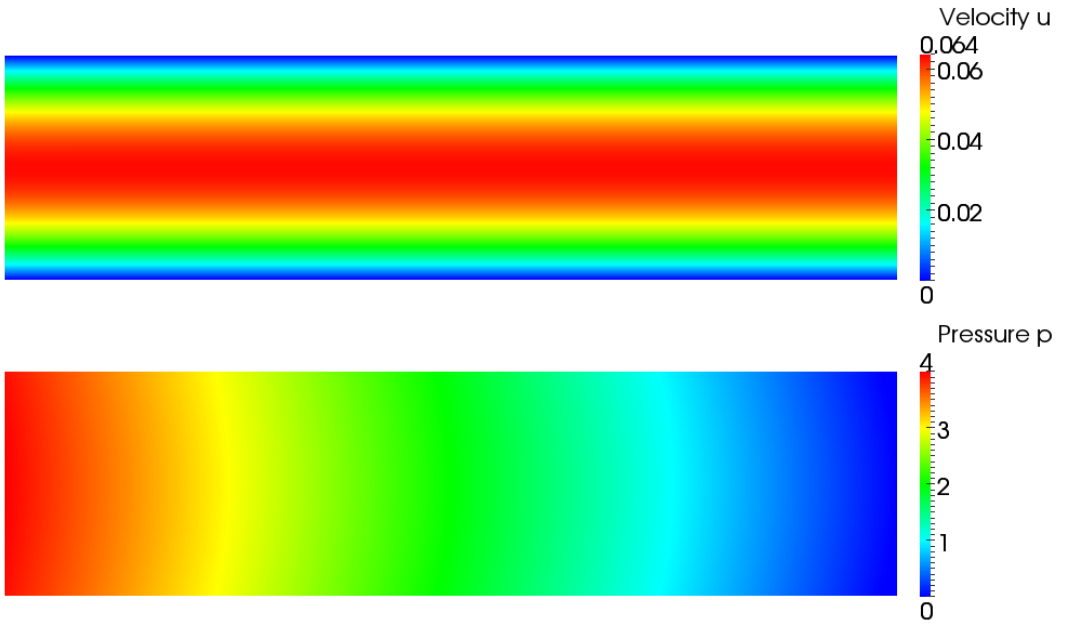

Figure 5.5: Full simulation of Poiseuille flow of model Quad1 for u and p.

5.4 Axisymmetric Couette flow

In this section we compare the numerical and analytical solution for steady axisymmetric Couette flow problem for the Oldroyd-B model (2.10) and model Quad1 (3.112). The domain is bordered with two concentric circles, radius of the inner one is 1 m, radius of the outer one is 2 m, the material flows inside these two circles and fully sticks to both boundaries. The inner circle is fixed and does not move, the outer one rotates with constant angular velocity $\omega = 0.5$ rad s^{-1}, thus the fluid rotates with it. The problem is depicted in Figure 5.7.

For the analytical solution we compute the problem using polar coordinates[4], we suppose that the fluid velocity is in the form

$$\mathbf{v} = (0, \mathbf{v}_\varphi(r)), \tag{5.103}$$

which automatically satisfies the balance of mass $\operatorname{div} \mathbf{v} = 0$. Then the Dirichlet boundary conditions are equivalent to

$$v_\varphi(r = 1) = 0, \quad v_\varphi(r = 2) = \omega r = 1. \tag{5.104}$$

The balance of linear momentum for this steady problem is equal to

$$\rho \mathbf{v} \cdot \nabla \mathbf{v} = \operatorname{div} \mathbf{T}, \tag{5.105}$$

where the convective term is with help of (5.103) in the form

$$\rho \mathbf{v} \cdot \nabla \mathbf{v} = \rho \begin{pmatrix} -\frac{v_\varphi^2}{r} \\ 0 \end{pmatrix}. \tag{5.106}$$

[4]See cylindrical coordinates in Appendix A.2, in case of polar coordinates all derivatives with respect to z and all z-components are equal to zero.

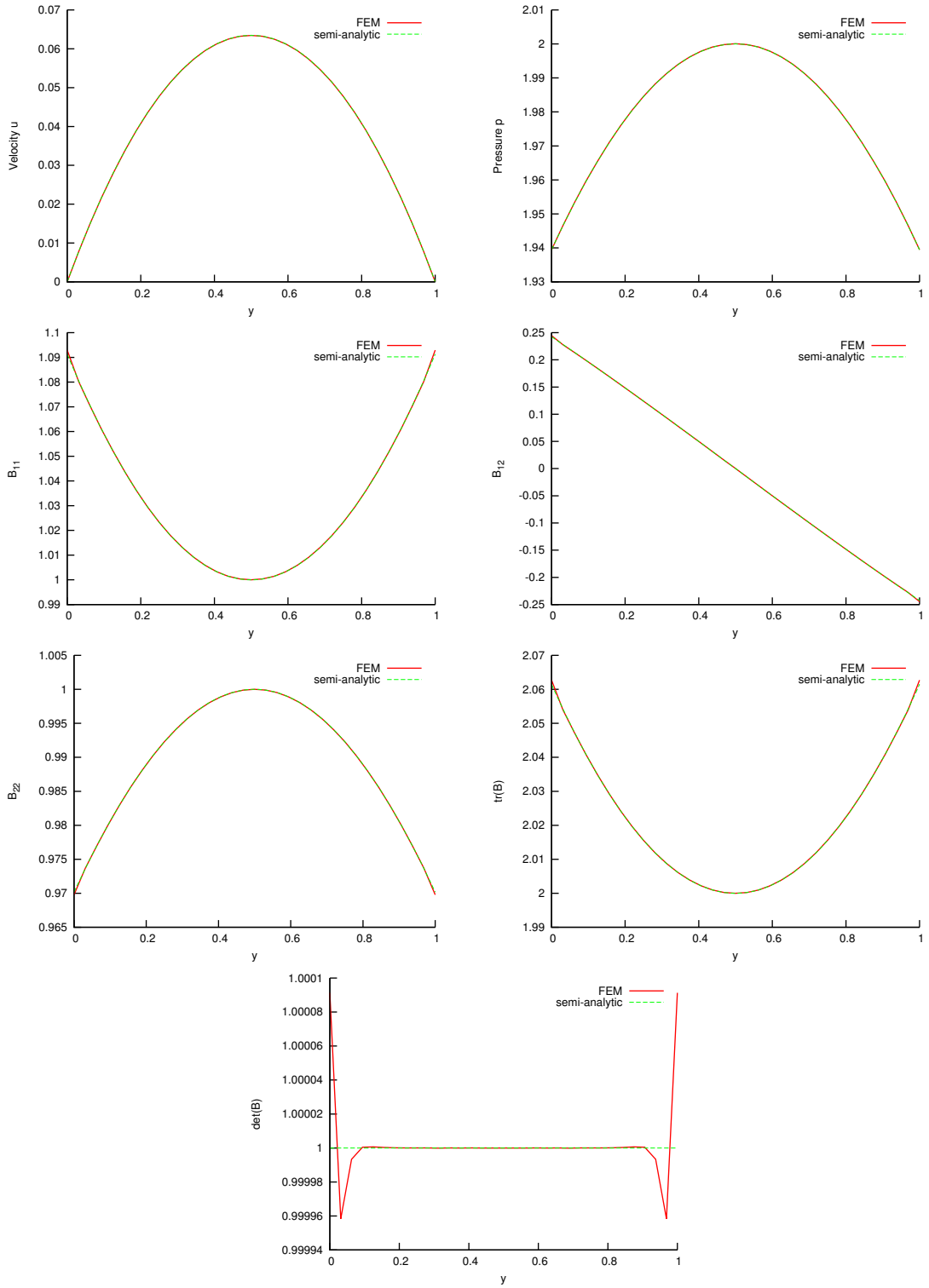

Figure 5.6: Comparison of semi-analytical solution with full simulation using FEM for Poiseuille flow of model Quad1, for $u, p, B_{11}, B_{12}, B_{22}, \mathrm{tr}(\mathbf{B}), \det(\mathbf{B})$ at $x = 2$.

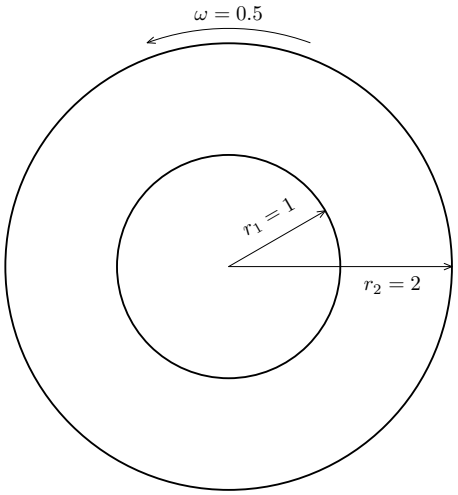

Figure 5.7: Couette flow, problem description.

For later use we compute the velocity gradient $\mathbf{L}$ and its symmetric part $\mathbf{D}$

$$\mathbf{L} = \begin{pmatrix} 0 & -\dfrac{v_\varphi}{r} \\ \dfrac{\partial v_\varphi}{\partial r} & 0 \end{pmatrix}, \quad \mathbf{D} = \frac{1}{2}\begin{pmatrix} 0 & \dfrac{\partial v_\varphi}{\partial r} - \dfrac{v_\varphi}{r} \\ \dfrac{\partial v_\varphi}{\partial r} - \dfrac{v_\varphi}{r} & 0 \end{pmatrix}. \tag{5.107}$$

5.4.1 Oldroyd-B model

We compute the problem using Oldroyd-B model where the Cauchy stress tensor $\mathbf{T}$ is in the form

$$\mathbf{T} = p\mathbf{I} + 2\mu_2\mathbf{D} + G(\mathbf{B} - \mathbf{I}), \tag{5.108}$$

due to symmetry $\mathbf{B} = \mathbf{B}(r), p = p(r)$ are only functions of r with the components

$$\mathbf{B} = \begin{pmatrix} B_{rr} & B_{r\varphi} \\ B_{r\varphi} & B_{\varphi\varphi} \end{pmatrix}. \tag{5.109}$$

Then the balance of linear momentum is in the form

$$-\frac{\partial p}{\partial r} + G\frac{\partial B_{rr}}{\partial r} + G\frac{B_{rr} - B_{\varphi\varphi}}{r} = -\rho\frac{v_\varphi^2}{r}, \tag{5.110}$$

$$G\frac{\partial B_{r\varphi}}{\partial r} + \mu_2\frac{\partial}{\partial r}\left[\frac{\partial v_\varphi}{\partial r} - \frac{v_\varphi}{r}\right] + \frac{2}{r}\left[GB_{r\varphi} + \mu_2\left(\frac{\partial v_\varphi}{\partial r} - \frac{v_\varphi}{r}\right)\right] = 0. \tag{5.111}$$

Now we rewrite the transport equation for $\mathbf{B}$

$$\mathbf{v}\cdot\nabla\mathbf{B} - \mathbf{L}\mathbf{B} - \mathbf{B}\mathbf{L}^{\mathrm{T}} + \frac{1}{\tau}(\mathbf{B} - \mathbf{I}) = 0$$

into components and we obtain

$$\begin{aligned} B_{rr} - 1 &= 0, \\ B_{r\varphi} + \tau \left(\frac{v_\varphi}{r} - \frac{\partial v_\varphi}{\partial r} \right) B_{rr} &= 0, \\ B_{\varphi\varphi} - 1 + 2\tau \left(\frac{v_\varphi}{r} - \frac{\partial v_\varphi}{\partial r} \right) B_{r\varphi} &= 0. \end{aligned}$$

The solution is

$$B_{rr} = 1, \quad B_{r\varphi} = \tau \left(\frac{\partial v_\varphi}{\partial r} - \frac{v_\varphi}{r} \right), \quad B_{\varphi\varphi} = 1 + 2\tau^2 \left(\frac{\partial v_\varphi}{\partial r} - \frac{v_\varphi}{r} \right)^2. \tag{5.112}$$

By inserting (5.112) into (5.111) we obtain

$$(G\tau + \mu_2) \left[\frac{2}{r} \left(\frac{\partial v_\varphi}{\partial r} - \frac{v_\varphi}{r} \right) + \frac{\partial}{\partial r} \left(\frac{\partial v_\varphi}{\partial r} - \frac{v_\varphi}{r} \right) \right] = 0. \tag{5.113}$$

Hence, we have to solve the following ODE

$$r^2 \frac{\partial^2 v_\varphi}{\partial r^2} + r \frac{\partial v_\varphi}{\partial r} - v_\varphi = 0, \tag{5.114}$$

which together with the boundary conditions (5.104) has the solution

$$v_\varphi = \frac{2}{3} \left(r - \frac{1}{r} \right). \tag{5.115}$$

Using (5.110), (5.115) and (5.112) we get pressure p

$$p = C + \rho \frac{4}{9} \left(\frac{r^2}{2} - 2 \ln r - \frac{1}{2r^2} \right) + \frac{8}{9} G\tau^2 \frac{1}{r^4} \tag{5.116}$$

upto constant C because there is only gradient of the pressure in the balance of linear momentum. We fix the constant C by imposing the condition $p(r = 1) = 0$, thus

$$p = \rho \frac{4}{9} \left(\frac{r^2}{2} - 2 \ln r - \frac{1}{2r^2} \right) + \frac{8}{9} G\tau^2 \frac{1}{r^4} - \frac{8}{9}. \tag{5.117}$$

Using (5.115) and (5.112) we find the elements of the tensor $\mathbf{B}$

$$B_{rr} = 1, \quad B_{r\varphi} = \frac{4\tau}{3r^2}, \quad B_{\varphi\varphi} = 1 + \frac{32\tau^2}{9r^4}. \tag{5.118}$$

For numerical simulation we use finite element method as described in Section 5.2. The mesh is depicted in Figure 5.8, it is three times refined locally near the boundaries (18 944 elements, 438 272 DOFS).

The full problem was computed in Cartesian coordinates with the material parameters $\rho = G = \mu_2 = \tau = 1$. Pressure p was fixed to be zero for $r = 1$. We plot pressure p and velocity magnitude $|\mathbf{v}|$ in Figure 5.9. Both solutions are symmetric[5]. Furthermore,

[5]Obviously, components v_x and v_y would not be symmetric, we would obtain components in polar coordinates by

$$\begin{pmatrix} v_r \\ v_\varphi \end{pmatrix} = \mathbf{A} \begin{pmatrix} v_x \\ v_y \end{pmatrix},$$

where $\mathbf{A}$ is coordinate transformation matrix defined by (5.120).

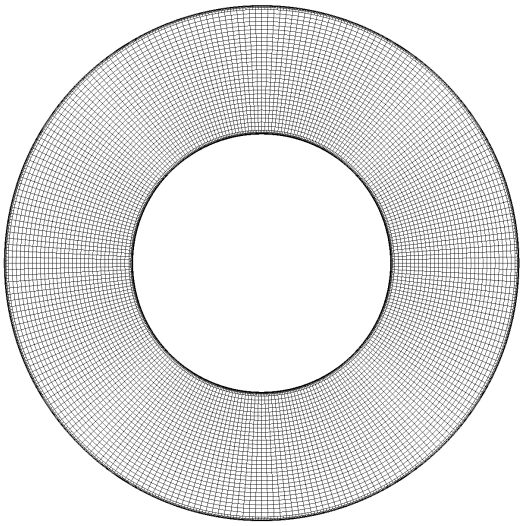

Figure 5.8: Mesh for Couette flow problem.

components of tensor $\mathbf{B}$: B_{xx}, B_{xy}, B_{yy} are plotted in the left column of Figure 5.10. The Cartesian components $\mathbf{B}$ are not symmetric, but after the transformation into polar coordinates according to relation

$$\begin{pmatrix} B_{rr} & B_{r\varphi} \\ B_{r\varphi} & B_{\varphi\varphi} \end{pmatrix} = \mathbf{A} \begin{pmatrix} B_{xx} & B_{xy} \\ B_{xy} & B_{yy} \end{pmatrix} \mathbf{A}^{\mathrm{T}}, \tag{5.119}$$

where $\mathbf{A}$ is the coordinate transformation matrix

$$\mathbf{A} = \frac{\partial\left(r(x,y), \varphi(x,y)\right)}{\partial(x,y)} = \begin{pmatrix} \dfrac{x}{\sqrt{x^2+y^2}} & \dfrac{y}{\sqrt{x^2+y^2}} \\ \dfrac{-y}{x^2+y^2} & \dfrac{x}{x^2+y^2} \end{pmatrix}, \tag{5.120}$$

the transformed components $B_{rr}, B_{r\varphi}, B_{\varphi\varphi}$ are symmetric (see right column of Figure 5.10).

We plot the solution of $v_\varphi(r)$, $p(r)$, $B_{rr}(r)$, $B_{r\varphi}(r)$, $B_{\varphi\varphi}(r)$ and also $\operatorname{tr}\mathbf{B}(r)$ and $\det\mathbf{B}(r)$ for $r \in [1,2]$, red solid line is the solution of FEM, green dashed line is the analytical solution given by (5.115), (5.117) and (5.118). The graphs are plotted in Figure 5.11. It is important to repeat that the full simulation was computed in Euclidean coordinates in the curved domain. Hence, this problem, that can be computed analytically in polar coordinates, is a good benchmark. Moreover, the solution is much complicated (see for example the solution for pressure (5.117)) than the solution of Poiseuille flow.

The numerical solution corresponds very well with the analytical solution. There is a little difference near boundaries ($r = 1$ and $r = 2$) as can be seen in case of B_{rr}.

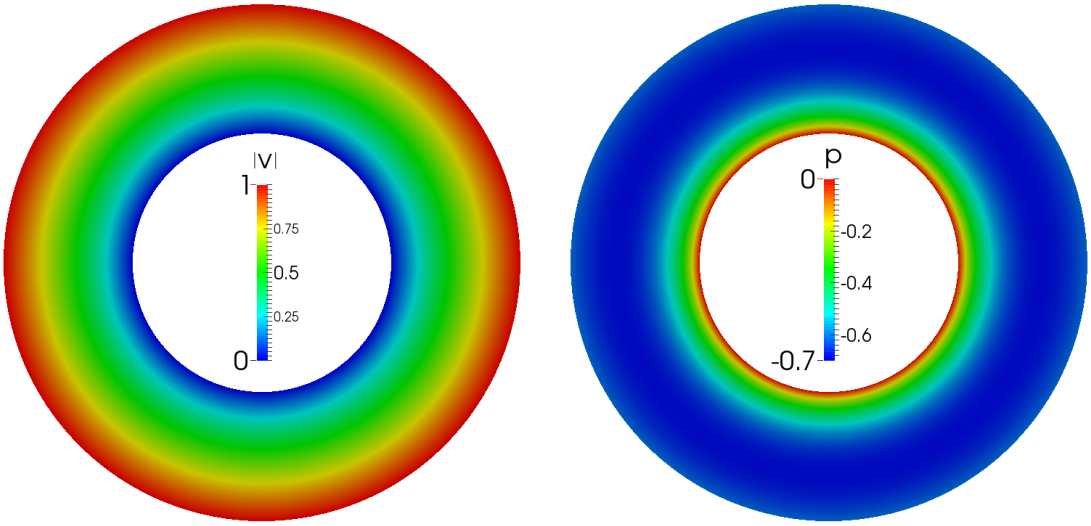

Figure 5.9: Full simulation for $|\mathbf{v}|$ and p for Oldroyd-B model.

5.4.2 Model Quad1

We compute the problem using model Quad1 for which the Cauchy stress tensor $\mathbf{T}$ is in the form

$$\mathbf{T} = p\mathbf{I} + 2\mu_2\mathbf{D} + G\left(\mathbf{B} - \frac{1}{2}(\operatorname{tr}\mathbf{B})\mathbf{I}\right). \tag{5.121}$$

Due to symmetry $\mathbf{B} = \mathbf{B}(r), p = p(r)$ are only functions of r, components of $\mathbf{B}$ are

$$\mathbf{B} = \begin{pmatrix} B_{rr} & B_{r\varphi} \\ B_{r\varphi} & B_{\varphi\varphi} \end{pmatrix}. \tag{5.122}$$

Then the balance of linear momentum is in the form

$$-\frac{\partial p}{\partial r} + \frac{G}{2}\frac{\partial}{\partial r}(B_{rr} - B_{\varphi\varphi}) + G\frac{B_{rr} - B_{\varphi\varphi}}{r} = -\rho\frac{v_\varphi^2}{r}, \tag{5.123}$$

$$G\frac{\partial B_{r\varphi}}{\partial r} + \mu_2\frac{\partial}{\partial r}\left[\frac{\partial v_\varphi}{\partial r} - \frac{v_\varphi}{r}\right] + \frac{2}{r}\left[GB_{r\varphi} + \mu_2\left(\frac{\partial v_\varphi}{\partial r} - \frac{v_\varphi}{r}\right)\right] = 0. \tag{5.124}$$

Now we rewrite the transport equation for $\mathbf{B}$ using alternative form (3.131)

$$\mathbf{v}\cdot\nabla\mathbf{B} - \mathbf{L}\mathbf{B} - \mathbf{B}\mathbf{L}^{\mathrm{T}} + \frac{1}{\tau}\left(\frac{\operatorname{tr}\mathbf{B}}{2}\mathbf{B} - \mathbf{I}\right) = 0$$

into components and we obtain

$$(B_{rr} + B_{\varphi\varphi})B_{rr} = 2, \tag{5.125}$$

$$(B_{rr} + B_{\varphi\varphi})B_{r\varphi} = 2\tau\left(\frac{\partial v_\varphi}{\partial r} - \frac{v_\varphi}{r}\right)B_{rr}, \tag{5.126}$$

$$\frac{1}{2}(B_{rr} + B_{\varphi\varphi})B_{\varphi\varphi} - 1 = 2\tau\left(\frac{\partial v_\varphi}{\partial r} - \frac{v_\varphi}{r}\right)B_{r\varphi}. \tag{5.127}$$

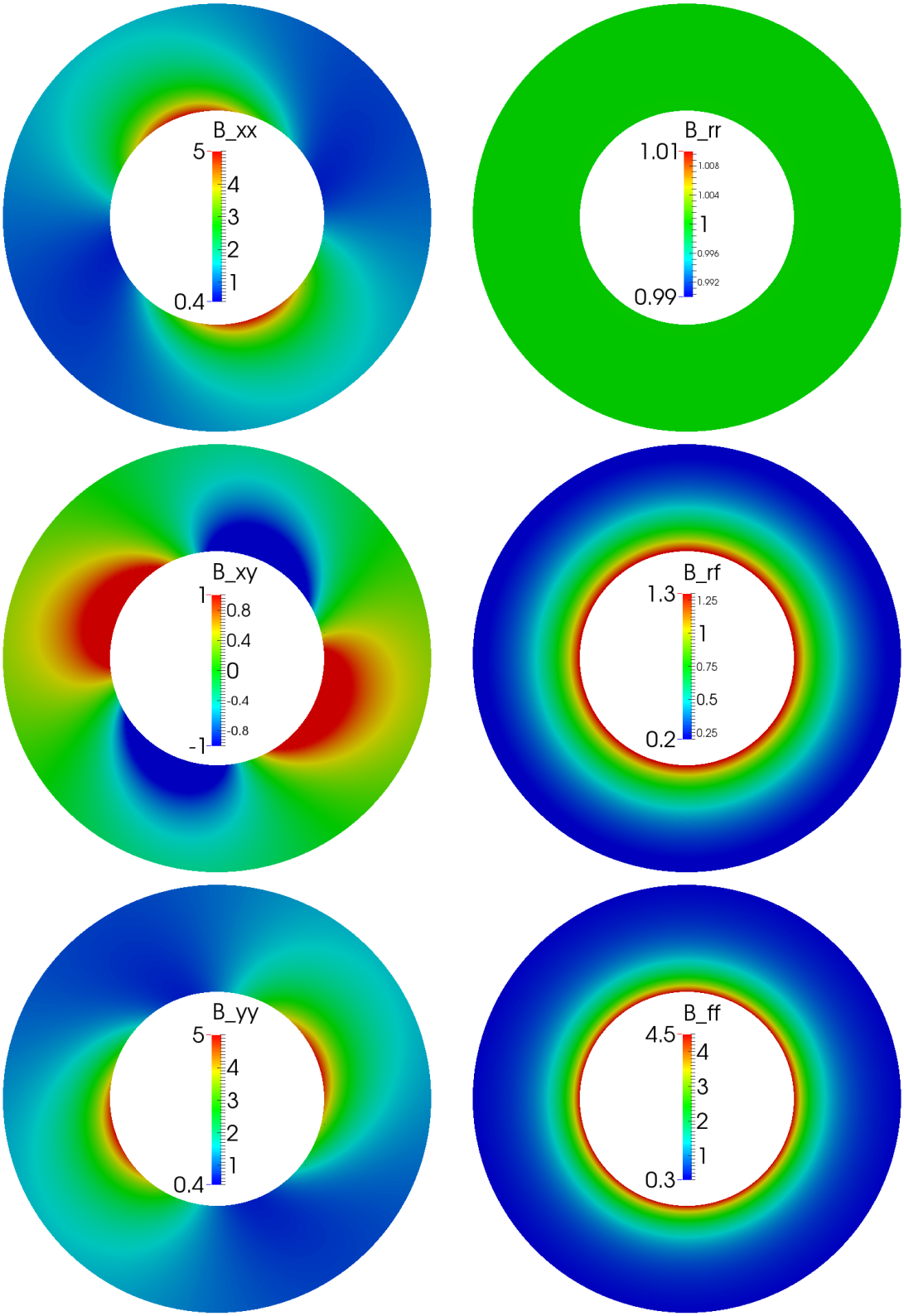

Figure 5.10: Full simulation for components of tensor **B** in Euclidean and polar coordinates for Oldroyd-B model.

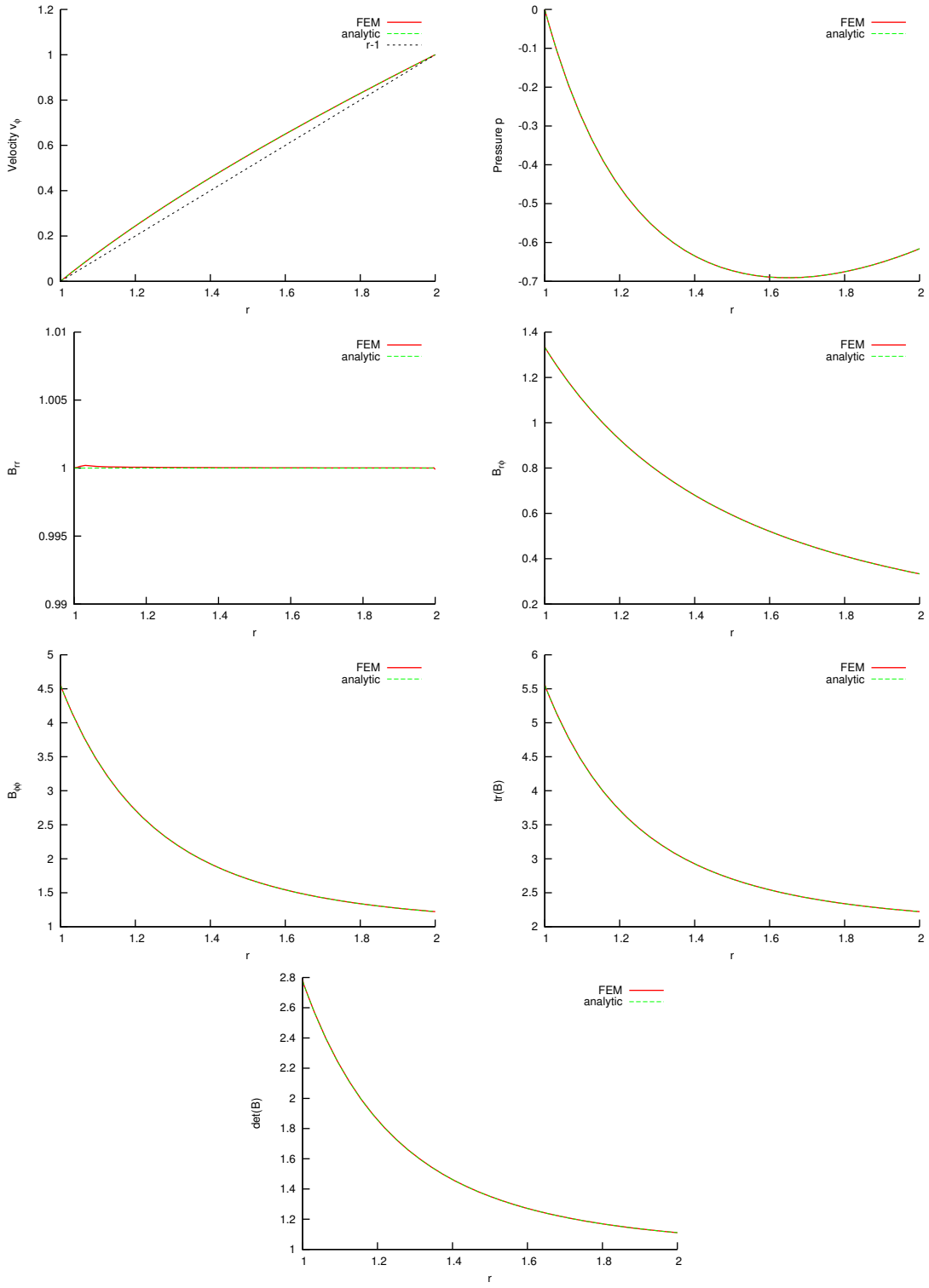

Figure 5.11: Comparison of analytical solution with full simulation using FEM for Couette flow of Oldroyd-B model, for $v_\varphi, p, B_{rr}, B_{r\varphi}, B_{\varphi\varphi}, \mathrm{tr}(\mathbf{B}), \det(\mathbf{B})$.

Let us denote

$$U := \frac{\partial v_\varphi}{\partial r} - \frac{v_\varphi}{r}, \tag{5.128}$$

then similarly as in case of Poiseuille flow we denote

$$0 \leq X := \frac{\sqrt{1+4\tau^2U^2}-1}{2\tau^2U^2}. \tag{5.129}$$

Then the solution of (5.125)–(5.127) is

$$B_{rr} = \sqrt{X}, \quad B_{r\varphi} = \tau U X = \frac{\sqrt{1+4\tau^2U^2}-1}{2\tau U}, \quad B_{\varphi\varphi} = \frac{2-B_{rr}^2}{B_{rr}} = \frac{2-X}{\sqrt{X}}. \tag{5.130}$$

By inserting (5.130) into (5.124) we obtain

$$\frac{\partial}{\partial r}\left[G\tau UX + \mu_2 U\right] + \frac{2}{r}\left[G\tau UX + \mu_2 U\right] = 0, \tag{5.131}$$

with the boundary conditions $v_\varphi(r=1)=0$ and $v_\varphi(r=2)=1$. This fully implicit boundary value problem can not be solved analytically. We solve it numerically with the material parameters $\rho = \mu_2 = G = \tau = 1$ in Matlab using BVPsuite (see [25]) that is based on a collocation method. This Matlab code provides the error estimate of the computed solution, the error was of the order 10^{-14}. Thus, we obtain v_φ and its derivative with respect to r, from this we compute $B_{rr}, B_{r\varphi}, B_{\varphi\varphi}$ using (5.130). Pressure p is obtained from (5.123)

$$p = \frac{1}{2}(B_{rr} - B_{\varphi\varphi}) + \int_0^r \frac{B_{rr} - B_{\varphi\varphi} + v_\varphi^2}{r}\,\mathrm{d}r + C, \tag{5.132}$$

where five-point Newton-Cotes integration formula is used for the integration and constant C is chosen such that $p(r=1)=0$.

For the full simulation we use finite element method as described in Section 5.2. The mesh is depicted in Figure 5.8. The full problem was computed in Cartesian coordinates with the material parameters $\rho = G = \mu_2 = \tau = 1$. Pressure p was fixed to be zero for $r = 1$. We plot pressure p and velocity magnitude $|\mathbf{v}|$ in Figure 5.12. Both solutions are symmetric. Further we plot components of tensor $\mathbf{B}$: B_{xx}, B_{xy}, B_{yy} in the left column of Figure 5.13. Again, the Cartesian components are not symmetric. We transform the tensor $\mathbf{B}$ from Cartesian to polar coordinates by the transformation (5.119). Components in polar coordinates $B_{rr}, B_{r\varphi}, B_{\varphi\varphi}$ are depicted in the right column of Figure 5.13 and they are symmetric.

We compare the solution of $v_\varphi(r), p(r), B_{rr}(r), B_{r\varphi}(r), B_{\varphi\varphi}(r), \operatorname{tr}\mathbf{B}(r)$ and $\det\mathbf{B}(r)$ for $r \in [1,2]$ obtained with FEM and collocation method. Red solid line is the solution of FEM, green dashed line is the solution obtained with collocation method (denoted by BVP). The graphs are plotted in Figure 5.14.

The FEM solution corresponds very well with the semi-analytical solution of BVP (5.131). There is a little difference near boundaries ($r = 1$ and $r = 2$) as can be seen in case of $\det(B)$ that should be identically equal to one. If we compare the results of Oldroyd-B model and model Quad1 we find out that in case of Quad1 v_φ differs much more from the linear function than v_φ that is obtained using Oldroyd-B model. The biggest difference is in the pressure p, in case of Oldroyd-B model p is a convex function that decreases for $r < 1.6$, in case of model Quad1 pressure p is an increasing function (if the axisymmetric Couette flow is computed using Navier-Stokes model, pressure p is also increasing function).

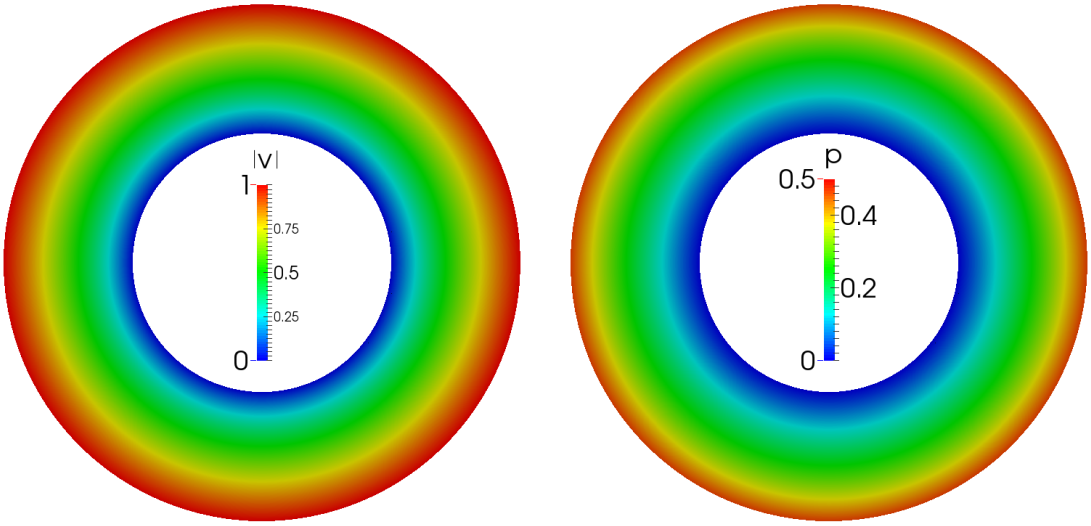

Figure 5.12: Full simulation for $|\mathbf{v}|$ and p for model Quad1.

5.5 Full simulation of the experiment performed by Narayan et al. (2012)

In this section we compute the full simulation of the experiment with unaged polymer modified binder at temperature 35 °C performed by Narayan et al. (2012). In the previous chapter we described and fitted this experiment with model Quad2 under the assumptions that the asphalt flows only in the direction of rotation and the velocity $\mathbf{v}$ is in the form

$$\mathbf{v} = (0, \omega r z/h, 0) \tag{5.133}$$

and neglecting the time derivative of ω in the balance of linear momentum. We compute the simulation with the material parameters given by Table 5.1 and with the density[6] $\rho = 1200$ kg/m^3: where we replaced ratios G_1/μ_1 and G_2/μ_2 with the relaxation times

Temp [°C]	G_1 [kPa]	G_2 [kPa]	τ_1 [s]	τ_2 [s]	μ_3 [kPa s]
35	130.4	27.7	0.17	1.52	45.3

Table 5.1: Fitted parameters for experiment by Narayan et al. (2012) using model Quad2.

τ_1 and τ_2.

We solve the full problem using the cylindrical coordinates in the fixed domain Ω. The only assumption that is used is that the solution does not depend on the φ coordinate. That is why we can solve the problem in the cross-section Σ, see Figure 5.15.

[6]Using the assumptions mentioned above the density is not presented in the simplified equations (4.42)–(4.46) and so it could have not been fitted.

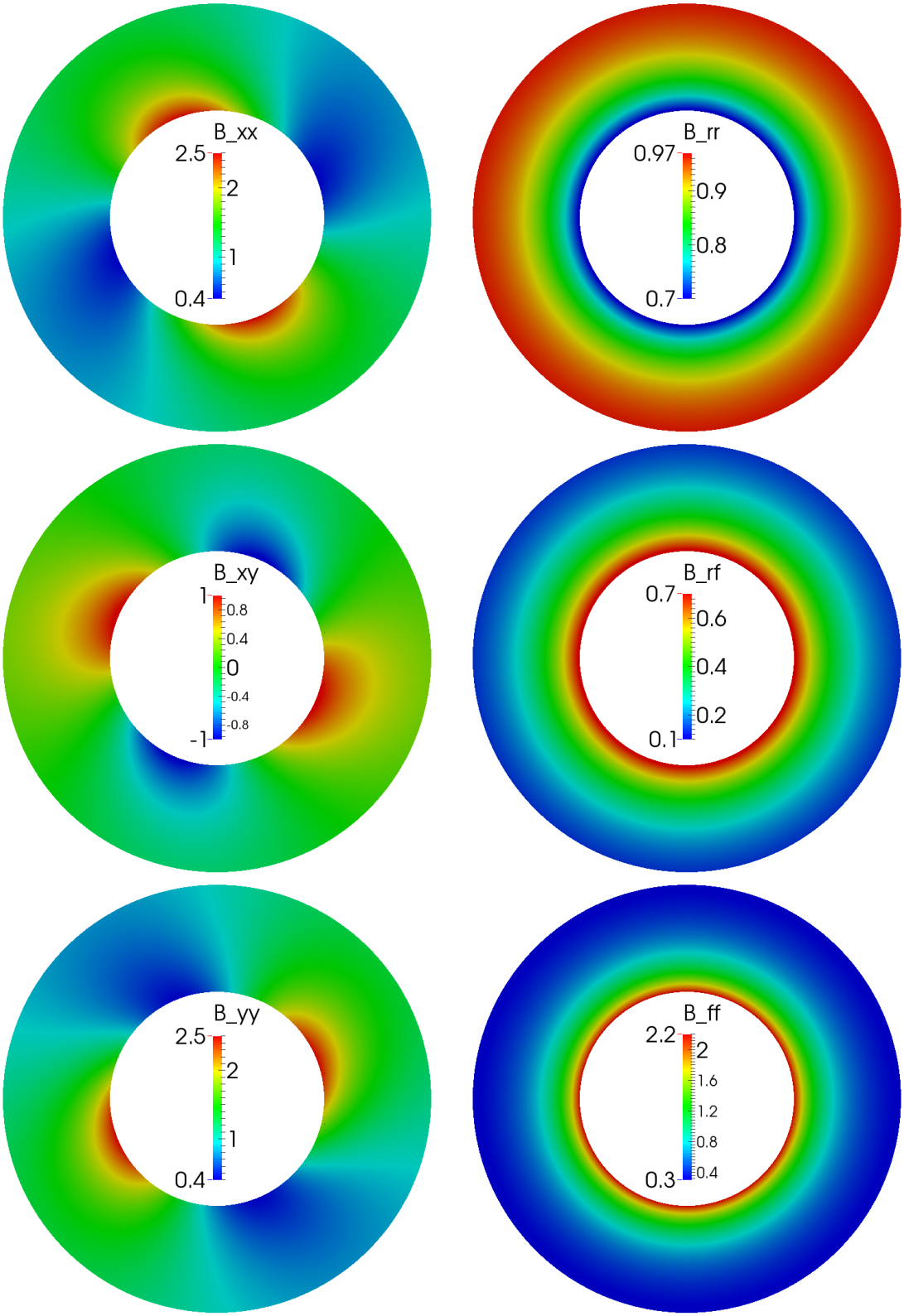

Figure 5.13: Full simulation for components of tensor **B** in Euclidean and polar coordinates for model Quad1.

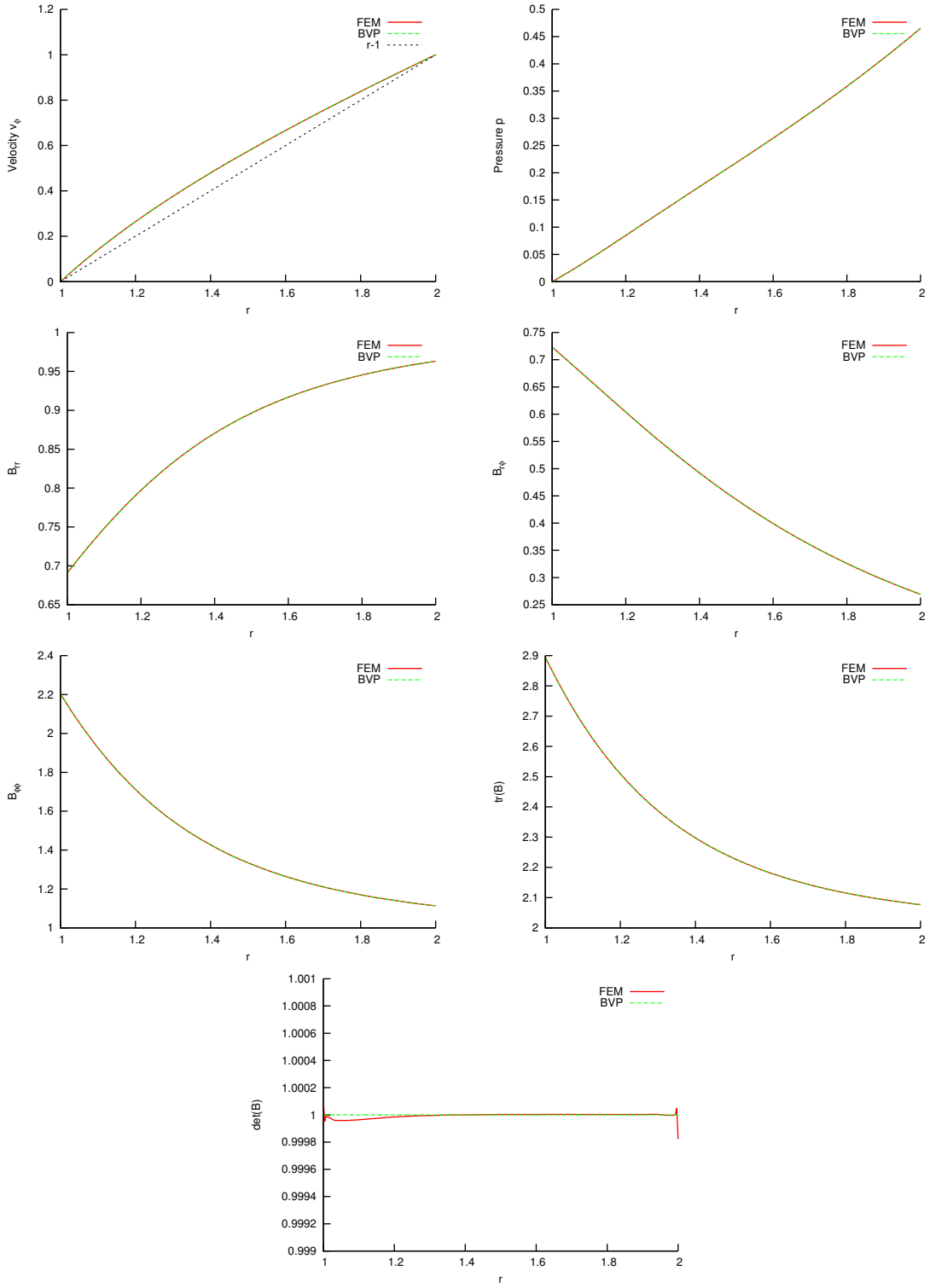

Figure 5.14: Comparison of numerical solution of simpler BVP using collocation method with full simulation using FEM for Couette flow of model Quad1, for $v_\varphi, p, B_{rr}, B_{r\varphi}, B_{\varphi\varphi}, \mathrm{tr}(\mathbf{B}), \det(\mathbf{B})$.

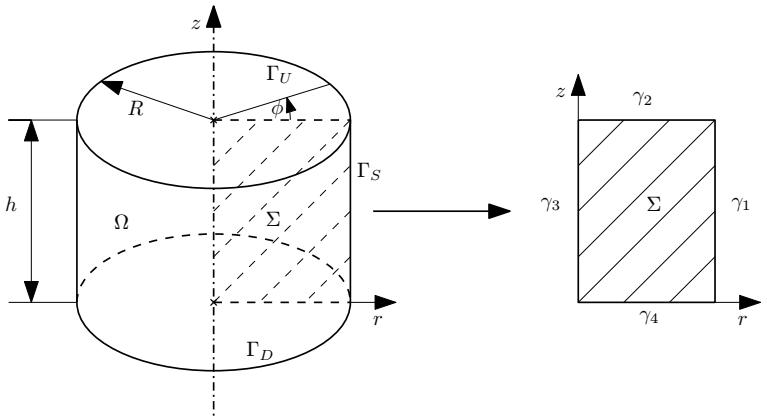

Figure 5.15: Cylindrical coordinates, cross-section Σ.

The unknowns of model Quad2 are in the form

$$p = p(r,z,t),\ \mathbf{v} = (v_r, v_\varphi, v_z)(r,z,t),\ \mathbf{B}_{\kappa_{p_1(t)}} = \begin{pmatrix} B_{1rr}, B_{1r\varphi}, B_{1rz} \\ B_{1r\varphi}, B_{1\varphi\varphi}, B_{1\varphi z} \\ B_{1rz}, B_{1\varphi z}, B_{1zz} \end{pmatrix}(r,z,t),$$

$$\mathbf{B}_{\kappa_{p_2(t)}} = \begin{pmatrix} B_{2rr}, B_{2r\varphi}, B_{2rz} \\ B_{2r\varphi}, B_{2\varphi\varphi}, B_{2\varphi z} \\ B_{2rz}, B_{2\varphi z}, B_{2zz} \end{pmatrix}(r,z,t), \quad (r,z) \in \Sigma,\ t \in [0,2].$$

The initial conditions are $p(0) = 0, \mathbf{v}(0) = \mathbf{0}, \mathbf{B}_{\kappa_{p_1(t)}}(0) = \mathbf{B}_{\kappa_{p_2(t)}}(0) = \mathbf{I}$ which means that the material is at rest and relaxed. The boundary conditions satisfy

$$\mathbf{Tn} = \mathbf{0} \text{ on } \gamma_1, \tag{5.134}$$

$$v_r = v_z = 0,\ v_\varphi = \omega r \text{ on } \gamma_2, \tag{5.135}$$

$$v_r = v_\varphi = v_z = 0 \text{ on } \gamma_4 \tag{5.136}$$

and the symmetry boundary conditions on γ_3

$$v_r = v_\varphi = 0, T_{rz} = 0 \text{ on } \gamma_3. \tag{5.137}$$

The Dirichlet conditions on γ_2, γ_3 and γ_4 are taking into account by choosing appropriate space and the Neumann conditions on γ_1 ad γ_3 are part of the weak formulation.

Under the assumption of axial symmetry, the weak formulation of the equations is transformed from 3D to 2D in the following way

$$\int_\Omega \operatorname{div}\mathbf{v}\ q\,\mathrm{d}\mathbf{x} = \int_0^R \int_0^h \int_0^{2\pi} r \operatorname{div}\mathbf{v}\ q\,\mathrm{d}\varphi\,\mathrm{d}z\,\mathrm{d}r = \int_\Sigma r \operatorname{div}\mathbf{v} \left(\int_0^{2\pi} q\,\mathrm{d}\varphi\right)\mathrm{d}\Sigma = \int_\Sigma r \operatorname{div}\mathbf{v}\ \hat{q}\,\mathrm{d}\Sigma, \tag{5.138}$$

where we denoted by $\hat{q}$ a new 2D test function computed from the old 3D test function q

$$\hat{q}(r,z) = \int_0^{2\pi} q(r,\varphi,z)\,\mathrm{d}\varphi.$$

The same procedure is applied to the rest of equations

$$\int_\Sigma r \operatorname{div} \mathbf{v}\ \hat{q}\ \mathrm{d}\Sigma = 0, \quad (5.139a)$$

$$\int_\Sigma \rho r \left(\frac{\partial \mathbf{v}}{\partial t} + \mathbf{v} \cdot \nabla \mathbf{v} \right) \cdot \mathbf{q}\ \mathrm{d}\Sigma + \int_\Sigma r \mathbf{T} \cdot \nabla \hat{\mathbf{q}}\ \mathrm{d}\Sigma = 0, \quad (5.139b)$$

$$r\mathbf{T} = -rp\mathbf{I} + r\nu \left(\nabla \mathbf{v} + (\nabla \mathbf{v})^{\mathrm{T}} \right) + rG_1 \mathbf{B}^d_{\kappa_{p_1(t)}} + rG_2 \mathbf{B}^d_{\kappa_{p_2(t)}}, \quad (5.139c)$$

$$\int_\Sigma r \left[\frac{\partial \mathbf{B}_{\kappa_{p_1(t)}}}{\partial t} + \mathbf{v} \cdot \nabla \mathbf{B}_{\kappa_{p_1(t)}} - (\nabla \mathbf{v}) \mathbf{B}_{\kappa_{p_1(t)}} - \mathbf{B}_{\kappa_{p_1(t)}} (\nabla \mathbf{v})^{\mathrm{T}} + \frac{1}{\tau_1} \mathbf{B}_{\kappa_{p_1(t)}} \mathbf{B}^d_{\kappa_{p_1(t)}} \right] \cdot \hat{\mathbf{Q}}_1\ \mathrm{d}\Sigma = 0, \quad (5.139d)$$

$$\int_\Sigma r \left[\frac{\partial \mathbf{B}_{\kappa_{p_2(t)}}}{\partial t} + \mathbf{v} \cdot \nabla \mathbf{B}_{\kappa_{p_2(t)}} - (\nabla \mathbf{v}) \mathbf{B}_{\kappa_{p_2(t)}} - \mathbf{B}_{\kappa_{p_2(t)}} (\nabla \mathbf{v})^{\mathrm{T}} + \frac{1}{\tau_2} \mathbf{B}_{\kappa_{p_2(t)}} \mathbf{B}^d_{\kappa_{p_2(t)}} \right] \cdot \hat{\mathbf{Q}}_2\ \mathrm{d}\Sigma = 0, \quad (5.139e)$$

where

$$\hat{\mathbf{q}}(r,z) = \int_0^{2\pi} \mathbf{q}(r,\varphi,z)\,\mathrm{d}\varphi, \quad \hat{\mathbf{Q}}_1(r,z) = \int_0^{2\pi} \mathbf{Q}_1(r,\varphi,z)\,\mathrm{d}\varphi, \quad \hat{\mathbf{Q}}_2(r,z) = \int_0^{2\pi} \mathbf{Q}_2(r,\varphi,z)\,\mathrm{d}\varphi \quad (5.140)$$

and all gradients are in the cylindrical coordinates.

Numerical results

We solve the problem using Finite element method that is based on weak formulation in cylindrical coordinates given by (5.139a) – (5.139e). The problem is solved on three different meshes with 40×10, 60×15 and 80×20 elements.

Pressure p / velocity $\mathbf{v}$ / tensors $\mathbf{B}_{\kappa_{p_1(t)}}$ and $\mathbf{B}_{\kappa_{p_2(t)}}$ are approximated by $\mathrm{P}_1^{\mathrm{disc}}$ / Q_2 / Q_2 elements as described in Section 5.2. Two different time schemes were used: BE time scheme and TH time scheme.

The angular velocity ω described by (4.1) changes in jumps. Instead of jumps we increase ω from zero to the desired value 0.5 rad s^{-1}, or decrease to zero smoothly on the time scale $t_1 = 0.001$s. It turns out that the result does not depend on t_1 if it is small enough. In fact, in the experiment the asphalt binder did not start/stop rotating immediately and so this approximation is very realistic.

No adaptive time step was used, it was given apriori, the lowest time step was used when the rotating started/stopped and was of the order 10^{-5}s, the largest time step was of the order 10^{-3}s (two different sets of time steps were used). We have checked, that the results are independent of the mesh, time step size and used time scheme.

We present here the result obtained with TH time scheme and the mesh containing 1600 elements (simple mesh consisting of 80×20 squares). The number of degrees of freedoms was 103 815 that is approximately 65 DOFs per one element (the set of 16 PDEs had to be solved at once using monolithic solver).

We found out that the assumptions (5.133) made in deriving ODE system were correct because it turns that the velocity magnitude in the rz direction was of the order 10^{-13} m/s, i.e. 10 magnitudes lower than in the φ direction. In the Figure 5.17 are the snapshots of the full simulation at times $t = 0.025\mathrm{s}, 0.5\mathrm{s}, 0.6\mathrm{s}, 2.0\mathrm{s}$. It can be seen that at the beginning at $t = 0.025$s when it already rotates with the full speed the clockwise vortex creates and it remains there upto $t = 0.5$s when the rotation starts to stop. After the rotation stops, the velocity in rz direction decreases, and around $t = 0.6$s the counter-clockwise vortex creates and with the increasing time the velocity decreases. The velocity in the φ direction almost does not differ from $\omega rz/h$.

We also verified that the torque M and the normal force F on the upper plate computed in the full simulation by

$$M = \int_{\Gamma_U} rT_{\varphi z}\,\mathrm{d}S = 2\pi \int_0^R r^2 T_{\varphi z}\,\mathrm{d}r, \tag{5.141}$$

$$F = \int_{\Gamma_U} T_{zz}\,\mathrm{d}S = 2\pi \int_0^R rT_{zz}\,\mathrm{d}r. \tag{5.142}$$

is the same as the torque and the normal force obtained in Chapter 4, see Figure 5.16.

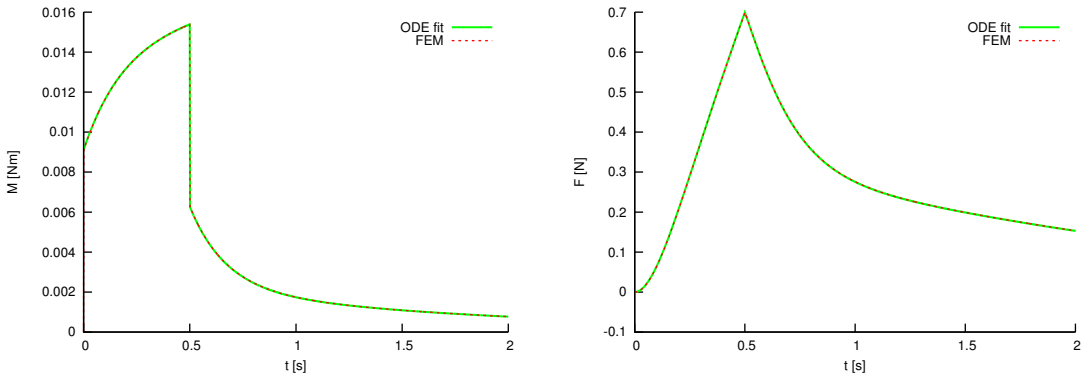

Figure 5.16: Comparison ODE and FEM.

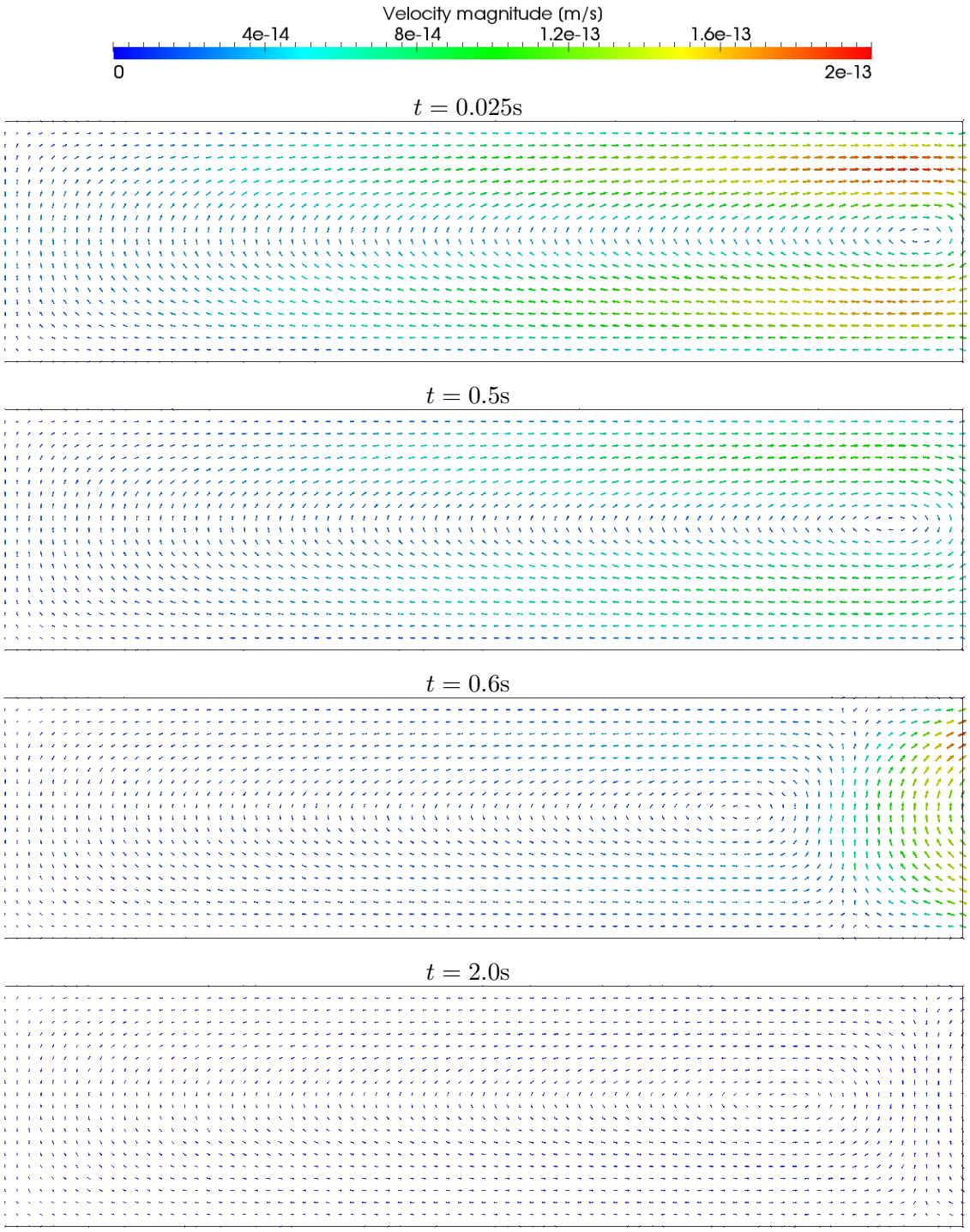

Figure 5.17: Snapshots of the full simulation of the experiment performed by Narayan et al. (2012).

5.6 Computation in the time varying domains

In this section we show the way how the problems in deforming domains are solved. Since we are using a robust Finite element code with a monolithic non-linear solver we decided to transform the equations describing the viscoelastic models – Oldroyd-B, Burgers, Quad1 and Quad2 – from Eulerian description where the domain deforms into a description with a fixed domain. In order to do this we add a new variable deformation $\hat{\mathbf{u}}$. The mapping $\hat{\varphi}$ maps fixed domain Ω_χ into the deforming domain Ω_x, see Figure 5.18.

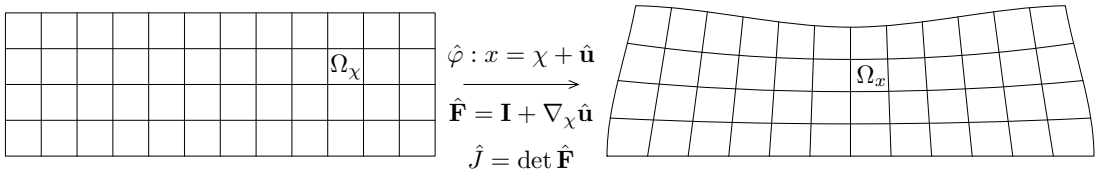

Figure 5.18: Deformation of the domain.

There are two popular ways how this transformation is made. First, the fixed domain corresponds to the Lagrangian description where all points in the domain are material points and $\mathbf{u}$ (without the hat above the letter) is the physical deformation. However, some problems, that are shown later, are connected with this approach. Second, the so-called Arbitrary Lagrangian-Eulerian (ALE) formulation where deformation $\hat{\mathbf{u}}$ is arbitrary with the restriction that the deformation is physical on the boundary of the domain. We present the application of both transformations on the example of model Quad2.

5.6.1 Lagrangian formulation

We identify the fixed computational mesh with the reference Lagrangian configuration Ω_X which is mapped into the current Eulerian configuration Ω_x (see Section 1.1) by

$$\varphi : X \to x := X + \mathbf{u}. \tag{5.143}$$

The velocity $\mathbf{v}$ is defined by

$$\mathbf{v} := \left.\frac{\partial \varphi}{\partial t}\right|_X = \frac{\partial \mathbf{u}}{\partial t}, \tag{5.144}$$

the deformation gradient $\mathbf{F}$ and its Jacobian J are defined as

$$\mathbf{F} = \frac{\partial \varphi}{\partial X} = \mathbf{I} + \nabla_X \mathbf{u}, \quad J = \det \mathbf{F}. \tag{5.145}$$

We want to solve the problem on the fixed mesh corresponding to the domain Ω_X where all the unknowns live. We use a monolithic approach and solve the problem as one big coupled system of equations including the equation for the deformation of the mesh (5.143).

We transform the Eulerian weak formulation (5.52) into the Lagrangian by substituting all derivatives with respect to x to derivatives with respect to X. We need to transform the velocity gradient $\nabla_x \mathbf{v}$ and the material time derivatives, i.e.

$$\nabla_X \mathbf{v} = \frac{\partial \mathbf{v}(\varphi(X,t),t)}{\partial X} = \frac{\partial \mathbf{v}}{\partial x}\frac{\partial \varphi}{\partial X} = (\nabla_x \mathbf{v})\mathbf{F} \quad \Rightarrow \quad \nabla_x \mathbf{v} = (\nabla_X \mathbf{v})\mathbf{F}^{-1} \tag{5.146}$$

and the material time derivatives of scalar α

$$\frac{\partial \alpha}{\partial t}\Big|_X = \frac{\mathrm{d}\alpha(\varphi(X,t),t)}{\mathrm{d}t}\Big|_X = \frac{\partial \alpha}{\partial t}\Big|_x + \frac{\partial \alpha}{\partial x}\frac{\partial \varphi}{\partial t}\Big|_X = \frac{\partial \alpha}{\partial t}\Big|_x + \mathbf{v}\cdot\nabla_x\alpha. \tag{5.147}$$

Further, the integrals over Ω_x are transformed to the integrals over Ω_X by using the integral substitution theorem. The last tool that is used in the balance of linear momentum is the Piola identity that states that $\mathrm{div}_X\left((\det\mathbf{F})\mathbf{F}^{-\mathrm{T}}\right) = 0$. Let us compute the $\mathrm{div}_x\,\mathbf{T}$ term in the weak formulation

$$\int_{\Omega_x}\mathrm{div}_x\,\mathbf{T}\cdot\mathbf{q}\,\mathrm{d}x = \int_{\Omega_X} J(\nabla_X\mathbf{T})\mathbf{F}^{-\mathrm{T}}\cdot\mathbf{q}\,\mathrm{d}X =$$

$$\int_{\Omega_X}\left(J(\nabla_X\mathbf{T})\mathbf{F}^{-\mathrm{T}} + \mathbf{T}\underbrace{\mathrm{div}_X\left(J\mathbf{F}^{-\mathrm{T}}\right)}_{0}\right)\cdot\mathbf{q}\,\mathrm{d}X = \int_{\Omega_X}\mathrm{div}_X(J\mathbf{T}\mathbf{F}^{-\mathrm{T}})\cdot\mathbf{q}\,\mathrm{d}X. \tag{5.148}$$

Using the weak formulation (5.52) the Eulerian description in Ω_x is transformed into the Lagrangian description in Ω_X

$$\int_{\Omega_X} J\,\mathrm{tr}\left((\nabla_X\mathbf{v})\mathbf{F}^{-1}\right)q\,\mathrm{d}X = 0, \tag{5.149}$$

$$\int_{\Omega_X} J\rho\frac{\partial\mathbf{v}}{\partial t}\cdot\mathbf{q}\,\mathrm{d}X - \int_{\Omega_X}\mathrm{div}_X\left(J\mathbf{T}\mathbf{F}^{-T}\right)\cdot\mathbf{q}\,\mathrm{d}X = 0, \tag{5.150}$$

$$\mathbf{T} = -p\mathbf{I} + \mu_3\left((\nabla_X\mathbf{v})\mathbf{F}^{-1} + \mathbf{F}^{-\mathrm{T}}(\nabla_X\mathbf{v})^{\mathrm{T}}\right) + G_1\mathbf{B}^d_{\kappa_{p_1(t)}} + G_2\mathbf{B}^d_{\kappa_{p_2(t)}}, \tag{5.151}$$

$$\int_{\Omega_X} J\left(\frac{\partial\mathbf{B}_{\kappa_{p_1(t)}}}{\partial t} - (\nabla_X\mathbf{v})\mathbf{F}^{-1}\mathbf{B}_{\kappa_{p_1(t)}} - \mathbf{B}_{\kappa_{p_1(t)}}\mathbf{F}^{-\mathrm{T}}(\nabla_X\mathbf{v})^{\mathrm{T}} + \frac{1}{\tau_1}\mathbf{B}_{\kappa_{p_1(t)}}\mathbf{B}^d_{\kappa_{p_1(t)}}\right)\cdot\mathbf{Q}_1\,\mathrm{d}X = 0, \tag{5.152}$$

$$\int_{\Omega_X} J\left(\frac{\partial\mathbf{B}_{\kappa_{p_2(t)}}}{\partial t} - (\nabla_X\mathbf{v})\mathbf{F}^{-1}\mathbf{B}_{\kappa_{p_2(t)}} - \mathbf{B}_{\kappa_{p_2(t)}}\mathbf{F}^{-\mathrm{T}}(\nabla_X\mathbf{v})^{\mathrm{T}} + \frac{1}{\tau_2}\mathbf{B}_{\kappa_{p_2(t)}}\mathbf{B}^d_{\kappa_{p_2(t)}}\right)\cdot\mathbf{Q}_2\,\mathrm{d}X = 0. \tag{5.153}$$

We need to add equation (5.144) to close the system of equations (unknown $\mathbf{u}$ is hidden in $\mathbf{F}$ and J).

The above formulation can be used if the changes in the domain are not too big. The main problem is in virtue of the fact that all points in the domain are material points and for example vortices in the flow can damage the deformed mesh[7]. Such example can be seen in Figure 5.19.

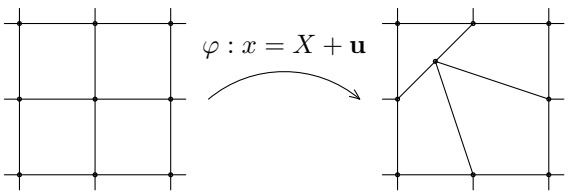

Figure 5.19: Damaged mesh in case of Lagrangian formulation.

[7]Here a monolithic approach with a fixed mesh is used, the deformation of the mesh is computed by (5.143). The damage of the mesh is a consequence of the fact that the consecutive set of linear equations creates a singular matrix (or at least a matrix with extremely high conditionally number).

5.6.2 Arbitrary Lagrangian-Eulerian formulation

In view of such difficulties with the purely Lagrangian formulation, we choose to use the ALE formulation which does not present such difficulties (for more details, see for example lecture notes [61], or papers [19], [23]). Instead of identifying the mesh with the Lagrangian domain Ω_X we identify it with a new domain Ω_χ (see Figure 5.20), where $\hat{\varphi}$ maps Ω_χ into Ω_x by

$$\hat{\varphi} : \chi \to x := \chi + \hat{\mathbf{u}}, \tag{5.154}$$

where $\hat{\mathbf{u}}$ is an arbitrary deformation (i.e. the deformation of the mesh). If the time derivative of $\hat{\mathbf{u}}$ was equal to the velocity $\mathbf{v}$ then all points would be the material points, $\Omega_\chi = \Omega_X$ and we would obtain the Lagrange formulation. Instead of this we only require to have the material points on the boundary $\partial\Omega_\chi$, inside the domain Ω_χ we just need to have a unique solution for $\hat{\mathbf{u}}$, for simplicity we use a Laplace equation, i.e.

$$\hat{\mathbf{u}} = \begin{cases} \dfrac{\partial \hat{\mathbf{u}}}{\partial t} = \mathbf{v} & \text{on } \partial\Omega_\chi \\ -\Delta_\chi \hat{\mathbf{u}} = 0 & \text{inside } \Omega_\chi. \end{cases} \tag{5.155}$$

We define the deformation gradient and its Jacobian by

$$\hat{\mathbf{F}} = \frac{\partial \hat{\varphi}}{\partial \chi} = \mathbf{I} + \nabla_\chi \hat{\mathbf{u}}, \quad \hat{J} = \det \hat{\mathbf{F}}. \tag{5.156}$$

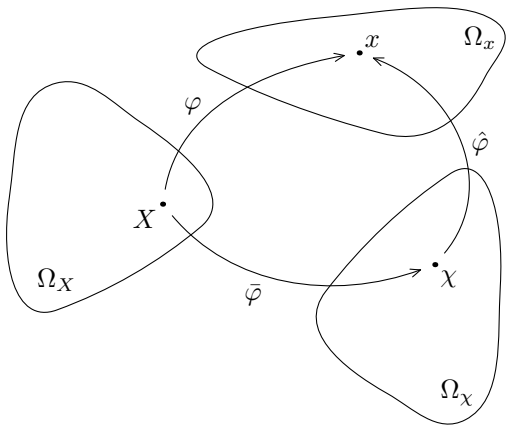

Figure 5.20: ALE formulation.

The same procedure as in the Lagrangian case is used to transform (5.52) from Ω_x to Ω_χ. The velocity gradient transforms in the same way as before

$$\nabla_\chi \mathbf{v} = \frac{\partial \mathbf{v}(\hat{\varphi}(\chi,t),t)}{\partial \chi} = \frac{\partial \mathbf{v}}{\partial x}\frac{\partial \hat{\varphi}}{\partial \chi} = (\nabla_x \mathbf{v})\hat{\mathbf{F}} \quad \Rightarrow \quad \nabla_x \mathbf{v} = (\nabla_\chi \mathbf{v})\hat{\mathbf{F}}^{-1}. \tag{5.157}$$

The transformation of the material time derivative is more difficult, first we compute

$$\frac{\partial \alpha}{\partial t}\Big|_\chi = \frac{\mathrm{d}\alpha(\hat{\varphi}(\chi,t),t)}{\mathrm{d}t}\Big|_\chi = \frac{\partial \alpha}{\partial t}\Big|_x + \frac{\partial \alpha}{\partial x}\frac{\partial \hat{\varphi}}{\partial t}\Big|_\chi = \frac{\partial \alpha}{\partial t}\Big|_x + \frac{\partial \hat{\mathbf{u}}}{\partial t}\cdot \nabla_x \alpha. \tag{5.158}$$

Using (5.158) we obtain

$$\begin{aligned}\frac{\partial\alpha}{\partial t}\Big|_x + \mathbf{v}\cdot\nabla_x\alpha &= \frac{\partial\alpha}{\partial t}\Big|_\chi + \left(\mathbf{v} - \frac{\partial\hat{\mathbf{u}}}{\partial t}\right)\cdot\nabla_x\alpha \\ &= \frac{\partial\alpha}{\partial t}\Big|_\chi + \left(\mathbf{v} - \frac{\partial\hat{\mathbf{u}}}{\partial t}\right)\cdot(\nabla_\chi\alpha)\hat{\mathbf{F}}^{-1} \\ &= \frac{\partial\alpha}{\partial t}\Big|_\chi + \left(\hat{\mathbf{F}}^{-1}\left(\mathbf{v} - \frac{\partial\hat{\mathbf{u}}}{\partial t}\right)\right)\cdot\nabla_\chi\alpha. \end{aligned} \tag{5.159}$$

Using (5.157), (5.159), the integral substitution theorem and Piola identity as in the Lagrangian case we transform the weak formulation (5.52) to

$$\int_{\Omega_\chi} \hat{J}\,\mathrm{tr}\left((\nabla_\chi\mathbf{v})\hat{\mathbf{F}}^{-1}\right) q\,\mathrm{d}\chi = 0, \tag{5.160a}$$

$$\int_{\Omega_\chi} \hat{J}\rho\left[\frac{\partial\mathbf{v}}{\partial t} + (\nabla_\chi\mathbf{v})\left(\hat{\mathbf{F}}^{-1}\left(\mathbf{v} - \frac{\partial\hat{\mathbf{u}}}{\partial t}\right)\right)\right]\cdot\mathbf{q}\,\mathrm{d}\chi - \int_{\Omega_\chi}\mathrm{div}_\chi\left(\hat{J}\hat{\mathbf{T}}\hat{\mathbf{F}}^{-T}\right)\cdot\mathbf{q}\,\mathrm{d}\chi = 0, \tag{5.160b}$$

$$\hat{\mathbf{T}} = -p\mathbf{I} + \mu_3\left((\nabla_\chi\mathbf{v})\hat{\mathbf{F}}^{-1} + \hat{\mathbf{F}}^{-\mathrm{T}}(\nabla_\chi\mathbf{v})^{\mathrm{T}}\right) + G_1\mathbf{B}^d_{\kappa_{p_1(t)}} + G_2\mathbf{B}^d_{\kappa_{p_2(t)}}, \tag{5.160c}$$

$$\begin{aligned}\int_{\Omega_\chi}\hat{J}\Bigg[&\frac{\partial\mathbf{B}_{\kappa_{p_1(t)}}}{\partial t} + (\nabla_\chi\mathbf{B}_{\kappa_{p_1(t)}})\left(\hat{\mathbf{F}}^{-1}\left(\mathbf{v} - \frac{\partial\hat{\mathbf{u}}}{\partial t}\right)\right) \\ &-(\nabla_\chi\mathbf{v})\hat{\mathbf{F}}^{-1}\mathbf{B}_{\kappa_{p_1(t)}} - \mathbf{B}_{\kappa_{p_1(t)}}\hat{\mathbf{F}}^{-\mathrm{T}}(\nabla_\chi\mathbf{v})^{\mathrm{T}} + \frac{1}{\tau_1}\mathbf{B}_{\kappa_{p_1(t)}}\mathbf{B}^d_{\kappa_{p_1(t)}}\Bigg]\cdot\mathbf{Q}_1\,\mathrm{d}\chi = 0, \end{aligned} \tag{5.160d}$$

$$\begin{aligned}\int_{\Omega_\chi}\hat{J}\Bigg[&\frac{\partial\mathbf{B}_{\kappa_{p_2(t)}}}{\partial t} + (\nabla_\chi\mathbf{B}_{\kappa_{p_2(t)}})\left(\hat{\mathbf{F}}^{-1}\left(\mathbf{v} - \frac{\partial\hat{\mathbf{u}}}{\partial t}\right)\right) \\ &-(\nabla_\chi\mathbf{v})\hat{\mathbf{F}}^{-1}\mathbf{B}_{\kappa_{p_2(t)}} - \mathbf{B}_{\kappa_{p_2(t)}}\hat{\mathbf{F}}^{-\mathrm{T}}(\nabla_\chi\mathbf{v})^{\mathrm{T}} + \frac{1}{\tau_2}\mathbf{B}_{\kappa_{p_2(t)}}\mathbf{B}^d_{\kappa_{p_2(t)}}\Bigg]\cdot\mathbf{Q}_2\,\mathrm{d}\chi = 0. \end{aligned} \tag{5.160e}$$

This set of equations is closed with the equation (5.155) written in the weak formulation as

$$\int_{\Omega_\chi}\nabla_\chi\hat{\mathbf{u}}\cdot\nabla_\chi\mathbf{t}\,\mathrm{d}\chi = 0. \tag{5.161}$$

5.6.3 Finite element method for ALE formulation

In order to compute problems with deforming domains numerically, a discrete approximation has to be introduced, here the Finite element method is used a described in Section 5.2. It is based on the weak formulation consisting of (5.160) and (5.161) with one difference in the balance of linear momentum where the divergence theorem is used

$$\int_{\Omega_\chi}\hat{J}\rho\left[\frac{\partial\mathbf{v}}{\partial t} + (\nabla_\chi\mathbf{v})\left(\hat{\mathbf{F}}^{-1}\left(\mathbf{v} - \frac{\partial\hat{\mathbf{u}}}{\partial t}\right)\right)\right]\cdot\mathbf{q}\,\mathrm{d}\chi = -\int_{\Omega_\chi}\hat{J}\hat{\mathbf{T}}\hat{\mathbf{F}}^{-T}\cdot\nabla_\chi\mathbf{q}\,\mathrm{d}\chi + \int_{\partial\Omega_\chi}\left(\hat{J}\hat{\mathbf{T}}\hat{\mathbf{F}}^{-T}\right)\mathbf{n}_\chi\cdot\mathbf{q}\,\mathrm{d}S_\chi, \tag{5.162}$$

where $\mathbf{n}_\chi$ is the outer unit normal vector in the domain Ω_χ. The last term in (5.162) is used for prescribing the Neumann boundary condition. To be precise, we prescribe $\left(\hat{J}\hat{\mathbf{T}}\hat{\mathbf{F}}^{-T}\right)\mathbf{n}_\chi$ as a force acting on the part of boundary $\partial\Omega_\chi$. This means that we prescribe a vector that is parallel with the normal vector in the actual configuration and so we can easily push the material perpendicular to the boundary. For the sake of simplicity, when we discuss the boundary conditions later in the text instead of writing the component $(\hat{J}\hat{\mathbf{T}}\hat{\mathbf{F}}^{-T})_{ij}$ we will write the component as T_{ij}.

Time derivatives in (5.160) are implicitly fully mixed (see for example the transformed convective terms). Since it was not clear to us how for example CR time scheme

should be implemented, BE time scheme and GL time scheme are used. In space pressure p / velocity $\mathbf{v}$ / deformation $\hat{\mathbf{u}}$ / tensors $\mathbf{B}_{\kappa_{p_1(t)}}$ and $\mathbf{B}_{\kappa_{p_2(t)}}$ are approximated by P_1^{disc} / Q_2 / Q_2 / Q_2 / Q_2 elements.

Using ALE method several problems that differ only in the domain and the boundary conditions are computed. In all problems the material is at rest at $t = 0$, the initial conditions are

$$p(0) = 0, \quad \hat{\mathbf{u}}(0) = \mathbf{0}, \quad \mathbf{v}(0) = \mathbf{0}, \tag{5.163}$$

$$\mathbf{B}(0) = \mathbf{B}_{\kappa_{p(t)}}(0) = \mathbf{I} \text{ for Oldroyd-B model and model Quad1,} \tag{5.164}$$

$$\mathbf{B}_1(0) = \mathbf{B}_2(0) = \mathbf{I} \text{ for Burgers model,} \tag{5.165}$$

$$\mathbf{B}_{\kappa_{p_1(t)}}(0) = \mathbf{B}_{\kappa_{p_2(t)}}(0) = \mathbf{I} \text{ for model Quad2.} \tag{5.166}$$

The boundary conditions are different in each problem, but all problems have the same Dirichlet boundary condition given by (5.155)

$$\frac{\partial \hat{\mathbf{u}}}{\partial t} = \mathbf{v} \text{ on } \partial\Omega.$$

5.7 Numerical simulations in the deforming domains

We use the ALE method for simulation of four problems with viscoelastic material in deforming domains.

The first problem is a square made from a material described by Oldroyd-B model and model Quad1 and this square is pushed in order to rotate. We use this problem to compare BE time scheme and GL time scheme and we show that GL time scheme is much better for describing the problems with deforming domains.

The second problem is a block of viscoelastic material that is initially at rest and it is suddenly compressed with a constant load on a part of the top surface of the block and after 0.5s the force is released. This problem is computed with all four models: Oldroyd-B, Burgers, Quad1 and Quad2 and we study how the response of the material depends on chosen material parameters. This problem is also used to show the dependence of the solution on time step Δt, mesh size h and perturbation of inner nodes of the mesh.

The third problem is a generalization of the second problem, repeated application of force at two different locations is considered which is connected to the problem of rutting that is observed on roadways due to the loading of the roadways by transportation vehicles. This problem is computed with the model Quad2 using both unrealistic and also realistic material parameters that were obtained by fitting unaged polymer modified asphalt binder.

In the fourth problem, we consider a load that is moving on the top surface which is connected with the problem of rolling of asphalt. The problem is computed with the model Quad2 using the same material parameters as in the third problem.

5.7.1 Spinning of a square from the viscoelastic material

The first problem with deforming domain that we compute is a problem of a spinning of a square that is made from viscoelastic material described by model Quad1. In this problem the square with the side $a = 1$ m is pushed for $0 \leq t \leq 0.2$s asymmetrically with respect to its center, so it starts to rotate, see Figure 5.21. It is pushed with

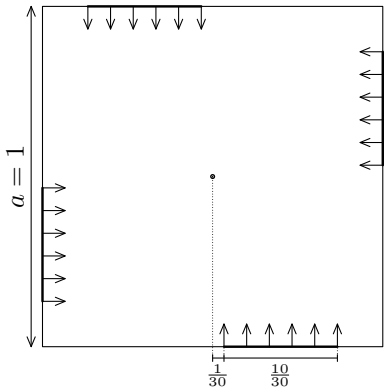

Figure 5.21: Spinning of a square made from viscoelastic material.

constant normal stress $p_p = 3$ kPa at four areas. The following material parameters are used: density $\rho = 1000$ kg.m^{-3}, solvent viscosity $\mu_2 = 100$ Pa s, elastic modulus $G = 1000$ Pa, relaxation time $\tau = 2.0$s.

In case that the square was rigid, it would obtain the angular momentum

$$L_{\text{rigid}} = 4 \int_{t_1=0}^{t_2=0.2} \int_{r_1=1/30}^{r_2=11/30} r p_p \, \mathrm{d}r \, \mathrm{d}t = 160\text{Nm s}. \tag{5.167}$$

Since no external force is applied on the square after the pushing, the balance of angular momentum says that the angular momentum L has to be preserved.

We use this problem to show the influence of the chosen time scheme on the result. We compute this problem using two different time schemes as described in Section 5.2 – standard backward Euler time scheme (BE) and less usual Glowinski time scheme (GL) – on one fixed mesh (30×30, refined locally near the boundary, 40 000 DOFs)[8]. The problem is computed with three different time steps Δt, see Table 5.2, at the beginning for $t \leq 0.3$, when the square starts to rotate, four times smaller current time step Δt^c is used, i.e.

$$\Delta t^c = \begin{cases} \frac{1}{4}\Delta t & t \leq 0.3 \\ \Delta t & t > 0.3. \end{cases}$$

The time step Δt for GL time scheme is twice greater than the time step for BE time scheme because GE time scheme is two times more CPU time consuming. We show that the first order backward Euler time scheme is not sufficient for these problems.

Time scheme	Time steps Δt [s]		
BE	0.005	0.01	0.02
GL	0.01	0.02	0.04

Table 5.2: Sets of time steps Δt used for the simulation of rotating square.

We compute the angular momentum of the square in the computational domain Ω_χ

[8]We computed the problem also on a coarser mesh and found out that the differences caused by different time schemes are significantly higher than the differences caused by the resolution of the mesh.

by

$$L = \int_{\Omega_x} \rho \mathbf{r} \times \mathbf{v} \, \mathrm{d}x = \int_{\Omega_\chi} \hat{J}(\mathbf{r}_\chi + \hat{\mathbf{u}}) \times \mathbf{v} \, \mathrm{d}\chi, \tag{5.168}$$

where $\mathbf{r}_\chi$ is the position vector in Ω_χ. The volume V is computed by

$$V = \int_{\Omega_x} 1 \, \mathrm{d}x = \int_{\Omega_\chi} \hat{J} \, \mathrm{d}\chi \tag{5.169}$$

and the kinetic energy E_k is computed by

$$E_k = \int_{\Omega_x} \frac{1}{2} \rho |\mathbf{v}|^2 \, \mathrm{d}x = \int_{\Omega_\chi} \frac{1}{2} \hat{J} \rho |\mathbf{v}|^2 \, \mathrm{d}\chi. \tag{5.170}$$

The comparison of angular momentum L, volume V and kinetic energy E_k for two time schemes each with three different sets of time steps is depicted in Figure 5.23. First we verified how the angular momentum L is preserved, Figures 5.23(ab). We found out that BE time scheme does not preserve this quantity for any time step Δt and L decreases with time t, for smaller time step Δt the descent is lower. The other time scheme GL is much better, the angular momentum L is almost constant, it slightly increases with the time t, for smaller time step Δt the increase is smaller. The computed value $L \approx 172$ Nms is similar to the value L_{rigid} given by (5.167).

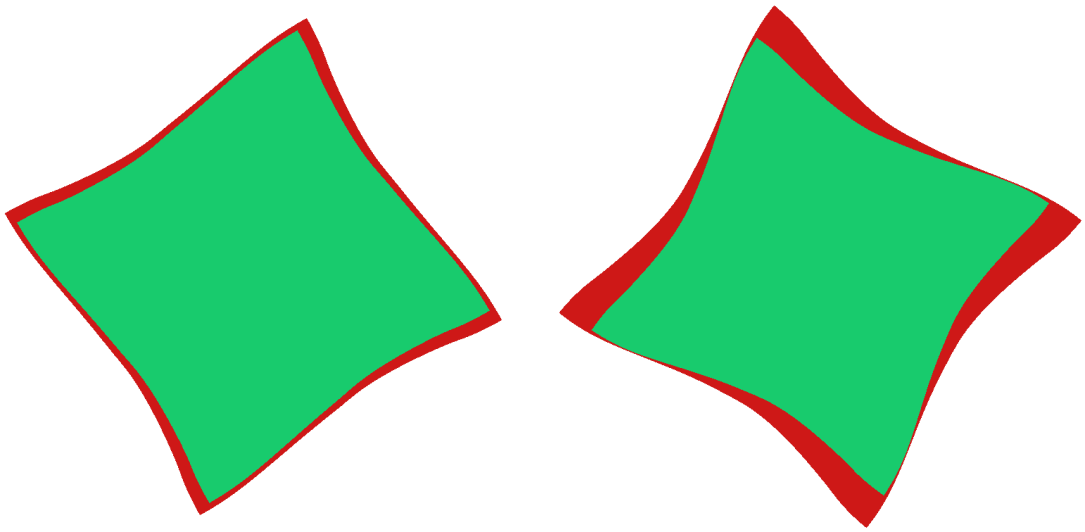

(a) $t = 10$s (b) $t = 20$s

Figure 5.22: Comparison of BE (green) and GL (red) time schemes, both $\Delta t = 0.01$, BE does not preserve volume.

After watching the movie of the full simulation (which is attached on the DVD) we found out that the incompressibility is violated, concretely the volume of the material is decreasing in case where BE time scheme was used, see Figures 5.23(cd). The comparison of the solution for BE and GL time schemes at $t = 10$s and $t = 20$s is depicted in Figure 5.22, BE time scheme does not preserve the volume V.

The graph of kinetic energy E_k is depicted in Figure 5.23(ef), one can see that in case of BE time scheme E_k decreases faster with larger time step, this is caused because

the volume is decreasing, results for GL time scheme are almost the same for all time steps. Further, it can be seen in Figure 5.22(f) that the amplitude of peak of the kinetic energy E_k around time $t = 0.5$s changes significantly less with changing time step Δt for GL time scheme. The amplitude of peak of the kinetic energy E_k obtained by BE time scheme converge with decreasing time step Δt to the value obtained by GL time scheme .

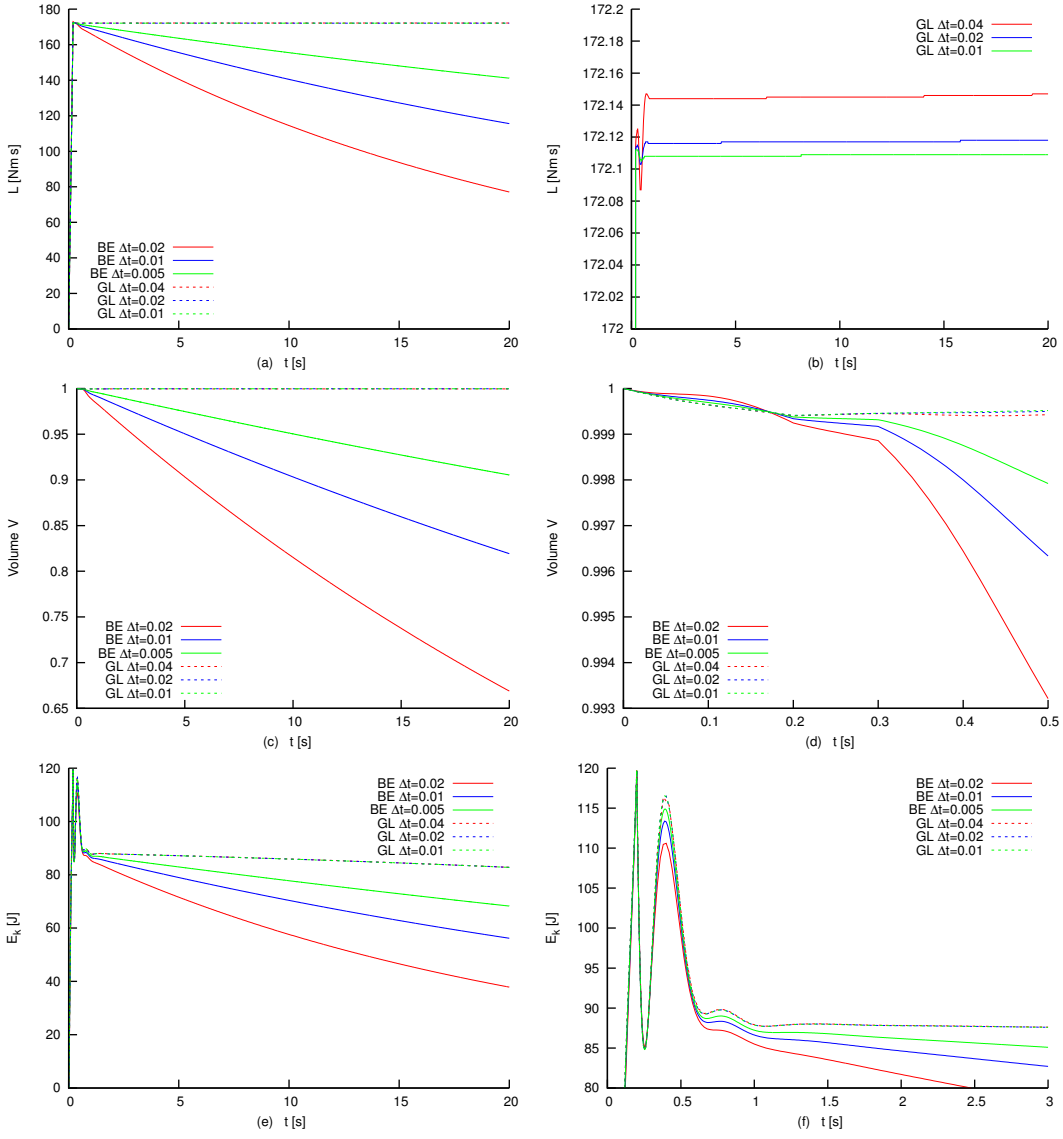

Figure 5.23: Comparison of BE and GL time schemes using (a), (b): angular momentum L, (c), (d): volume V and (e), (f): kinetic energy E_k, zooms of the graphs are depicted in the right columns (b), (d) and (f).

Results obtained in this problem lead us to the conclusion that for problems in deforming domains GL time scheme is much better than BE time scheme and we will use only GL time scheme. In the next Subsection we show the convergence analysis

with respect to the time step and the mesh size.

We computed this problem also using Oldroyd-B model with the same material parameters. We found out that the difference in the solution is very small, similar to the difference caused by numerical discretization. This is probably caused because the applied force is not big enough to create high stresses in the material.

5.7.2 Benchmark – pressing of the rectangular piece of viscoelastic material

In this problem let us consider a rectangular piece of material, see Figure 5.24. Its width is 3m, the height is 1m.[9] The material is put on the ground where it can fully slip in the x-direction, but it can not move in the y-direction. All other sides of the rectangle can freely move. We ignore the effect of gravity. At $t = 0$ the material is at rest and does not move. Suddenly at time $t = 0$ the body is pushed at the top by a constant normal stress $T_{yy} = -5$ kPa. This stress acts till the time $t = 0.5$s, and then it suddenly ceases to exist. We observe how the boundary continues to deform after the applied traction ceases.

The boundary conditions are:

Bottom Dirichlet: $v_y = 0$, Neumann: $T_{xy} = 0$

Top and sides Neumann: $\mathbf{Tn} = \mathbf{0}$, during the pressing $T_{yy} = -5$ kPa on a part of the boundary.

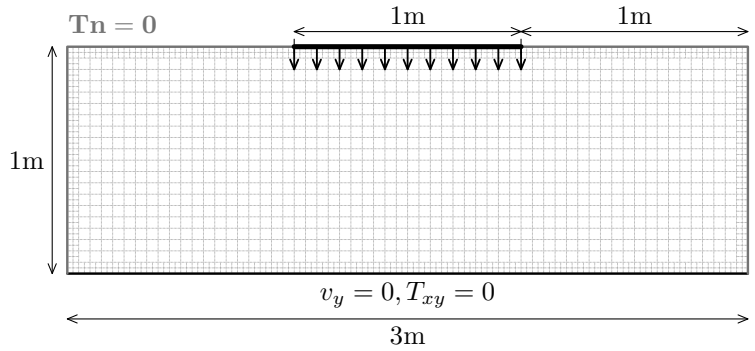

Figure 5.24: Pressing of the rectangular piece of viscoelastic material.

We solve this problem using 4 different models – Oldroyd-B, Burgers, Quad1 and Quad2 model – with the material parameters given by Table 5.3. In case of the model with only one relaxation time τ and one elastic modulus G, these parameters[10] are given in the column corresponding to τ_1 and G_1. Density $\rho = 1000$ kg/m^3 in all cases. All problems are computed on a fixed mesh 60×20 (locally refined near the boundary) with constant time step $\Delta t = 0.01$ and GL time scheme.

[9] We use a thick layer of viscoelastic material in order to capture elastic response. Later, we shall use much thinner domains as an application we have in mind are pavements which are usually modeled as rate type viscoelastic fluids, which are much wider than thick.

[10] In fact, Oldroyd-B model with material parameters μ_2, τ, G is equivalent to Burgers model with $G_1 + G_2 = G$ and $\tau_1 = \tau_2 = \tau$ and the same holds for model Quad1 and model Quad2. We numerically verified this equivalence.

Model	μ_3 [Pa s]	τ_1 [s]	τ_2 [s]	G_1 [kPa]	G_2 [kPa]
Oldroyd-B	100.0	0.2	—	15.0	—
	100.0	0.8	—	15.0	—
	100.0	2.0	—	15.0	—
Burgers	100.0	0.2	2.0	10.0	5.0
Quad1	100.0	0.2	—	15.0	—
	100.0	0.8	—	15.0	—
	100.0	2.0	—	15.0	—
Quad2	100.0	0.2	2.0	10.0	5.0

Table 5.3: Material parameters used in the simulation of rectangle compression for each model.

We found out that the differences in the solution between Burgers model and model Quad2, and between Oldroyd-B model and model Quad1 are very small, comparable to the difference obtained with different mesh size or different time step. Hence, presented results of models Quad1 and Quad2 are very similar to the results of the standard viscoelastic models. However, note that standard linear models are incapable of capturing experimental data in another physical settings (even in the full simulation, see Subsection 5.5) and one can not simply state that the models give the same results.

In case of the model Quad2 two relaxation times are $\tau = 0.2$s and $\tau = 2.0$s. The elastic moduli G_1 and G_2 in model Quad2 determine the weights corresponding to the relaxation times τ_1 and τ_2. The more G_1 is higher than G_2, the more the material behaves as a material with the relaxation time τ_1 as the dominant relaxation time. That is why we also use a model Quad1 with relaxation time $\tau = 0.8$s which is a weighted average of the previous two in the sense

$$\tau = \frac{G_1\tau_1 + G_2\tau_2}{G_1 + G_2}.$$

We will see that the steady solution of the model Quad1 with this averaged relaxation time and the model Quad2 is almost the same.

We carried out the full simulations for four materials described by non-linear model Quad1 and Quad2 listed in Table 5.3 and we have a fully dynamic movie of the response of each of these materials from which we have picked five snapshots of the deformation of the top side (lateral sides are not depicted). Figure 5.25 depicts how the y-component of the deformation at the center line depends on time. Vertical lines in the graph denote the times when the snapshots are captured: 0.53s (minimum for model Quad2), 0.7s, 0.94s (maximum for model Quad1 with $\tau = 2.0$s) and 1.14s (maximum for model Quad2). The snapshots are depicted in Figure 5.26.

In [22] we computed this problem also with the standard models with zero Newtonian viscosity (i.e. Maxwell and Burgers without additional Newtonian dissipation), and we found out that the materials described with these models behave more elastically and oscillate more than the models with corresponding non-zero Newtonian viscosity.

Further model Quad1 with relaxation time $\tau = 2.0$s exhibits both elasticity and damping, and the material with relaxation time $\tau = 0.8$s exhibits with similar behavior but with less elasticity (or with more damping). The material having a relaxation time $\tau = 0.2$s behaves mostly like a fluid, on pressing the top surface there is only one small

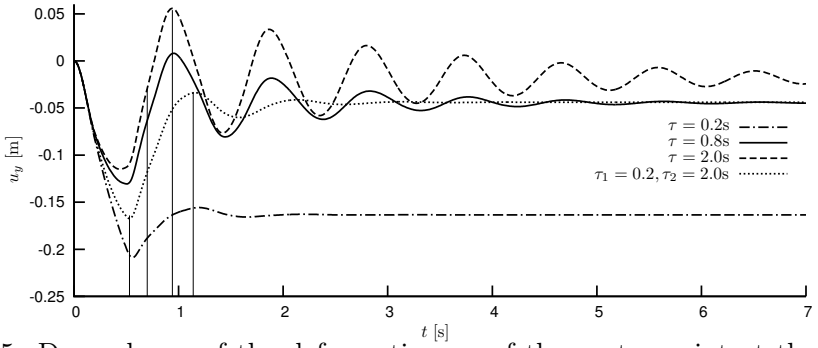

Figure 5.25: Dependency of the deformation u_y of the center point at the top surface with time t. Vertical lines: 0.53s, 0.7s, 0.94s, 1.14s.

wave and the material remains deformed. The most interesting response characteristics are exhibited by the model Quad2 with relaxation times $\tau_1 = 0.2$s, $\tau_2 = 2.0$s, in that the displacement after an initial oscillation remains essentially constant with the value very close to that of model Quad1 with the relaxation time $\tau = 0.8$s.

All the simulations were carried out upto the time $t = 40.0$s when even the viscoelastic fluid with the greatest elastic response ceases to deform further.

The snapshots in Figure 5.26 show that in the case of model Quad1 with $\tau = 2.0$s the shape of the surface at its maximum is almost concave compared to the other materials. Further it can be seen that at time 40.0s when all materials cease to deform, the deformations of model Quad2 with $\tau_1 = 0.2$s, $\tau_2 = 2.0$s and model Quad1 with $\tau = 0.8$s are almost the same (dotted line merges the dot-and-dashed line), that is, asymptotically in time both these models have the same response, though their transient response is different.

Convergence and mesh stability analysis

To verify that our simulations are correct we computed this problem with Oldroyd-B model with $\tau = 0.8$s on four different meshes (see Table 5.4) and with four different time steps. All meshes are locally refined near the boundary, in the Table 5.4 the dimensions of the mesh before the local refinement are provided. The mesh size h is computed from the refined elements. Table 5.4 also contains information about the dimension of the system of linear equations and the solver that was used.

	mesh dimension	mesh size h	$1/h$	# DOFs	lin. solver
mesh1	15×5	0.1	10	6 016	umfpack
mesh2	30×10	0.05	20	16 991	umfpack
mesh3	60×20	0.025	40	52 891	umfpack
mesh4	120×40	0.0125	80	180 491	gmres

Table 5.4: Parameters for the meshes used in converge analysis for the problem of the compression of rectangle, corresponding number of degrees of freedom and the linear solver that was used.

We computed the problem with four different constant time steps: 0.05s, 0.02s, 0.01s

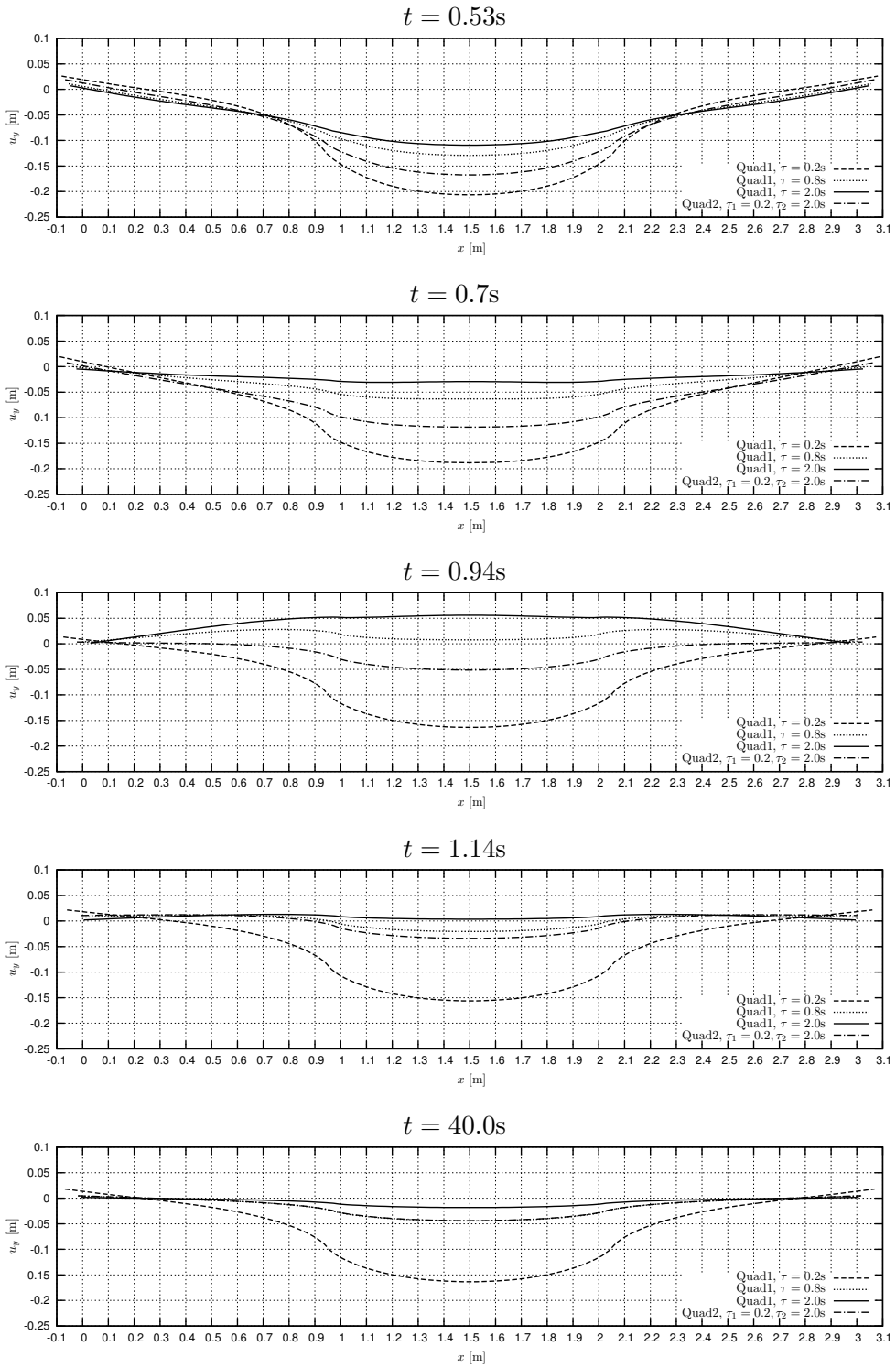

Figure 5.26: Snapshots of the top side at five different times for models Quad1 and Quad2.

and 0.005s (CPU time on mesh4 with $\Delta t = 0.0005$s was 16 days), GL time scheme was used. We compared the deformation u_y in the middle of the top side and the kinetic energy of the whole body

$$E_k = \int_{\Omega_x} \frac{1}{2}\rho|\mathbf{v}|^2 \,\mathrm{d}x = \int_{\Omega_\chi} \hat{J}\frac{1}{2}\rho|\mathbf{v}|^2 \,\mathrm{d}\chi$$

at time $t = 0.6$s (0.1s after the release of the force) and time $t = 20$s when the material with this relaxation time is almost at rest[11], see Tables 5.5, 5.6 and 5.7.

mesh\timestep	0.05	0.02	0.01	0.005
mesh1	-0.10926	-0.10857	-0.10852	-0.10851
mesh2	-0.10675	-0.10603	-0.10598	-0.10597
mesh3	-0.10604	-0.10531	-0.10526	-0.10525
mesh4	-0.10573	-0.10498	-0.10493	-0.10492

Table 5.5: Deformation u_y at the middle of the top surface at $t = 0.6$s for all four meshes and all four time steps with GL time scheme.

mesh\timestep	0.05	0.02	0.01	0.005
mesh1	97.6757	96.8109	96.6711	96.6358
mesh2	95.4497	94.5366	94.3909	94.3542
mesh3	94.3437	93.4059	93.2570	93.2195
mesh4	93.7926	92.8423	92.6919	92.6540

Table 5.6: Kinetic energy E_k at $t = 0.6$s for all four meshes and all four time steps with the GL time scheme.

mesh\timestep	0.05	0.02	0.01	0.005
mesh1	-0.0452265	-0.0452183	-0.0452161	-0.0452156
mesh2	-0.0443225	-0.0443169	-0.0443155	-0.0443152
mesh3	-0.0441374	-0.0441317	-0.0441305	-0.0441301
mesh4	-0.0440739	-0.0440683	-0.0440671	-0.0440667

Table 5.7: Deformation u_y in the middle of the top side at $t = 20.0$s for all four meshes and all four time steps with GL time scheme.

Using these data we computed the relative error related to the the value obtained with the smallest time step $\Delta t = 0.005$s and the densest mesh4. We have plotted the dependence of the relative error on the mesh size h and the time step Δt in Figures 5.27 (a) – (f) in log-log scale.

The plots show that the relative error is decreasing with the mesh size h and the time step Δt, and the experimental order of convergence with regard to space is between h and h^2 and for time of the order between Δt^2 and Δt^3, for the densest mesh. In the

[11] Kinetic energy E_k is not compared at $t = 20$s because it is numerically equal to zero.

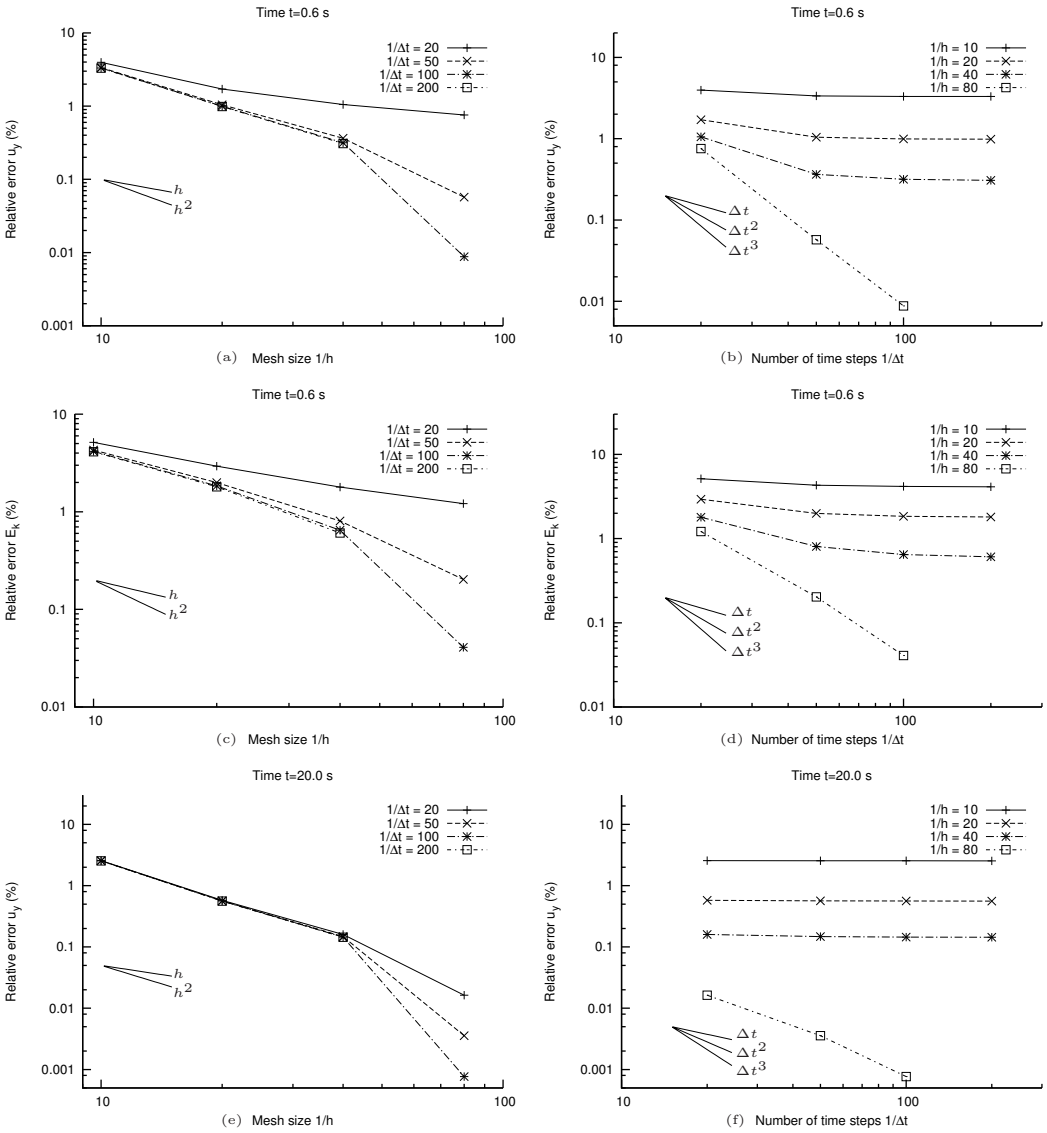

Figure 5.27: (a), (b): Dependence of the relative error of deformation u_y on the mesh size h and the time step Δt at $t = 0.6$s, (c), (d): relative error for E_k for the mesh size h and time step Δt at $t = 0.6$s, (e), (f):relative error for u_y for the mesh size h and the time step Δt at $t = 20$s.

graphs a combination of discretization errors (space+time) is depicted. In case of the coarse mesh the space discretization error is much higher than the time discretization error and so the relative error decreases very slowly with smaller time step and vice versa the relative error decreases slower with a smaller mesh size for a long time step.

Mesh stability We compared the result obtained with mesh3 and time step $\Delta t = 0.01$ with the results obtained with the meshes where all inner nodes are randomly perturbed by 20% of h (mesh3d20) and 25% of h (mesh3d25, see Figure 5.28). The computational

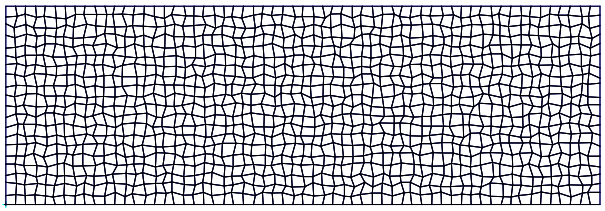

Figure 5.28: Mesh3d25 is mesh3 where all inner nodes are randomly perturbed by 25% of h (before refinement).

mesh is again the mesh locally refined near the boundary. In Table 5.8 one can see the deformation u_y at the center of the top surface and kinetic energy E_k at times $t = 0.6$s and $t = 20$s for these meshes. The change of relative error caused by the perturbed mesh

	u_y at $t = 0.6$	u_y at $t = 20$	E_k at $t = 0.6$
mesh3	-0.1052579	-0.04413047	93.2570
mesh3d20	-0.1052592	-0.04413016	93.2864
mesh3d25	-0.1052596	-0.04413021	93.2936

Table 5.8: Comparison of the results for perturbed meshes in the problem of rectangle compression.

is very small, approximately 200 times smaller than the relative error of u_y observed in the convergence analysis for mesh3 and $\Delta t = 0.01$ and approximately 20 times smaller than the relative error of E_k.

5.7.3 Rutting in the road

The problem that we study next is connected to the problem of rutting that is observed on roadways due to the loading of the roadways by heavy transportation vehicles. The tires of these vehicles constantly go over a small part of the roadway and one can clearly observe the depression that is made on the roadway.

We assume that the roadway is made from material described by model Quad2, the material parameters are given in Table 5.3. Let us consider a rectangular piece of roadway as given in Figure 5.29. The width is 3m, the height is 0.2m. The vehicles are assumed to move along the z-direction and the tires of the vehicles apply a load on the roadway as shown. We have assumed that the tires are 0.25m wide. At the bottom surface we will assume that the material can fully slip in the x-direction, but it can not

move in the y-direction. The material can not flow through the lateral sides but it can fully slip in the y-direction. It can freely move on the top.

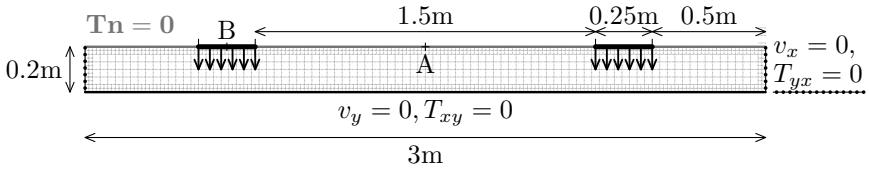

Figure 5.29: Problem of rutting in the road.

The material is pushed by constant normal stress $T_{yy} = -2$ kPa due to the contact of the tires with the roadway as depicted in Figure 5.29. Let us assume that there are twenty passes of the vehicles over a particular region and that the tire of vehicle stays in contact with the roadway at that location for 0.5s. Let us also assume the time interval between two vehicles approaching the same location is 3.5s. Thus, the body is given 3.5s to relax. Let us suppose that the material is pressed between the times t_1^k and t_2^k, where $t_1^k = (4.0k)$s and $t_2^k = (0.5 + 4.0k)$s for $k = 0, \ldots, 19$.

The boundary conditions are:

Bottom surface Dirichlet: $v_y = 0$, Neumann: $T_{xy} = 0$

Lateral sides Dirichlet: $v_x = 0$, Neumann: $T_{yx} = 0$

Bottom corners Dirichlet: $v_x = v_y = 0$

Top surface Neumann: $\mathbf{Tn} = \mathbf{0}$, during the pressing $T_{yy} = -2$ kPa on a part of the boundary.

The problem is computed on a fixed mesh 90×6 (locally refined near the boundary) with constant time step $\Delta t = 0.01$ and GL time scheme.

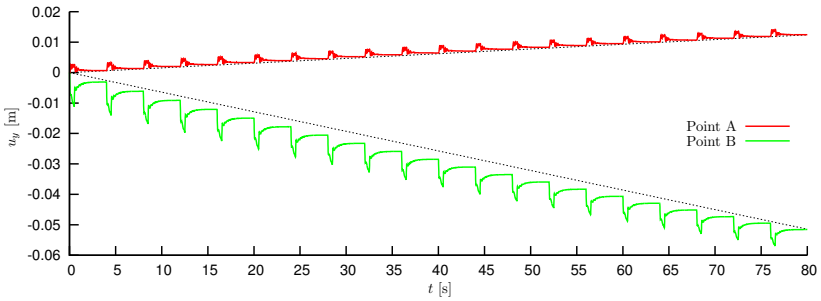

Figure 5.30: The time dependence of the deformation u_y at the points A (upper line) and B (lower line).

The time dependence of the deformation u_y of two points A and B on the top surface (see Figure 5.29) is depicted in Figure 5.30. We observe that the deformation u_y is non-linear with time t, for the point B this can be seen clearly (compare with the dotted linear line), in case of point A the deformation is also non-linear but this can not be

seen in the presented scale. The non-linear deformation is caused because the non-linear model was used and it is also the result of the boundary condition at the bottom.

In Figure 5.31 we depict the result of compressing a roadway. For the purpose of illustration, only the evolution of the deformation of the top surface with time for their first, the tenth and the twentieth compression is portrayed. Each compression is drawn in a different color. The beginning of the compression is denoted by a dotted line and the end by a dashed line and the deformation four seconds after the beginning of the compression by a solid line. It can be seen that the material is most deformed during the first compression, and least deformed during the last twentieth compression.

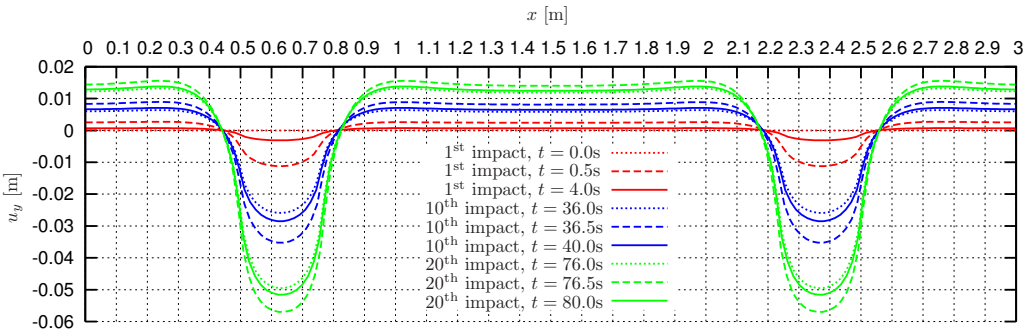

Figure 5.31: Time snapshots of the top side depicting the first (red line), the tenth (blue line) and the twentieth (green line) application of force. Corresponding to these applications of compressive loads at the top surface the beginning of the application by a dotted line, the end of the application by a dashed line and the deformation four seconds after the beginning of the application by a solid line.

The movie of the full simulation is attached on the DVD, the problem was computed with two sets of material parameters: one set is given by Table 5.3 where the applied normal stress is equal to 2 kPa, the other are the real material parameters that we fitted for unaged polymer modified binder at temperature 35 °C given in Table 5.1 and the applied normal stress is ten times higher, i.e. 20 kPa.

5.7.4 Rolling over a viscoelastic material

The last problem is the rolling of the asphalt on the runway. Let us consider the rectangular piece of material, 3m wide and 0.5m high. Model Quad2 is used with the material parameters given by Table 5.3. The problem is depicted in the Figure 5.32.

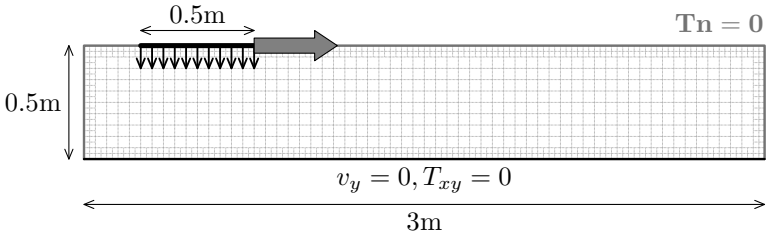

Figure 5.32: Rolling over a viscoelastic material.

The material is on the ground where it can fully slip in the x-direction, but it can not move in the y-direction. All other sides of the rectangle can freely move. At $t = 0$ the material is at rest and does not move. Suddenly at time $t = 0$ it is pushed at the top with a constant normal stress $T_{yy} = -5$ kPa. The force is applied on the constant area $l = 50$cm, which moves with the velocity 40 cm/s from the left to the right and then back to the left, i.e. the material is rolled forward and back. In the Figure 5.33 the location of the area borders is depicted with respect to time t. The force is released at $t = 10.4$s and the material is let to relax.

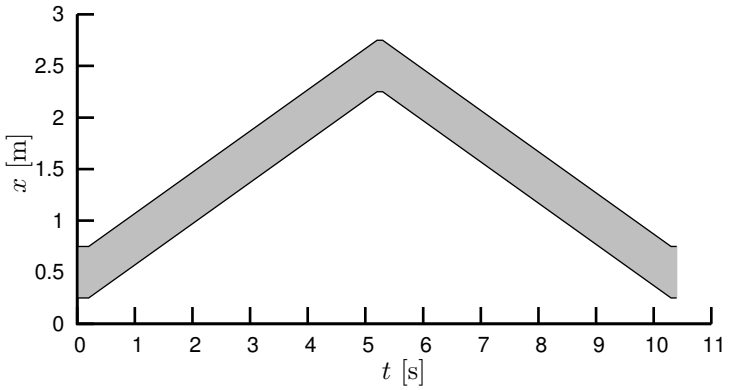

Figure 5.33: The location of the area where the force is applied with respect to time.

The boundary conditions are:

Bottom surface Dirichlet: $v_y = 0$, Neumann: $T_{xy} = 0$

Top and sides Neumann: $\mathbf{Tn} = \mathbf{0}$, during the pressing $T_{yy} = -5$ kPa on the moving part of the boundary.

The problem is computed on a fixed mesh 60×10 (locally refined near boundary as can be seen in Figure 5.32) with time constant time step $\Delta t = 0.01$ and GL time scheme.

In the Figure 5.34 there are five snapshots of the whole simulation. It can be seen how the material is rolled into the sides, the snapshot at $t = 6.5$s shows how the roller pushes the material ahead. The last two snapshots show the relaxation of the material due to the elastic part of response.

The full simulation was done for two set of material parameters. In order to show the viscoelastic behavior of the model Quad2 we computed the problem with unrealistic educational parameters given by Table 5.3 where the applied normal stress is equal to 5 kPa. Further, we computed the problem also for real material parameters given by Table 5.1 where the applied stress is equal to 50 kPa. The movies of both simulations are attached on the DVD.

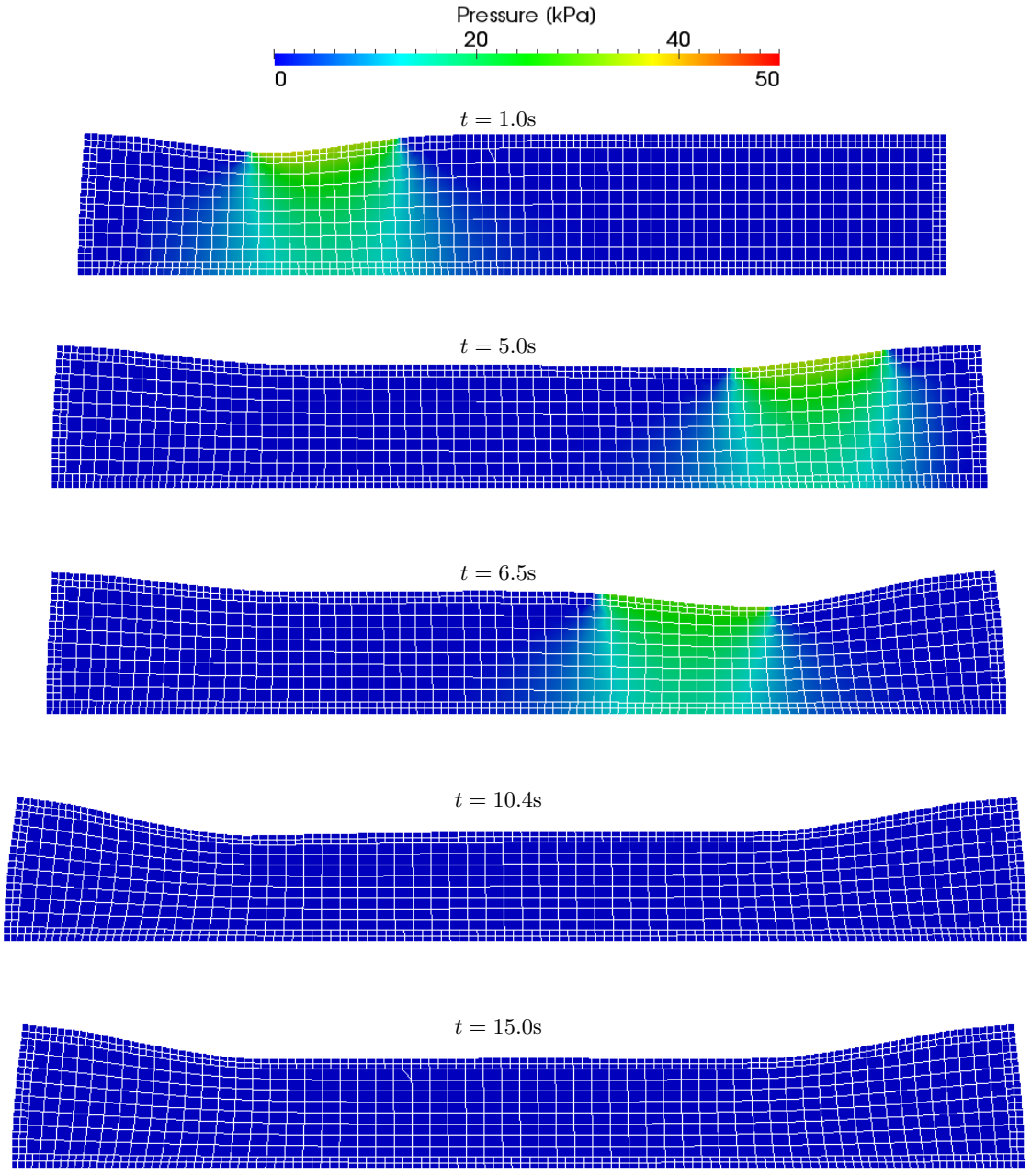

Figure 5.34: Snapshots of the rolling over a viscoelastic material, real material parameters given by Table 5.1.

Chapter 6

Conclusions

We have been interested in identifying the models, with the class of rate-type fluids, that are capable of describing the response of asphalt binders. Although geomaterials like asphalt binder or asphalt concrete may exhibit several non-Newtonian phenomena, as listed in Chapter 2, we have concentrated in this study on two of them associated with viscoelastic properties of the materials: stress relaxation and non-linear creep test. We considered the results of the classical experimental work by Monismith, Secor on asphalt concrete and two experiments with asphalt binder. Regarding asphalt binders the first torsional experiment was performed by Krishnan and Narayan in 2007 with an interesting output, which is a torque overshoot that is not possible to simulate by standard linear viscoelastic models like Oldroyd-B or Burgers model. Later, in 2012 Narayan et al. performed a new torsional experiment that showed that the relaxation time for the normal force and the torque are very different, in fact an order of magnitude apart, and this suggests that asphalt binders exhibit at least two different relaxation mechanisms.

In Chapter 3 we showed a new way of deriving thermodynamically compatible viscoelastic rate-type fluid models proposed by Rajagopal and Srinivasa (2000). The derivation is based on two notions – a natural configuration and the principle of maximum rate of entropy production. Using the concept of natural configuration the whole deformation is split into purely elastic and purely dissipative part, thus it can be controlled how the elastic response looks like and how the energy in the body dissipates.

In 2000 Rajagopal and Srinivasa derived a non-linear version of Maxwell model, where the elastic response corresponds to that of incompressible neo-Hookean solid and the dissipative mechanism takes into account the mutual interaction of the amorphous phase and macromolecules. We added Newtonian dissipative mechanism to this model and obtained a non-linear version of Oldroyd-B model. We fitted the torque overshoot experiment with this model with qualitatively better agreement that the standard models.

Furthermore, we derived another model where the dissipation was in the form of power-law like model and we obtained a viscoelastic model containing six material parameters. When imposing restriction on these parameters the model simplifies to the original viscoelastic model from Rajagopal and Srinivasa (2000). The agreement of this model with experiment was very good, however, it contained two times more material parameters than the original non-linear version of Oldroyd-B model. Our next task was therefore to develop a simpler model with comparably good behavior as this

one. On that account we developed a viscoelastic model containing only three material parameters using a purely quadratic form of dissipation which also exhibits the torque overshoot.

However, none of these models were capable to describe two different relaxation mechanisms revealed by the experiment from 2012. We included this phenomenon in our thermodynamic framework by considering two natural configurations. This new model fits the second experiment very well having only five material parameters. We also showed that this model can be linearized to standard Burgers model and after imposing special parameters restriction it leads to Oldroyd-B model.

Furthermore, we showed that also the standard Oldroyd-B model can be derived using this thermodynamic approach under the assumption that elastic response corresponds to that of compressible neo-Hookean solid. This seems to be a very interesting result because it leads to the conclusion that this standard model is thermodynamically compatible (i.e. it satisfies the second law of thermodynamics), moreover, it reveals how the elastic response looks like. Similarly, other standard viscoelastic models like upper convected Maxwell and Burgers model can be derived as well, one should however view them as the fluids where the elastic response corresponds to that of a compressible neo-Hookean solid and it dissipates the energy as in the original paper by Rajagopal and Srinivasa (2000) [57].

In addition to the model development in Chapter 5 we also performed extensive full simulations of all new viscoelastic models together with the standard ones. For this purpose we modified an in-house finite element code written by J. Hron in C and we carried out some benchmark tests in order to confirm that the implementation is correct. On simple problems like the steady solution of Poiseuille flow in plane geometry and Couette flow in polar geometry (which can be computed analytically in case of Oldroyd-B model and semi-analytically in case the new non-linear model) we verified that the full simulation is correct. Afterwards, we computed the full simulation of the experiment performed by A. Narayan et al. in 2012 using the new model with the fitted material parameters and confirmed that the assumptions imposed on reducing the problem are justified and the whole method of fitting gives the same answer.

Our next task was to compute the problems of viscoelastic flows in deforming domains and to simulate real life problems with asphalt. For this purpose we transformed the equations from the physical deforming domain to the computational fixed domain using Arbitrary Lagrangian-Eulerian method. The obtained set of highly non-linear equations was solved on this fixed mesh using the monolithic solver that treats all unknowns simultaneously. The performed set of benchmark problems revealed the need to replace the standard backward Euler time scheme with better one because the incompressibility was violated (volume of the physical domain was decreasing). We solved this problem by using a higher order Glowinski time scheme. We used the improved FEM implementation combined with the ALE formulation for full simulation of rolling of the asphalt (response to the constant load moving forward and back), the problem was computed with the real fitted material parameters. We also simulated the impact of the wheel of landing plane, or the origin of rutting in asphalt.

Bibliography

[1] M. Anand and K. R. Rajagopal, *A shear-thinning viscoelastic fluid model for describing the flow of blood*, International Journal of Cardiovascular Medicine and Science 4 (2004), no. 2, 59 – 68.

[2] S. Bair, M. Khonsari, and W. O. Winer, *High-pressure rheology of lubricants and limitations of the Reynolds equation*, Tribology International 31 (1998), no. 10, 573–586.

[3] C. Barus, *Isothermals, isopiestics and isometrics relative to viscosity*, American Journal of Science 45 (1893), no. 3, 87–96.

[4] O. Bejaoui and M. Majdoub, *Global weak solutions for some Oldroyd models*, Journal of Differential Equations 254 (2012), no. 2, 660–685.

[5] E. C. Bingham, *Fluidity and plasticity*, vol. 1, McGraw-Hill New York, 1922.

[6] R. B. Bird, C. F. Curtiss, R. C. Armstrong, and O. Hassager, *Dynamics of polymeric liquids*, vol. 2, Wiley, 1987.

[7] S. Boyaval, T. Lelièvre, and C. Mangoubi, *Free-energy-dissipative schemes for the Oldroyd-B model*, ESAIM: Mathematical Modelling and Numerical Analysis 43 (2009), no. 3, 523–561.

[8] R. B. Bramley and X. Wang, *SPLIB: A library of iterative methods for sparse linear systems*, Tech. report, Indiana University, Bloomington, IN, 1997.

[9] P. W. Bridgman, *The effect of pressure on the viscosity of forty-three pure liquids*, Proceedings of the American Academy of Arts and Sciences, vol. 61, 1926, pp. 57–99.

[10] J. M. Burgers, *Mechanical considerations – Model systems – Phenomenological theories of relaxation and viscosity*, First report on viscosity and plasticity, Nordemann Publishing, New York, 1939, pp. 5–67.

[11] B. D. Coleman and W. Noll, *An approximation theorem for functionals, with applications in continuum mechanics*, Archive for Rational Mechanics and Analysis 6 (1960), no. 1, 355–370.

[12] T. A. Davis, *Algorithm 832: UMFPACK V4. 3 – an unsymmetric-pattern multifrontal method*, ACM Transactions on Mathematical Software (TOMS) 30 (2004), no. 2, 196–199.

[13] R. Edgeworth, B. J. Dalton, and T. Parnell, *The pitch drop experiment*, European journal of Physics 5 (1984), no. 4, 198–202.

[14] R. P. Feynman, *Record of R. P. Feynman teaching at Cornell University*, `http://www.youtube.com/watch?v=b240PGCMwV0`, 1964.

[15] C. W. Gardiner et al., *Handbook of stochastic methods*, vol. 3, Springer Berlin, 1985.

[16] R. Glowinski, *Viscous flow simulation by finite element methods and related numerical techniques*, Progress and Supercomputing in Computational Fluid Dynamics (E. M. Murman and S. S. Abarbanel, eds.), Progress in Scientific Computing, vol. 6, Birkhäuser Boston, 1985, pp. 173–210.

[17] R. Glowinski, *Finite element methods for incompressible viscous flow*, Handbook of Numerical Analysis 9 (2003), 3–1176.

[18] C. Guillopé and J. C. Saut, *Global existence and one-dimensional nonlinear stability of shearing motions of viscoelastic fluids of Oldroyd type*, ESAIM: Mathematical Modelling and Numerical Analysis-Modélisation Mathématique et Analyse Numérique 24 (1990), no. 3, 369–401.

[19] C. W. Hirt, A. A. Amsden, and J. L. Cook, *An Arbitrary Lagrangian-Eulerian computing method for all flow speeds*, Journal of Computational Physics 14 (1974), no. 3, 227–253.

[20] J. Hron, *Fluid structure interaction with applications in biomechanics*, Ph.D. thesis, Charles University in Prague, 2001.

[21] J. Hron, J. Kratochvíl, J. Málek, K. R. Rajagopal, and K. Tůma, *A thermodynamically compatible rate type fluid to describe the response of asphalt*, Mathematics and Computers in Simulation 82 (2012), no. 10, 1853–1873.

[22] J. Hron, K. R. Rajagopal, and K. Tůma, *Flow of a Burgers fluid due to time varying loads on deforming boundaries*, to be submitted for publication to Journal of Non-Newtonian Fluid Mechanics (2014).

[23] T. Hughes, W. K. Liu, and T. K. Zimmermann, *Lagrangian-Eulerian finite element formulation for incompressible viscous flows*, Computer Methods in Applied Mechanics and Engineering 29 (1981), no. 3, 329–349.

[24] R. R. Huilgol, *Continuum mechanics of viscoelastic liquids*, Hindustan Publishing Corporation Delhi, 1975.

[25] G. Kitzhofer, O. Koch, and E. Weinmüller, *Numerical treatment of singular BVPs: The new Matlab code bvpsuite*, AIP Conference Proceedings, vol. 1168, 2009, p. 39.

[26] O. Kreml and M. Pokorný, *On the local strong solutions for a system describing the flow of a viscoelastic fluid*, Banach Center Publications 86 (2009), 195 – 206.

[27] J. M. Krishnan and A. Narayan, *Steady shear experiments on ashpalt*, Internal Report, IIT Madras, Chennai, 2007.

[28] J. M. Krishnan and K. R. Rajagopal, *Review of the uses and modeling of bitumen from ancient to modern times*, Applied Mechanics Reviews 56 (2003), no. 2, 149–214.

[29] J. M. Krishnan and K. R. Rajagopal, *Triaxial testing and stress relaxation of asphalt concrete*, Mechanics of Materials 36 (2004), no. 9, 849–864.

[30] W. Kuhn, *Über die Gestalt fadenförmiger Moleküle in Lösungen*, Kolloid-Zeitschrift 68 (1934), no. 1, 2–15 (German).

[31] Z. Lei, C. Liu, and Y. Zhou, *Global solutions for incompressible viscoelastic fluids*, Archive for Rational Mechanics and Analysis 188 (2008), no. 3, 371–398.

[32] F. Lin, C. Liu, and P. Zhang, *On hydrodynamics of viscoelastic fluids*, Comm. Pure Appl. Math. 58 (2005), no. 11, 1437–1471.

[33] P. L. Lions and N. Masmoudi, *Global solutions for some Oldroyd models of non-Newtonian flows*, Chinese Annals of Mathematics 21 (2000), no. 2, 131–146.

[34] J. Málek, *Lecture notes for the series of lectures given in Warsaw*, `http://ssdnm.mimuw.edu.pl/pliki/wyklady/skrypt-malek.pdf`, 2012.

[35] J. Málek and K. R. Rajagopal, *Mathematical issues concerning the Navier-Stokes equations and some of its generalizations*, Evolutionary equations. Vol. II, Handbook of Differential Equations, Elsevier/North-Holland, Amsterdam, 2005, pp. 371–459.

[36] J. Málek and K. R. Rajagopal, *Incompressible rate type fluids with pressure and shear-rate dependent material moduli*, Nonlinear Analysis: Real World Applications 8 (2007), no. 1, 156–164.

[37] J. Málek and K. R. Rajagopal, *Compressible generalized Newtonian fluids*, Zeitschrift für angewandte Mathematik und Physik 61 (2010), no. 6, 1097–1110.

[38] J. Málek, K. R. Rajagopal, and K. Tůma, *A thermodynamically compatible model for describing the response of asphalt binders*, second revised version submitted for publication to Mechanics of Materials (2013).

[39] Z. Martinec, *Continuum mechanics (lecture notes)*, `http://geo.mff.cuni.cz/vyuka/Martinec-ContinuumMechanics.pdf`, 2011.

[40] J. C. Maxwell, *On the dynamical theory of gases*, Philosophical Transactions of the Royal Society 157 (1867), 49–88.

[41] C. L. Monismith and K. E. Secor, *Viscoelastic behavior of asphalt concrete pavements*, Structural Design of Asphalt Pavements, 1962, Univ of California, Berkeley.

[42] C. L. Monismith and K. E. Secor, *Analysis and interrelation of stress-strain-time data for asphalt concrete*, Transactions of The Society of Rheology 8 (1964), no. 19, 19–32.

[43] A. Narayan, J. M. Krishnan, A. P. Deshpande, and K. R. Rajagopal, *Nonlinear viscoelastic response of asphalt binders: An experimental study of the relaxation of torque and normal force in torsion*, Mechanics Research Communications 43 (2012), 66–74.

[44] J. Nelder and R. Mead, *A simplex method for function minimization*, Computer Journal 7 (1965), no. 4, 308–313.

[45] R. W. Ogden, *Non-linear elastic deformations*, Dover Civil and Mechanical Engineering Series, Dover Publications, 1997.

[46] J. G. Oldroyd, *On the formulation of rheological equations of state*, Proceedings of the Royal Society A 200 (1950), no. 1063, 523–541.

[47] H. C. Öttinger, *Stochastic processes in polymeric fluids: tools and examples for developing simulation algorithms*, Springer Berlin, 1996.

[48] R. G. Owens and T. N. Phillips, *Computational rheology*, vol. 2, World Scientific, 2002.

[49] M. Pavelka, *Simple flows of visco-elastic fluids*, bachelor thesis, Charles University in Prague, 2010.

[50] N. Phan-Thien, *Understanding viscoelasticity: Basics of rheology*, Springer, Berlin, 2002.

[51] V. Průša and K. R. Rajagopal, *Jump conditions in stress relaxation and creep experiments of Burgers type fluids: a study in the application of Colombeau algebra of generalized functions*, Zeitschrift für angewandte Mathematik und Physik 62 (2011), no. 4, 707–740.

[52] V. Průša and K. R. Rajagopal, *On implicit constitutive relations for materials with fading memory*, Journal of Non-Newtonian Fluid Mechanics 181 (2012), 22–29.

[53] K. R. Rajagopal, *Mechanics of non-Newtonian fluids*, Recent Developments in Theoretical Fluid Mechanics (G.P. Galdi and J. Nečas, eds.), vol. 291, 1993, pp. 129–162.

[54] K. R. Rajagopal, *Multiple natural configurations in continuum mechanics*, Tech. Report 6, Institute for Computational and Applied Mechanics, University of Pittsburgh, 1995.

[55] K. R. Rajagopal and A. R. Srinivasa, *Mechanics of the inelastic behavior of materials – Part I: Theoretical underpinnings*, International Journal of Plasticity 14 (1998), no. 10, 945–967.

[56] K. R. Rajagopal and A. R. Srinivasa, *Mechanics of the inelastic behavior of materials – Part II: Inelastic response*, International Journal of Plasticity 14 (1998), no. 10–11, 969–995.

[57] K. R. Rajagopal and A. R. Srinivasa, *A thermodynamic frame work for rate type fluid models*, Journal of Non-Newtonian Fluid Mechanics 88 (2000), no. 3, 207–227.

[58] K. R. Rajagopal and A. R. Srinivasa, *On the thermomechanics of materials that have multiple natural configurations Part I: Viscoelasticity and classical plasticity*, Zeitschrift für angewandte Mathematik und Physik 55 (2004), no. 5, 861–893.

[59] K. R. Rajagopal and A. R. Srinivasa, *On thermomechanical restrictions of continua*, Proceedings of the Royal Society A 460 (2004), no. 2042, 1074–1093.

[60] W. R. Schowalter, *Mechanics of non-Newtonian fluids*, Pergamon press Oxford, 1978.

[61] G. Scovazzi and T. Hughes, *Lecture notes on continuum mechanics on arbitrary moving domains*, Tech. report, SAND-2007-6312P, Sandia National Laboratories, 2007.

[62] V. R. Smith, *Application of the triaxial test to bituminous mixtures California research corporation method*, ASTM Special Technical Publication 106 (1951), 55–72.

[63] R. Temam, *Navier-Stokes equations: Theory and numerical analysis*, North-Holland publishing, New York, 1977.

[64] S. Turek, L. Rivkind, J. Hron, and R. Glowinski, *Numerical study of a modified time-stepping θ-scheme for incompressible flow simulations*, Journal of Scientific Computing 28 (2006), no. 2-3, 533–547.

[65] P. Vojtěchovský, *Mechanical analogs of viscous-elastic materials*, sophomore thesis, Charles University in Prague, in Czech, 2007.

[66] C. C. Wang, *The principle of fading memory*, Archive for Rational Mechanics and Analysis 18 (1965), no. 5, 343–366.

[67] S. A. White, A. D. Gotsis, and D. G. Baird, *Review of the entry flow problem: Experimental and numerical*, Journal of Non-Newtonian Fluid Mechanics 24 (1987), no. 2, 121–160.

[68] A. S. Wineman and K. R. Rajagopal, *Mechanical response of polymers: An introduction*, Cambridge University Press, 2000.

List of Tables

List of Figures

List of Notations

$\mathbf{a}$	acceleration
$\overset{\triangledown}{\mathbf{A}}$	$\frac{\partial \mathbf{A}}{\partial t} + \mathbf{v} \cdot \nabla \mathbf{A} - \mathbf{L}\mathbf{A} - \mathbf{A}\mathbf{L}^{\mathrm{T}}$, upper convected Oldroyd material time derivative
$\mathbf{A}^d$	$\mathbf{A} - \frac{1}{d}(\operatorname{tr} \mathbf{A})\mathbf{I}$, deviatoric part of tensor
b	$\operatorname{tr} \mathbf{B}_{\kappa_{p(t)}}$
$\mathbf{b}$	volume force
$\mathbf{B}$	$\mathbf{F}\mathbf{F}^{\mathrm{T}}$, left Cauchy-Green tensor
$\mathbf{B}_{\kappa_{p(t)}}$	$\mathbf{F}_{\kappa_{p(t)}}\mathbf{F}^{\mathrm{T}}_{\kappa_{p(t)}}$, left Cauchy-Green tensor associated with natural configuration
$\mathbf{C}$	$\mathbf{F}^{\mathrm{T}}\mathbf{F}$, right Cauchy-Green tensor
$\mathbf{C}_{\kappa_{p(t)}}$	$\mathbf{F}^{\mathrm{T}}_{\kappa_{p(t)}}\mathbf{F}_{\kappa_{p(t)}}$, right Cauchy-Green tensor associated with natural configuration
(CCC)	fully compressible variant: total deformation is compressible, both elastic and dissipative parts are compressible
(CIC)	compressible variant: total deformation is compressible, elastic part is compressible, dissipative part is incompressible
(CCI)	compressible variant: total deformation is compressible, elastic part is incompressible, dissipative part is compressible
d	space dimension
$\mathbf{D}$	$\frac{1}{2}\left(\mathbf{L} + \mathbf{L}^{\mathrm{T}}\right)$, symmetric part of velocity gradient, stretching
$\mathbf{D}_{\kappa_{p(t)}}$	$\frac{1}{2}\left(\mathbf{L}_{\kappa_{p(t)}} + \mathbf{L}^{\mathrm{T}}_{\kappa_{p(t)}}\right)$, rate of deformation of natural configuration
e	specific internal energy
E	specific total energy; experimental data (Chapter 4)
$\mathbf{F}_{\kappa_R}$	$\frac{\partial \chi_{\kappa_R}}{\partial X}$, deformation gradient
$\mathbf{F}_{\kappa_{p(t)}}$	mapping of infinitesimal line from natural configuration $\kappa_{p(t)}$ to current configuration $\kappa(t)$
g_{abs}	absolute error
g_{rel}	relative error
$\mathbf{G}$	mapping of infinitesimal line from reference configuration κ_R to natural configuration $\kappa_{p(t)}$
G, G_i	elastic modulus
$\mathcal{G}$	stress relaxation function
$\mathbf{I}$	identity matrix
(III)	fully incompressible variant: total deformation is incompressible, both elastic and dissipative parts are incompressible
(ICC)	incompressible/compressible variant: total deformation is incompressible, both elastic and dissipative parts are compressible

$\mathcal{J}$	creep function
k	Boltzmann constant
K	stiffness of the spring in dumbbell model
$\mathbf{L}$	$\nabla\mathbf{v}$, $\dot{\mathbf{F}}_{\kappa_R}\mathbf{F}_{\kappa_R}^{-1}$, velocity gradient
$\mathbf{L}_{\kappa_{p(t)}}$	$\dot{\mathbf{F}}_{\kappa_{p(t)}}\mathbf{F}_{\kappa_{p(t)}}^{-1}$, quantity related to the rate of deformation of natural configuration
m	$(\operatorname{tr}\mathbf{T})/3$
p	thermodynamic pressure
$\mathbf{q}$	heat flux; elongation vector in dumbbell model (Chapter 2)
r	density of energy sources
$\mathbf{v}$	fluid velocity
t	time
$\mathbf{T}$	Cauchy stress tensor
$\mathbf{W}$	$\frac{1}{2}\left(\mathbf{L}-\mathbf{L}^{\mathrm{T}}\right)$, antisymmetric part of velocity gradient, spin
x	point in the current configuration
X	point in the reference configuration
ε	strain
η	specific entropy
$\dot{\gamma}$	shear rate
κ_t	current configuration of the body $\mathcal{B}$, abbreviate $\kappa_t(\mathcal{B})$
κ_R	reference configuration of the body $\mathcal{B}$, abbreviate $\kappa_R(\mathcal{B})$
$\kappa_{p(t)}$	natural configuration associated to current configuration κ_t
λ	Lagrange multiplicator and bulk viscosity (Chapter 3); strain in stress relaxation experiment by Monismith, Secor (Chapter 4)
μ, μ_i	viscosity
μ_{g}	generalized viscosity
ξ	rate of entropy production
ψ	Helmholtz free energy; dumbbell probability density function (Chapter 2)
ρ	density
σ	one dimensional stress
τ	relaxation time
θ	temperature
χ	point in the fixed domain Ω_χ used in ALE formulation
χ_{κ_R}	mapping between the reference configuration κ_R and current configuration κ_t
ω	angular velocity

Appendix A

Differential operators

A.1 Cartesian coordinates

Cartesian system of coordinates is a system of coordinates where all axes are lines perpendicular to each other and a point in the three-dimensional space is defined by the coordinate triplet (see Figure A.1)

$$\mathrm{A} = (A_x, A_y, A_z).$$

Let us denote the scalar function by

$$s = s(x, y, z),$$

vector functions with the letters $\mathbf{v}, \mathbf{w}$ with the components

$$\mathbf{v} = (v_x, v_y, v_z)(x, y, z), \quad \mathbf{w} = (w_x, w_y, w_z)(x, y, z).$$

The second order tensor $\mathbf{T}$ with the components

$$\mathbf{T} = \begin{pmatrix} T_{xx} & T_{xy} & T_{xz} \\ T_{yx} & T_{yy} & T_{yz} \\ T_{zx} & T_{zy} & T_{zz} \end{pmatrix} (x, y, z).$$

Now, the components of the differential operators used in continuum mechanics are written

$$\nabla s = \begin{pmatrix} \dfrac{\partial s}{\partial x} \\ \dfrac{\partial s}{\partial y} \\ \dfrac{\partial s}{\partial z} \end{pmatrix}, \quad \mathbf{v} \cdot \nabla s = v_x \frac{\partial s}{\partial x} + v_y \frac{\partial s}{\partial y} + v_z \frac{\partial s}{\partial z}, \quad \operatorname{div} \mathbf{v} = \frac{\partial v_x}{\partial x} + \frac{\partial v_y}{\partial y} + \frac{\partial v_z}{\partial z},$$

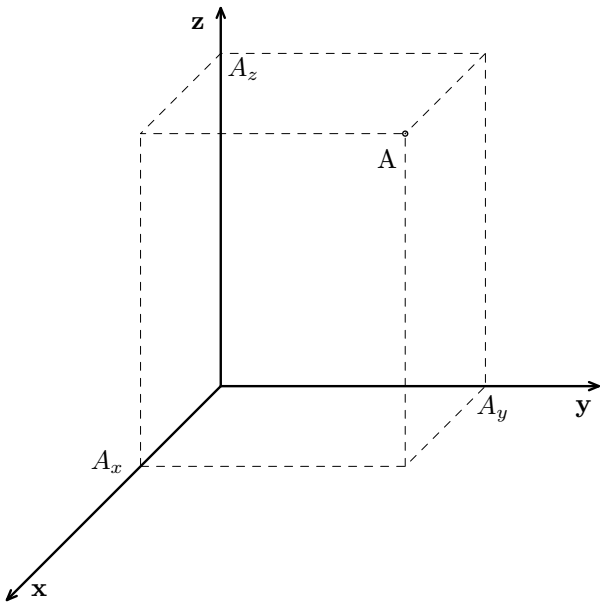

Figure A.1: Cartesian coordinates.

$$\nabla \mathbf{v} = \begin{pmatrix} \frac{\partial v_x}{\partial x} & \frac{\partial v_x}{\partial y} & \frac{\partial v_x}{\partial z} \\ \frac{\partial v_y}{\partial x} & \frac{\partial v_y}{\partial y} & \frac{\partial v_y}{\partial z} \\ \frac{\partial v_z}{\partial x} & \frac{\partial v_z}{\partial y} & \frac{\partial v_z}{\partial z} \end{pmatrix}, \quad \operatorname{div} \mathbf{T} = \begin{pmatrix} \frac{\partial T_{xx}}{\partial x} + \frac{\partial T_{yx}}{\partial y} + \frac{\partial T_{zx}}{\partial z} \\ \frac{\partial T_{xy}}{\partial x} + \frac{\partial T_{yy}}{\partial y} + \frac{\partial T_{zy}}{\partial z} \\ \frac{\partial T_{xz}}{\partial x} + \frac{\partial T_{yz}}{\partial y} + \frac{\partial T_{zz}}{\partial z} \end{pmatrix},$$

$$(\mathbf{v} \cdot \nabla)\mathbf{w} = \begin{pmatrix} \mathbf{v} \cdot \nabla w_x \\ \mathbf{v} \cdot \nabla w_y \\ \mathbf{v} \cdot \nabla w_z \end{pmatrix}, \quad (\mathbf{v} \cdot \nabla)\mathbf{T} = \begin{pmatrix} \mathbf{v} \cdot \nabla T_{xx} & \mathbf{v} \cdot \nabla T_{xy} & \mathbf{v} \cdot \nabla T_{xz} \\ \mathbf{v} \cdot \nabla T_{yx} & \mathbf{v} \cdot \nabla T_{yy} & \mathbf{v} \cdot \nabla T_{yz} \\ \mathbf{v} \cdot \nabla T_{zx} & \mathbf{v} \cdot \nabla T_{zy} & \mathbf{v} \cdot \nabla T_{zz} \end{pmatrix}.$$

In the two-dimensional space the terms corresponding to z components are missing.

A.2 Cylindrical coordinates

In the cylindrical system of coordinates is the point in three-dimensional space defined by the coordinate triplet (see Figure A.2)

$$\mathrm{A} = (A_r, A_\varphi, A_z),$$

where the coordinate r denotes the distance between the point and the axis z, the coordinate φ denotes the angle between the reference direction on the given plane and the line from the origin to the projection of the point on the same plane. The coordinate z is the distance between the point and the given plane perpendicular to the axis z.

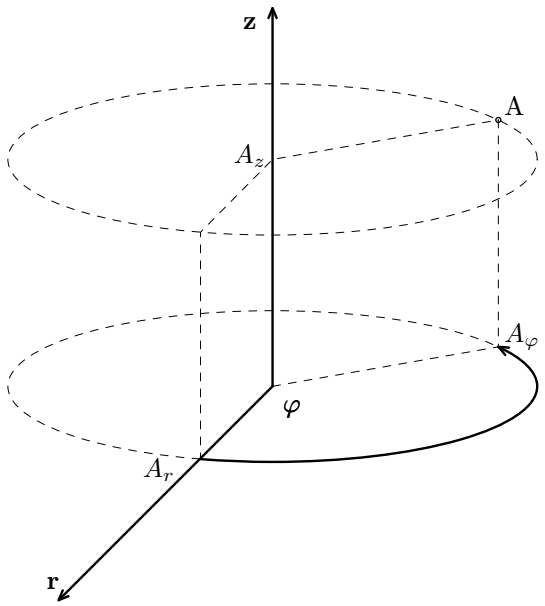

Figure A.2: Cylindrical coordinates.

Let us denote the scalar function

$$s = s(r, \varphi, z),$$

vector functions $\mathbf{v}, \mathbf{w}$ with the components

$$\mathbf{v} = (v_r, v_\varphi, v_z)(r, \varphi, z), \quad \mathbf{w} = (w_r, w_\varphi, w_z)(r, \varphi, z).$$

The second order tensor $\mathbf{T}$ with the components

$$\mathbf{T} = \begin{pmatrix} T_{rr} & T_{r\varphi} & T_{rz} \\ T_{\varphi r} & T_{\varphi\varphi} & T_{\varphi z} \\ T_{zr} & T_{z\varphi} & T_{zz} \end{pmatrix} (r, \varphi, z).$$

The components of the differential operators used in continuum mechanics are written on the following page.

$$\nabla s = \begin{pmatrix} \dfrac{\partial s}{\partial r} \\ \dfrac{1}{r}\dfrac{\partial s}{\partial \varphi} \\ \dfrac{\partial s}{\partial z} \end{pmatrix}, \quad \mathbf{v}\cdot\nabla s = v_r\frac{\partial s}{\partial r} + \frac{v_\varphi}{r}\frac{\partial s}{\partial \varphi} + v_z\frac{\partial s}{\partial z}, \quad \operatorname{div}\mathbf{v} = \frac{\partial v_r}{\partial r} + \frac{v_r}{r} + \frac{1}{r}\frac{\partial v_\varphi}{\partial \varphi} + \frac{\partial v_z}{\partial z},$$

$$\nabla\mathbf{v} = \begin{pmatrix} \dfrac{\partial v_r}{\partial r} & \dfrac{1}{r}\dfrac{\partial v_r}{\partial \varphi} - \dfrac{v_\varphi}{r} & \dfrac{\partial v_r}{\partial z} \\ \dfrac{\partial v_\varphi}{\partial r} & \dfrac{1}{r}\dfrac{\partial v_\varphi}{\partial \varphi} + \dfrac{v_r}{r} & \dfrac{\partial v_\varphi}{\partial z} \\ \dfrac{\partial v_z}{\partial r} & \dfrac{1}{r}\dfrac{\partial v_z}{\partial \varphi} & \dfrac{\partial v_z}{\partial z} \end{pmatrix}, \quad (\mathbf{v}\cdot\nabla)\mathbf{w} = \begin{pmatrix} \mathbf{v}\cdot\nabla w_r - \dfrac{v_\varphi w_\varphi}{r} \\ \mathbf{v}\cdot\nabla w_\varphi + \dfrac{v_\varphi w_r}{r} \\ \mathbf{v}\cdot\nabla w_z \end{pmatrix},$$

where $\mathbf{v}\cdot\nabla w_\alpha = v_r\dfrac{\partial w_\alpha}{\partial r} + v_\varphi\dfrac{\partial w_\alpha}{\partial \varphi} + v_z\dfrac{\partial w_\alpha}{\partial z}, \quad \alpha = r, \varphi, z.$

$$\operatorname{div}\mathbf{T} = \begin{pmatrix} \dfrac{\partial T_{rr}}{\partial r} + \dfrac{1}{r}\dfrac{\partial T_{\varphi r}}{\partial \varphi} + \dfrac{T_{rr} - T_{\varphi\varphi}}{r} + \dfrac{\partial T_{zr}}{\partial z} \\ \dfrac{\partial T_{r\varphi}}{\partial r} + \dfrac{1}{r}\dfrac{\partial T_{\varphi\varphi}}{\partial \varphi} + \dfrac{T_{r\varphi} + T_{\varphi r}}{r} + \dfrac{\partial T_{z\varphi}}{\partial z} \\ \dfrac{\partial T_{rz}}{\partial r} + \dfrac{1}{r}\dfrac{\partial T_{\varphi z}}{\partial \varphi} + \dfrac{T_{rz}}{r} + \dfrac{\partial T_{zz}}{\partial z} \end{pmatrix},$$

$$(\mathbf{v}\cdot\nabla)\mathbf{T} = \begin{pmatrix} \mathbf{v}\cdot\nabla T_{rr} - \dfrac{v_\varphi}{r}(T_{r\varphi} + T_{\varphi r}) & \mathbf{v}\cdot\nabla T_{r\varphi} - \dfrac{v_\varphi}{r}(T_{\varphi\varphi} - T_{rr}) & \mathbf{v}\cdot\nabla T_{rz} - \dfrac{v_\varphi}{r}T_{\varphi z} \\ \mathbf{v}\cdot\nabla T_{\varphi r} + \dfrac{v_\varphi}{r}(T_{rr} - T_{\varphi\varphi}) & \mathbf{v}\cdot\nabla T_{\varphi\varphi} + \dfrac{v_\varphi}{r}(T_{\varphi r} + T_{r\varphi}) & \mathbf{v}\cdot\nabla T_{\varphi z} + \dfrac{v_\varphi}{r}T_{rz} \\ \mathbf{v}\cdot\nabla T_{zr} - \dfrac{v_\varphi}{r}T_{z\varphi} & \mathbf{v}\cdot\nabla T_{z\varphi} + \dfrac{v_\varphi}{r}T_{zr} & \mathbf{v}\cdot\nabla T_{zz} \end{pmatrix},$$

where $\mathbf{v}\cdot\nabla T_{\alpha\beta} = v_r\dfrac{\partial T_{\alpha\beta}}{\partial r} + v_\varphi\dfrac{\partial T_{\alpha\beta}}{\partial \varphi} + v_z\dfrac{\partial T_{\alpha\beta}}{\partial z}, \quad \alpha, \beta = r, \varphi, z.$

Appendix B

Symmetric positive definite matrices

In this chapter we summarize several properties of symmetric positive definite matrices needed in the thesis.

B.1 Some properties of symmetric positive definite matrices

Lemma B.1.1. *Let* $\mathbf{A}$ *be a function* $(0,T)\times\Omega \to \mathbb{R}^{d\times d}_{\mathrm{sym}}$. *Let* D *stands for any derivative (partial time derivative, space gradient, material time derivative). Then it holds*

$$\mathrm{D}(\det \mathbf{A}) = (\det \mathbf{A}) \operatorname{tr}\left((\mathrm{D}\mathbf{A})\mathbf{A}^{-1}\right). \tag{B.1}$$

Proof. For scalar a let us denote $a' := \mathrm{D}a$ some derivative of a, then

$$\mathrm{D}(\det \mathbf{A}) = \sum_{j=1}^{d} \det(\mathbf{A}^{(j)}),$$

where $\mathbf{A}^{(j)}$ contains derivatives in the $j-$th column i.e.

$$\mathbf{A}^{(j)} = \begin{pmatrix} a_{11} & \dots & a'_{1j} & \dots & a_{1d} \\ a_{21} & \dots & a'_{2j} & \dots & a_{2d} \\ \vdots & & \vdots & & \vdots \\ a_{d1} & \dots & a'_{dj} & \dots & a_{dd} \end{pmatrix}.$$

Further, continue with the expansion with respect to the $i-$th row

$$\sum_{j=1}^{d} \det(\mathbf{A}^{(j)}) = \sum_{i=1}^{d}\sum_{j=1}^{d} a'_{ij}(-1)^{i+j} \det\left(\mathbf{A}_{ij}\right) =$$

$$(\det \mathbf{A}) \sum_{i,j=1}^{d} a'_{ij} \underbrace{(-1)^{i+j} \det\left(\mathbf{A}_{ij}\right) (\det \mathbf{A})^{-1}}_{a^{-1}_{ji}} =$$

$$(\det \mathbf{A}) \sum_{i,j=1}^{d} a'_{ij} a^{-1}_{ji} = (\det \mathbf{A}) \operatorname{tr}\left((\mathrm{D}\mathbf{A})\mathbf{A}^{-1}\right). \tag{B.2}$$

□

Using (B.1) we obtain

$$\frac{\mathrm{d}}{\mathrm{d}t}\ln(\det\mathbf{A}) = \mathrm{tr}\left(\dot{\mathbf{A}}\mathbf{A}^{-1}\right). \tag{B.3}$$

Lemma B.1.2. *Let* $\mathbf{A}$ *be a symmetric positive definite matrix of dimension* $d\times d$*. Then it holds*

$$\mathrm{tr}(\mathbf{A}) \geq d\,(\det\mathbf{A})^{1/d}, \quad \mathrm{tr}(\mathbf{A}^{-1}) \geq d\left(\det\left(\mathbf{A}^{-1}\right)\right)^{1/d}. \tag{B.4}$$

Proof. As $\mathbf{A}$ is symmetric and positive definite, we can do a diagonalization

$$\mathbf{A} = \mathbf{C}\mathbf{\Lambda}\mathbf{C}^{\mathrm{T}}$$

where $\mathbf{C}$ is orthogonal matrix and $\mathbf{\Lambda} = diag(\lambda_1, \lambda_2, \ldots, \lambda_d)$, where $\lambda_i > 0$ is the i-th eigenvalue of matrix $\mathbf{A}$, then

$$\det\mathbf{A} = \det\mathbf{C}\det\mathbf{\Lambda}\det\left(\mathbf{C}^{\mathrm{T}}\right) = \lambda_1\lambda_2\ldots\lambda_d, \tag{B.5}$$

$$\mathrm{tr}(\mathbf{A}) = \mathrm{tr}(\mathbf{C}\mathbf{\Lambda}\mathbf{C}^{\mathrm{T}}) = \mathrm{tr}(\mathbf{\Lambda}) = \lambda_1 + \lambda_2 + \cdots + \lambda_d. \tag{B.6}$$

Now, we use inequality of arithmetic and geometric means for $\lambda_1, \lambda_2, \ldots, \lambda_d > 0$

$$\frac{1}{d}\left(\lambda_1 + \lambda_2 + \cdots + \lambda_d\right) \geq \sqrt[d]{\lambda_1\lambda_2\ldots\lambda_d}, \tag{B.7}$$

which together with (B.5) and (B.6) gives

$$\mathrm{tr}\,\mathbf{A} \geq d\,(\det\mathbf{A})^{1/d}. \tag{B.8}$$

Similarly we can proceed with the inverse of matrix $\mathbf{A}$

$$\mathbf{A}^{-1} = \mathbf{C}\mathbf{\Lambda}^{-1}\mathbf{C}^{\mathrm{T}}$$

where $\mathbf{\Lambda}^{-1} = diag\left(\lambda_1^{-1}, \lambda_2^{-1}, \ldots, \lambda_d^{-1}\right)$, then

$$\left(\det\left(\mathbf{A}^{-1}\right)\right) = \det\mathbf{C}\det\left(\mathbf{\Lambda}\right)^{-1}\det\left(\mathbf{C}^{\mathrm{T}}\right) = \lambda_1^{-1}\lambda_2^{-1}\ldots\lambda_d^{-1}, \tag{B.9}$$

$$\mathrm{tr}(\mathbf{A}^{-1}) = \mathrm{tr}(\mathbf{C}\mathbf{\Lambda}^{-1}\mathbf{C}^{\mathrm{T}}) = \mathrm{tr}(\mathbf{\Lambda}^{-1}) = \lambda_1^{-1} + \lambda_2^{-1} + \cdots + \lambda_d^{-1}. \tag{B.10}$$

Again, using (B.7) we obtain

$$\mathrm{tr}\left(\mathbf{A}^{-1}\right) \geq d\left(\det\left(\mathbf{A}^{-1}\right)\right)^{1/d}. \tag{B.11}$$

□

Lemma B.1.3. *Let* $\mathbf{A}$ *be a symmetric positive definite matrix of dimension* $d\times d$*. Then it holds*

$$A_{ij}^2 < A_{ii}A_{jj} \quad \forall i, j = 1, \ldots, d, i \neq j. \tag{B.12}$$

Proof. We use the definition of positive definiteness of matrix $\mathbf{A}$

$$\sum_{k,l=1}^{d} A_{kl}x_k x_l > 0 \quad \forall \mathbf{x} \neq \mathbf{0}.$$

Choose $\mathbf{x} = \mathbf{e}_i + \lambda \mathbf{e}_j$, where $\mathbf{e}_i = (0, \ldots, 0, 1, 0, \ldots, 0)$ (all components zero, i-th component equal to one) and λ is an arbitrary real number

$$0 < \sum_{k,l=1}^{d} A_{kl}(\delta_{il} + \lambda\delta_{jl})(\delta_{ik} + \lambda\delta_{jk}) = A_{ii} + \lambda A_{ij} + \lambda(A_{ji} + \lambda A_{jj}) = A_{ii} + 2\lambda A_{ij} + \lambda^2 A_{jj}. \tag{B.13}$$

The right-hand-side of (B.13) is a quadratic equation for λ, which (since $\mathbf{A}$ is positive definite $A_{jj} > 0$) describes a convex parabola. We want the inequality (B.13) to hold for all λ, hence the parabola can not cross the real axis and the discriminant

$$D = 4A_{ij}^2 - 4A_{ii}A_{jj} < 0 \tag{B.14}$$

has to be negative. □

Lemma B.1.4. *Let* $\mathbf{A}$ *be a symmetric positive definite matrix of dimension* $d \times d$*. Then all components of the matrix* $\mathbf{A}$ *are bounded by its trace, i.e.,*

$$|A_{ij}| < \operatorname{tr} \mathbf{A}. \tag{B.15}$$

Proof. The inequality is proved by Lemma B.1.3.

$$(\operatorname{tr} \mathbf{A})^2 = \left(\sum_{i=1}^{d} A_{ii}\right)^2 = \sum_{i=1}^{d} A_{ii}^2 + \sum_{i\neq j} A_{ii}A_{jj} > \sum_{i=1}^{d} A_{ii}^2 + \sum_{i\neq j} A_{ij}^2 = \sum_{i,j=1}^{d} A_{ij}^2.$$

Hence

$$A_{ij}^2 \leq \sum_{i,j=1}^{d} A_{ij}^2 < (\operatorname{tr} \mathbf{A})^2 \;\Rightarrow\; |A_{ij}| < \operatorname{tr} \mathbf{A}.$$

□

Lemma B.1.5 (Trace of inverse matrix)**.** *Let* $\mathbf{A}$ *be a positive definite matrix of dimension* $d \times d$*. Then it holds*

$$\operatorname{tr}\left(\mathbf{A}^{-1}\right) = \frac{\operatorname{tr} \mathbf{A}}{\det \mathbf{A}}, \text{ for } d = 2, \tag{B.16}$$

$$\operatorname{tr}\left(\mathbf{A}^{-1}\right) = \frac{(\operatorname{tr} \mathbf{A})^2 - \operatorname{tr}\left(\mathbf{A}^2\right)}{2 \det \mathbf{A}}, \text{ for } d = 3. \tag{B.17}$$

Proof. We use Cayley-Hamilton theorem saying that matrix $\mathbf{A}$ is a root of its characteristic polynom $p(\lambda) = \det(\lambda\mathbf{I} - \mathbf{A})$, i.e. $p(\mathbf{A}) = \mathbf{0}$. In two-dimensional space the characteristic polynom is equal to

$$p(\lambda) = \lambda^2 - \operatorname{tr}(\mathbf{A})\lambda + (\det \mathbf{A}), \tag{B.18}$$

using Cayley-Hamilton theorem we have

$$\mathbf{0} = \mathbf{A}^2 - \mathrm{tr}(\mathbf{A})\mathbf{A} + (\det \mathbf{A})\mathbf{I}. \tag{B.19}$$

Multiplying (B.19) by $\mathbf{A}^{-1}$ and taking the trace of the result we get (B.16).

In three-dimensional space the characteristic polynom is equal to

$$p(\lambda) = \lambda^3 - \mathrm{tr}(\mathbf{A})\lambda^2 + \frac{1}{2}\left[(\mathrm{tr}\,\mathbf{A})^2 - \mathrm{tr}\left(\mathbf{A}^2\right)\right]\lambda + (\det \mathbf{A}), \tag{B.20}$$

using Cayley-Hamilton theorem we obtain

$$\mathbf{0} = \mathbf{A}^3 - \mathrm{tr}(\mathbf{A})\mathbf{A}^2 + \frac{1}{2}\left[(\mathrm{tr}\,\mathbf{A})^2 - \mathrm{tr}\left(\mathbf{A}^2\right)\right]\mathbf{A} + (\det \mathbf{A})\mathbf{I}. \tag{B.21}$$

Multiplying (B.21) by $\mathbf{A}^{-1}$ and taking the trace of the result we get (B.17). □

Lemma B.1.6. *Let* $\mathbf{A}$ *be a positive definite matrix of dimension* 2×2. *Then it holds*

$$\mathbf{A}\mathbf{A}^d = \frac{1}{2}(\mathrm{tr}\,\mathbf{A})\mathbf{A} - (\det \mathbf{A})\mathbf{I}. \tag{B.22}$$

Proof. Again, we use Cayley-Hamilton theorem saying that matrix $\mathbf{A}$ is a root of its characteristic polynom $p(\lambda) = \det(\lambda\mathbf{I} - \mathbf{A})$, i.e. $p(\mathbf{A}) = \mathbf{0}$. In two-dimensional space the characteristic polynom is equal to

$$p(\lambda) = \lambda^2 - \mathrm{tr}(\mathbf{A})\lambda + (\det \mathbf{A}), \tag{B.23}$$

using Cayley-Hamilton theorem we have

$$\mathbf{0} = \mathbf{A}^2 - \mathrm{tr}(\mathbf{A})\mathbf{A} + (\det \mathbf{A})\mathbf{I} \tag{B.24}$$

from which we express

$$\mathbf{A}\mathbf{A}^d = \mathbf{A} - \frac{1}{2}(\mathrm{tr}\,\mathbf{A})\mathbf{A} = \frac{1}{2}(\mathrm{tr}\,\mathbf{A})\mathbf{A} - (\det \mathbf{A})\mathbf{I}. \tag{B.25}$$

□

Appendix C

Objectivity and material symmetry

Let $\mathbf{F}_{\kappa_{p(t)}}$ maps the infinitesimal line from the natural configuration $\kappa_{p(t)}$ to the current configuration κ_t, and $\mathbf{F}$ is the deformation gradient between the reference configuration κ_R and the actual configuration κ_t, see Fig. C.1.

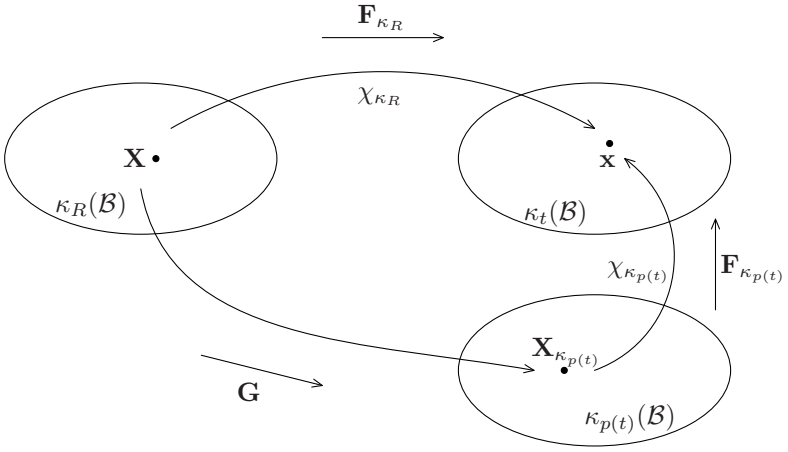

Figure C.1: Mapping between the configurations.

Suppose that $\mathbf{F}_{\kappa_{p(t)}}$ is gradient of some mapping $\chi_{\kappa_{p(t)}}$ (this is not generally true since natural configuration is only a local notion)

$$\mathbf{F}_{\kappa_{p(t)}} = \frac{\partial \chi_{\kappa_{p(t)}}}{\partial X_{\kappa_{p(t)}}}, \quad (F_{\kappa_{p(t)}})_{iJ} = \frac{\partial (\chi_{\kappa_{p(t)}})_i}{\partial (X_{\kappa_{p(t)}})_J}.$$

Deformation gradient is defined as

$$\mathbf{F}_{\kappa_R} = \frac{\partial \chi_{\kappa_R}}{\partial X}, \quad (F_{\kappa_R})_{iJ} = \frac{\partial (\chi_{\kappa_R})_i}{\partial X_J}.$$

For more details concerning observer transformation and material symmetry see the lecture notes by Z. Martinec [39].

C.1 Observer transformation

The constitutive relations should be independent of the movement of an observer.

Definition C.1.1. *Second order tensor* $\mathbf{A}$ *is objective or frame indifferent if under the observer transformation* (C.2) *it holds*

$$\mathbf{A}^* = \mathbf{Q}(t)\mathbf{A}\mathbf{Q}^{\mathrm{T}}(t). \tag{C.1}$$

Under the change of coordinates

$$\mathbf{x}^* = \mathbf{Q}(t)\mathbf{x} + \mathbf{c}(t), \quad \mathbf{Q}(t)\mathbf{Q}(t)^{\mathrm{T}} = \mathbf{Q}(t)^{\mathrm{T}}\mathbf{Q}(t) = \mathbf{I} \tag{C.2}$$

the deformation gradient $\mathbf{F}_{\kappa_{p(t)}}$ transforms as

$$(F^*_{\kappa_{p(t)}})_{i^*J} = \frac{\partial(\chi^*_{\kappa_{p(t)}})_{i^*}}{\partial(X_{\kappa_{p(t)}})_J} = \frac{\partial}{\partial(X_{\kappa_{p(t)}})_J}(Q_{i^*i}(\chi_{\kappa_{p(t)}})_i + \mathbf{c}_i) = Q_{i^*i}\frac{\partial(\chi_{\kappa_{p(t)}})_i}{\partial X_J} = Q_{i^*i}(F_{\kappa_{p(t)}})_{iJ}$$

and thus the gradient $\mathbf{F}_{\kappa_{p(t)}}$

$$\mathbf{F}^*_{\kappa_{p(t)}} = \mathbf{Q}\mathbf{F}_{\kappa_{p(t)}} \tag{C.3}$$

transforms as a vector, which implies that $\mathbf{F}_{\kappa_{p(t)}}$ is not an objective tensor. However, the three columns of $\mathbf{F}_{\kappa_{p(t)}}$ are objective vectors. Now we can compute how transforms the left Cauchy-Green tensor $\mathbf{B}_{\kappa_{p(t)}}$ and right Cauchy-Green tensor $\mathbf{C}_{\kappa_{p(t)}}$

$$\mathbf{C}^*_{\kappa_{p(t)}} = \mathbf{F}^{\mathrm{T}*}_{\kappa_{p(t)}}\mathbf{F}^*_{\kappa_{p(t)}} = \mathbf{F}^{\mathrm{T}}_{\kappa_{p(t)}}\underbrace{\mathbf{Q}^{\mathrm{T}}\mathbf{Q}}_{\mathbf{I}}\mathbf{F}_{\kappa_{p(t)}} = \mathbf{F}^{\mathrm{T}}_{\kappa_{p(t)}}\mathbf{F}_{\kappa_{p(t)}} = \mathbf{C}_{\kappa_{p(t)}}$$

$$\mathbf{B}^*_{\kappa_{p(t)}} = \mathbf{F}^*_{\kappa_{p(t)}}\mathbf{F}^{\mathrm{T}*}_{\kappa_{p(t)}} = \mathbf{Q}\mathbf{F}_{\kappa_{p(t)}}\mathbf{F}^{\mathrm{T}}_{\kappa_{p(t)}}\mathbf{Q}^{\mathrm{T}} = \mathbf{Q}\mathbf{B}_{\kappa_{p(t)}}\mathbf{Q}^{\mathrm{T}}$$

and so, the right Cauchy-Green tensor $\mathbf{C}_{\kappa_{p(t)}}$ transforms as an objective scalar and the left Cauchy-Green tensor $\mathbf{B}_{\kappa_{p(t)}}$ transforms as an objective tensor under the change of the coordinates.

Similarly as the tensor $\mathbf{F}_{\kappa_{p(t)}}$ transforms also the deformation gradient $\mathbf{F}_{\kappa_R}$ transforms under the change of coordinates (C.2)

$$\mathbf{F}^*_{\kappa_R} = \mathbf{Q}\mathbf{F}_{\kappa_R}. \tag{C.4}$$

Using (C.4) we shod how the velocity gradient $\mathbf{L}$ and its symmetric part transforms

$$\mathbf{L}^* = \dot{\mathbf{F}}^*_{\kappa_R}\mathbf{F}^{*-1}_{\kappa_R} = \left(\dot{\mathbf{Q}}\mathbf{F}_{\kappa_R} + \mathbf{Q}\dot{\mathbf{F}}_{\kappa_R}\right)\mathbf{F}^{-1}_{\kappa_R}\mathbf{Q}^{\mathrm{T}} = \dot{\mathbf{Q}}\mathbf{Q}^{\mathrm{T}} + \mathbf{Q}\dot{\mathbf{F}}_{\kappa_R}\mathbf{F}^{-1}_{\kappa_R}\mathbf{Q}^{\mathrm{T}} = \dot{\mathbf{Q}}\mathbf{Q}^{\mathrm{T}} + \mathbf{Q}\mathbf{L}\mathbf{Q}^{\mathrm{T}},$$

thus $\mathbf{L}$ is not an objective tensor. Since

$$\mathbf{0} = \dot{\overline{\mathbf{Q}\mathbf{Q}^{\mathrm{T}}}} = \dot{\mathbf{Q}}\mathbf{Q}^{\mathrm{T}} + \mathbf{Q}\dot{\mathbf{Q}}^{\mathrm{T}} = \dot{\mathbf{Q}}\mathbf{Q}^{\mathrm{T}} + \left(\dot{\mathbf{Q}}\mathbf{Q}^{\mathrm{T}}\right)^{\mathrm{T}},$$

the symmetric part of velocity gradient $\mathbf{D}$ is an objective tensor. Further it can be shown that material time derivative of objective tensor $\mathbf{A}$ is not objective tensorial quantity, briefly

$$\frac{\mathrm{d}\mathbf{A}^*}{\mathrm{d}t} = \dot{\mathbf{Q}}\mathbf{A}\mathbf{Q}^{\mathrm{T}} + \mathbf{Q}\frac{\mathrm{d}\mathbf{A}}{\mathrm{d}t}\mathbf{Q}^{\mathrm{T}} + \mathbf{Q}\mathbf{A}\dot{\mathbf{Q}}^{\mathrm{T}} \neq \mathbf{Q}\frac{\mathrm{d}\mathbf{A}}{\mathrm{d}t}\mathbf{Q}^{\mathrm{T}}.$$

Using (C.3) and (C.4) we find out how the rate of deformation of the natural configuration $\mathbf{L}_{\kappa_{p(t)}} = \dot{\mathbf{G}}\mathbf{G}^{-1}$ (remind that $\mathbf{G} = \mathbf{F}^{-1}_{\kappa_{p(t)}}\mathbf{F}_{\kappa_R}$) transforms

$$\begin{aligned}\mathbf{L}^*_{\kappa_{p(t)}} = \dot{\mathbf{G}}^*\mathbf{G}^{*-1} = \mathbf{F}^{*-1}_{\kappa_{p(t)}}\left(-\dot{\mathbf{F}}^*_{\kappa_{p(t)}} + \dot{\mathbf{F}}^*_{\kappa_R}\mathbf{F}^{-1*}_{\kappa_R}\mathbf{F}^*_{\kappa_{p(t)}}\right) = \\ \mathbf{F}^{-1}_{\kappa_{p(t)}}\mathbf{Q}^{-1}\left(-(\dot{\mathbf{Q}}\mathbf{F}_{\kappa_{p(t)}} + \mathbf{Q}\dot{\mathbf{F}}_{\kappa_{p(t)}}) + (\dot{\mathbf{Q}}\mathbf{F}_{\kappa_R} + \mathbf{Q}\dot{\mathbf{F}}_{\kappa_R})\mathbf{F}^{-1}_{\kappa_R}\mathbf{Q}^{-1}\mathbf{Q}\mathbf{F}_{\kappa_{p(t)}}\right) = \\ -\mathbf{F}^{-1}_{\kappa_{p(t)}}\mathbf{Q}^{-1}\dot{\mathbf{Q}}\mathbf{F}_{\kappa_{p(t)}} - \mathbf{F}^{-1}_{\kappa_{p(t)}}\dot{\mathbf{F}}_{\kappa_{p(t)}} + \mathbf{F}^{-1}_{\kappa_{p(t)}}\mathbf{Q}^{-1}\dot{\mathbf{Q}}\mathbf{F}_{\kappa_{p(t)}} + \mathbf{F}^{-1}_{\kappa_{p(t)}}\dot{\mathbf{F}}_{\kappa_R}\mathbf{F}^{-1}_{\kappa_R}\mathbf{F}_{\kappa_{p(t)}} = \mathbf{L}_{\kappa_{p(t)}}\end{aligned}$$

and the rate of deformation $\mathbf{L}_{\kappa_{p(t)}}$ and its symmetric part $\mathbf{D}_{\kappa_{p(t)}}$ transforms as an objective scalar

$$\mathbf{L}^*_{\kappa_{p(t)}} = \mathbf{L}_{\kappa_{p(t)}}, \quad \mathbf{D}^*_{\kappa_{p(t)}} = \mathbf{D}_{\kappa_{p(t)}}. \tag{C.5}$$

C.2 Material symmetry

We suppose that the material is homogeneous isotropic and so the constitutive equations do not depend on the change (translation and rotation) of the natural configuration κ_p. Suppose we have two natural configurations $\kappa_{p(t)}$ and $\tilde{\kappa}_{p(t)}$ and the relation between the points in two configurations is the following

$$\tilde{X}_{\kappa_{p(t)}} = \mathbf{P}X_{\kappa_{p(t)}} + \mathbf{a}, \quad \mathbf{P}\mathbf{P}^{\mathrm{T}} = \mathbf{P}^{\mathrm{T}}\mathbf{P} = \mathbf{I} \text{ and } \mathbf{P} = \mathbf{P}(X_{\kappa_{p(t)}})$$

Then with this change, the gradient $\mathbf{F}_{\kappa_{p(t)}}$ changes as

$$(\tilde{F}_{\kappa_{p(t)}})_{iJ} = \frac{\partial(\chi_{\kappa_{p(t)}})_i}{\partial(\tilde{X}_{\kappa_{p(t)}})_J} = \frac{\partial(\chi_{\kappa_{p(t)}})_i}{\partial(X_{\kappa_{p(t)}})_K}\frac{\partial(P_{IK}((\tilde{X}_{\kappa_{p(t)}})_I - a_I))}{\partial(\tilde{X}_{\kappa_{p(t)}})_J} = \frac{\partial(\chi_{\kappa_{p(t)}})_i}{\partial(X_{\kappa_{p(t)}})_K}P_{JK} = (F_{\kappa_{p(t)}})_{iK}P_{JK} \tag{C.6}$$

and so

$$\tilde{\mathbf{F}}_{\kappa_{p(t)}} = \mathbf{F}_{\kappa_{p(t)}}\mathbf{P}^{\mathrm{T}}.$$

Note, that the change of natural configuration does not cause any change of the deformation gradient $\mathbf{F}_{\kappa_R}$. Then the right Cauchy-Green tensor $\mathbf{C}_{\kappa_{p(t)}}$ and the left Cauchy-Green tensor $\mathbf{B}_{\kappa_{p(t)}}$ changes as

$$\tilde{\mathbf{C}}_{\kappa_{p(t)}} = \tilde{\mathbf{F}}^{\mathrm{T}}_{\kappa_{p(t)}}\tilde{\mathbf{F}}_{\kappa_{p(t)}} = \mathbf{P}\mathbf{F}^{\mathrm{T}}_{\kappa_{p(t)}}\mathbf{F}_{\kappa_{p(t)}}\mathbf{P}^{\mathrm{T}} = \mathbf{P}\mathbf{C}_{\kappa_{p(t)}}\mathbf{P}^{\mathrm{T}}, \tag{C.7}$$

$$\tilde{\mathbf{B}}_{\kappa_{p(t)}} = \tilde{\mathbf{F}}_{\kappa_{p(t)}}\tilde{\mathbf{F}}^{\mathrm{T}}_{\kappa_{p(t)}} = \mathbf{F}_{\kappa_{p(t)}}\mathbf{P}^{\mathrm{T}}\mathbf{P}\mathbf{F}^{\mathrm{T}}_{\kappa_{p(t)}}\mathbf{F}_{\kappa_{p_1(t)}} = \mathbf{B}_{\kappa_{p(t)}} \tag{C.8}$$

and so: For the material symmetry the right Cauchy-Green tensor $\mathbf{C}_{\kappa_{p(t)}}$ transforms as a tensor and the left Cauchy-Green tensor $\mathbf{B}_{\kappa_{p(t)}}$ transforms as a scalar.

Now, again we want to show how changes the rate of deformation of the natural configuration $\mathbf{L}_{\kappa_{p(t)}}$ under the change of the natural configuration.

$$\tilde{\mathbf{L}}_{\kappa_{p(t)}} = \dot{\tilde{\mathbf{G}}}\tilde{\mathbf{G}}^{-1} = \tilde{\mathbf{F}}^{-1}_{\kappa_{p(t)}}\left(-\dot{\tilde{\mathbf{F}}}_{\kappa_{p(t)}} + \dot{\mathbf{F}}_{\kappa_R}\mathbf{F}^{-1}_{\kappa_R}\tilde{\mathbf{F}}_{\kappa_{p(t)}}\right) = \mathbf{P}\mathbf{F}^{-1}_{\kappa_{p(t)}}\left(-(\dot{\mathbf{F}}_{\kappa_{p(t)}}\mathbf{P}^{\mathrm{T}} + \mathbf{F}_{\kappa_{p(t)}}\dot{\mathbf{P}}^{\mathrm{T}}) + \dot{\mathbf{F}}\mathbf{F}^{-1}\mathbf{F}_{\kappa_{p(t)}}\mathbf{P}^{\mathrm{T}}\right) = \mathbf{P}\left(\mathbf{F}^{-1}_{\kappa_{p(t)}}(-\dot{\mathbf{F}}_{\kappa_{p(t)}} + \dot{\mathbf{F}}_{\kappa_R}\mathbf{F}^{-1}_{\kappa_R}\mathbf{F}_{\kappa_{p(t)}})\right)\mathbf{P}^{\mathrm{T}} - \mathbf{P}\dot{\mathbf{P}}^{\mathrm{T}}.$$

Since $\mathbf{P}$ is not a function of t, $\dot{\mathbf{P}} = 0$ and so the rate of deformation of the natural configuration $\mathbf{L}_{\kappa_{p(t)}}$ transforms as a tensor and also its symmetric part $\mathbf{D}_{\kappa_{p(t)}}$ transforms as a tensor [1].

$$\tilde{\mathbf{D}}_{\kappa_{p(t)}} = \mathbf{P}\mathbf{D}_{\kappa_{p(t)}}\mathbf{P}^{\mathrm{T}}. \tag{C.9}$$

[1] $\mathbf{D}_{\kappa_{p(t)}}$ transforms as objective tensor even in case that $\mathbf{P}$ depends on time t because $\mathbf{P}\dot{\mathbf{P}}^{\mathrm{T}}$ is an antisymmetric tensor.

C.3 Application to the choice of internal energy and to the choice of rate of entropy production

We use derived relations for the transformation of $\mathbf{B}_{\kappa_{p(t)}}, \mathbf{C}_{\kappa_{p(t)}}$ and $\mathbf{D}_{\kappa_{p(t)}}$ to determine if the choice of constitutive relation for the internal energy and rate of entropy production satisfies the objectivity and the material symmetry.

Choice of the internal energy e We test two different constitutive relations for the internal energy:

1. with left Cauchy-Green tensor $\mathbf{B}_{\kappa_{p(t)}}$: $e = e_0 + \frac{G}{2\rho}\left(\operatorname{tr}\mathbf{B}_{\kappa_{p(t)}} - 3\right)$

   Material symmetry – change of natural configuration

   $$\frac{G}{2\rho}\left(\operatorname{tr}\mathbf{B}_{\kappa_{p_2(t)}} - 3\right) = \frac{G}{2\rho}\left(\operatorname{tr}\mathbf{B}_{\kappa_{p_1(t)}} - 3\right).$$

   Objectivity – change of observer

   $$\frac{G}{2\rho}\left(\operatorname{tr}\mathbf{B}^*_{\kappa_{p(t)}} - 3\right) = \frac{G}{2\rho}\left(\operatorname{tr}\mathbf{B}_{\kappa_{p(t)}} - 3\right).$$

2. with right Cauchy-Green tensor $\mathbf{C}_{\kappa_{p(t)}}$: $e = e_0 + \frac{G}{2\rho}\left(\operatorname{tr}\mathbf{C}_{\kappa_{p(t)}} - 3\right)$

   Material symmetry – change of natural configuration

   $$\frac{G}{2\rho}\left(\operatorname{tr}\tilde{\mathbf{C}}_{\kappa_{p(t)}} - 3\right) = \frac{G}{2\rho}\left(\operatorname{tr}\mathbf{C}_{\kappa_{p(t)}} - 3\right).$$

   Objectivity – change of observer

   $$\frac{G}{2\rho}\left(\operatorname{tr}\mathbf{C}^*_{\kappa_{p(t)}} - 3\right) = \frac{G}{2\rho}\left(\operatorname{tr}\mathbf{C}_{\kappa_{p(t)}} - 3\right).$$

Both constitutive relations for the internal energy satisfy objectivity and material symmetry.

Choice of the rate of entropy production ξ We test three different constitutive relations for the rate of entropy production:

1. with left Cauchy-Green tensor $\mathbf{B}_{\kappa_{p(t)}}$: $\xi = \mathbf{D}_{\kappa_{p(t)}}\mathbf{B}_{\kappa_{p(t)}} \cdot \mathbf{D}_{\kappa_{p(t)}}$

   Material symmetry – change of natural configuration

   $$\tilde{\mathbf{D}}_{\kappa_{p(t)}}\tilde{\mathbf{B}}_{\kappa_{p(t)}} \cdot \tilde{\mathbf{D}}_{\kappa_{p(t)}} = (\mathbf{D}_{\kappa_{p(t)}}\mathbf{P}^{\mathrm{T}}\mathbf{B}_{\kappa_{p(t)}}) \cdot (\mathbf{D}_{\kappa_{p(t)}}\mathbf{P}^{\mathrm{T}}) \neq \mathbf{D}_{\kappa_{p(t)}}\mathbf{B}_{\kappa_{p(t)}} \cdot \mathbf{D}_{\kappa_{p(t)}}.$$

   Objectivity – change of observer

   $$\mathbf{D}^*_{\kappa_{p(t)}}\mathbf{B}^*_{\kappa_{p(t)}} \cdot \mathbf{D}^*_{\kappa_{p(t)}} = (\mathbf{D}_{\kappa_{p(t)}}\mathbf{Q}\mathbf{B}_{\kappa_{p(t)}}) \cdot (\mathbf{D}_{\kappa_{p(t)}}\mathbf{Q}) \neq \mathbf{D}_{\kappa_{p(t)}}\mathbf{B}_{\kappa_{p(t)}} \cdot \mathbf{D}_{\kappa_{p(t)}}.$$

2. with right Cauchy-Green tensor $\mathbf{C}_{\kappa_{p(t)}}$: $\xi = \mathbf{D}_{\kappa_{p(t)}}\mathbf{C}_{\kappa_{p(t)}} \cdot \mathbf{D}_{\kappa_{p(t)}}$

Material symmetry – change of natural configuration

$$\tilde{\mathbf{D}}_{\kappa_{p(t)}}\tilde{\mathbf{C}}_{\kappa_{p(t)}}\cdot\tilde{\mathbf{D}}_{\kappa_{p(t)}}=\mathbf{D}_{\kappa_{p(t)}}\mathbf{C}_{\kappa_{p(t)}}\cdot\mathbf{D}_{\kappa_{p(t)}}.$$

Objectivity – change of observer

$$\mathbf{D}^{*}_{\kappa_{p(t)}}\mathbf{C}^{*}_{\kappa_{p(t)}}\cdot\mathbf{D}^{*}_{\kappa_{p(t)}}=\mathbf{D}_{\kappa_{p(t)}}\mathbf{C}_{\kappa_{p(t)}}\cdot\mathbf{D}_{\kappa_{p(t)}}.$$

3. purely quadratic rate of entropy production in terms of $\mathbf{D}_{\kappa_{p(t)}}$: $\xi=\mathbf{D}_{\kappa_{p(t)}}\cdot\mathbf{D}_{\kappa_{p(t)}}$

   Material symmetry – change of natural configuration

$$\tilde{\mathbf{D}}_{\kappa_{p(t)}}\cdot\tilde{\mathbf{D}}_{\kappa_{p(t)}}=\mathbf{D}_{\kappa_{p(t)}}\cdot\mathbf{D}_{\kappa_{p(t)}}.$$

   Objectivity – change of observer

$$\mathbf{D}^{*}_{\kappa_{p(t)}}\cdot\mathbf{D}^{*}_{\kappa_{p(t)}}=\mathbf{D}_{\kappa_{p(t)}}\cdot\mathbf{D}_{\kappa_{p(t)}}.$$

The constitutive relation for the rate of entropy production $\xi=\mathbf{D}_{\kappa_{p(t)}}\mathbf{B}_{\kappa_{p(t)}}\cdot\mathbf{D}_{\kappa_{p(t)}}$ satisfies neither objectivity nor material symmetry. The constitutive relation for the rate of entropy production $\xi=\mathbf{D}_{\kappa_{p(t)}}\mathbf{C}_{\kappa_{p(t)}}\cdot\mathbf{D}_{\kappa_{p(t)}}$ and purely quadratic relation in terms of $\mathbf{D}_{\kappa_{p(t)}}$ satisfy objectivity and material symmetry.

Appendix D

Weak formulation for viscoelastic model Quad1

In this chapter we write components of weak formulation for viscoelastic model Quad1 in three situations: components in two-dimensional space using Cartesian corrdinates, three-dimensional space using cylindrical coordinates and ALE formulation in two-dimensional space using Cartesian coordinates.

We use the model Quad1 in the usual form given by (3.112)[1]:

$$\operatorname{div} \mathbf{v} = 0, \tag{D.1a}$$

$$\rho \left(\frac{\partial \mathbf{v}}{\partial t} + \mathbf{v} \cdot \nabla \mathbf{v} \right) = \operatorname{div} \mathbf{T}, \tag{D.1b}$$

$$\mathbf{T} = -p\mathbf{I} + 2\mu_2 \mathbf{D} + G\mathbf{B}^d_{\kappa_{p(t)}}, \tag{D.1c}$$

$$\frac{\partial \mathbf{B}_{\kappa_{p(t)}}}{\partial t} + \mathbf{v} \cdot \nabla \mathbf{B}_{\kappa_{p(t)}} - \mathbf{L}\mathbf{B}_{\kappa_{p(t)}} - \mathbf{B}_{\kappa_{p(t)}}\mathbf{L}^{\mathrm{T}} = -\frac{1}{\tau}\mathbf{B}_{\kappa_{p(t)}}\mathbf{B}^d_{\kappa_{p(t)}}, \tag{D.1d}$$

where $\tau = G/\mu_1$ is relaxation time.

D.1 Model Quad1 in two-dimensional Cartesian coordinates

Let us assume that all unknowns $p, \mathbf{v}, \mathbf{B}_{\kappa_{p(t)}}$ are in the form

$$p = p(x,y),\ \mathbf{v} = (v_x, v_y)(x,y),\ \mathbf{B}_{\kappa_{p(t)}} = \begin{pmatrix} B_{xx}, B_{xy} \\ B_{xy}, B_{yy} \end{pmatrix}(x,y).$$

The weak formulation is

$$\int_\Omega \operatorname{div} \mathbf{v}\ q = 0, \tag{D.2}$$

$$\int_\Omega \rho \left(\frac{\partial \mathbf{v}}{\partial t} + \mathbf{v} \cdot \nabla \mathbf{v} \right) \cdot \mathbf{q} + \int_\Omega \mathbf{T} \cdot \nabla \mathbf{q} = 0, \tag{D.3}$$

$$\mathbf{T} = -p\mathbf{I} + 2\mu_2 \mathbf{D} + G\mathbf{B}^d_{\kappa_{p(t)}}, \tag{D.4}$$

$$\int_\Omega \left(\frac{\partial \mathbf{B}_{\kappa_{p(t)}}}{\partial t} + \mathbf{v} \cdot \nabla \mathbf{B}_{\kappa_{p(t)}} - \mathbf{L}\mathbf{B}_{\kappa_{p(t)}} - \mathbf{B}_{\kappa_{p(t)}}\mathbf{L}^{\mathrm{T}} + \frac{1}{\tau}\mathbf{B}_{\kappa_{p(t)}}\mathbf{B}^d_{\kappa_{p(t)}} \right) \cdot \mathbf{Q} = 0 \tag{D.5}$$

[1] In two-dimension setting it is also possible to use alternative form of model Quad1 given by (3.131b).

with the test functions

$$q = q(x,y), \quad \mathbf{q} = (q_x, q_y)(x,y), \quad \mathbf{Q} = \begin{pmatrix} Q_{xx}, Q_{xy} \\ Q_{xy}, Q_{yy} \end{pmatrix}(x,y).$$

The components of the weak formulation of all equations are

(D.2)
$$\int_\Omega \left(\frac{\partial v_x}{\partial x} + \frac{\partial v_y}{\partial y} \right) q = 0.$$

(D.3)
$$\int_\Omega \rho \left(\frac{\partial v_x}{\partial t} + v_x \frac{\partial v_x}{\partial x} + v_y \frac{\partial v_x}{\partial y} \right) q_x + \int_\Omega T_{xx} \frac{\partial q_x}{\partial x} + T_{xy} \frac{\partial q_x}{\partial y} = 0.$$
$$\int_\Omega \rho \left(\frac{\partial v_y}{\partial t} + v_x \frac{\partial v_y}{\partial x} + v_y \frac{\partial v_y}{\partial y} \right) q_y + \int_\Omega T_{xy} \frac{\partial q_y}{\partial x} + T_{yy} \frac{\partial q_y}{\partial y} = 0.$$

(D.4)
$$\mathbf{T} = \begin{pmatrix} -p + 2\mu_2 \frac{\partial v_x}{\partial x} + \frac{G}{2}(B_{xx} - B_{yy}) & \mu_2 \left(\frac{\partial v_x}{\partial y} + \frac{\partial v_y}{\partial x} \right) + G B_{xy} \\ \mu_2 \left(\frac{\partial v_x}{\partial y} + \frac{\partial v_y}{\partial x} \right) + G B_{xy} & -p + 2\mu_2 \frac{\partial v_y}{\partial y} + \frac{G}{2}(B_{yy} - B_{xx}) \end{pmatrix}.$$

(D.5)
$$\int_\Omega \left(\frac{\partial B_{xx}}{\partial t} + v_x \frac{\partial B_{xx}}{\partial x} + v_y \frac{\partial B_{xx}}{\partial y} - 2 \left(\frac{\partial v_x}{\partial x} B_{xx} + \frac{\partial v_x}{\partial y} B_{xy} \right) + \frac{1}{\tau} \left(\frac{1}{2} B_{xx}(B_{xx} - B_{yy}) + B_{xy}^2 \right) \right) Q_{xx} = 0.$$

$$\int_\Omega \left(\frac{\partial B_{xy}}{\partial t} + v_x \frac{\partial B_{xy}}{\partial x} + v_y \frac{\partial B_{xy}}{\partial y} - \left(\frac{\partial v_y}{\partial x} B_{xx} + \left(\frac{\partial v_x}{\partial x} + \frac{\partial v_y}{\partial y} \right) B_{xy} + \frac{\partial v_x}{\partial y} B_{yy} \right) + \frac{1}{2\tau} B_{xy}(B_{xx} + B_{yy}) \right) Q_{xy} = 0.$$

$$\int_\Omega \left(\frac{\partial B_{yy}}{\partial t} + v_x \frac{\partial B_{yy}}{\partial x} + v_y \frac{\partial B_{yy}}{\partial y} - 2 \left(\frac{\partial v_y}{\partial x} B_{xy} + \frac{\partial v_y}{\partial y} B_{yy} \right) + \frac{1}{\tau} \left(\frac{1}{2} B_{yy}(B_{yy} - B_{xx}) + B_{xy}^2 \right) \right) Q_{yy} = 0.$$

D.2 Model Quad1 in the cylindrical coordinates

Let us assume that all unknowns $p, \mathbf{v}, \mathbf{B}_{\kappa_{p(t)}}$ are independent of φ. Then the problem is solved in the cross-section Σ. The unknowns are in the form

$$p = p(r,z), \ \mathbf{v} = (v_r, v_\varphi, v_z)(r,z), \ \mathbf{B}_{\kappa_{p(t)}} = \begin{pmatrix} B_{rr}, B_{r\varphi}, B_{rz} \\ B_{r\varphi}, B_{\varphi\varphi}, B_{\varphi z} \\ B_{rz}, B_{\varphi z}, B_{zz} \end{pmatrix}(r,z), \quad (r,z) \in \Sigma.$$

The weak formulation in the cylindrical coordinates in the cross-section Σ is

$$\int_\Sigma r \operatorname{div} \mathbf{v}\ q = 0, \tag{D.6}$$

$$\int_\Sigma \rho r \left(\frac{\partial \mathbf{v}}{\partial t} + \mathbf{v} \cdot \nabla \mathbf{v} \right) \cdot \mathbf{q} + \int_\Sigma r \mathbf{T} \cdot \nabla \mathbf{q} = 0, \tag{D.7}$$

$$r\mathbf{T} = -rp\mathbf{I} + 2r\mu_2 \mathbf{D} + rG\mathbf{B}^d_{\kappa_{p(t)}}, \tag{D.8}$$

$$\int_\Sigma r \left(\frac{\partial \mathbf{B}_{\kappa_{p(t)}}}{\partial t} + \mathbf{v} \cdot \nabla \mathbf{B}_{\kappa_{p(t)}} - \mathbf{L}\mathbf{B}_{\kappa_{p(t)}} - \mathbf{B}_{\kappa_{p(t)}}\mathbf{L}^{\mathrm{T}} + \frac{1}{\tau}\mathbf{B}_{\kappa_{p(t)}}\mathbf{B}^d_{\kappa_{p(t)}} \right) \cdot \mathbf{Q} = 0 \tag{D.9}$$

with the test functions

$$q = q(r,z), \quad \mathbf{q} = (q_r, q_\varphi, q_z)(r,z), \quad \mathbf{Q} = \begin{pmatrix} Q_{rr}, Q_{r\varphi}, Q_{rz} \\ Q_{r\varphi}, Q_{\varphi\varphi}, Q_{\varphi z} \\ Q_{rz}, Q_{\varphi z}, Q_{zz} \end{pmatrix} (r,z)$$

The components of the weak formulation of all equations are

(D.6)

$$\int_\Sigma \left(r\frac{\partial v_r}{\partial r} + v_r + r\frac{\partial v_z}{\partial z} \right) q = 0.$$

(D.7)

$$\int_\Sigma \rho \left(r\frac{\partial v_r}{\partial t} + rv_r\frac{\partial v_r}{\partial r} - v_\varphi^2 + rv_z\frac{\partial v_r}{\partial z} \right) q_r + \int_\Sigma \frac{rT_{\varphi\varphi}}{r} q_r + rT_{rr}\frac{\partial q_r}{\partial r} + rT_{rz}\frac{\partial q_r}{\partial z} = 0,$$

$$\int_\Sigma \rho \left(r\frac{\partial v_\varphi}{\partial t} + rv_r\frac{\partial v_\varphi}{\partial r} + v_\varphi v_r + rv_z\frac{\partial v_\varphi}{\partial z} \right) q_\varphi + \int_\Sigma -\frac{rT_{r\varphi}}{r} q_\varphi + rT_{r\varphi}\frac{\partial q_\varphi}{\partial r} + rT_{\varphi z}\frac{\partial q_\varphi}{\partial z} = 0,$$

$$\int_\Sigma \rho \left(r\frac{\partial v_z}{\partial t} + rv_z\frac{\partial v_r}{\partial r} + rv_z\frac{\partial v_z}{\partial z} \right) q_r + \int_\Sigma rT_{rz}\frac{\partial q_z}{\partial r} + rT_{zz}\frac{\partial q_z}{\partial z} = 0.$$

(D.8)

$$r\mathbf{T} = \begin{pmatrix} -rp + 2r\mu_2\dfrac{\partial v_r}{\partial r} + rG(B_{rr} - b) & \mu_2\left(-v_\varphi + r\dfrac{\partial v_\varphi}{\partial r}\right) + rGB_{r\varphi} & r\mu_2\left(\dfrac{\partial v_r}{\partial z} + \dfrac{\partial v_z}{\partial r}\right) + rGB_{rz} \\ \mu_2\left(-v_\varphi + r\dfrac{\partial v_\varphi}{\partial r}\right) + rGB_{r\varphi} & -rp + 2\mu_2 v_r + rG(B_{\varphi\varphi} - b) & r\mu_2\dfrac{\partial v_\varphi}{\partial z} + rGB_{\varphi z} \\ r\mu_2\left(\dfrac{\partial v_r}{\partial z} + \dfrac{\partial v_z}{\partial r}\right) + rGB_{rz} & r\mu_2\dfrac{\partial v_\varphi}{\partial z} + rGB_{\varphi z} & -rp + 2r\mu_2\dfrac{\partial v_z}{\partial z} + rG(B_{zz} - b) \end{pmatrix},$$

where $b = \dfrac{1}{3}(B_{rr} + B_{\varphi\varphi} + B_{zz})$.

(D.9)

$$\int_\Sigma \Big(r\frac{\partial B_{rr}}{\partial t} + rv_r\frac{\partial B_{rr}}{\partial r} + rv_z\frac{\partial B_{rr}}{\partial z} - 2v_\varphi B_{r\varphi} - 2\left(rL_{rr}B_{rr} + rL_{r\varphi}B_{r\varphi} + rL_{rz}B_{rz}\right) + \frac{r}{\tau}\left(\frac{1}{3}B_{rr}(2B_{rr} - B_{\varphi\varphi} - B_{zz}) + B_{r\varphi}^2 + B_{rz}^2\right)\Big) Q_{rr} = 0,$$

$$\int_\Sigma \Big(r\frac{\partial B_{r\varphi}}{\partial t} + rv_r\frac{\partial B_{r\varphi}}{\partial r} + rv_z\frac{\partial B_{r\varphi}}{\partial z} - v_\varphi\left(B_{\varphi\varphi} - B_{rr}\right) - rL_{rr}B_{r\varphi} - rL_{r\varphi}B_{\varphi\varphi} - rL_{rz}B_{\varphi z} - rL_{\varphi r}B_{rr} - rL_{\varphi\varphi}B_{r\varphi} - rL_{\varphi z}B_{rz} + \frac{r}{\tau}\left(\frac{1}{3}B_{r\varphi}(2B_{\varphi\varphi} + 2B_{rr} - B_{zz}) + B_{rz}B_{\varphi z}\right)\Big)Q_{r\varphi} = 0,$$

$$\int_\Sigma \Big(r\frac{\partial B_{rz}}{\partial t} + rv_r\frac{\partial B_{rz}}{\partial r} + rv_z\frac{\partial B_{rz}}{\partial z} - v_\varphi B_{\varphi z} - rL_{rr}B_{rz} - rL_{r\varphi}B_{\varphi z} - rL_{rz}B_{zz} - rL_{zr}B_{rr} - rL_{z\varphi}B_{r\varphi} - rL_{zz}B_{rz} + \frac{r}{\tau}\left(\frac{1}{3}B_{rz}(2B_{zz} + 2B_{rr} - B_{\varphi\varphi}) + B_{r\varphi}B_{\varphi z}\right)\Big)Q_{rz} = 0,$$

$$\int_\Sigma \Big(r\frac{\partial B_{\varphi\varphi}}{\partial t} + rv_r\frac{\partial B_{\varphi\varphi}}{\partial r} + rv_z\frac{\partial B_{\varphi\varphi}}{\partial z} + 2v_\varphi B_{r\varphi} - 2\left(rL_{\varphi r}B_{r\varphi} + rL_{\varphi\varphi}B_{\varphi\varphi} + rL_{\varphi z}B_{\varphi z}\right) + \frac{r}{\tau}\left(\frac{1}{3}B_{\varphi\varphi}(2B_{\varphi\varphi} - B_{rr} - B_{zz}) + B_{r\varphi}^2 + B_{\varphi z}^2\right)\Big)Q_{\varphi\varphi} = 0,$$

$$\int_\Sigma \Big(r\frac{\partial B_{\varphi z}}{\partial t} + rv_r\frac{\partial B_{\varphi z}}{\partial r} + rv_z\frac{\partial B_{\varphi z}}{\partial z} + v_\varphi B_{rz} - rL_{\varphi r}B_{rz} - rL_{\varphi\varphi}B_{\varphi z} - rL_{\varphi z}B_{zz} - rL_{zr}B_{r\varphi} - rL_{z\varphi}B_{\varphi\varphi} - rL_{zz}B_{\varphi z} + \frac{r}{\tau}\left(\frac{1}{3}B_{\varphi z}(2B_{zz} + 2B_{\varphi\varphi} - B_{rr}) + B_{r\varphi}B_{rz}\right)\Big)Q_{\varphi z} = 0,$$

$$\int_\Sigma \Big(r\frac{\partial B_{zz}}{\partial t} + rv_r\frac{\partial B_{zz}}{\partial r} + rv_z\frac{\partial B_{zz}}{\partial z} - 2\left(rL_{zr}B_{rz} + rL_{z\varphi}B_{\varphi z} + rL_{zz}B_{zz}\right) + \frac{r}{\tau}\left(\frac{1}{3}B_{zz}(2B_{zz} - B_{rr} - B_{\varphi\varphi}) + B_{rz}^2 + B_{\varphi z}^2\right)\Big)Q_{zz} = 0,$$

where

$$r\mathbf{L} = \begin{pmatrix} rL_{rr} & rL_{r\varphi} & rL_{rz} \\ rL_{\varphi r} & rL_{\varphi\varphi} & rL_{\varphi z} \\ rL_{zr} & rL_{z\varphi} & rL_{zz} \end{pmatrix} = \begin{pmatrix} r\dfrac{\partial v_r}{\partial r} & -v_\varphi & r\dfrac{\partial v_r}{\partial z} \\ r\dfrac{\partial v_\varphi}{\partial r} & v_r & r\dfrac{\partial v_\varphi}{\partial z} \\ r\dfrac{\partial v_z}{\partial r} & 0 & r\dfrac{\partial v_z}{\partial z} \end{pmatrix}.$$

D.3 ALE formulation of model Quad1 in two-dimensional Cartesian coordinates

ALE formulation of the model Quad1 is in the local form (in Ω_χ) equal to

$$\hat{J}\,\mathrm{tr}\left((\nabla_\chi \mathbf{v})\hat{\mathbf{F}}^{-\mathrm{T}}\right) = 0,$$

$$-\Delta\mathbf{u} = 0,$$

$$\hat{J}\rho\frac{\partial \mathbf{v}}{\partial t} + \hat{J}\rho(\nabla_\chi \mathbf{v})\left(\hat{\mathbf{F}}^{-1}\left(\mathbf{v} - \frac{\partial \mathbf{u}}{\partial t}\right)\right) = \nabla_\chi \cdot \left(\hat{J}\hat{\mathbf{T}}\hat{\mathbf{F}}^{-T}\right),$$

$$\hat{\mathbf{T}} = -p\mathbf{I} + \mu_2((\nabla_\chi \mathbf{v})\hat{\mathbf{F}}^{-1} + \hat{\mathbf{F}}^{-\mathrm{T}}(\nabla_\chi \mathbf{v})^{\mathrm{T}}) + G\mathbf{B}^d_{\kappa_{p(t)}},$$

$$\hat{J}\left[\frac{\partial \mathbf{B}_{\kappa_{p(t)}}}{\partial t} + \left(\hat{\mathbf{F}}^{-1}\left(\mathbf{v} - \frac{\partial \mathbf{u}}{\partial t}\right)\right)\nabla_\chi \mathbf{B}_{\kappa_{p(t)}} - (\nabla_\chi \mathbf{v})\hat{\mathbf{F}}^{-1}\mathbf{B}_{\kappa_{p(t)}} - \mathbf{B}_{\kappa_{p(t)}}\hat{\mathbf{F}}^{-\mathrm{T}}(\nabla_\chi \mathbf{v})^{\mathrm{T}}\right] = -\frac{\hat{J}}{\tau}\mathbf{B}_{\kappa_{p(t)}}\mathbf{B}^d_{\kappa_{p(t)}},$$

where $\dfrac{\partial \mathbf{u}}{\partial t} = \mathbf{v}$ on the boundary $\partial\Omega_\chi$, $\hat{\mathbf{F}} = \mathbf{I} + \nabla\mathbf{u}$, $\hat{J} = \det\hat{\mathbf{F}}$. Let assume that all unknowns $p, \mathbf{u}, \mathbf{v}, \mathbf{B}_{\kappa_{p(t)}}$ are in the form

$$p = p(x, y),\ \mathbf{u} = (u_x, u_y)(x, y),\ \mathbf{v} = (v_x, v_y)(x, y),$$

$$\mathbf{B}_{\kappa_{p(t)}} = \begin{pmatrix} B_{xx} & B_{xy} \\ B_{xy} & B_{yy} \end{pmatrix}(x,y), \quad (x,y) \in \Omega_\chi.$$

The weak formulation in the Cartesian coordinates is

$$\int_{\Omega_\chi} \hat{J}\,\mathrm{tr}\left((\nabla_\chi \mathbf{v})\hat{\mathbf{F}}^{-1}\right)\, q = 0, \quad \text{(D.10)}$$

$$\int_{\Omega_\chi} \nabla \mathbf{u} \cdot \nabla \mathbf{t} = 0, \quad \text{(D.11)}$$

$$\int_{\Omega_\chi} \hat{J}\rho\left(\frac{\partial \mathbf{v}}{\partial t} + (\nabla_\chi \mathbf{v})\left(\hat{\mathbf{F}}^{-1}\left(\mathbf{v} - \frac{\partial \mathbf{u}}{\partial t}\right)\right)\right) \cdot \mathbf{q} + \int_{\Omega_\chi} \hat{J}\hat{\mathbf{T}}\hat{\mathbf{F}}^{-T} \cdot \nabla \mathbf{q} - \int_{\partial\Omega_\chi} \hat{J}\hat{\mathbf{T}}\hat{\mathbf{F}}^{-T}\mathbf{n} \cdot \mathbf{q} = 0, \quad \text{(D.12)}$$

$$\hat{\mathbf{T}} = -p\mathbf{I} + \mu_2((\nabla_\chi \mathbf{v})\hat{\mathbf{F}}^{-1} + \hat{\mathbf{F}}^{-\mathrm{T}}(\nabla_\chi \mathbf{v})^{\mathrm{T}}) + G\mathbf{B}^d_{\kappa_{p(t)}}, \quad \text{(D.13)}$$

$$\int_{\Omega_\chi} \hat{J}\Big[\frac{\partial \mathbf{B}_{\kappa_{p(t)}}}{\partial t} + \left(\hat{\mathbf{F}}^{-1}\left(\mathbf{v} - \frac{\partial \mathbf{u}}{\partial t}\right)\right)\nabla_\chi \mathbf{B}_{\kappa_{p(t)}} - (\nabla_\chi \mathbf{v})\hat{\mathbf{F}}^{-1}\mathbf{B}_{\kappa_{p(t)}} - \mathbf{B}_{\kappa_{p(t)}}\hat{\mathbf{F}}^{-\mathrm{T}}(\nabla_\chi \mathbf{v})^{\mathrm{T}} + \frac{1}{\tau}\mathbf{B}_{\kappa_{p(t)}}\mathbf{B}^d_{\kappa_{p(t)}}\Big] \cdot \mathbf{Q} = 0 \quad \text{(D.14)}$$

with the test functions

$$q = q(x,y), \quad \mathbf{t} = (t_x, t_y)(x,y), \quad \mathbf{q} = (q_x, q_y)(x,y), \quad \mathbf{Q} = \begin{pmatrix} Q_{xx} & Q_{xy} \\ Q_{xy} & Q_{yy} \end{pmatrix}(x,y).$$

Using the components it can be comupted

$$\hat{\mathbf{F}} = \begin{pmatrix} 1 + \dfrac{\partial u_x}{\partial x} & \dfrac{\partial u_x}{\partial y} \\ \dfrac{\partial u_y}{\partial x} & 1 + \dfrac{\partial u_y}{\partial y} \end{pmatrix}, \quad \hat{J} = \det \hat{\mathbf{F}} = \left(1 + \frac{\partial u_x}{\partial x}\right)\left(1 + \frac{\partial u_y}{\partial y}\right) - \frac{\partial u_x}{\partial y}\frac{\partial u_y}{\partial x}.$$

Let us denote

$$\hat{\mathbf{F}}^{-1} = \begin{pmatrix} Fi_{xx} & Fi_{xy} \\ Fi_{yx} & Fi_{yy} \end{pmatrix} := \frac{1}{\hat{J}} \begin{pmatrix} 1 + \dfrac{\partial u_y}{\partial y} & -\dfrac{\partial u_x}{\partial y} \\ -\dfrac{\partial u_y}{\partial x} & 1 + \dfrac{\partial u_x}{\partial x} \end{pmatrix},$$

$$\widehat{\nabla \mathbf{v}} = (\nabla_\chi \mathbf{v})\hat{\mathbf{F}}^{-1} = \begin{pmatrix} \hat{L}_{xx} & \hat{L}_{xy} \\ \hat{L}_{yx} & \hat{L}_{yy} \end{pmatrix} := \begin{pmatrix} \dfrac{\partial v_x}{\partial x}Fi_{xx} + \dfrac{\partial v_x}{\partial y}Fi_{yx} & \dfrac{\partial v_x}{\partial x}Fi_{xy} + \dfrac{\partial v_x}{\partial y}Fi_{yy} \\ \dfrac{\partial v_y}{\partial x}Fi_{xx} + \dfrac{\partial v_y}{\partial y}Fi_{yx} & \dfrac{\partial v_y}{\partial x}Fi_{xy} + \dfrac{\partial v_y}{\partial y}Fi_{yy} \end{pmatrix}.$$

The components of the weak formulation of all equations are

(D.10)

$$\int_{\Omega_\chi} \hat{J}\left(\hat{L}_{xx} + \hat{L}_{yy}\right) q = 0.$$

(D.11)

$$\int_{\Omega_\chi} \frac{\partial u_x}{\partial x}\frac{\partial t_x}{\partial x} + \frac{\partial u_x}{\partial y}\frac{\partial t_x}{\partial y} = 0,$$

$$\int_{\Omega_\chi} \frac{\partial u_y}{\partial x}\frac{\partial t_y}{\partial x} + \frac{\partial u_y}{\partial y}\frac{\partial t_y}{\partial y} = 0.$$

(D.12) The equations are written without the boundary term.

$$\int_{\Omega_\chi} \rho\hat{J}\left(\frac{\partial v_x}{\partial t} + \hat{L}_{xx}\left(v_x - \frac{\partial u_x}{\partial t}\right) + \hat{L}_{xy}\left(v_y - \frac{\partial u_y}{\partial t}\right)\right) q_x + \int_{\Omega_\chi} \hat{J}\left(\hat{T}_{xx}Fi_{xx} + \hat{T}_{xy}Fi_{xy}\right)\frac{\partial q_x}{\partial x} + \hat{J}\left(\hat{T}_{xx}Fi_{yx} + \hat{T}_{xy}Fi_{yy}\right)\frac{\partial q_x}{\partial y} = 0,$$

$$\int_{\Omega_\chi} \rho\hat{J}\left(\frac{\partial v_y}{\partial t} + \hat{L}_{yx}\left(v_x - \frac{\partial u_x}{\partial t}\right) + \hat{L}_{yy}\left(v_y - \frac{\partial u_y}{\partial t}\right)\right) q_y + \int_{\Omega_\chi} \hat{J}\left(\hat{T}_{xy}Fi_{xx} + \hat{T}_{yy}Fi_{xy}\right)\frac{\partial q_y}{\partial x} + \hat{J}\left(\hat{T}_{xy}Fi_{yx} + \hat{T}_{yy}Fi_{yy}\right)\frac{\partial q_y}{\partial y} = 0.$$

(D.13)

$$\hat{\mathbf{T}} = \begin{pmatrix} -p + 2\mu_2\hat{L}_{xx} + \frac{G}{2}(B_{xx} - B_{yy}) & \mu_2\left(\hat{L}_{xy} + \hat{L}_{yx}\right) + GB_{xy} \\ \mu_2\left(\hat{L}_{xy} + \hat{L}_{yx}\right) + GB_{xy} & -p + 2\mu_2\hat{L}_{yy} + \frac{G}{2}(B_{yy} - B_{xx}). \end{pmatrix}$$

(D.14)

$$\int_{\Omega_\chi} \hat{J}\Big[\frac{\partial B_{xx}}{\partial t} + \left(Fi_{xx}\left(v_x - \frac{\partial u_x}{\partial t}\right) + Fi_{xy}\left(v_y - \frac{\partial u_y}{\partial t}\right)\right)\frac{\partial B_{xx}}{\partial x} + \left(Fi_{yx}\left(v_x - \frac{\partial u_x}{\partial t}\right) + Fi_{yy}\left(v_y - \frac{\partial u_y}{\partial t}\right)\right)\frac{\partial B_{xx}}{\partial y} - 2\left(\hat{L}_{xx}B_{xx} + \hat{L}_{xy}B_{xy}\right) + \frac{1}{\tau}\left(\frac{1}{2}B_{xx}(B_{xx} - B_{yy}) + B_{xy}^2\right)\Big]Q_{xx} = 0,$$

$$\int_{\Omega_\chi} \hat{J}\Big[\frac{\partial B_{xy}}{\partial t} + \left(Fi_{xx}\left(v_x - \frac{\partial u_x}{\partial t}\right) + Fi_{xy}\left(v_y - \frac{\partial u_y}{\partial t}\right)\right)\frac{\partial B_{xy}}{\partial x} + \left(Fi_{yx}\left(v_x - \frac{\partial u_x}{\partial t}\right) + Fi_{yy}\left(v_y - \frac{\partial u_y}{\partial t}\right)\right)\frac{\partial B_{xy}}{\partial y} - \left(\hat{L}_{yx}B_{xx} + \left(\hat{L}_{xx} + \hat{L}_{yy}\right)B_{xy} + \hat{L}_{xy}B_{yy}\right) + \frac{1}{2\tau}B_{xy}(B_{xx} + B_{yy})\Big]Q_{xy} = 0,$$

$$\int_{\Omega_\chi} \hat{J}\Big[\frac{\partial B_{yy}}{\partial t} + \left(Fi_{xx}\left(v_x - \frac{\partial u_x}{\partial t}\right) + Fi_{xy}\left(v_y - \frac{\partial u_y}{\partial t}\right)\right)\frac{\partial B_{yy}}{\partial x} + \left(Fi_{yx}\left(v_x - \frac{\partial u_x}{\partial t}\right) + Fi_{yy}\left(v_y - \frac{\partial u_y}{\partial t}\right)\right)\frac{\partial B_{yy}}{\partial y} - 2\left(\hat{L}_{yx}B_{xy} + \hat{L}_{yy}B_{yy}\right) + \frac{1}{\tau}\left(\frac{1}{2}B_{yy}(B_{yy} - B_{xx}) + B_{xy}^2\right)\Big]Q_{yy} = 0.$$